pennsylvania
DEPARTMENT OF TRANSPORTATION

Sensing Technology for Damage Assessment of Sign Supports and Cantilever Poles

FINAL REPORT

August 31, 2010

By Piervincenzo Rizzo and Xuan Zhu
University of Pittsburgh

COMMONWEALTH OF PENNSYLVANIA
DEPARTMENT OF TRANSPORTATION

CONTRACT # 510601
WORK ORDER # PIT 008

1. Report No. FHWA – PA – 2010 -10 – PIT008	2. Government Accession No.	3. Recipient's Catalog No.	
4. Title and Subtitle **Sensing Technology for Damage Assessment of Sign Supports and Cantilever Poles**		5. Report Date August 31, 2010	
		6. Performing Organization Code	
7. Author(s) Piervincenzo Rizzo and Xuan "Peter" Zhu		8. Performing Organization Report No.	
9. Performing Organization Name and Address University of Pittsburgh, SWANSON School of Engineering, Department of Civil & Environmental Engineering 949 Benedum Hall Pittsburgh, PA 15261-2294		10. Work Unit No. (TRAIS)	
		11. Contract or Grant No. 510601-PIT 008	
12. Sponsoring Agency Name and Address The Pennsylvania Department of Transportation Bureau of Planning and Research Commonwealth Keystone Building 400 North Street, 6th Floor Harrisburg, PA 17120-0064		13. Type of Report and Period Covered Final Report, March 1, 2008-September 1, 2010	
		14. Sponsoring Agency Code	

15. Supplementary Notes
PennDOT Technical Advisor: Jerry Bruck

16. Abstract
This report presents the results of research activities conducted under Contract No. 519691-PIT 008 on "Sensing Technology for Damage Assessment of Sign Supports and Cantilever Poles" between the University of Pittsburgh and the Pennsylvania Department of Transportation.
The two primary goals of the contract aimed at developing a finite element model for the prediction of fatigue life of sign supports, and at developing a low-cost sensing technology to detect damage in sign support structures.
The project has made use of test equipment and computer support at PITT's Laboratory for Nondestructive Evaluation and Structural Health Monitoring studies and the Watkins-Haggart Structural Engineering Laboratory.
Special acknowledgement goes to Jerry Bruck, technical advisor of the project for the Pennsylvania Department of Transportation, for his valuable guidance and comments, and for all the research materials that he provided.

17. Key Words Sign Support Structures, Nondestructive Evaluation, Structural Health Monitoring, Sign Structures Inspection	18. Distribution Statement No restrictions. This document is available from the National Technical Information Service, Springfield, VA 22161		
19. Security Classif. (of this report) Unclassified	20. Security Classif. (of this page) Unclassified	21. No. of Pages 222	22. Price

Form DOT F 1700.7   **(8-72)**   **Reproduction of completed page authorized**

University of Pittsburgh

Department of Civil and Environmental Engineering

**Sensing Technology for Damage Assessment of Sign Supports and Cantilever Poles
(Final Report)**

By

Piervincenzo Rizzo, Ph.D.

Assistant Professor

Xuan "Peter" Zhu

Graduate Student Researcher

Final Report submitted to the Pennsylvania Department of Transportation

under Contract No. 510601-PIT 008

Department of Civil and Environmental Engineering

University of Pittsburgh

Pittsburgh, Pennsylvania 15261

August 2010

PREFACE and ACKNOWLEDGEMENTS

DISCLAIMER

TABLE OF CONTENTS

LIST OF FIGURES

LIST OF TABLES

LIST OF ACRONYMS

AE	Acoustic Emission
AASHTO	American Association of State Highway and Transportation Officials
AISI	American Iron and Steel Institute
APDL	ANSYS Parametric Design Language
ASTM	American Society for Testing And Materials
AWS	American Welding Society
CAFL	Constant Amplitude Fatigue Limits
cf	Crest Factor
DOT	Department of Transportation
ECT	Eddy Current Testing
EMI	Electromechanical Impedance
FEM	Finite Element Method
FHWA	Federal Highway Administration
GUW	Guided Ultrasonic Wave
kf	K-Factor
Krt	Kurtosis
Max	Maximum
MPI	Magnetic Particle Inspection
MSD	Mahalanobis Squared Distance
NCDC	National Climatic Data Center
NCHRP	National Cooperative Highway Research Program
NDE	Nondestructive Evaluation
NDT	Nondestructive Testing
NI	National Instruments
PennDOT	Pennsylvania Department of Transportation
PCI	Peripheral Component Interconnect
PITT	University of Pittsburgh
Ppk	Peak-to-Peak
PT	Penetrant Testing
PXI	PCI Extensions for Instrumentation
RMS	Root Mean Square
SAFE	Semi-Analytical Finite Element
SHM	Structural Health Monitoring
SPBW	Superposition of Bulk Waves
UT	Ultrasonic Testing

UV	Ultraviolet
VIM	Visual Inspection Method
VMS	Variable Message Sign

CHAPTER 1: INTRODUCTION

1.1 PROBLEM STATEMENT AND MOTIVATION

Sign support structures including the cantilever, butterfly, and bridge support (also known as overhead or span type supports) can be found along any major highway across the United States. These are most commonly found on roads or pedestals built into the highway side or median barriers or built into parapets or other parts of a bridge. These structures support signages that help commuters navigate their way. Similarly, Variable Message Sign (VMS) are used to control, inform, and warn the commuters through the display of a number of messages that may be changed or switched on or off as necessary.

Overhead cantilever consists of a mast arm extending out over the roadway supported by a single roadside column, typically a single or double pole or a box-truss structure. The vertical columns are sometimes referred to as an uprights, posts, or poles. The horizontal part of the structure is referred to as the mast arm (usually in reference to a monotube, that is a single tube without joints), the truss (for other than monotubes), or the cantilever.

In the fourth edition of the *Standard Specifications for Structural Supports for Highway Signs, Luminaries, and Traffic Signals* (AASHTO 2001), structures supported on both sides of the roadway are referred to as bridge supports. Bridge supports are also called span-type structures, sign bridges, or overhead structures (although the latter term is sometimes used to describe both cantilever and bridge supports) (Dexter and Ricker 2002). The roadside columns that support the mast range from single poles to box-truss structures. Each vertical column truss is composed of two to four chord members braced by web members using the same pipe-to-pipe connections as in the overhead truss-type structure.

Cantilevered support structures can be an attractive option because the cost is typically less than 40 percent of the cost of bridge supports. Also, the single upright increases motorist safety by reducing the probability of vehicle collision (Dexter and Ricker 2002). In Pennsylvania two types of overhead sign support structures are mainly used, namely the cantilever with single pole and overhead bridge truss with bridge pole.

Figure 1.1 – Examples of: (a) overhead cantilever with single pole; (b) overhead bridge truss with truss poles.

Figure 1.2 - Examples of (clockwise from top left): overhead truss with single pole supports, cantilevered single pole, overhead truss with truss supports, cantilever with double pole, a structure mounted sign, pole mounted VMS, monotube structure.

Photos of these two structures taken in the Pittsburgh area are presented in Fig. 1.1.

Nationwide and through the years, the configuration of the full-span overhead sign supports has evolved, and today many structures consist of a truss-type structure that contains fully welded pipe-to-pipe connections (Ginal 2003). A gallery of different sign support structures is provided in Fig. 1.2.

Sign structures are made of structural steel and aluminum. However, aluminum structures are no longer being constructed, because steel structures have proven to be more cost effective (Ginal 2003).

In general, highway sign supports must withstand in-service dynamic loads, which largely constitute the fatigue environment. Sources of these loads include natural winds, seismic events (in seismic areas), artificial gusts created by passing vehicles, and vibrations induced in bridges by passing vehicles (sign supports mounted on a bridge).

During the past two decades, sign structures have shown problems associated with reduced fatigue performance. Defective welds, aging material, and harsh environmental conditions have exacerbated these problems.

Most of the underlying problems involve cracks induced into welds by fatigue loading. Generally, cracks are found propagating within the leg of a fillet weld or at the toe. Depending upon the amount of time the crack has to grow, these cracks can propagate into the main supporting member (e.g., the chord of a truss) (Ginal 2003).

A report (Dexter and Ricker 2002) for the National Cooperative Highway Research Program (NCHRP) included the following factors that increased the number of such problems: a) the advent of backplates (used on signal fixtures to block the sun and enhance the visibility of the signal) has increased the susceptibility to galloping (FHWA 2000); b) the size and location of flat panel signs —larger signs are now placed asymmetrically with their center of gravity above the center of gravity of the horizontal mast arm or support truss, increasing the torsional motion of the mast arms; c) the use of large VMSs which implies the presence of a large horizontal surface that increases the effect of truck-induced gusts (Dexter et al. 2000). It was also identified that the structural connections of all these types of sign supports are susceptible to fatigue loadings, wind induced vibration and crack propagations on the surface or deep inside.

While the optimal design of such structures is paramount to prevent damage and consequent collapse, the determination of proper inspection technology is important in preventing collapses such as those shown in Fig. 1.3.

The AASHTO specifications (AASHTO 2001) affirm that "*a regular maintenance program should be established that includes periodic inspection, maintenance, and repair of structural supports*." Despite this, no regulations for the inspection of highway sign structures in the United States exist, and those states that do inspect do so without any uniform process. Different states use different inspection methods over different time periods to make sure that their sign structures continue to function properly.

(a)

(b)

Figure 1.3 – (a) Collapse of a sign structure along I-65 in Tennessee. http://updatewindowssecurity.com/?id=34452915477 (b) Cantilever Sign Structure Failure: (Source: http://www.fhwa.dot.gov/BRIDGE/signinspection03.cfm**.**

1.2 SCOPE OF WORK

The main objective of the project, conducted under the aegis of the Pennsylvania Department of Transportation (PennDOT), was the development of a sensing technology to assess the structural soundness of sign supports, cantilever poles, and VMS supports. The sensing technology aims to shift the maintenance paradigm from time-based (periodic inspection) to real-time monitoring.

The work was articulated in two main directions. First an analytical model based on the Finite Element Method (FEM) was developed to correlate stress-crack severity and/or damage location to the integrity and residual lifetime of the sign support structures. Second, a sensing technology coupled to signal processing and feature extraction was developed to provide a means to detect damage. The project included the following research efforts:

a) Improve the finite element modeling of loaded structure in light of the latest advancement in structural modeling and wind simulation.

b) Apply Nondestructive Evaluation (NDE) / Structural Health Monitoring (SHM) strategies able to monitor the structure in real-time

4

c) Distribute and examine a survey sent to U.S. and Canadian Departments of Transportation about this report provides an overview of the NDE methods currently used to assess the health of support structures for highways and roadways signs and VMSs.

d) Use signal-processing algorithms for damage identification and classification.

The aim of the research activities is twofold: 1) formulate a numerical model able to predict fatigue life and correlate stress-crack severity and/or location to the structural integrity and residual lifetime of sign structures; 2) develop a robust and low-cost sensing technology to assess the structural soundness of sign structures.

1.3 REPORT OUTLINE

The outline of the report is as follows.

Chapter 2 presents in detail the different types of sign structures used in the U.S. and the terminology used throughout the report. Descriptions of the materials used in the construction of sign support structures are given. The list and the cause of the main issues associated with service life are discussed.

Chapter 3 describes the survey sent to the U.S. and Canadian DOTs. The analysis of the received responses is presented. The results of previous surveys are briefly reviewed wherever they were found relevant to this project.

Chapter 4 presents the analytical study conducted to model fatigue by means of a FEM algorithm. The work presented in this chapter has been reported in the journal paper:

> Kacin, J., Rizzo, P., and Tajari M. (2010). "Fatigue Analysis of Overhead Sign Support Structures," Engineering Structures, Engineering Structures, 32(6), pp. 1659-1670.

Interested readers are also referred to the following:

> Kacin, J., **Rizzo, P.**, and Annamdas, V.G.M. (2009). *Sensing Technology for Damage Assessment of Sign Supports and Cantilever Poles – Tasks 2-3*, Year 1 Report, Pennsylvania Department of Transportation, Contract No. 519691-PIT 008, University of Pittsburgh.

Chapter 5 reports on the background and the technical requirements to deploy the NDE methods that have emerged from the survey. The methods of visual inspection, liquid penetrant, magnetic particles, and ultrasonic testing are illustrated. This chapter overviews the potential technologies that can be adapted, especially from the oil and gas industry. In fact, many support structures are made of tubular components and therefore technologies used in the pipeline industry may be adapted.

Attention is also given to the requirements needed to operate a transition from a time-based to permanent-based monitoring approach. Few feasible techniques to develop the SHM approach are illustrated. The estimated cost to run an inspection is also provided based on the figures collected in the years 2008-2009.

Chapter 6 presents the hardware, software, and equipment used in the experimental program conducted at the Laboratory for Nondestructive Evaluation and Structural Health Monitoring studies and the Watkins-Haggart Structural Engineering Laboratory, both at the University of Pittsburgh. The test protocol and signal processing utilized to process the ultrasonic data are presented as well.

5

Chapter 7 describes the results obtained from the application of ultrasonic data applied to the three tests performed in the laboratory. The first test consisted of monitoring the onset and growth of an artificial crack under dynamic loading. The second test consisted of monitoring the onset and growth of a second artificial crack under dynamic loading. Finally, during the third test the structure was monitored under different environmental conditions (dry, rainy, snowy) and temperatures (cold, warm). Part of the work presented in this chapter was reported in the journal paper:

Zhu, X., Rizzo, P., Marzani, A., and Bruck, J. (2010). "Ultrasonic Guided Waves for NDE/SHM of Trusses," Measurement Science and Technology, 21, 045701, doi: 10.1088/0957-0233/21/4/045701.

Chapter 8 illustrates the results obtained from the application of the electromechanical impedance method applied to some of the laboratory tests.

Chapter 9 presents the experimental results of tests conducted in the field. Two structures were monitored.

Chapter 10 concludes the report with some final remark and recommendation for future studies.

CHAPTER 2: SIGN SUPPORT STRUCTURES

2.1 NOMENCLATURE

The classification of sign support structures is not unique. They may be classified based on material types, support dimensions, etc. In general sign structures can be divided in to **single supported** or **twin supported ends**. Single supported structures have one end fixed on the ground, can have an electric light at the top or can carry a message board, whereas twin supported ends have two supports fixed on the ground with several components over their head and these components are inter-linked with each other.

As described in the introduction cantilevered signal, sign, and light support structures have a single vertical column referred to as an upright, post, or pole (Fig. 2.1a). Structures supported on both sides of the roadway are referred to as bridge supports, also called span-type structures, sign bridges, or overhead structures. The horizontal span of the structure can have the shape of a monotube or a tri-chord truss (Fig. 2.1b) or a four-chord truss (Fig. 2.2). Across the United States there is great variety in the types of sign structures used.

Currently highway signs, luminaries, and traffic signal support structures are designed in accordance to the AASHTO standard specifications (AASHTO 2001).

Figure 2.1 – (a) Cantilever sign support structure with a damping plate (along top) to combat the destructive forces of sympathetic wind vibrations. (b) Trichord overhead sign support Source: http://www.burgesseng.com/sign.htm

For the sake of completeness the following definitions are provided (FHWA 2005):

- **Cantilever sign structure**: a structure that extends over traffic and has a support on only one side of the roadway.

- **Sign bridge:** a structure supporting sign panels or other devices such as VMSs that span over the road with supports on both the sides of the roadway. It may also be referred to as a Span Structure.

- **Mast arm structure:** a structure that cantilevers over traffic with a single mast arm. This is different than a cantilever sign structure that may have a truss or dual arm as the cantilever support for signs or other attachments. A mast arm usually supports small signs or traffic signals.

- **Signal supports:** a structure, usually a mast arm type, which supports traffic signals. The primary components are the foundation, base plate, anchor rods, pole to base plate connection, pole, mast arm to pole connection, and mast arm.

- **Light poles:** a structure supporting lighting, such as a high mast lighting tower. The primary components are the foundation, base plate, anchor rods, pole to base plate connection, pole, and luminaire. High mast poles also have a luminaire raising device and generally a slip joint (or more) in the post.

Figure 2.2 – Four-chord overhead truss structure in Pittsburgh, PA. (a) Front view; (b) rear view; (c) side view.

Nomenclature	Description
Anchor rod	The rods that connect the sign structure base to the foundation
Base plate	The plate used to connect the post base to the foundation.
Catwalk	The walkway used by maintenance personnel, usually located in front of the sign.
Chords	The main horizontal members of the truss.
Diagonals	The diagonal members of the truss.
Foundation	The portion of the sign structure that directs the load into the ground, usually constructed of concrete pedestal on pile, spread or caisson foundations.
Post or Tower	The vertical supporting members of a sign structure.
Splice	Usually referred to as the connection between the truss chords, may also occur in long mast arms and high poles.
Truss	Superstructure that is composed of truss members. These can be tubular or angular.

Table 2.1 - Components, nomenclature and their description as followed by NewYork state DOT

Table 2.1 describes the nomenclature followed by NewYork state DOT (NYDOT 1999).

2.2 MATERIALS

2.2.1 Main Support frames

Most support structures are fabricated from structural steel tubes, angles, and plates or from aluminum tubes, angles, and plates. Round steel tubes may be either cold formed tubing conforming to ASTM A500 or steel pipe conforming to ASTM A53 for resistance welded pipe, or one of the several other ASTM or API (American Petroleum Institute) specifications. Multi-sided tubes are manufactured by the successive bending of a plate and welding the longitudinal seam. Common material specifications are shown in Table 2.2.

Aluminum alloys 6061-T6 and 6063-T5 are also used. In order to increase strength, aluminum is alloyed with other elements and heat treated (T-series alloys). When these tempers are used in welded construction, their allowable stresses are reduced as the heat from welding reduces the beneficial heat treatment. Aluminum is both lightweight and corrosion resistant. However, the fatigue strength of aluminum is only about 40 percent of that of steels with comparable yield strength, and the modulus of elasticity is one third of that of steel, which increases the member deflections.

Materials	Specifications/grades	Components
Steel	ASTM A36, A572 or A709 (or AASHTO equivalent)	
	ASTM F1554-97	• Anchor rods
	ASTM A706-96	• Reinforcing bars (Foundation)
	ASTM A572 W or A588	• Tubes (Weathering resistance)
	ASTM A500	• Tubes
	ASTM A53, Grade B; A595 A, A135, API 52	• Mast arm • Pipes (resistance welded)
	ASTM F593	• Fasteners (Stainless Steel Bolts, Hex Cap Screws, and Studs)
	ASTM F594	• Stainless Steel Nuts and washers
Aluminum tempers and alloys (5083 - H111/H321 5456 - H111/H116/H321 6061 - T6/T651 6063 - T5/T6)	ASTM B209, B210, B211, B221, B241, B247, B308, B429	• Miscellaneous applications such as sign connections • Fasteners
(2024-T4, 6061-T6)	ASTM B316	• Bolts

Table 2.2 – Materials' specifications for sign support structure elements (adapted from FHWA 2003).

2.2.2 Bolted connections

The following are the guidelines from the FHWA (2005) about bolting systems.

Sign, signal, and lighting structures utilize a variety of bolted fasteners in their construction. These range from large anchor rods and high strength bolted structural connections to "secondary" fasteners for signs, wind beams, saddles, and the like. Fasteners also include U-bolts, bolted clips, and similar items. While procedures for installing high strength bolts are established in AASHTO, and recommended procedures for anchor rod nut installation are provided herein, installation practices for other types of bolted fasteners vary. Ancillary structures are subject to vibration due to fluctuating wind loads, and unless properly tensioned, this can cause fasteners to become lose and contribute to their failure.

2.2.2.1 <u>High-Strength Bolts</u>

The design, specification, handling, installation, and inspection of bolted joints in steel support structures should be in accordance with the *Specification for Structural Joints Using ASTM A325 or A490 Bolts* dated June, 2000 by the Research Council on Structural Connections (RCSC). […]. The Federal Highway Administration Report No. FHWA-SA-91-031, "High-Strength Bolts for Bridges" provides an in depth treatment of bolt supply, installation, and testing (this manual is available for download at fhwa.dot.gov/bridge). The U-bolts and other details for connecting luminaries, signs, and signal heads to the structure are not discussed. The manufacturers design these details, and there have been few problems with them in the past. Structural joints for galvanized steel sign, signal, and light support structures should only utilize galvanized ASTM A325 high strength bolts or galvanized ASTM F1852 twist-off-type, tension control bolt assemblies. The joints should be between steel members, and it is essential that the joints be properly pretensioned to resist vibration. These bolts have a very high strength so that they can supply high forces to compress the joint when they are tightened to their prescribed pretension. When a bolted joint is not properly pretensioned, all the load range is transferred through the bolts and they may quickly fail by fatigue. The bolt length used in a connection should be such that the end of the bolt is flush with or projecting beyond the face of the nut when properly installed.

2.2.2.2 <u>Fasteners</u>

Connections for stainless steel structures, which are rare, and aluminum structures, utilize stainless steel bolts and related fasteners. Stainless steel offers excellent corrosion resistance. Stainless fasteners are most often supplied from the American Iron and Steel Institute (AISI) Type 304 or 316 stainless material. Type 304 is the most common. Nuts and washers should match the steel type of the bolt or fastener. Stainless fasteners should conform to the requirements of ASTM F593, "Standard Specification for Stainless Steel Bolts, Hex Cap Screws, and Studs" and ASTM F594 "Standard Specification for Stainless Steel Nuts." Stainless steel bolts are supplied either hot finished or cold finished. Cold finished Type 304 and 316 bolts have an ultimate tensile strength of 620 MPa (90 ksi), versus 516 MPa (75 ksi) for hot finished. However, cold finished bolts are only supplied if specified and are not normally "off-the-shelf" items. Since installation tension for stainless fasteners is not as high, or as well controlled as it is for high strength steel bolts, the use of lock washers is common with stainless fasteners. Lock washers are placed under the nut and help to reduce loosening due to structure vibration and load fluctuation.

Aluminum fasteners are sometimes used for miscellaneous applications, such as sign connections. Aluminum bolts are not generally used in structural connections, even on aluminum sign structures, due to a tendency to stretch and hence loosen under cyclic tension loadings.

Aluminum bolts should conform to ASTM B316 "Structural Specification for Aluminum-Alloy Rivet and Cold Heading Wire and Rods." Bolts are available in several alloy-tempers, with 2024-T4 and 6061-T6 being the most common. Off-the-shelf bolts are typically alloy-temper 2024-T4, which has an allowable shear stress of 96 MPa (14 ksi) and an allowable tension stress of 158 MPa (23 ksi) as given in the "Aluminum Design Manual" published by the Aluminum Association.

2.3 DAMAGE AND FACTORS INDUCING DAMAGE

'Damage' is by definition the change of the material or geometrical properties of a structural or mechanical system. To be critical, damage should affect the current or future performance of that system. Under appropriate loading, damage may grow and coalesce to the point where it produces component-level failure.

To detect damage non-invasively, one or more Nondestructive Testing (NDT) techniques are employed. NDT is generally defined as the examination of an object with technology that does not affect the object's future usefulness. All of these methods help to determine the presence, location, and extension of damage. Usually, the examination is conducted on a time-based schedule and a remedial action is taken only after the examination has been conducted.

The major factors affecting the soundness of sign support structures are defect originated during the manufacturing process, corrosion, loadings, wind, and fatigue. Both sign support and VMS structures installed on cantilever-type designs are susceptible to galloping, natural wind gusts, and truck-induced wind gusts, whereas VMSs mounted on bridge supports are not expected to be susceptible to galloping due to the torsional rigidity of the sign bridge. However, bridge supports are still expected to be susceptible to natural wind gusts and truck induced wind gusts. Thus, there will be many factors influencing sign supports depending on type of material, type of installation, location of installation, terrain, climate etc.

Some of the crucial issues connected with sign supports along with protection steps are corrosion, load, fatigue, wind, and fabrication.

2.3.1 Corrosion

Corrosion is the deterioration of a material (usually a metal) as a result of interaction with its surroundings. Aside from the foundation, the majority of a highway sign structure is made of steel or aluminium, which are susceptible to corrosion.

Corrosion is facilitated by the presence of cracks that allow water ingress in the hollow structural tubes that make up the truss and posts. This built up pond water can lead to internal corrosion, which can lead to more intense problems such as section loss. Members are not only susceptible to internal corrosion, but also external corrosion.

2.3.2 Load

According to Section 3 of the AASHTO standards (AASHTO 2001) structural supports are subjected to the following four loads:

1) dead load consisting of the weight of the structural support, sign, luminaries, traffic signals, lowering devices, and any other appurtenances permanently attached to and supported by the structure.

2) live load consisting of a single load of 2200 N (495 lbs) distributed over 0.6 m (23 3/5 in) transversely to the member will be used for designing members for walkways and service platforms.

3) ice load applied around the surfaces of the supports, but only on one face of sign panels.

4) wind load consisting of the pressure of the wind acting horizontally on the supports, signs, and other attachments.

2.3.3 Fatigue

Fatigue has been shown to be a problem in highway sign structures. The low levels of stiffness and damping of the structures can lead to large amplitude vibrations. In extreme cases, these vibrations lead to problems that may cause the catastrophic collapse of sign structures. To avoid large amplitude vibrations, which may lead to the development of fatigue cracks, there are four types of wind loading that should be accounted for: natural wind, truck induced gusts, galloping, and vortex shedding. All four of these wind loads have design specifications given in Section 11 of the AASHTO Manual (AASHTO 2001).

As trucks pass under a sign structure, they produce an upward force on attachments mounted to said structures. A suction pressure is then applied downward after the truck passes, effectively doubling the load. Vibration problems due to truck induced gusts are particularly critical in VMS structures due to their large area parallel to the road as compared to that of a standard flat sign structure. The fact that many large trucks are outfitted with deflectors to divert wind flow upward increases the problem.

Over a period of several years, fatigue cracking from truck induced gusts can develop. These cracks usually appear at the connection of the mast arm to the pole, at truss connections, and at the base of the pole to the weld joining the pole to the base plate, at the top of the stiffeners, at hand holes, or at the anchor rods (FHWA 2005).

The direction of **natural wind** load on a sign structure is largely unpredictable and constantly changing. All sign supports are subject to this type of wind loading and are thus susceptible to fatigue cracking over a period of several years. Cracks can be caused in locations similar to those given by **truck-induced gusts**. The severity of these problems will depend upon the location and the inherent flexibility of the sign structure.

When the structure starts to vibrate in the air, the air flow begins to oscillate relative to the motion of the structure. An aerodynamic force is then produced on the structure due to this oscillation. The vibration induced by this air flow is referred to as **galloping**. "Galloping results in large amplitude, resonant oscillations in a plane normal to the direction of wind flow. It is usually limited to structures with nonsymmetrical cross sections, such as sign structures with attachments to the horizontal cantilevered arm" (AASHTO 2001). According to Dexter and Ricker (2002), a large portion of the vibration and fatigue problems that have been investigated for cantilevered signals and sign support structures were caused by galloping.

12

Characteristics of the galloping phenomena include the sudden onset of large amplitude, across wind vibrations that increase with increases in wind velocity. Galloping is generally caused by the attachments to a cantilevered structure.

"**Vortex shedding-induced vibrations** of a structure occur when wind vortices are shed alternately from opposite sides of the 'bluff' body present to the wind flow" (Ginal 2003). Unlike galloping, vortex shedding is dependent on the cross section of the structure. Any cross section used in sign structure construction could be subjected to vortex shedding. Vortex shedding has to do with the turbulent nature of the wind flow around the sign structure. As the air flow's Reynolds number reaches a certain range, vortices are shed off the structure's members as shown in Fig. 2.3.
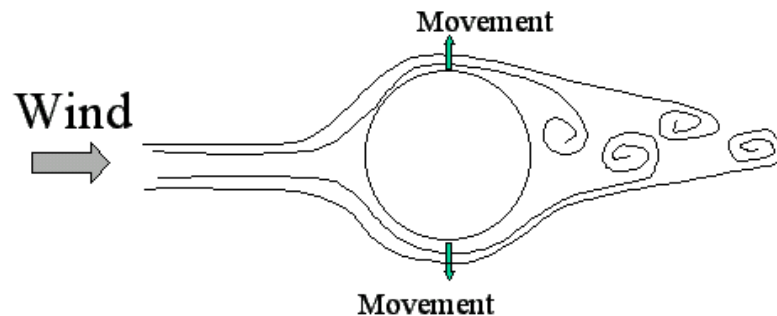
Figure 2.3 – Vortex Shedding (http://www.mecaenterprises.com/images/vortex4.gif)

As these vortices form on one side, the wind speed increases on the other leading to a reduced pressure. A lateral force is then formed on the side of the member opposite the vortices. If the wind is turbulent and changing directions and the vortices are shedding on alternating sides of the structure, a changing lateral load develops. Because this load is varying in the direction at which it hits the structure, large vibrations can occur if the frequency of vortex shedding is equal to the natural frequency of the structure. According to chapter 11 of AASHTO (2001), sign structures are not susceptible to vortex shedding.

Numerous defects found during condition assessment inspections have been attributable to poor fabrication or erection practices. As such the FHWA has recommended that the owners or their representatives should perform inspection during the erection (FHWA 2005).

Inspection of ancillary structures is encouraged, particularly for welded cantilever signs and overhead bridge structures. The 2001 Specification requires weld inspection, which should be performed and documented by the fabricator. Weld quality for steel structures should conform to the D1.1 and D1.2 codes from the American Welding Society (AWS). Due to the types of joint configurations and welds found in ancillary structures, weld inspection requirements contained in current fabrication specifications are not sufficient to ensure defect free welds during shop fabrication. This is one reason that close field inspection of ancillary structures to find detectable cracks is particularly important.

13

CHAPTER 3: STATE OF PRACTICE

A survey was sent to U.S. DOTs, Canadian MOTs, and to each PennDOT district. The main objectives were to determine the most common causes of structural deficiencies, to establish the state of practice for the inspection of sign supports structures, and to estimate the cost to inspect, repair, or replace such structures. The questionnaire prepared at the University of Pittsburgh, was approved by PennDOT and the University of Pittsburgh Institutional Review Board. The respondents were asked to consider all types of structures and not to consider fabrication, shipping or erection-induced damage.

Twenty-two responses were received. Fourteen state DOTs responded including Arkansas (AR), Connecticut (CT), Illinois (IL), Iowa (IA), Kansas (KS), Maryland (MD), Michigan (MI), Missouri (MO), New Jersey (NJ), New York (NY), Tennessee (TN), Utah (UT), Washington (WA), Wisconsin (WI), and Wyoming (WY). Along with these states, the Canadian Province of Alberta (AB) participated. Finally, we received responses from PennDOT Districts 4, 5, 8, 9, 10, 11, and 12 (PA4, PA5, PA8, PA9, PA10, PA11, and PA12).

The Utah DOT has responded that currently they do not "*have an inspection program for sign supports and cantilevers structures*".

The next section shows the blank questionnaire which was sent to all DOTs. Section 3.2 describes the analysis of the filled survey. Section 3.3 compares the results from this survey with two surveys published in 1999 and 2002, sponsored by the National Cooperative Highway Research Program (NCHRP) and the Michigan DOT, respectively. Section 3.4 provides some considerations and conclusions stemming from the analyses in section 3.2.

3.1 QUESTIONNAIRE

State-of-Practice Survey
Inspection Methods for Sign Supports and Cantilever Poles Structures

Survey completed by:

Name: _____   Title: _____

Jurisdiction: _____   email: _____

Address: _____   Telephone: _____

_____

PLEASE RETURN COMPLETED SURVEY BY <u>MAY 31</u> TO:

> Piervincenzo Rizzo
> University of Pittsburgh
> Department of Civil and Environmental Engineering
> 941 Benedum Hall
> Pittsburgh, PA 15261
> Phone: (412) 624-9575
> Fax: (412) 624-0135
> pir3@pitt.edu

Introduction
In responding to this survey, please consider only sign structures and cantilever poles once they have been placed in service in your jurisdiction. Do not consider fabrication, shipping or non-structural erection-induced damage.

> The purpose of this research study is to assess the current state of practice associated with the inspection of sign support structures and cantilever poles. This survey is being distributed to all PennDOT district offices, US states DOTs, Canadian MOTs and other jurisdictions having responsibility for such structures. If you are willing to participate, you will be asked to provide your professional contact information and direct responses to the survey questioned asked. There are no foreseeable risks associated with this project, nor are there any direct benefits to you. Your participation is voluntary. All surveys will be kept in confidence and responses will be stripped of remarks identifying an individual, organization or jurisdiction. This study is being conducted by Dr. Piervincenzo Rizzo, who can be reached at 412.624.9575 or at pir3@pitt.edu, if you have any questions.

1. Overhead sign support structure types (see figure below) used in your jurisdiction (check all that apply):

☐	1. Cantilever truss with single pole
☐	2. Overhead bridge truss with single pole
☐	3. Overhead cantilever with single pole
☐	4. Overhead bridge truss with truss pole
☐	5. Planar taper tube
☐	6. Monotube
☐	7. Other 1 (please describe) _____
☐	8. Other 2 (please describe) _____

2. Provide the number of sign support structure type (see figure below) existing in your jurisdiction.

	< 500	500 – 2000	> 2000	Exact number (if known)
1.Cantilever truss with single pole				
2. Overhead bridge truss with single pole				
3. Overhead cantilever with single pole				
4. Overhead bridge truss with truss pole				
5. Planar taper tube				
6. Overhead Monotube				
7. Other 1 (please describe) _____				
8. Other 2 (please describe) _____				

1. Cantilever Truss w/ single pole   2. Overhead Bridge Truss w/ single pole   3. Cantilever w/ single pole

4. Overhead Bridge Truss w/ truss pole   5. Planar Taper Tube   6. Overhead Monotube

Figure 3.1 – Sketch of different structure types (front view):

3. How often are the overhead sign support structures inspected (check all that apply):

☐ Once a year
☐ Once every two years
☐ Only after some environmental-related hazard (excessive wind, earthquake, hurricane/tornado, etc.)
☐ Only after some human-related hazard (vehicle impact)
☐ Other 1 (please describe) _____
☐ Other 2 (please describe) _____

4. IS either nondestructive evaluation (NDE) or destructive evaluation method adopted to assess the presence or the extent of damage in overhead structures (check all that apply):

☐ NDE: Visual inspection
☐ NDE: liquid penetrant
☐ NDE: magnetic particle
☐ NDE: ultrasonic testing
☐ NDE: other (please describe) _____
☐ Destructive evaluation methods (please describe) _____
☐ Neither NDE nor destructive (please describe) _____

5. If NDE or destructive methods are adopted please briefly describe for each method how many persons are usually involved, and on average how many work hours per person the inspection require.

_____

_____

_____

_____

_____

6. Identify main problems observed in the overhead sign support structures in your jurisdiction (check all that apply):

☐ Fatigue cracks in the column to base connections
☐ Cracks in the tube-to-tube welded connections
☐ Loose or missing bolts at the base
☐ Welded connection between the mast and the pole
☐ Other 1 (please describe) _____
☐ Other 2 (please describe) _____
☐ Other 3 (please describe) _____

7. Estimate the number of overhead sign structures damaged in your jurisdiction over the last five years with the following degrees of damage:

☐	**Minor damage** Visible through visual inspection; not affecting structure's residual life; no action taken
☐	**Moderate damage** Hidden or visible damage; may affect structure's residual life; some repair conducted but no replacement required
☐	**Significant damage** Loss of portion of cross section which induced structural deficiency; affect structure's residual life; require the replacement of one or more elements
☐	**Severe damage** Damage severe enough to result in full structure decommissioning
☐	**Catastrophic damage** Unexpected catastrophic failure

8. If your jurisdiction does not track the level of damage identified in question 7, please list the levels of damage (0 low damage – 5 catastrophic failure) and the damage criteria identified:

☐	_____
☐	_____
☐	_____
☐	_____
☐	_____
☐	_____

9. What is the percentage of the types of damage sources to overhead structures members that require repair action to be taken (indicate all that apply)**:**

☐	Vehicle impact
☐	Corrosion occurring at unrepaired site of vehicle impact
☐	Corrosion resulting from source **other than** vehicle impact
☐	Natural hazard (wind action, earthquake, hurricane/tornado, etc.)
☐	Construction/design error (misplaced welding, low strength bolts, etc.)
☐	Nonspecific deterioration due to aging
☐	Missing bolts
☐	Other 1 (please describe): _____
☐	Other 2 (please describe): _____
100%	Total

10. Sort (in decreasing order) the five most expensive (in term of estimated cost for repair/replacement) types of defects encountered in overhead sign supports during the last five years:

18

Damage type	Estimated cost ($)

11. Provide (if known) the estimate cost over the last five years of the following actions:

	Estimated cost ($)
Scheduled inspection of overhead sign structures	
Unscheduled inspection of overhead sign structures	
Repair to overhead sign structures	
Replace of overhead sign structures	

12. Briefly describe what analytical procedures (finite element method software, structural design software, etc…) are used to assess the damage and the need for repair overhead structures (include names of software if appropriate)

13. Briefly describe the most common repair methods

_____

_____

_____

_____

_____

14. Rate the following factors by importance in the determination of the inspection method or repair.

	low	moderate	high	not considered
Cost of repair				
Time required to make repair				
Aesthetics of repair				
Interruption of service				
Load capacity				
Expected service life of repair				
Maintenance required				
Other, please specify:_____				

3.2 SURVEY ANALYSIS

The results presented here are broken up by question. The responses of the PennDOT districts and the responses of other state DOTs are compared to one another to see the common practices that States follow and the things that States do differently from one another.

3.2.1 Question 1 (Overhead sign support structure types used in your jurisdiction)

The question aimed at determining which type of structure is present in each jurisdiction. This question was accompanied by the schematic drawing of six types of structures (Fig. 3.1). The drawing was used to avoid any ambiguity associated with the use of the term overhead (see chapter 1.1). Table 3.1 details the response from the PennDOT districts.

Structure Type	PA 4	PA 5	PA 8	PA 9	PA 10	PA 11	PA 12
Cantilever truss				x			
Overhead bridge truss with single pole				x	x	x	x
Overhead cantilever with single pole	x	x	x	x	x	x	x
Overhead truss with truss pole	x	x	x	x	x	x	x
Planar taper tube							
Monotube							x
Other	x	x		x			

Table 3. 1 Types of sign structures in use - PennDOT response to Question 1.

Figure 3.2– (a) Pole mounted VMS (http://www.paturnpike.com/newsletters/summer99/vmstest.jpg); (b) structure mounted sign ((http://www.universalindustrialsales.com/images/pic-001.jpg)

District 4 reported the use of overhead cantilever with double pole and district 5 uses a pole mounted VMS (Fig. 3.2a) and a structure mounted sign (Fig. 3.2b).

The response from other States is summarized in the histogram of Fig. 3.3. Over 90% of the responders reported the use of cantilever truss structures in their jurisdiction. On the other end, less than 10% of the responders reported the use of planar taper tube structure. While PennDOT fits the trend of using overhead cantilevers and overhead trusses, it should be noted that the majority of other responders use the cantilever trusses while none of the PennDOT districts do so.
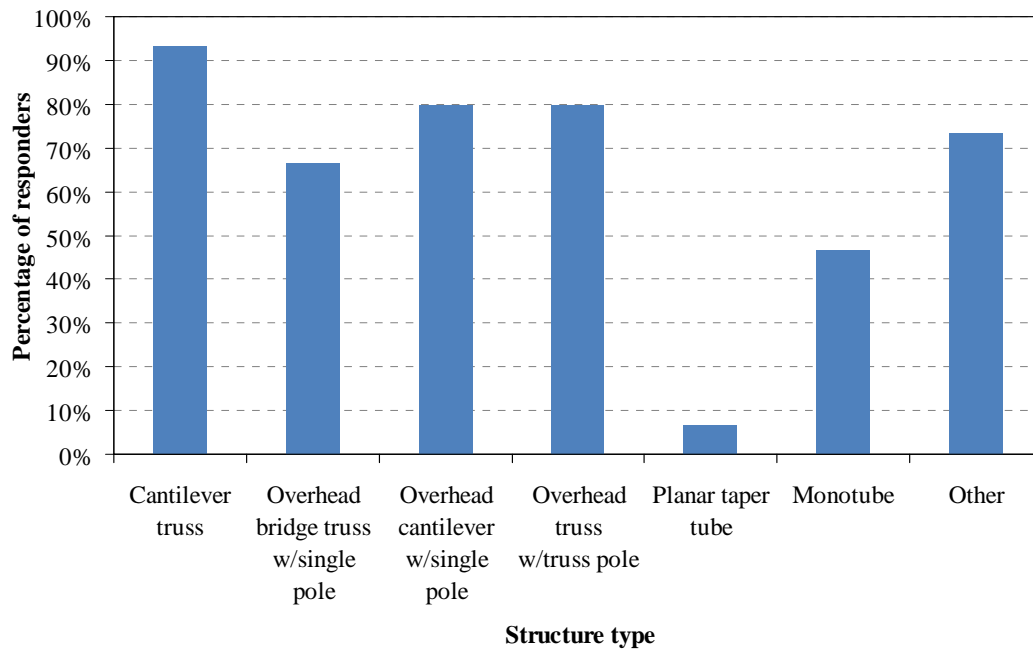
Figure 3.3 – Sign Structures in use among responding DOTs

Over 70% of the responders reported the use of "other" types of structures not illustrated in Fig. 3.1. The complete listing of these *other* structures is given below, in alphabetical order:

- Box truss with cantilever (MO)
- Bridge mounted frame (CN, TN)
- Bridge truss with truss pole parallel to traffic (WA)
- Butterfly cantilever with single pole (CN, IL, NY. See Fig. 3.4)
- Butterfly truss (KS, NY, TN, MO)
- Cantilever monotube (WA)
- Cantilever truss with truss pole (AR)
- Cantilever with double poles (PA 9)
- Double tube butterfly (MO)
- Overhead spans in highway cuts supported on retaining walls with no poles (NY)
- Propped cantilever with truss pole (AR)
- Single tube with hinge at top of pole (IA)
- Single tube tapered span (KS, MO)
- Timber poles with steel cables (WI)
- T-mount truss on truss pole (AR)

Figure 3.4 – Butterfly cantilever structure (NYDOT, 2-11)

The Missouri DOT provided the drawings (Fig. 3.5) of typical truss configuration codes used in its jurisdiction.
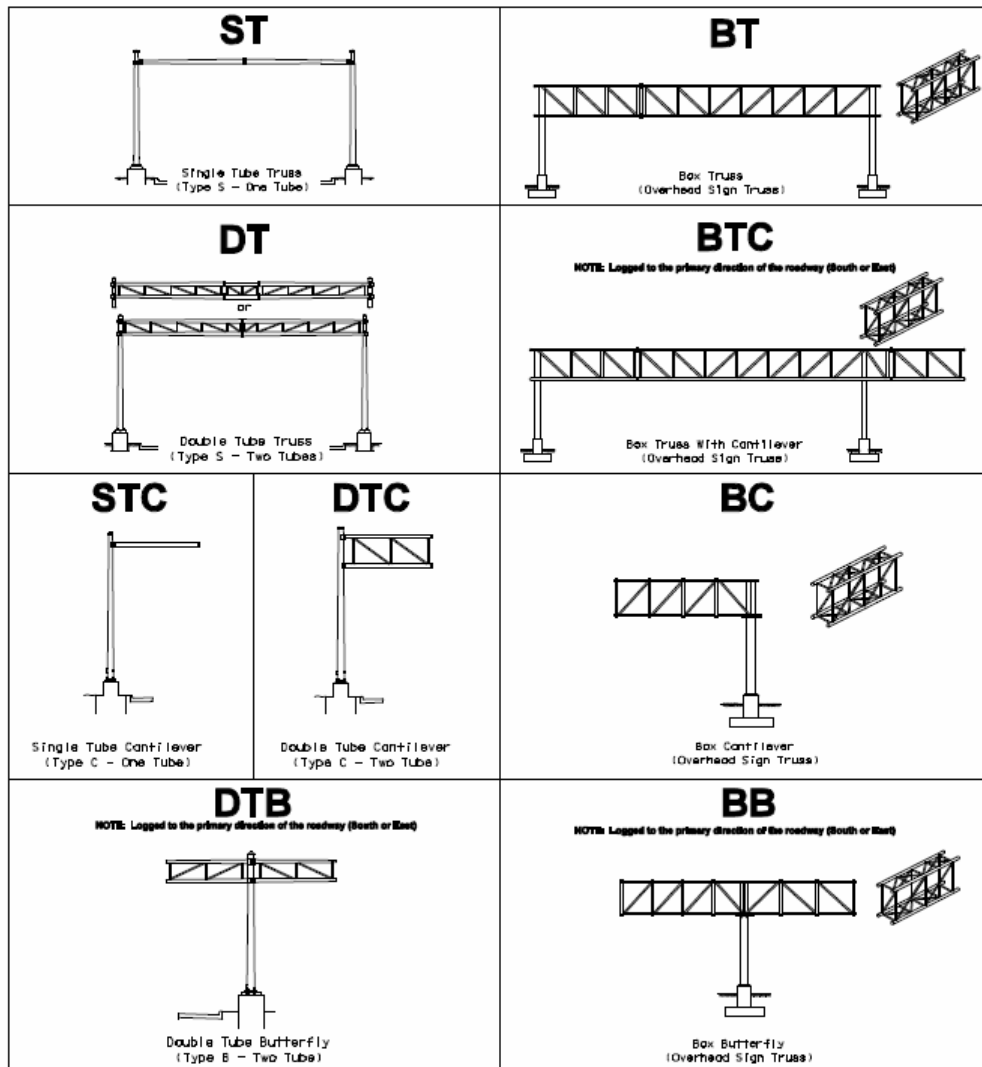
Figure 3.5 - Missouri typical truss configuration codes.

3.2.2 Question 2 (Provide the number of sign support structure type (see figure below) existing in your jurisdiction)

The aim of this question was to take a census of the structures currently deployed along highways and roadways. The responses from PennDOT districts and other States are summarized in Tables 3.2a and Table 3.2b, respectively.

	PA 4	PA 5	PA 8	PA 9	PA 10	PA 11	PA 12
Cantilever truss				1			
Overhead bridge truss w/ single pole				13	<500	<500	5
Overhead cantilever w/ single pole	<500	125	<500	9	<500	<500	40
Overhead truss with truss pole	<500	180	<500	62	<500	<500	76
Planar taper tube							
Monotube							3
Other*	<500	<500		29			

Table 3.2a – Inventory of sign support structures in Pennsylvania DOT Districts.

State	Structure type						
	1	2	3	4	5	6	7
AB	<500	<500	<500	<500	0	<500	0
AR	0	0	0	187	0	0	88
CT	145	0	451	332	0	288	476
IL	500-2000	<500	<500	500-2000	0	<500	<500
IA	89	0	0	350	0	0	5
KS	427	0	30	535	0	0	160
MI	500-2000	500-2000	500-2000	<500	<500	<500	0
MO	N/A	N/A	N/A	N/A	N/A	N/A	N/A
NJ	530	20	9	1100	0	2	22
NY	1568	423	833	1955	0	0	28
TN	674	30	20	603	0	0	372
WA	387	13	56	0	0	188	630
WI	<500	<500	<500	<500	<500	<500	2
WY	<500	<500	<500	<500	0	<500	0

Table 3.2b – Inventory of sign support structures in state DOTs. The type in column 1 identifies the following: 1 Cantilever truss with single pole; 2 Overhead bridge truss with single pole; 3 Overhead cantilever with single pole; 4 Overhead truss with truss pole; 5 Planar taper tube; 6 Overhead monotube; 7 other structures listed on page 10. N/A Not answered.

There seems to be a mixture of DOTs that do and do not keep track of the number of sign structures in their jurisdiction. Among the states that have responded, the cantilever truss and the overhead truss with truss pole have the largest numbers of structures in use

throughout the country. This coincides with the results of Question 1. Michigan DOT does "*not track each specific category of overhead signs in our inventory to my knowledge. See website for our standard plans and special details at http://mdotwas1.mdot.state.mi.us/public/tands/plans.cfm*"

3.2.3 Question 3 (How often are the overhead sign support structures inspected)

Because no federal regulation mandates the inspection of sign support structures at a specified frequency, Question 3 aimed to determine a common trend among state DOTs. Tables 3.3a and 3.3b summarize the responses obtained from PennDOT districts and the other states. All but two state DOTs checked the *other* box. Examples of inspection policy include: 1) inspection frequency based the type of sign being inspected (WA), 2) routine inspections on one cycle and more in depth inspections on another cycle (NY and PA12); 3) structures age and material (IL, MO, PA4, and PA8).

	Every year	Every two years	Post environmental hazard	Post human hazard	Other
PA 4					x
PA 5		x			x
PA 8					x
PA 9					x
PA 10					x
PA 11		x	x	x	x
PA 12			x	x	x

	Every year	Every two years	Post environmental hazard	Post human hazard	Other
AB					x
AR		x	x	x	x
CT					x
IL					x
IA					x
MD					x
MI		x	x	x	
MO					x
NJ					x
NY	x	x			x
TN			x	x	
WA				x	x
WI					x
WY					x

Table 3.3 – Sign Inspection frequency among (a) PA districts and (b) U.S. DOTs

25

These last two reasons are why we assume that New York checked both once/year and once every two years.

Five out of the seven PA districts said that they use a three year cycle. PA district 9 inspects structures in accordance with SOL 431-04-03. After a cantilever with single pole carrying traffic signs failed, a number of such structures were re-inspected. The last regular inspection cycle occurred in 2005. Seven DOTs inspect some structures on a four year cycle, five DOTs follow a five year cycle. The state of Washington inspects cantilevers with only four anchor bolts every four years, monotube cantilevers every eight years, and monotube bridges every ten years, and the remaining structures every five years. In the state of Illinois "*if no deficiencies are found the structure is placed in a five year detailed inspection cycle. If minor cracks are found in welds and internal members, the structure is placed on a three year detailed inspection cycle with a ground inspection cycle in eighteen months. If there are numerous cracked welds and broken members the structure is placed in annual inspection cycle until replaced or repaired*". Missouri noted that they are in a three year contract to inspect all of their sign structures and will use the results of these inspections to plan future inspection intervals. Finally, the province of Alberta reported an inspection cycle of 21 months.

3.2.4 Question 4 (Is either nondestructive evaluation (NDE) or destructive evaluation method adopted to assess the presence or the extent of damage in overhead structures)

Question 4 was formulated to identify the nondestructive methodologies currently in practice. Four different approaches, namely visual inspection, liquid penetrant, magnetic particle, and ultrasonic testing, were considered separately. Respondents were also asked to include any destructive method eventually used to assess the condition of the structures.

Table 3.4 summarized the survey responses. All DOTs use visual inspection. The advantages and disadvantages of this will be pointed out in chapter 4. Arkansas, Missouri, and Tennessee do not use any inspection method other than visual inspection. In most cases liquid penetrant and magnetic particle testing are used as an extension of visual inspection. NJ-DOT reported that liquid penetrant is used if crack is suspected, while NY and WA DOTs use if crack is visually located, i.e. if potential cracks have been located visually. Wisconsin DOT uses all three methods if a crack is suspected.

Liquid and magnetic particles are used: 1) "*to determine the limits of cracked welds or internal members that can not be visually determined when recommended by the Bureau of Bridges & Structures after a review of the structure's inspection report*" (IL_DOT), 2) if crack is suspected (CT_DOT and IA_DOTs), and 3) if a defect is found (WY_DOT). PA 9 reported that liquid penetrant are used if visual signs of cracks in paint or protective coating or cracks in welds and/or steel are visible. In the aftermath of the failure of a cantilever with single pole carrying traffic signs, magnetic particles were used to inspect all of the pole/base plate welds of all of the similar signs.

Ultrasonic testing is most often used to test the anchor bolts at the base of the structure. Connecticut DOT has reported that UT is used to inspect all anchor bolts in tension on cantilever sign supports. Kansas, Iowa, New Jersey, and New York DOTs use UT to determine length and to detect the presence of defects in anchor bolts. It is estimated that the

inspection time is five minutes per bolt. The state of New York has reported that UT testing is used to routinely determine the thickness at the base of poles. This inspection can be conducted using an ultrasonic thickness gauge and it can be extended to determine internal corrosion as well.

	Visual inspection	Liquid penetrant	Magnetic particle	Ultrasonic testing	Other
PA 4	x	x	x		
PA 5	x	x		x	
PA 8	x	x			
PA 9	x	x	x		
PA 10	x	x			
PA 11	x	x			
PA 12	x				

Table 3.4a – Various inspection methods followed in PA districts.

	Visual inspection	Liquid penetrant	Magnetic particle	Ultrasonic testing	Other
AB	x	x	x	x	
AR	x				
CT	x	x	x	x	
IL	x	+	+	x	
IA	x	x	x	x	
KS	x			x	
MD	x			x	
MI	x	x		x	
MO	x				
NJ	x	x		x	
NY	x	x	x	x	x
TN	x				
WA	x	x		x	
WI	x	x	x	x	
WY	x	x	x		

+ these are used to determine the limits of cracked welds or internal members that cannot be visually determined when recommended by the Bureau of Bridges & Structures after a review of the structure's inspection report

Table 3.4b – Various DOT inspection methods

NY-DOT uses methods like hammer-based impact sounding as part of the regular inspection of loose foundation bolts and ultrasonic thickness gauging to routinely determine the thickness of the base of the pole. Once NY_DOT hired a company to do digital radiograph imaging on one particular structure.

No DOTs selected "*destructive evaluation methods*" or "*Neither NDE nor destructive evaluation*" so those two options are not included in Table 3.4.

3.2.5 Question 5 (If NDE or destructive methods are adopted please briefly describe for each method how many persons are usually involved, and on average how many work hours per person the inspection require)

To estimate the cost of labor for each inspection, Question 5 was devoted to gathering information on the number of people usually involved in the inspection. The results of the survey indicate that most DOTs (67%) use two people for all types of inspection, however all the numbers given vary between needing one and five people to do the job. For instance the Connecticut DOT has indicated that for visual inspection (conducted on every sign support) and liquid penetrant and magnetic particle (conducted only if crack is suspected) two inspectors are involved. For ultrasonic testing, used on all anchor bolts in tension on cantilever sign supports, one inspector and one technician are involved. The DOT that specified five people (PA District 4) included the people needed to aid in traffic control.

The time length of time required for different types of inspections was less uniform across the board then was the number of people required. This is shown in Table 3.5.

Method	Inspection Time	Number of responders
Visual Inspection	2 hours	4
	1 hour	3
	2 - 5 hours	1
	4 - 8 hours	1
	1 - 3 hours	1
	2.5 hours	1
Liquid Penetrant	1 – 2 hours	2
	0.5 hours	2
	2.5 hours	1
	4 – 8 hours	1
	< 1 hour	1
Magnetic Particle	1 – 2 hours	1
	0.5 hours	1
	3 hours	1
	< 1 hour	1
Ultrasonic Testing	1 – 2 hours	1
	0.5 hours	1
	1 hours	1
	4 – 8 hours	1
	< 1 hour	1
	5 min/bolt	1
	20 min	1

Table 3.5 – Time required to perform inspections.

The amount of time actually required undoubtedly depends on the experience of the inspector.

3.2.6 Question 6 (Identify main problems observed in the overhead sign support structures in your jurisdiction)

To sort the main problems associated with sign supported structures, Question 6 was formulated. Four main options were given, namely fatigue cracks in the column to base connections, cracks in the tube-to-tube welded connections, loose or missing bolts at the base, and welded connection between the mast and the pole.

	Column to base cracks	Tube to tube welded connection cracks	Loose or missing bolts at the base	Welded connection	Other
PA 4		x	x		
PA 5		x	x	x	x
PA 8		x			
PA 9	x		x		x
PA 10	x		x		x
PA 11					x
PA 12					x

	Column to base cracks	Tube to tube welded connection cracks	Loose or missing bolts at the base	Welded connection	Other
AB	x				x
AR	x		x		
CT		x	x	x	x
IA		x			x
IL		x	x		x
KS		x	x		
MD		x	x		
MI		x	x	x	
MO		x	x		
NJ		x			x
NY	x	x	x	x	x
TN			x		x
WA			x		x
WI	x	x	x	x	x
WY		x	x		

Table 3.6 – Problems observed during sign structure inspections in (a) PennDOT district and (b) State DOTs.

The responses in Table 3.6 indicate that the tube to tube welded connection cracks and loose or missing bolts at the base are the problems most often observed. This is true for the majority of PennDOT districts that responded too.

Many states reported "other" problems. The list of these problems is provided below sorted by the alphabetical order:

- Bolted connection between mast and pole (WI)
- Concrete foundations that have delaminated exposing rebar and anchor bolts (IL)
- Corrosion of anchor bolts within grout pad (WA)
- Corrosion on bolts at base (TN)
- Cracked welds in overhead truss (AB)
- Cracking of aluminum lock nuts which attach sign panel (PA 12)
- Cracking/falling luminaries (NY)
- Cracks in cast base plate connectors (NY)
- Cracks in truss diagonal chord welds (NY)
- Crooked assembly of fittings at junctures (NY)
- Damaged aluminum truss members from ice bursts or torsion failures (WA)
- Debris in the post base (NY)
- Deteriorated luminary housing attachment bolts (PA 12)
- Eccentric base loading (NY)
- Fatigue cracks at the arm to column weld (CT)
- Fatigue on bolts at the base (TN)
- Gaps between support beam and saddle plate (NY)
- Impact damage (NY, PA 10, PA 11)
- Internal corrosion of galvanized structures (WA)
- Loose sign connectors (IA)
- Loose or missing bolts at various locations (NJ)
- Missing fasteners and clips (PA 5, PA9)
- Missing post caps and covers (NY)
- Missing utility locks (PA 5)
- Painted tubular steel end supports deteriorating from the inside out (IL)
- Section loss at post interiors near base plate due to standing water in vertical poles (NY)

The fact that so many potential problems can occur on such structures gives rise to the need for more comprehensive inspection procedures.

3.2.7 Question 7 (Estimate the number of overhead sign structures damaged in your jurisdiction over the last five years with the following degrees of damage)

To assess the condition of the existing structures the number and the severity of the damaged structures was asked. Five levels of damage were proposed ranging from minor damage that did not affect the structure residual life and no intervention was required, to catastrophic failure. The assessment was limited to the last five years.

Table 3.7a and 3.7b summarizes the responses from the PennDOT districts and from other State DOTs, respectively. Compared to other states, the structures in the Pennsylvania districts that responded seem to be functioning rather well. New York appears to have by far the highest number of damaged structures. The discrepancy in the number of damaged structures is perhaps the combination of one of more of the following: 1) total number of structures existing in the jurisdiction; i.e. larger the inventory, larger the number of damaged structures; 2) effectiveness of the inspection program adopted; 3) structure types; 4) interpretation of the survey's question; 5) track record of the inventory. Figure 3.6 shows the histogram relative to the total number of damaged structures as a function of the level of damage.

	Minor	Moderate	Significant	Severe	Catastrophic
PA 4	7	0	1	0	0
PA 5	20	10	2	0	0
PA 8	4	1	0	1	0
PA 9	1	0	0	0	1
PA 10	5	2	0	0	0
PA 11	2	0	0	1	1
PA 12	54	3	0	0	0

	Minor	Moderate	Significant	Severe	Catastrophic
AB	25	5	0	1	0
AR	45	25	15	2	7
CT	75	50	30	50	3
IL	350	150	100	10	0
IA			N/A		
KS	2	2	10	2	0
MD	15	10	2	0	0
MI	N/S	N/S	N/S	N/S	N/S
MO	N/S	N/S			
NJ			N/A		
NY	997	804	177	115	11
TN	0	0	0	1	2
WA	50	50	50	5	2
WI	N/S	50	5	2	0
WY	<50	<50	0	0	0

Table 3.7 – Number of sign structures found with flawed components in (a) Pennsylvania (b) participating states. **Note**: N/S: category selected but number not specified. N/A: not answered.
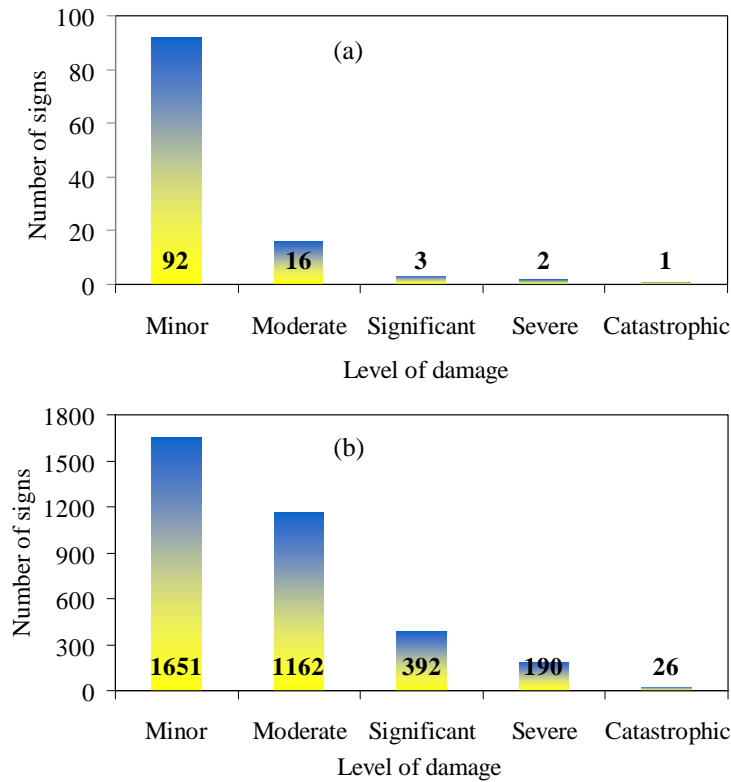
Figure 3.6 – Number of Signs reported with each level of damage

3.2.8 Question 8 (If your jurisdiction does not track the level of damage identified in question 7, please list the levels of damage (0 low damage – 5 catastrophic failure) and the damage criteria identified)

Similar to Question 7, Question 8 was aimed at providing a qualitative estimation of the existing sign support inventory. The question asked the responder to rank the state of the signs in the jurisdiction on a scale of 1 to 5 (1 being low damage to 5 being catastrophic). Only the state of New Jersey answered this question. However they stated that they "*do not track as described above*". They "*refer to the Guidelines for the Installation, Inspection, Maintenance and Repair of Structural Supports for Highway Signs, Luminaries, and Traffic Signals, pages 63-65 (Publication No. FHWA NHI 05-036). New Jersey's guidelines were the basis of this section. Also, see Appendix C of this document for a sample NJDOT report*".

Condition	Description	Feasible Action	NJ response
0	Not applicable	None	1250
1	Element performs intended function with high degree of reliability (good)	None	330
2	Element performs intended function with small reduction in reliability (fair)	Repair element, increase inspection frequency, do nothing	110
3	Element performs intended function with significant reduction in reliability (poor)	Repair or replacement of element within specified time frame	4
4	Element does not perform intended function with any degree of reliability (critical)	Immediate repair or replacement of element	0

Table 3.8 – Structure condition classification as referred by *FHWA NHI 05-03.6*

According to this set of guidelines, the structures' conditions are rated from 0 to 4 according to Table 3.8. The number of damaged structures reported by NJDOT is reported in the fourth column of the table. This gives New Jersey a similar number of damaged structures as New York.

3.2.9 Question 9 (What is the percentage of the types of damage sources to overhead structures members that require repair action to be taken)

To investigate the origin of the detected problems question 9 was formulated. Seven sources of damage were initially considered, namely vehicle impact, corrosion occurring at unrepaired site of vehicle impact, corrosion resulting from a source other than vehicle impact, natural hazard, construction/design error, nonspecific deterioration due to aging, and missing bolts.

	PA 4	PA 5	PA 8	PA 9	PA 10	PA 11	PA 12
Vehicle impact	0%	1%	80%	5%	20%	5%	5%
Corrosion at unrepaired site of vehicle impact	0%	0%	0%	0%	0%	0%	0%
Corrosion from source other than vehicle impact	0%	50%	0%	10%	0%	25%	15%
Natural hazard	0%	0%	0%	0%	0%	0%	0%
Construction/design error	0%	0%	0%	5%	0%	50%	0%
Nonspecific deterioration due to aging	0%	24%	5%	0%	0%	0%	10%
Missing bolts	100%	15%	15%	80%	50%	20%	70%
Other *	0%	10%	0%	0%	30%	0%	0%

Table 3.9a – Percentage of damage given by specific damage sources.

	AB	AR	CT	IL	KS	MD	NY	TN	WA	WI	WY
Vehicle impact	98%	10%	3%	20%	65%	80%	5%	0%	5%	5%	1%
Corrosion at unrepaired site of vehicle impact	1%	0%	1%	0%	0%	0%	0%	0%	0%	0%	0%
Corrosion from source other than vehicle impact	1%	30%	27%	35%	0%	0%	30%	0%	80%	80%	7%
Natural hazard	0%	5%	3%	0%	25%	10%	0%	0%	5%	5%	0%
Construction/design error	0%	0%	12%	13%	5%	10%	10%	0%	5%	5%	7%
Nonspecific deterioration due to aging	0%	30%	30%	20%	0	0%	20%	0%	5%	5%	85%
Missing bolts	0%	5%	24%	12%	0%	0%	0%	0%	0%	0%	0%
Other *	0%	20%[1]	0%	0%	5%[2]	0%	35%[3]	100%[4]	0%	0%	0%

Table 3.9b – Percentage of damage given for specific damage sources by State DOTs.

---

[1] Fatigue cracks and mower impact
[2] Ice damage in enclosed tube
[3] Cracks in truss diagonal to chord welds and loose anchor bolt nuts
[4] Fatigue of anchor bolts in the concrete footing of the cantilever truss sign structures

Tables 3.9a and 3.9b report the responses from the PA DOTs and from those states that provided a quantitative estimation of the damage source, respectively.

Each PennDOT district listed missing bolts as causing some level of damage. This does not reflect the national trend because only three other DOTs listed missing bolts as damage causing. This is interesting because in Question 6 nearly all responding DOTs checked loose or missing bolts at the base as a problem observed.

This could lead to the conclusion that while missing bolts are a problem, they does not cause an overwhelming amount of damage. Like the PennDOT Districts, most State DOTs listed vehicle impact as causing some damage, if not the majority of damage, to a sign structure.

Corrosion occurring at an unrepaired site of vehicle impact was only chosen by two states, while all other damage causes received similar numbers of responses.

3.2.10 Question 10 (Sort (in decreasing order) the five most expensive (in term of estimated cost for repair/replacement) types of defects encountered in overhead sign supports during the last five years)

To assess the costs of the damages identified in the last two questions, Question 10 was proposed. As an open-ended question, Question 10 had a wide spectrum of responses and costs. The three most common responses (including the average given costs) and the most expensive documented repairs are presented in Table 3.10. Cracked weld repair is the only thing common between the two. Other types of damage that at least one DOT listed are Structural replacement, corrosion damage, fatigue cracks, old age, and tornado damage. Many DOTs did not know the exact cost of fixing these damages. PennDOT district 11 usually budgets $100,000 for high priority fixes, and then wrap the costs of other maintenance into upcoming construction projects.

PA 9 estimated that to replace a sign structure may cost *$175,000 (3 chord), $25,000 (double pole), and $15,000 (single pole).* Moreover *removing, metalizing sign structure, and reassembling structure cost $85,000 (3&4 chord).*

	Type of repair	Cost
Most common repair	Bolt tightening/replacement	$71,667
	Vehicle impact damage	$77,563
	Cracked welds	$12,500
Most costly repairs	Cracking in welds of cantilever truss arm to column connection (CT)	$2,500,000
	Rusted through truss members (CT)	$2,000,000
	Full replacement (NY)	$130,000-$250,000

Table 3.10 – Most commonly listed types of damage and most expensive repairs reported. Note that most common repair the average cost is reported.

3.2.11 Question 11 (Provide (if known) the estimate cost over the last five years of the following actions)

The information gathered in Question 10 was integrated with the information obtained in Question 11, that aimed at estimating the cost over the last five years of the following actions: 1) Scheduled inspection of overhead sign structures, 2) Unscheduled inspection of overhead sign structures; 3) Repair of overhead sign structures, and 4) Replacement of overhead sign structures.

Not all DOTs gave responses to Question 11 and those that did respond gave very different values. Because of this the given values were averaged and are summarized below in Table 3.11 as a list of the average, median, high, low, and total value spent on each item by all reporting DOTs. Replacement is the highest cost item, which is reasonable because it is a large option to undertake. Because of this high cost, DOTs rightly spend a large amount of money on inspection and subsequent repairs. Spending money in these two areas will probably allow them to spend less money on future replacements.

	Average	High	Low	Total
Scheduled inspection	$3,115,886	$21,500,000	$50,000	$40,506,513
Unscheduled inspection	$86,750	$250,000	$2,500	$520,500
Repair to structure	$1,284,100	$4,000,000	$500	$6,420,500
Replacement of structure	$6,420,566	$25,000,000	$85,000	$57,785,000

Table 3.11 – Values for reported costs given as answers to Question 11

3.2.12 Question 12 (Briefly describe what analytical procedures (finite element method software, structural design software, etc…) are used to assess the damage and the need for repair overhead structures (include names of software if appropriate))

To gather insight about the analytical procedures adopted to assess the soundness of sign structures, Question 12 was formulated. Many DOTs did not answer this question or did not know if they use any analytical procedures. The PennDOT district 11 responder said that "*generally it is difficult to model sign structures that are damaged. The type of damage typically associated with sign structures is due to vehicular collision, a crack in a member, or damage due to overload. This type of damage is difficult to accurately analyze due to questionable section properties. Sometimes the evaluation is handled by engineering judgment.*" Those that do use analytical software gave the following responses:

- STAAD – Connecticut, Kansas, New York
- SABRE – Connecticut, Maryland
- In house/consultant developed programs – Connecticut, Kansas, New York
- Excel – New York
- None – Alberta, Illinois, New Jersey, PennDOT District 10, Tennessee, Washington

3.2.13 Question 13 (Briefly describe the most common repair methods)

This question asked for the most common repair methods, and the most common response to this question is that the State removes and replaces whatever is damaged. In the case of loose anchor bolts, those that are not replaced are tightened. Cracks can be fixed by re-welding the offending weld. All DOTs that answered gave similar answers; the only unique answer is that New York State reported the use of fiber reinforced polymer to strengthen truss members with weld cracks.

3.2.14 Question 14 (Rate the following factors by importance in the determination of the inspection method or repair)

Table 3.12 shows the number of DOTs that responded that each given repair factor had a low, moderate, or high importance in determining if the damage would be repaired. The highest rated factor chosen was fixing damage that affects the load bearing capacity of the structure. This makes sense because we found out in Question 11 that sign replacement is the most expensive cost associated with sign structures, and if a sign cannot bear a load it will likely collapse and need to be replaced. Because some DOTs marked some of the factors *not considered*, the numbers in the fifth column differ.

On the other end of the spectrum, the aesthetics of the repair was chosen as the least important factor.

	Low	Moderate	High	Total
Cost of repair	2	6	10	18
Time to make repair	6	8	6	20
Aesthetics of repair	13	4	1	18
Interruption of service	4	7	9	20
Load capacity	2	3	14	19
Expected life of service repair	2	4	13	19
Maintenance required	2	11	6	19

Table 3.12 – Number of DOTs in each repair priority response category.

3.3 COMPARISON WITH PREVIOUS SURVEYS

In 1999 and 2002 the NCHRP and MIDOT, respectively, sponsored surveys on sign support structures. Although the focus of those surveys was more oriented toward design methodologies and structural fatigue issues, it is possible to compare some of the outcomes of those surveys with the present one.

3.3.1 NCHRP survey vs. PITT survey

The 1999 NCHRP sought to gain information about the "*fatigue and vibration of non-cantilevered support structures, foundations, drag coefficients for round and multi-sided*

sections, structure-specific connection plate and base plate flatness tolerances for erection, bending about the diagonal axis of rectangular sections, fiber-reinforced composite support structures, design examples, and retrofit/rehabilitation for fatigue damaged support structures" (Dexter and Ricker 2002). The numbers and the jurisdictions that responded were not indicated. Similar to PITT's survey, the 1999 survey inquired about the states that inspect their support structures. They found that 66.7% of states perform inspections and 29.17% do not perform inspections while 4.17% of states did not respond. More specifically they found that 60.42% inspect overhead cantilevered structures and 58.33% inspect overhead bridge structures. All states except UTAH who responded to the PITT's survey indicated that they inspect their structures. As was noted in Section 3.3.3 there is no nationwide time table on which these structures are inspected, but after comparing the results of the 2008 survey to the 1999 survey it is clear that the importance placed on sign structure inspection has grown.

3.3.2 Michigan Survey vs. Pitt Survey

Thirty-eight states responded to the 2002 survey (Alhborn et al. 2003). Figure 3.7 compares the states that responded to the survey conducted for the 2002 and 2008 (PITT's) survey. The Canadian Province of Alberta also responded to the Pittsburgh Survey, but there is no mention of surveying Canadian Provinces in the Michigan Tech survey, so only the responses of US states will be used to compare the two. The only state that responded to the current survey and not to Michigan's is Washington.

There are two common questions between the two surveys. The first asks what types of sign support structures are used. Figure 3.8 shows the results of this question and Figure 3.9 shows a comparison between the two reports.

Figure 3.7 – States responding to (a) Michigan Tech and (b) University of Pittsburgh survey

Several conclusions can be drawn from Figure 3.8. The percentage of states using cantilevered trusses is similar now to what it was in 2002. Fewer states use overhead trusses with single poles now than in 2002, and the percentage of states with cantilevered poles, overhead trusses with truss poles, and other structures has increased. Looking closely at the common state's answers in each survey, those for cantilevered trusses are exactly the same. Interestingly, the results are very different for each survey for the other three structure types.

Figure 3.8 – Structure type response for 2002 Michigan Tech Survey

For example, Connecticut, Maryland, and Kansas reported using overhead trusses in 2002 but not in 2008. It is unlikely that in the last six years such structures were dismantled. It is possible though that different terminolgy used in both surveys have generated different responses. The comparison of which states reported use of which structure type in each survey is shown in Table 3.14.

The second similar question between the 2002 Michigan Tech survey and the 2008 University of Pittsburgh survey involved finding out if the responding state experienced problems with overhead sign structures. More specifically, the 2002 survey asked if there were problems with excessive vibration or cracking and also allowed the responder to fill in an "other" response.
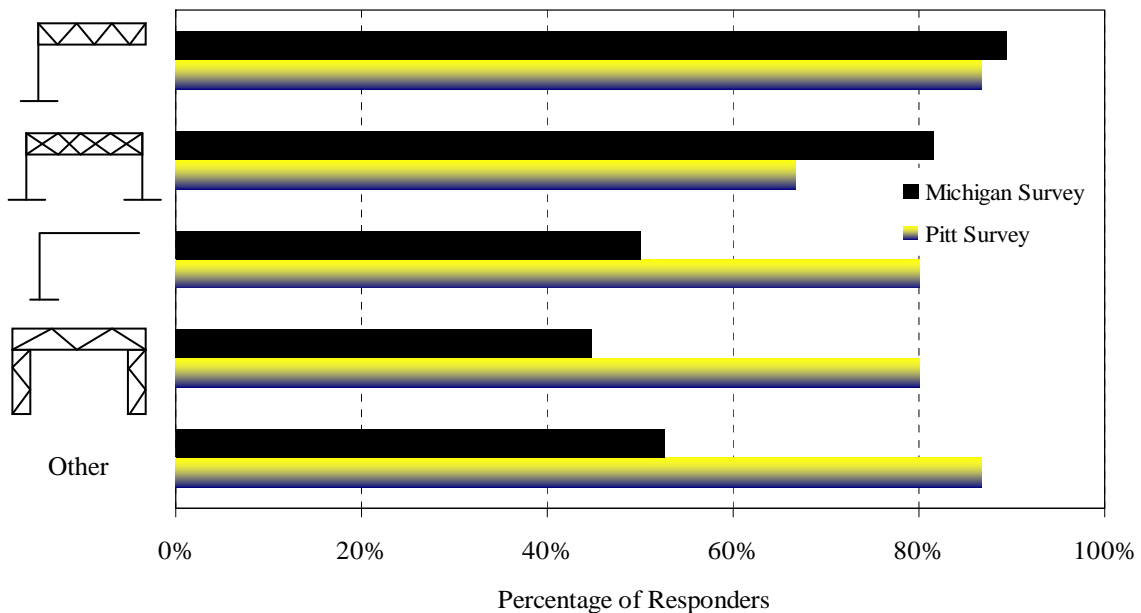
Figure 3.9 – Comparison of structure types in use

	Cantilevered Truss		Overhead Truss		Cantilevered Pole		Truss w/ truss pole	
	2002	2008	2002	2008	2002	2008	2002	2008
AR							x	x
CN	x	x	x		x	x		x
IL	x	x		x		x	x	x
IA	x	x					x	x
KS	x	x	x		x	x		x
MD	x	x	x		x		x	x
MI	x	x		x	x	x		
NJ	x	x	x	x		x		x
NY	x	x	x	x		x	x	x
PA			x	x	x	x	x	x
TN	x	x	x	x		x		x
WI	x	x	x	x	x	x		x
WY	x	x	x	x		x		x

Table 3.13 – Structures used across certain States according to 2002 and 2008 survey.

The present survey divided cracks into tube to tube weld cracks and column to base cracks, and also asked about loose or missing bolts and the mast arm to column connection. The results of the 2002 survey are shown in Fig. 3.10.

Recall from Section 3.3.6 that the current survey found loose or missing bolts as the most commonly listed problem. Of all 38 states responding to the 2002 survey only Wyoming listed loose bolts as a problem. Along with this, nearly all states reported some form of cracking as a problem in the current survey while only 11 of 38 states listed cracking as a problem in 2002.

Illinois, Iowa, Michigan, Tennessee, and Wyoming listed cracking as a problem in both surveys and New York listed corrosion of the posts at the base plate as a problem both times. It could be interpreted from the differences between the results of the two surveys that either more problems exist in sign structures today then in 2002 or that DOTs are more aware of the problems that exist now than they were in the past.

No: 58%

Yes: 42%

States that answered yes:
Cracking: 69%
Excessive Vibration: 19%
Other: 36%
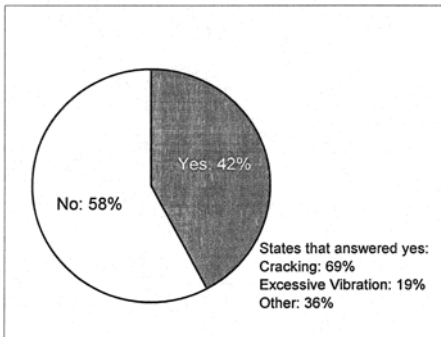
Figure 3.10 – Results of Michigan's survey about whether or not states experienced problems with sign structures.

3.4 Summary and Conclusion of the Survey Results

This chapter presented the results of a survey conducted by the University of Pittsburgh. In general the following other information was given.

MODOT reported that: "*Missouri originally had a 2 year inspection program that was conducted in house by our District Traffic Staff. Many of these inspections were not being faithfully conducted, primarily due to the high concentrations of structures in the two urban areas and a lack of personnel. In addition, the personnel were not adequately trained as structural inspectors. As a result, the department pursued a contract to have our overhead sign structures inspected by a structural consultant. Given our funding and the number of structures we have this program will take three years to complete ... the first year is just now being completed. As a result, we are not able to completely fill out your questionnaire as much of the information will not be complete until after the last year of this program. So far, however, the majority of the issues we have seen have been loose or missing anchor bolts, minor impact damage (major damage is replaced as it is very evident) and a few cases of weld failures on diagonal members in box trusses. Nothing found to date has not been correctable. To date, we have no record of having a catastrophic failure other than impacts by oversized loads*".

The Tennessee DOT reported that they "*went through a sign structure inspection process several years ago (2000) and followed that with a retrofit program of the four bolt cantilever sign structures. Our main problem with the cantilever sign structures have been fatigue of the back anchor bolts causing failure of the structure. Currently any cantilever sign structure constructed on any state road in Tennessee requires a special designed footing with a pipe pile projecting up through the center of the footing and into the annular opening of the vertical mast of the sign structure. The void between the concrete filled pipe piling and the wall of the column is filled with grout so that in the event of a bolt failure the structure will not catastrophically fail. […]. However we are trying to avoid the use of the cantilever structure and use more overhead or sign bridge structures*".

New Jersey *has "heavy" overhead sign structures inspected through the Bureau of Structural Engineering (Structural Evaluation)."Light" sign supporting cantilever poles (the standard types typically used for various traffic control purposes, that may have been given the task of holding a sign) are the purview of the maintenance arm of the Department, and would be maintained by them according to their procedures for maintaining all traffic control structures.* The data reported here applies to *the "heavy" structures only.*

The answers given by the responding DOTs show that while sign structures across the U.S. are pretty similar and are damaged in similar ways, the inspection processes are not very similar. Most likely this is the origin of the quantitative discrepancies reported in this chapter.

CHAPTER 4: FATIGUE ANALYSIS

A general algorithm that includes wind action, fatigue stress analysis and finite element modeling was developed as a part of the project. The algorithm was specifically applied to the case study of an overhead structure. This algorithm determined the effect of wind loads on the fatigue performance and established a relationship between damage severity and residual fatigue lifetime.

The following steps were performed:

1. review the algorithms utilized to model the action of wind on structures;

2. review the fatigue theories applied to dynamic analysis to determine residual fatigue life of structures;

3. formulate an accurate loading scenario that sign structures are subjected to while in service;

4. identify the elements of the structures more prone to develop fatigue cracks;

5. calculate the fatigue life of critical elements under pristine conditions of the whole sign support structures;

6. calculate the fatigue life of the critical elements in the presence of simulated damaged conditions.

Steps 3 through 6 were accomplished by examining a real structure deployed in the Pittsburgh area. The damaged scenario was modeled by reducing the material elastic properties of some components within the structure.

Fatigue failure can be identified as a structural failure under a repeated loading. It is not caused by one application of loading, but rather by several over a period of time. Fatigue may occur as either low-cycle or high cycle fatigue (Pun 2001). In low-cycle fatigue, there are high stresses that cause plastic deformation and lead to a short life. Conversely, in high-cycle fatigue stress cycles occur in the elastic range. They are caused by low loads and allow for a longer life. Low-cycle fatigue takes place in highway sign structures.

Interested readers can refer to the following publication,

Kacin, J., **Rizzo, P.**, and Annamdas, V.G.M. (2009). *Sensing Technology for Damage Assessment of Sign Supports and Cantilever Poles – Tasks 2-3*, Year 1 Report, Pennsylvania Department of Transportation, Contract No. 519691-PIT 008, University of Pittsburgh.

to gain more insights about the program codes and more details about the analytical formulation developed during this part of the project.

4.1 PROBLEM STATEMENT

Owing to their functionality, highway sign support structures must span great distances to provide drivers with needed information without introducing the danger associated with the occurrence of intermediate supports on medians or other locations adjacent to the roadway (Kozy and Earls 2007). Because of their long span length and relatively small cross-sectional

area and mass, these sign structures are flexible. This flexibility gives sign structures low natural frequencies. The damping is also low, typically around 1% of critical damping. These properties make these structures susceptible to large-amplitude vibration and fatigue cracking under wind loading (Li et al. 2005).

The AASHTO 2001 specifications (AASHTO 2001) divide wind loadings into the following: galloping, vortex shedding, natural wind gusts, and truck induced gusts. Galloping is an aeroelastic phenomenon that occurs when the across-wind oscillations of a structure create variations in the angle of attack of the wind flow. Galloping does not occur on cylindrical elements alone; it is caused by wind loading acting on the attachments. Vortex shedding is caused by the shedding of tiny whirlpools of air created as the structure disrupts the natural air flow. Wind gust loading is the result of varying gust patterns. Wind flow velocity components can fluctuate within a broad range of frequencies, causing strong fluctuating pressures that can induce vibration.

Truck-induced gusts occur as a result of the passage of large trucks underneath the sign structure. Higher speeds cause a significant disturbance in airflow, causing gust loading on both the frontal area of the structure and the underside of the members, creating torsional and bending moments in the connections (Ahlborn et al. 2004). The horizontal gust created by a truck is much smaller than that created by natural wind. The magnitude of the vertical pressure is directly proportional to the speed of the truck. Also, the higher the sign is above the roadway, the lower the magnitude of the gust (Creamer 1979).

The magnitude, direction, and frequency of pressure distributions on VMS caused by trucks passing underneath were determined by Cook et al. (1997). It was found that the truck induced gusts caused both negative and positive pressure as they passed and that the maximum positive pressure occurred at an angle of 75º to the front of the sign while the maximum negative pressure occurred normal to the sign face. By studying the effect of height on pressure, a 10% reduction in pressure for each foot of sign elevation increase was observed. Kaczinski et al. (1998) characterized the susceptibility of cantilevered structures to excessive displacement or fatigue damage.

An equivalent static load range was developed for the four common wind related causes of fatigue to identify the fatigue sensitive connection details in a sign structure and to determine the fatigue strength of anchor bolts. Fouad et al. (2003) and Fouad and Calvert (2005) studied fatigue and vibration in overhead structures to determine the impact of the extreme wind load and fatigue provisions on the design of cantilevered overhead sign support structures.

Natural wind on sign structures is usually characterized by a fluctuating wind force (Ginal 2003, Kaczynski 1998, Dexter and Ricker 2002, Li 2005). A wind force spectrum can be obtained by using either the Davenport wind velocity spectrum (Davenport 1961) or the Kaimal wind spectrum (Kaimal et al. 1972). Dexter and Ricker (2002) applied a randomly occurring wind load with base wind speeds ranging from 0 to 26.8 m/s (0 to 60 mph). Extreme speeds with a mean occurrence of greater than 1 year were considered not relevant for the fatigue analysis. Ginal (2003) studied three overhead sign structures by considering a 2.24-22.4 m/s (5-50) mph wind speed range and the Kaimal spectrum. Finally, Li (2005) developed a wind load time history to be used in a finite element analysis of several sign

support structures types. The range of wind speeds used in the analysis varied from 0-13.4 m/s (0-30 mph) and the Kaimal spectrum was used.

Fatigue modeling of highway sign structures was carried out by several researchers (Zalewski and Huckelbridge 2005, Ginal 2003, Fouad et al. 2003, Dexter and Ricker 2002, Li 2005, Van de Lindt and Ahkborn 2005, Park and Stallings 2006). Such studies varied by the type of wind loading included, the type of structure analyzed, the wind spectrum considered, and the method to carry out the transient analysis. Desantis and Haig (1996) analyzed the fatigue failure of a cantilever sign structure using the commercial finite element analysis program ANSYS. Two tapered poles formed the chords of the cantilevered truss and a VMS was attached at the end. Dexter and Ricker (2002) performed a finite element fatigue analysis of a cantilevered two-chord truss and a cantilevered four-chord box truss, both of which support VMSs and experienced excessive vibration in the field. The structures were modeled using ABAQUS.

Natural wind gusts were applied to the entire exposed area of the sign and structure. The horizontal component of truck induced gusts was neglected because it was considered small when compared to the magnitude of natural gusts, while the vertical component was applied to the bottom of the VMS. Ginal (2003) evaluated the fatigue performance of three full span overhead sign support structures using ANSYS. The effect of fatigue life due to both truck induced pulses and natural wind were determined separately. Wind data were collected in terms of speed and direction from the National Climatic Data Center (NCDC) (http://cdo.ncdc.noaa.gov). A rainflow counting algorithm to transform stress histories into stress ranges was used and the Palmgren-Miner rule to assess yearly fatigue damage was employed. The fatigue life predicted for the critical members in the three structures under investigation ranged between four years and 27 years.

Finally, Li (2005) utilized ANSYS to model a cantilevered double mast arm, a cantilevered single mast arm, a box truss, a monotube, and a tri-chord sign structure, focusing on the modeling of critical connections in these structures. Only natural wind was considered. As such, all loads other than natural wind were ignored, because galloping has rarely been observed in the field except for single mast arms, only structures with large dimensions are subjected to vortex shedding, and truck induced gusts are more critical in structures with large areas parallel to the ground. Similar to Ginal's work, the fatigue analytical method included the use of SN curves, Miner's rule, rainflow counting, and fatigue limits. Transient analyses were performed on the finite element models to obtain stress-time histories at critical details. Li found that practically all connections in the box truss, cantilevered monotube, and tri-chord truss have an infinite lifetime.

Park and Stallings (2006) performed a fatigue evaluation of two overhead box trusses to investigate the applicability of the AASHTO 2001 sign support specifications to non-cantilevered structures. Field monitoring tests were performed using strain gauges and a wind anemometer. The response associated with both natural and truck induced gusts was measured, and it was found that natural wind caused most of the significant cycles. Very few members were found to have a finite fatigue life.

In the study presented in this chapter the finite element software ANSYS was used to create the model of an overhead sign structure to: a) determine the effect of wind loads on the

fatigue life performance, b) identify the elements of the structure prone to fatigue cracking, and c) establish a relationship between damage severity and reduction of the fatigue lifetime.

Natural wind load was considered and the Kaimal wind spectrum was used. Wind data relative to the Pittsburgh International Airport were considered. Three welded diagonal members were specifically analyzed, being among the most critical. The stress history of such elements was found and coupled with a rainflow counting algorithm in order to calculate the complete stress cycles within the time history. The AASHTO stress-life curves were adopted to estimate the damage associated with a particular stress cycle. Finally, the Palmgren Miner rule of linear damage accumulation was used to find the fatigue life of each critical member.

The method was employed to analyze the structure in pristine condition and with simulated damaged elements. The reduction of the fatigue life when damage is present was quantified.

4.2 SIGN STRUCTURE AND FINITE ELEMENT MODEL

The overhead four-chord box truss shown in Fig. 4.1 was studied. The structure, built in 1988, spans 59.1 m (194 ft) over nine lanes of traffic. The structure is made of steel members, while the signs are flat aluminum panels. Both the box truss and the upright webs are constructed with angles, while the uprights posts are made of wide flanges. Design plan and drawings of the structure are in Kacin (2009) and Kacin et al. (2009).

Figure 4.1 – Overhead sign structure modeled in this study for fatigue analysis.

The structure mounts five signs of varying shapes and sizes, though the original plans for the structure showed four signs. Since erection, another sign has been added. A catwalk spans over the northbound lanes. Both welded and bolted connections are present. The chords are continuous members that are spliced in four locations. On the top and bottom truss sections a plate is welded to the chord and the diagonals are connected to this plate via high strength bolts. The cross bracing is connected with bolts to a separate plate that is welded to the chord. On the front and back truss the diagonals and the vertical members are

fillet welded to the chord. The signs on the structure are attached to the truss through vertical W sections.

The commercial software ANSYS version 11.0 software was chosen to model the structure and to run a transient analysis with a wind load applied as a traction force. The model was linear elastic and the small deformations caused by the wind loading were assumed to cause an elastic response.
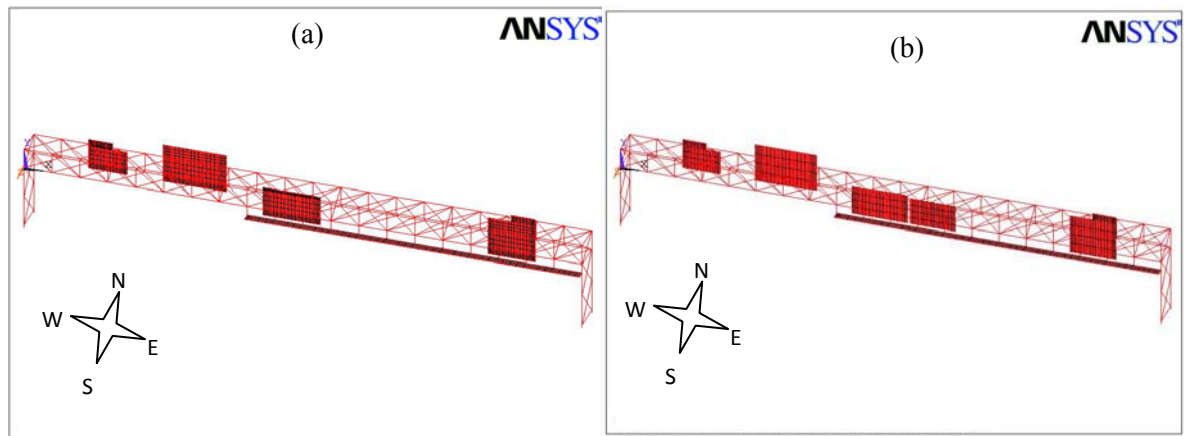
Figure 4.2 - ANSYS model of sign structure 511-76. (a) Model with 4 four aluminum signs attached. (b) Model with 5 five aluminum signs attached.

Because the gravity is not a time-variant variable, its effect was not included in the analysis.

Nodes and lines were built by using the ANSYS Parametric Design Language (APDL) and the implicit time integration was used. The model shown in Fig. 4.2 represents the structure with 4 and 5 signs, respectively.

The steel components were modeled using a three dimensional two-node beam element, and the aluminum signs and the catwalk were modeled using a three dimensional four-node shell element. The beam elements were Bernoulli-Euler beams. The sign mesh was cut in such a way that the nodes on the vertical beam lined up with those on the sign. These coincident nodes were then merged in order to connect the sign to the beam at finite points. All connections were modeled as fixed connections.

The model's inputs were cross sectional area, moment of inertia, member thickness, Young's modulus, and material density. Table 4.1 summarizes the section properties used for each member.

Before proceeding with the thorough analysis of the truss, in order to verify that the numerical model converged, a mesh convergence study was performed by comparing the stresses obtained with different mesh densities. Time integration was equal to 0.002 sec. Both mesh density and integration's time step were considered a good tradeoff between computational speed and solution accuracy to guarantee the convergence of the solution. For instance, the values of stresses changed less than 1% when the time step was halved to 0.001 sec.

Span	194'	59.13 m
Truss Depth	7.5'	2.29 m
Truss Width	10'	3.05 m
Tower A Height	26'-5"	8.05 m
Panel Point Spacing	22'-8"	6.91 m
Tower B Height	28'	8.53 m
Panel Point Spacing	24'-3"	7.39 m
Element type 1	Beam4	
Element type 2	SHELL63	
Section Property 1	L 8x8x7/8	
Section Property 2	L 4x4x3/8	
Section Property 3	L 4x4x5/8	
Section Property 4	L 3.5x3.5x5/16	
Section Property 5	C 15x33.9	
Section Property 6	C 4x5.4	
Section Property 7	W 30x124	
Section Property 8	W 6x12	
Section Property 9	W 6x8.5	
Section Property 10	Thickness = 1/4"	
Section Property 11	Thickness = 4"	
Section Property 12	L8x8x5/8	

Elastic properties of steel		
Young's Modulus	2.9×10^6 psi	210 GPa
Poisson's Ratio	0.3	0.3
Density	0.282 lb/in^3	7.85 g/cm^3

Elastic properties of aluminum		
Young's modulus	10^6 psi	69 GPa
Poisson's ratio	0.35	0.35
Density	0.093 lb/in^3	2.7 g/cm^3

Table 4.1 - Model information in U.S. Customary system and in SI units.

4.3 WIND LOADING ON SIGN STRUCTURES

The action of natural wind on the structure was simulated by using a Matlab program that generated data to be read into ANSYS. Truck induced gusts were neglected because they mainly affect VMS support structures that, unlike flat aluminum signs, have a large area parallel to the road (McLean 2004).

4.3.1 Basic Characteristics Of Natural Wind

In general, wind velocity is dependent on the time t and on the height z from the ground. The wind time history $V(t)$ can be considered as the resultant of two components: a mean component $\overline{V}(t)$ and a fluctuating component $V'(t)$. This concept can be expressed through the equation $V(t) = \overline{V}(t) + V'(t)$.

Two empirical formulas describe the effect of the height from the ground on wind speed over flat areas. These relationships are the power law:

$$V(z) = V_1 \left(\frac{z}{z_1} \right)^\alpha \tag{4.1}$$

and the logarithmic law

$$V(z) = \frac{1}{k} V_* \ln \left(\frac{z}{z_0} \right) \tag{4.2}$$

where $V(z)$ is the wind speed at a height z above the ground, V_* is the shear velocity or friction velocity equal to the square root of the ratio between the shear stress of wind at ground level and the air density, $k \approx 0.4$ is the von Karman constant, z_0 is the ground roughness elements; V_1 is the wind speed at a reference height z_1, and α is the power law exponent which is based on the terrain (Liu 1991). Because the logarithmic law produces negative wind speeds when $z < z_0$, the power law is generally used in engineering applications.

Because the structure is a bluff body, the wind pressure can be quantified by using the Bernoulli equation

$$p_s = p_a + \frac{1}{2} \rho V^2 \tag{4.3}$$

that predicts the stagnation pressure p_s at the stagnation point. In Eq. (4.3) p_a is the ambient pressure, ρ is the air density and V is the speed of the upstream wind. In the case when the ambient pressure is equal to the atmospheric pressure, $p_a = 0$. This is the case for the wind acting on the sign structure, therefore the equation for pressure reduces to the equation:

$$p = \frac{1}{2} \rho V^2 \tag{4.4}$$

Drag was considered. The magnitude of the drag force varies depending on the size and shape of the object that a wind flow is acting on. For a highway sign structure there will be a different coefficient of drag (C_d) for the signs and truss members. The drag force on the signs was found by subtracting the leeward pressure from the windward pressure on the panel's face and multiplying this number by the total frontal area of the panel. It is estimated that 60% of the drag is caused by pressure on the front face while the remaining 40% is caused by pressure on the rear face (Holmes 2007). The drag coefficient C_d for a square plate in perfectly smooth wind flow is about 1.1, but all of the signs on the modeled structure are rectangular so they have a slightly larger value of C_d.

Aspect Ratio	C_d	Sign #	Aspect Ratio	C_d
1.0	1.12	1	1.5	1.16
2.0	1.19	2	1.52	1.16
5.0	1.20	3	1.8	1.18
10.0	1.23	4	1.14	1.13
15.0	1.30	5	1.6	1.16

Table 4.2 - AASHTO coefficients of drag for sign panels. (b) Coefficients of drag used in this report.

The AASHTO sign support specifications provide a table of drag coefficient values (Table 4.2a). These values are based on the sign's aspect ratio (length to height ratio). Table 4.2b summarizes the aspect ratio and the corresponding value of C_d for the signs of the modeled structure. In the table, the panels are numbered from west to east. In order to apply the same wind loading to each sign, these drag coefficients were averaged so that the value of C_d = 1.16 was used.

The drag coefficients shown in Table 4.2 cannot be used for the truss, because the truss is not a solid plate. When wind flows through a truss, the reduction of the difference in windward and leeward pressures must be taken into account. This reduction then causes a smaller drag force. The overall reduction in drag depends on the solidity ratio (δ), which is the ratio of solid area to the total area, and the porosity factor K_p, which represents the reduction in drag, is expressed as follows:

$$K_p \cong 1 - (1 - \delta)^2 \tag{4.5}$$

Once the porosity factor is known, the reduced drag coefficient $C_{d\delta}$, can be calculated as [23]:

$$C_{d\delta} = C_d \cdot K_p \tag{4.6}$$

In this study the values of C_d = 1.62, K_p = 0.467, and δ = 0.27 were used. Details about the calculation of such values are in McLean (2007) and Kacin (2009). The drag coefficient for both the signs and the truss members were used to find the pressure load applied to the structure.

4.3.2 Wind Simulation

Much research has been done in the past to develop a spectrum that could accurately predict the dynamic characteristic of wind. Owing to its gusty nature, the complexity of wind cannot be perfectly predicted. Wind spectra assume that over a time period the statistical characteristics of wind can be regarded as constant (Davenport 1961).

In this study the Kaimal spectrum (Kaimal et al. 1972) was used, for it accounts for the height of the structure. The following relationship relative to the horizontal component of the wind was considered:

$$S_{ka}(f) = \frac{200 z u_*^2}{u_z \left(1 + 50 \dfrac{fz}{u_z}\right)} \tag{4.7}$$

where S_{ka} is the Kaimal spectrum, z is height above the ground, u_* is the shear velocity, u_z is the mean wind velocity at z. From Eq. (4.2), the shear velocity can be expressed as follows:

$$u_* = \frac{u_z \cdot k}{\ln(\frac{z}{z_0})} \tag{4.8}.$$

For the ground roughness coefficient z_0, the value of 35.56 mm (1.4 in) valid for open terrain (Liu 1991) was used.

4.3.3 Analytical Wind Simulation Process

To model the turbulent nature of wind in the horizontal direction, a five-second period time history load with sampling rate equal to 100 Hz was considered.

Base wind speeds of 0-25 mph were used to simulate the action of wind load on the structure. Weather data collected at the Pittsburgh International Airport and provided by the NCDC were used to measure the probability of occurrence of each of these speeds. Typically, the hourly measurements record the wind velocity over pre-defined one-minute period. This measurement therefore does not necessarily record the maximum value during the hour. Data collected between January 1999 and December 2008 were used.

Wind data were then clustered into 5 mph bins with the center point of each bin being a value from 0-25 mph spaced at increments of 5. For example, the bin containing the value of 10 mph includes all wind speeds between 7.5 and 12.5 mph. The only exception to this rule is the bin ranging from >0 – 7.5 mph.

Similarly, the directions were divided into bins containing the four cardinal directions and the four primary inter-cardinal directions. The resulting histograms presented in Fig. 4.3 show a positively skewed distribution with the maximum number of speeds occurring in the 2.24 m/s (5 mph) bin. Figure 4.3b shows that the prevailing wind flows along west direction.

The frequency of the occurrence of wind speeds above 13.4 m/s (30 mph) was statistically negligible; it was ignored in the subsequent analysis. A basic statistical analysis was performed in order to determine the probability of the occurrence of a particular speed or direction. Since there are two variables that must occur, speed and direction, their probability can either be analyzed as a joint probability or an independent probability. A joint probability is the probability that both events A and B will occur, while an independent probability is the probability that event A will occur. The joint probability is based on conditional probability, which is the probability that A occurs given that B has taken place (or will take place). Both cases were analyzed. To compare the results of the present study with the existing literature, only the joint probability was used to calculate the fatigue life by using the following equation:

$$P(A \cap B) = P(B) \cdot P(A \mid B) = P(A) \cdot P(B \mid A) \tag{4.9}$$

where, $P(A \cap B)$ is the joint probability, $P(A)$ is the independent probability of A, and a conditional probability is written as $P(A|B)$ and read "probability of A given B."
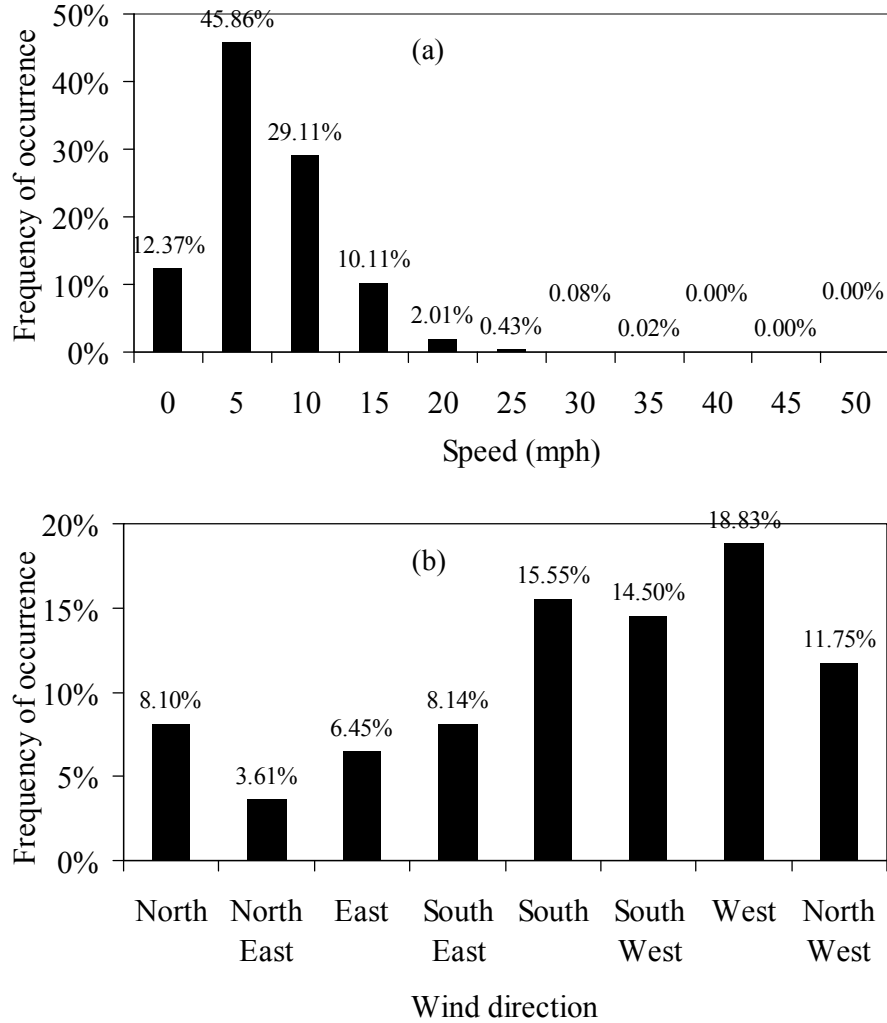
Figure 4.3 - (a) Frequency of wind speeds in Pittsburgh, PA; (b) Frequency of wind direction in Pittsburgh, PA

The individual P(A) and P(B) are known from the histograms shown in Fig. 4.3. In order to find the conditional probabilities, the partnered daily speed and direction were sorted into bins falling into the 5 mph increments discussed earlier. The results of this procedure are presented in the P(A|B) histograms of Fig. 4.4 where direction is event A and speed is event B. Equation (4.9) was used to calculate the joint probability.

The joint probabilities of directions at the Pittsburgh International Airport are presented in Fig. 4.5.

The mean component $\bar{u}$ was found using the power law. The turbulent component $u'(t)$ was found by using the weighted amplitude wave superposition (Iannuzzi and Spinelli 1987):

$$u'(t) = \sum_{k=1}^{N} \sqrt{2S_{ka}f_k \Delta f} \cdot \cos(2\pi f_k t + \phi_k) \tag{4.10}$$

where ϕ_k is the phase angle randomly distributed between 0 and 2π. The wind pressure *P(t)* and the applied force *F(t)* were obtained

$$P(t) = \frac{1}{2}\rho C_d u(t)^2 \hspace{4cm} (4.11)$$

$$F(t) = AP(t) \hspace{5cm} (4.12),$$

where ρ is the air density, $u(t) = \bar{u} + u'(t)$, and A is the gross area over which the pressure is applied.

The above procedure was implemented into a Matlab script to obtain the five wind time histories associated with five different wind speeds. Wind pressures acting on the signs are shown in Fig. 4.6a. The effect of wind pressure acting on the truss elements and modeled as concentrated forces on the truss' joints are shown in Fig. 4.6b.
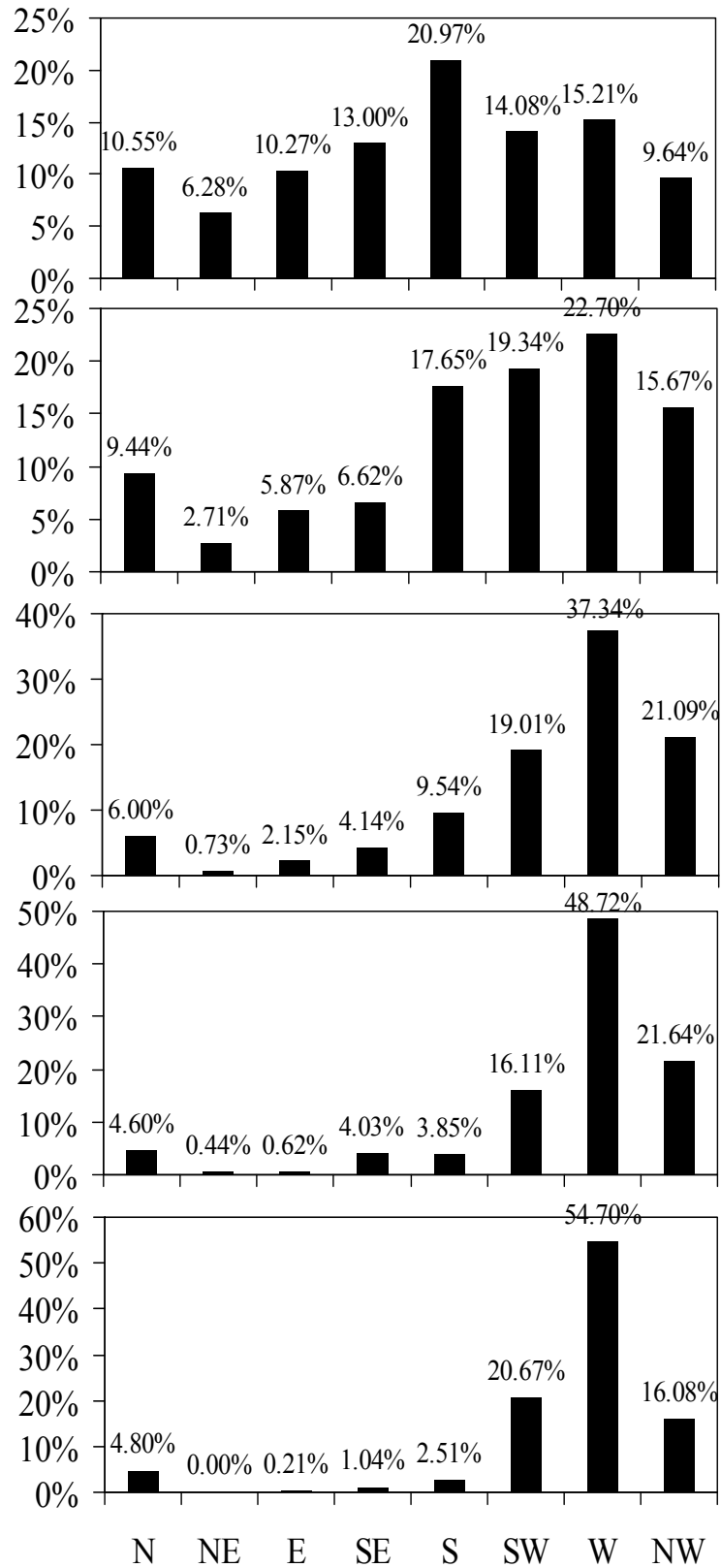
Figure 4.4 - Probabilities of directions given a certain wind speed. P(A|B) for A= wind direction and B= wind speed. Figures (a) through (e) are associated to wind speed of 5, 10, 15, 20, and 25 mph.
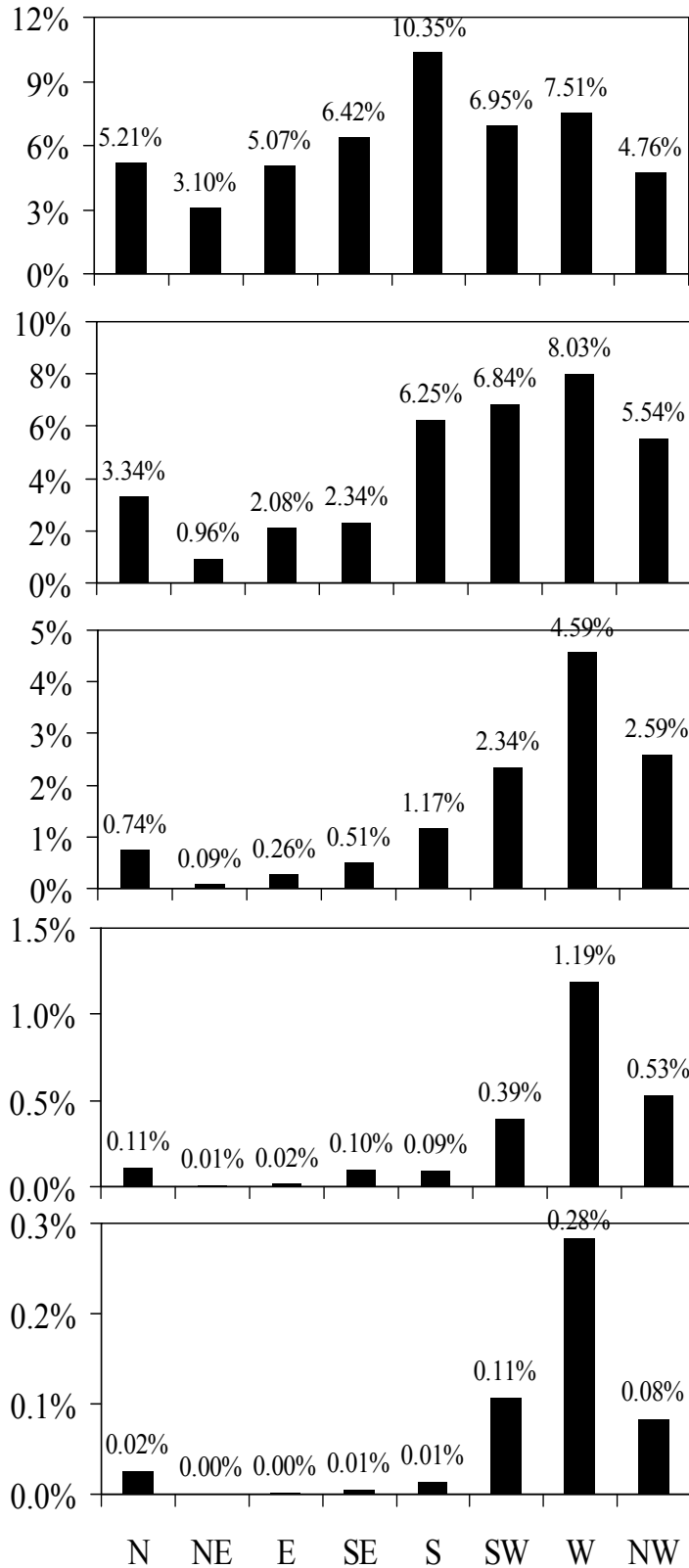
Figure 4.5 - Joint probabilities of directions recorded at the Pittsburgh International Airport. Figures (a) through (e) are associated to wind speed of 5, 10, 15, 20, and 25 mph.
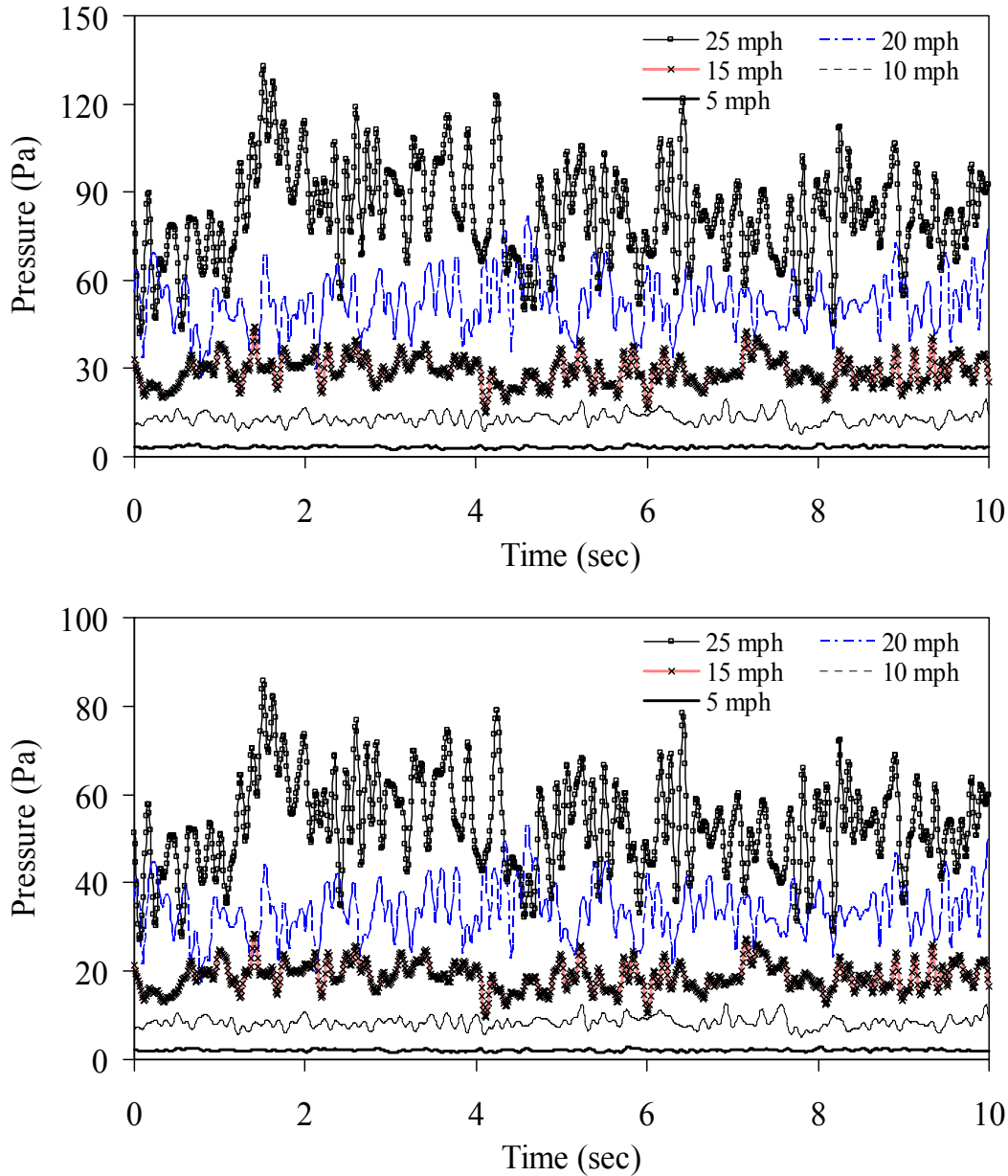
Figure 4.6 -. (a) Wind pressures to be applied to signs. (b) Wind pressures to be applied to truss's elements joints

4.4 FATIGUE LIFE CALCULATION

The S-N method was used to calculate the fatigue life of the structure. In order to use this method the applied stress must be in the elastic range. The basis of this method is the stress-life curve which plot the stress range S versus the number of cycles to failure N. The basic equation of each curve is given by the following:

$$N_i = \frac{A'}{S_i^3}$$
(4.13)

where A' is a constant given in the AASHTO 2004 manual (AASHTO 2004) and associated with the member connection, S_i is the stress range acting on the detail at cycle i, and N_i is the number of cycles of the stress range. A representation of the S-N curve adapted from AASHTO 2004 is shown in Figure 4.7. For convenience the curve are presented in U.S. Customary system and SI Units. Each S-N curve has a discontinuity point after which the value of the stress range is independent on the number of cycles (dashed horizontal lines in Fig. 4.7).
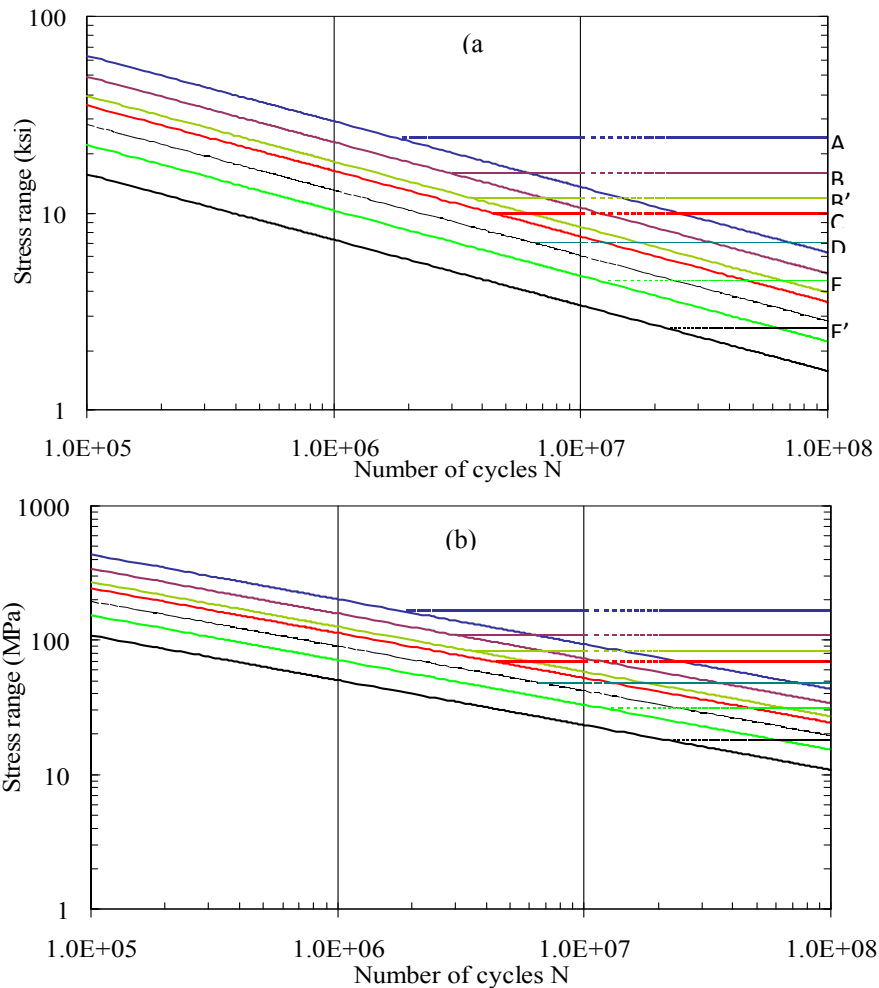
Figure 4.7 - Stress-Life curves adapted from (AASHTO 2004). (a) U.S. Customary system; (b) SI units.

Fatigue provisions utilize an infinite life design basis, requiring that the maximum stress range within the load spectra be less than the corresponding constant amplitude fatigue limit (CAFL) for the connection detail (Azzam and Menzemer 2008). The discontinuity points in Fig. 4.7 identify the CAFL. When the design stress range is less than one-half of the CAFL, the detail theoretically provides infinite life (AASHTO 2004). The AASHTO specifications

contain nine design categories, labeled A through K2 in order of decreasing fatigue strength. Examples of details are anchor bolts (Category D detail), post-to–base plate socket weld connection (Category E′ details), mast arm–to–flange plate socket connections (Category E′ details), and hand hole openings (Category E detail). Many of the connection details for cantilevered sign structures are classified as having low levels of fatigue resistance (Li et al. 2005). Table 4.3 shows the CAFL values for each detail category.

In the analysis, the maximum stress varied with time and the stress was measured at both ends (nodes i and j) of the element. Once the stress history of an element was found the following steps were performed:

1. Establish a histogram of stress ranges for the critical elements in the structure;

2. Associate each critical member with a particular AASHTO fatigue detail category by using the member end connections;

3. Use the appropriate S-N diagram associated with the connection being considered to calculate fatigue damage of the critical members;

4. Assess the fatigue life of each critical member.

Detail Category	CAFL (ksi)	CAFL (MPa)
A	24	165
B	16	110
B'	12	83
C	10	69
D	7	48
E	4.5	31
E'	2.6	18
ET	1.2	8
K	1	7

Table 4.3 - Constant amplitude fatigue limits.

Time histories were calculated for five members. The locations of these elements are shown in Fig. 4.8a and 4.8b and include three diagonal members on the front and back face of the truss and two vertical members that connect the top truss chord to the bottom chord. Figure 4.8c shows the location of the connections while Table 4.4 illustrates the truss details according to the TC-7718 from the Commonwealth of Pennsylvania Department of Transportation.
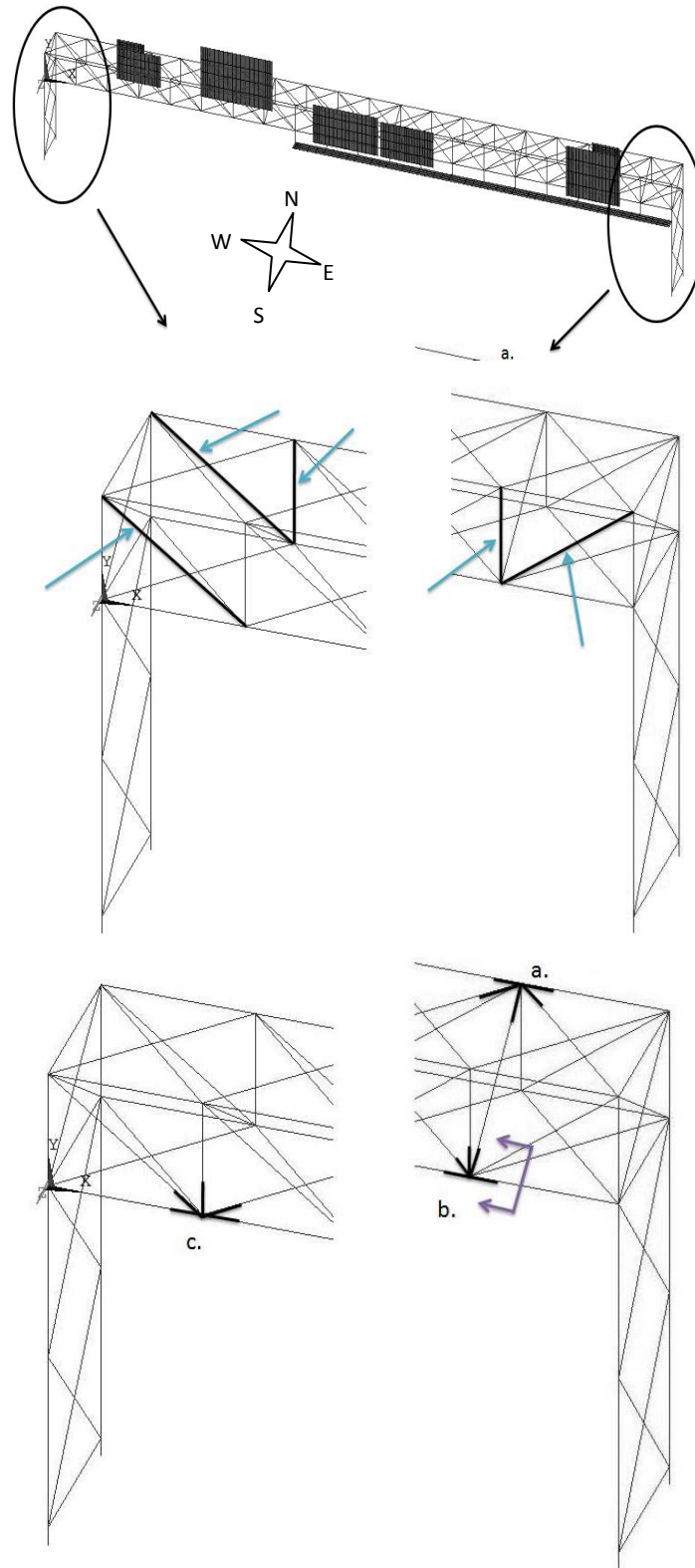
Figure 4.8 - (a) Finite element model. (b) Close-up view of the critical members considered in the present analysis. (c) location of connection details.

As can be seen in Table 4.4 illustrates the connections for the critical members selected in this study. Because welded connections have more severe initial cracking, and cracks in welds can propagate from one element into another (Fisher et al. 1998), fixed connections were used in the finite element model.

Location in Structure	Connection Detail
 PLAN a.	 DETAIL A
 PLAN b.	 SECTION AA
 ELEVATION c.	 DETAIL C

Table 4.4 - Connection details and their locations within the structure

Table 4.5 summarizes the characteristics of these critical elements.

In order to perform step 1 of the fatigue analysis, a rainflow counting algorithm was used to determine the critical stress ranges within each member. The algorithm was introduced by (Matsuishi and Endo) and was later standardized by the American Society for Testing and Materials (ASTM E1049-85).

ANSYS Element #	Type	Shape	Length	Length	Stress Category
1710	Vertical	L4x4x3/8	7'-6"	22.9 m	E
1725	Vertical	L4x4x3/8	7'-6"	22.9 m	E
1826	Elevation Diagonal	L4x4x3/8	12'-3"	37.3 m	E
1926	Elevation Diagonal	L4x4x3/8	12'-3"	37.3 m	E
1921	Elevation Diagonal	L4x4x3/8	12'-3"	37.3 m	E

Table 4.5 - Critical element stress categories.

The approach identifies closed hysteresis loops in a non-periodic stress response.

Because wind is a non-periodic loading, the structural response has no measureable constant amplitude or period. The rainflow counting algorithm was used to reduce the load's time history into a number of constant amplitude ranges.

A damage summing method was used to calculate the fatigue damage. The Palmgren-Miner rule was employed. This method assumes that each cycle causes some amount of damage over a time duration T (Ahlborn 2004). Moreover all cycles of a given stress range cause the same amount of damage regardless of when they occur in a structure's lifetime and that the presence of one stress range does not affect the damage caused by a different stress range. The relationship between the fraction of damage D_i that results from a specific stress range S_i, and the stress range n_i is given by

$$D_i = \frac{n_i}{N_i} \tag{4.14}$$

where N_i is the number of cycles it would take to cause failure (the fatigue life) at stress range i. The value of N_i can be found using equation (4.13). According to Palmgren-Miner rule failure occurs when the total damage D given by

$$D = \sum D_i \tag{4.15}$$

reaches unity.

4.5 RESULTS

4.5.1 Pristine Structure

The fatigue life of the diagonal angle located at the left end on the rear face of the truss (element 1921) is described. This member is connected to the truss chord via a filet weld and therefore falls into the fatigue detail category E.

Figure 4.9 shows the stress history for a 25 mph base wind, at both ends of the element (nodes i and j). Time histories were found for all of the wind speeds from 2.24 m/s (5 mph) to 11.8 m/s (25 mph).
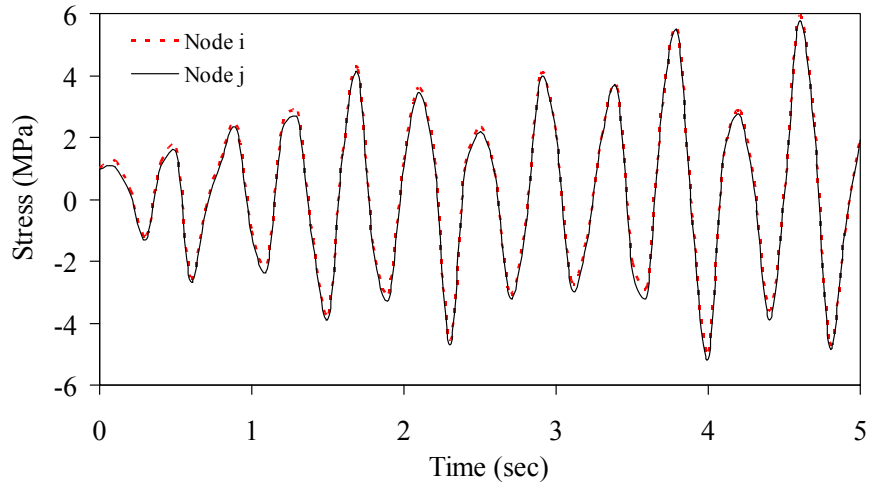
Figure 4.9 - Stress time history for element 1921 at a base speed of 11.8 m/s (25 mph).

Table 4.6 lists the stress values calculated at the completion of each cycle by means of the rainflow algorithm. If a stress range contains the starting point s of the distribution, when using the rainflow method that stress range only counts as a half a cycle rather than a full cycle. Those ranges for which this is the case are highlighted in Table 4.6. Detailed calculation of these stress ranges are in (Kacin 2009, Kacin et al. 2009).

According to the stress life method, only those stress ranges with a value greater than half of the CAFL, i.e. 15.51 MPa (2250 psi), will cause fatigue damage. None of the stress ranges in Table 4.6 are above 15.51 MPa (2250 psi), but for the sake of this example they will all be used to show how damage is calculated.

The number of cycles (N) required to induce damage was calculated by using the S-N equation (4.13).

Stress at node *i*		Stress at node *j*	
psi	MPa	psi	MPa
349.78	2.4127	345.09	2.3793
414.83	2.8602	410.68	2.8316
608.54	4.1958	605.85	4.1772
649.56	4.4786	657.64	4.5343
775.23	5.3451	766.49	5.2848
777.04	5.3576	779.58	5.3751
905.54	6.2435	927.54	6.3952
945.49	6.5190	936.50	6.4570
946.48	6.5258	967.84	6.6731
966.74	6.6655	973.28	6.7106
995.23	6.8619	1022.57	7.0504
1462.67	10.084	1466.41	10.111

Table 4.6 - Stress ranges in psi in element 1921 at 11.8 m/s (25 mph).

For fatigue category E, constant $A' = 3.61 \times 10^{11}$ MPa (11×10^{8} ksi^3). The Palmgren-Miner rule states that the total damage can be found by summing all of the individual damages. As shown in Table 4.7, the total damage in nodes i and j are equal to 7.43×10^{-9} and 7.65×10^{-9}, respectively.

In order to turn these damages into fatigue lives the wind probability data is needed. Because the sign structure is north-south oriented, only the wind probability occurring among north and south directions should be considered.

Node i				Node j			
S_i (kPa)	n_i (cycles)	N_i (cycles)	D_i	S_i (psi)	n_i (cycles)	N_i (cycles)	D_i
2411.65	0.5	2.57E+10	1.95E-11	2379.33	0.5	2.68E+10	1.87E-11
2860.15	0.5	1.54E+10	3.24E-11	2831.56	0.5	1.59E+10	3.15E-11
4195.76	0.5	4.88E+09	1.02E-10	4177.21	0.5	4.95E+09	1.01E-10
4478.59	1	4.01E+09	2.49E-10	4534.30	1	3.87E+09	2.59E-10
5345.06	0.5	2.36E+09	2.12E-10	5284.80	0.5	2.44E+09	2.05E-10
5357.54	1	2.34E+09	4.27E-10	5375.05	1	2.32E+09	4.31E-10
6243.52	1	1.48E+09	6.75E-10	6395.20	1	1.38E+09	7.25E-10
6518.96	1	1.30E+09	7.68E-10	6456.98	0.5	1.34E+09	3.73E-10
6525.79	0.5	1.30E+09	3.85E-10	6673.06	1	1.21E+09	8.24E-10
6665.48	1	1.22E+09	8.21E-10	6710.57	1	1.19E+09	8.38E-10
6861.91	1	1.12E+09	8.96E-10	7050.42	1	1.03E+09	9.72E-10
10084.82	1	3.52E+08	2.84E-09	10110.6	1	3.49E+08	2.87E-09
		ΣD	7.43E-09			ΣD	7.65E-09

Table 4.7 - The damage at node i and j of element 1921 caused by a 11.8 m/s (25 mph) wind.

Because the load was applied to the model for a 5 second time period, the number (6,307,200) of such periods over one year was found first. Then, this number is multiplied by the joint probability plot associated with the north and south direction. These values were plotted in Fig. 4.5 and are given in Table 4.8. Finally, the damage caused in one year is found by multiplying the summed damage at a particular wind speed by the number of 5 second cycles/year of the corresponding wind speed and direction.

Wind speed (m/s)	North wind probability	Number of 5-second cycles/year (North)	South wind probability	Number of 5-second cycles/year (South)
2.25	5.210%	328,577	10.353%	653,000
4.5	3.338%	210,537	6.245%	393,898
6.7	0.738%	46,521	1.173%	73,971
9.0	0.112%	7,084	0.094%	5,926
11.2	0.025%	1,567	0.013%	817

Table 4.8 – Probability of wind blowing in a certain direction for a certain speed.

For example, the damage caused by a 11.8 m/s (25 mph) wind in the northern direction at node *i* of element 1921 is given by the following:

$$7.43 \cdot 10^{-9}\left(\frac{1}{cycle}\right)*1567\left(\frac{cycles}{year}\right)=1.16 \cdot 10^{-5}\left(\frac{1}{year}\right)$$

The amount of damage per year caused at each wind speed in each direction is summed. Since failure occurs when D = 1, the fatigue life is equal to the inverse of the amount of damage per year. Table 4.9 summarizes the fatigue life for the three critical elements 1826, 1921, and 1926.

			Total Damage		
			5 mph	10 mph	15 mph	20 mph	25 mph	sum	Life (years)
1826	i	north	4.15E-10	9.17E-09	2.84E-08	1.61E-07	5.39E-08	4.78E-07	2,092,343
		south	8.25E-10	1.72E-08	4.51E-08	1.34E-07	2.81E-08		
	j	north	3.88E-10	7.57E-09	3.22E-08	4.24E-08	5.31E-08	2.65E-07	3,775,050
		south	7.72E-10	1.42E-08	5.11E-08	3.55E-08	2.77E-08		
1921	i	north	1.93E-10	3.30E-08	9.72E-08	2.24E-07	1.09E-07	9.25E-07	1,081,096
		south	3.83E-10	6.18E-08	1.55E-07	1.88E-07	5.68E-08		
	j	north	3.05E-10	3.40E-08	8.13E-08	2.63E-07	1.11E-07	9.61E-07	1,041,087
		south	3.66E-10	6.36E-08	1.29E-07	2.20E-07	5.81E-08		
1926	i	north	3.52E-10	5.51E-08	7.53E-08	4.72E-08	3.51E-07	9.74E-07	1,026,406
		south	6.99E-10	1.03E-07	1.20E-07	3.95E-08	1.83E-07		
	j	north	2.44E-10	6.53E-08	2.48E-08	3.96E-07	4.18E-07	1.62E-06	618,741
		south	4.85E-10	1.22E-07	3.95E-08	3.32E-07	2.18E-07		

Table 4.9 - Fatigue life for the structure modeled with four signs.
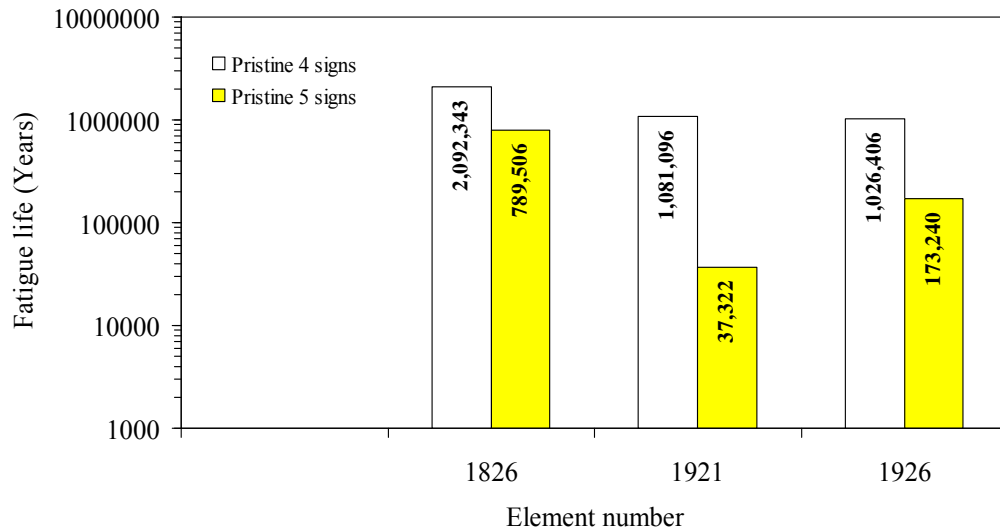
Figure 4.10 - Expected fatigue life in three critical members for the 5-signs and 4-signs pristine structures.

In order to make a comparison between the 4 and 5 sign model, the complete fatigue life calculations shown in the example calculation were carried out for all base wind speeds. The fatigue life of elements 1826, 1921, and 1926 are shown in Fig. 4.10. It is evident that the life is longer for all of the members in the four sign model. This is expected since the load transmitted to the critical members is lower when the amount of signs attached to the truss is lower. The stress ranges in the members in the four sign model were much lower than those in the five sign model, leading to a longer lifetime.

The analysis method adopted here assumes that the connections between members are made to code. A connection may be weakened by anomalies like loose bolts or a weak weld resulting in a reduced life. As such, albeit the results show that the structure will have an infinite life, it cannot be concluded that the structure will never sustain any fatigue damage.

4.5.2   Damaged Structure

The fatigue life of the same structure with five signs mounted and simulated damage was calculated. In order to simulate damage, a few randomly selected members near the two
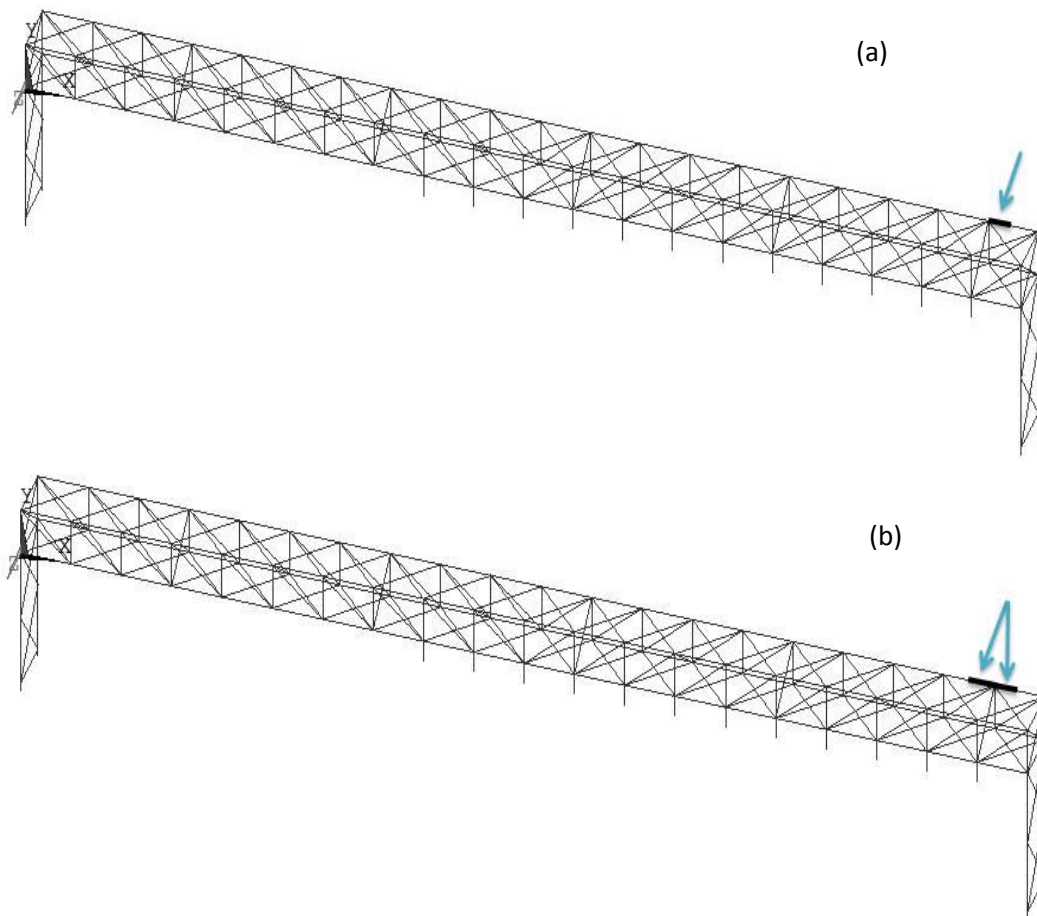
Figure 4.11 - Sign support structure with reduced capacity. (a) One member with Young's modulus halved. (b) Two members with Young's modulus halved. (Note that the signs are not shown to ease the visibility of the chosen element).

tower supports were assigned with reduced Young's Modulus. The reduction of the Young's modulus simulates that these members had a lower load carrying capacity.

Three simulations were run: the first simulation involved one member only, the second simulation involved the same member and an adjacent member having the same amount of damage, and the third simulation considered member 1926 with Young's modulus equal to zero.

The first member that was selected to be damaged was the chord member shown in Fig. 4.11. To estimate the effect of damage on the fatigue life, the same critical members discussed in section 4.5.1 were analyzed. A model with two damaged adjacent chord members was made and shown in Fig. 4.11b. The fatigue lives of critical members in these two models were found. Like the pristine model, the fatigue lives are once again infinite.

The fatigue lives of critical elements were found even though all of the stress ranges were below the CAFL. Figure 4.12a shows the fatigue life predicted in the 5-signs structure for the pristine structure and all simulations with damage. It can be seen that the fatigue life of the critical members is reduced although it still can be considered infinite. Thus, damage in the chord members will impact fatigue life, but not enough to result in their imminent failure. Figure 4.12b quantifies the fatigue life variation of the damaged condition with respect to the
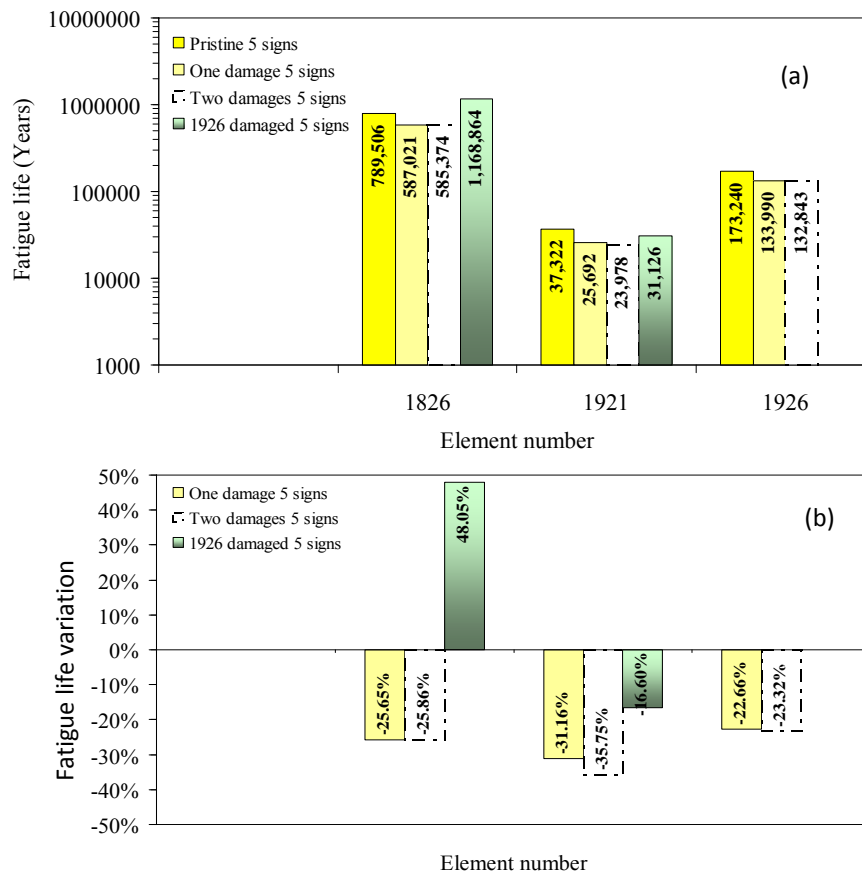
Figure 4.12 - Expected fatigue life in the five-signs support structure that has no damage, one member, two members, or member 1826 damaged; (b) variation of fatigue life with respect to the pristine structure when one member, two members, or member 1826 are damages.

pristine structure. When critical element 1926 carries no load, it was found that the fatigue life of element 1826 increases. It can be argued that when a member is severely damaged, the stress distribution along the truss changes. This may reduce the stress range in certain members.

4.6. CONCLUSION

This chapter presents the results of a methodology aimed at determining the fatigue life of critical structural members in overhead sign structures. Particularly, a four-chord box truss deployed in the State of Pennsylvania, was studied. The structure was modeled using the finite element program ANSYS, and a dynamic structural analysis was conducted to evaluate the effect of natural wind on the fatigue life of five critical elements of the truss. A 5-second natural wind load was considered by using the Kaimal wind spectrum and base speeds in the range of 5-25 mph. The wind data were gathered from the NCDC website showed. The data from the Pittsburgh International Airport were considered.

The critical members were chosen based on their connection type, with the welded diagonal members being the most critical. The stress history of such elements was found. Because the stress histories from ANSYS are not periodic, a rainflow counting algorithm was then used in order to find the complete stress cycles within the time history and the AASHTO stress-life curves were used to find the damage associated with a particular stress cycle. Lastly, the Palmgren Miner rule of linear damage accumulation was used to find the fatigue life each critical member.

The analysis was carried out by considering: a) the structure in pristine conditions; b) the structure having one or two members partially damaged; c) the structure having one critical member fully damaged. It was found that the selected critical members have an infinite fatigue life. Even though the results predicted an infinite life, the exact conditions in the field cannot be predicted without monitoring the real structure and measuring the real wind loading.

It should be pointed out that the single angle elements present is the truss may generate large secondary moments, which, cannot be captured by the ANSYS BEAM4 element used in this study. The deflection of all five elements discussed in this study associated with this secondary moment was estimated by using conventional structural analysis. It was found that the largest deflection was equal to 0.038 inches, which caused a stress increase in the order of 3.5% at the most.

In this research it was assumed that natural wind is the loading that most significantly contributes to fatigue damage. The hypothesis supported by studies carried out, for instance, for double–mast arm cantilevered sign structures (Li et al. 2005), may not be true for other sign structures, such as single–mast arm cantilevered structures. As overhead sign structure design varies from state-to-state within the U.S., an agreement among the different studies should not be expected.

The computer procedure developed in this study is general and can be adapted to any type of overhead sign structure. The geometry and material properties of the new structure need to be accurately modeled in ANSYS or a similar program and the wind load algorithm described in Chapter 4.4 can be applied.

CHAPTER 5: NONDESTRUCTIVE TESTING METHODS

This chapter reviews the NDT methods that have been proposed or utilized to inspect sign support structures. Based on the responses to the survey discussed in Chapter 3, the methods of visual inspection, magnetic particle, dye penetrant, and ultrasonic testing are discussed. An estimate of the cost of equipment needed to carry out these inspections is provided based on feedback received from companies operating in the field of NDE.

A general outline of the inspection procedures is described. The example of the state of Arkansas provided with the survey is presented.

The last part of the chapter examines the NDT techniques that show promise for application in sign support structures. A description of potential transition from "time-based" to "condition-based" maintenance is also given.

5.1. CURRENT METHODS

5.1.1 Visual inspection

Aided or unaided, direct or remote, visual inspection methods (VIMs) are one of the most basic NDT techniques. Generally VIM is the first method utilized to locate suspected defects areas in large structures. Inspectors follow procedures that range from simply looking at a part to see surface imperfections to performing various gauging operations, which assure compliance with acceptable physical standards (Mix 2005).

Once suspected areas are identified, they can be thoroughly examined using other approaches.

In the past the successful result of a visual inspection relied on the inspectors' skill, surface conditions of the structure under investigation, quality of any aid tools, and proper illumination. The development of sophisticated optical systems such as high-definition cameras, special probes, spectrometers, and notebook computers has greatly improved the inspection outcomes.

Depending on the field of application, visual inspection procedures can be tedious, time consuming, and characterized by high implementation costs (Kessler et al. 2002). Sometimes, inspection requires the dismantling of critical components before inspections and reassembling afterwards (Boller 2002), which could consume up to 45% of the entire inspection time, as in the case of the aviation sector (Bhalla 2004).

Tools that inspectors can use to perform visual inspection and to enhance the ability to remotely view critical area are borescopes, videoscopes, and crawlers. **Borescopes** are optical instruments for remote viewing of objects. They have long been used for the inspection of pipe and tubing (Mix 2005). Analogue to borescopes, **videoscopes** reduce many of the deficiencies of traditional borescopes by adding the quality and advantages of digital imaging.

The cost of such tools may range within few hundred dollars.

In the sign supports, visual inspection is normally conducted using a pair of binoculars of at least ten power magnification or a telescope such as a shooter's spotting telescope. The latter offers higher magnification, with the ability to identify smaller cracks. Several efforts have also been made to develop a robotic device that can climb, for instance, the vertical poles (FHWA).

A private communication with a Pennsylvania-based company stated: "*we* [the company] *used visual inspections only for the entire sign structures. If we see any suspected cracks, we may use dye penetrate testing or ultrasonic testing. However, we have never used any NDT on any sign structures yet*". "*Camera is a must toll for any inspection. We also use a bucket truck to get access to the signs. I know some cracks were found on some new VMS structures. NDT might have been used on those structures*".

Although VIM is the primary inspection method, it cannot detect all structural deficiencies. Examples include small fatigue cracks in welds, corrosion occurring on the interior of the structural element, and cracked anchor rods.

Future improvement of remotely operated crawlers able to climb structures while carrying a video camera may bring the VIM to a superior level of performance.

5.1.2 Liquid penetrant

Liquid (or dye) Penetrant Testing (PT) is a rapid, simple, and relatively inexpensive NDE method (Shull). It can be considered as an extension of visual inspection and it is used in the detection of surface-breaking flaws on any non-absorbent material's surface.

In penetrant testing the surface being inspected is cleaned thoroughly to remove all traces of dirt and grease. A bright coloured or fluorescent liquid is applied to the component surface and allowed to penetrate any surface-breaking cracks or cavities. After a pre-selected time interval (dwell time), the excess dye is removed from the surface. Another material, called the developer, is placed on the surface. The developer is usually a dry white powder. It draws some of the penetrant from the defects by reverse capillary action to produce indications on the surface, and it provides a contrasting background to make the penetrant easier to see. With fluorescent dyes, an ultraviolet lamp is used to make the "bleed out" fluoresce brightly. These (coloured) indications are broader than the actual flaw and are therefore more easily visible. After the indications from the penetrant/developer have been interpreted and perhaps recorded, the surface is cleaned a third time, to remove the developer and any remaining
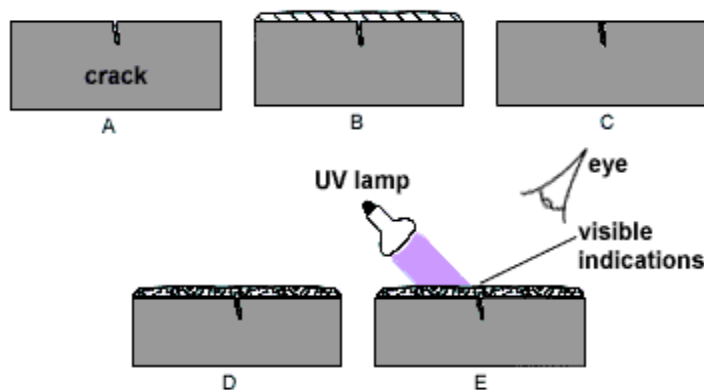
Figure 5.1 - Steps of an inspection conducted by using liquid penetrant testing. (a) Sample before testing; (b) liquid penetrant applied; (c) surplus wiped off leaving penetrant in crack; (d) developer powder applied, dye soaks into powder; (e) View coloured indications, or UV lamp shows up fluorescent indications. (http://www.twi.co.uk/content/ksijm001.html)

67

penetrant. The procedural steps are as shown in Figure 5.1 (Shull 2002, TWI 2008).

A number of different liquid penetrant systems are used. Fluorescent penetrants are normally used when maximum flaw sensitivity is required. However, these penetrants must be viewed under darkened conditions with an ultraviolet (UV) lamp, which may not always be practical. The most commonly used systems are solvent removable, or water washable, red dye systems, which typically are comprised of three aerosol cans - cleaning fluid, penetrant and developer.

Inspection using visible light and UV light differ also in price. Three aerosol cans (cleaning, penetrant, and developer) can cost from \$30 to \$140. Each can contain 16 oz. of product. The price of UV lamps to conduct in-shop in-dark inspection ranges from \$600 to \$2500. The cost of each bulb is \$50-\$60. For instance, to inspect a typical I-section beam 1 to 5 gallons of penetrants are necessary for level II inspection[1]. The gallon can cost around \$300 per gallon. Based on the people interviewed, it has been estimated that a system of three aerosol cans, may cover around 25-40 sq.ft. of surface area. The cost associated with the inspection of sign structures is dependent on the number and size of the structural elements that need to be examined.

The aerospace industry uses fluorescent PT to look for fatigue cracking in turbine blades. The construction industry uses dye PT to check welds and other susceptible areas prone to surface-breaking flaws.

The drawbacks associated with this technique can be summarized as follows:

1. the test surfaces need to be cleaned adequately, the contact time between the penetrant and the test surface should be sufficiently long, and the excess penetrant must be removed carefully.

2. minute hair line cracks cannot be detected.

3. the inspection cannot be automated.

4. only surface discontinuities are detectable.

5. environmental and safety issues associated with the use of dye penetrant are present.

According to the survey discussed in Chapter 3 Michigan, New Jersey, and New York DOTs, and some Pennsylvania districts have used liquid penetrant to inspect sign supports. NJ-DOT reported that liquid penetrant is used if a crack is suspected, while NY and WA DOTs only if crack is visually located.

5.1.3 Magnetic particle inspection

Magnetic Particle Inspection (MPI) is used to detect surface and near-surface flaws in ferromagnetic materials, to look for cracking at welded joints and in areas identified as being susceptible to environmental cracking (e.g. stress corrosion cracking or hydrogen induced cracking), fatigue cracking, or creep cracking. The procedure is relatively simple. A magnetic field is applied to the specimen, either locally or overall, using a permanent magnet,

---

[1] For ASNT (American Society for Nondestructive Testing) certification levels see
http://www.asnt.org/certification/leveliii/pd-accp.pdf

electromagnet, flexible cables, or hand-held prods. Fine ferromagnetic particles are then applied into the specimen's surface. If the material is sound, most of the magnetic flux is concentrated below the material's surface and the particles follow the induced magnetic field (Shull 2002, TWI 2008). However, if a flaw is present, such that it interacts with the magnetic field, the flux is distorted locally and 'leaks' from the surface of the specimen in the region of the flaw. The particles create a visible indication of the flaw. Magnetic particles commonly used are black iron particles and red (Fig. 5.2) or yellow iron oxides. In some cases, the iron particles are coated with a fluorescent material enabling them to be viewed under a UV lamp in darkened conditions.

Magnetic particles are usually applied as a suspension in water or paraffin. This enables the particles to flow over the surface and to migrate to any flaws. On hot surfaces, or where contamination is a concern, dry powders may be used as an alternative to wet inks. On dark surfaces, a thin layer of white paint is usually applied, to increase the contrast between the background and the black magnetic particles. The most sensitive technique, however, is to use fluorescent particles viewed under UV (black) light.

Figure 5.2 - Magnetic particle testing of a welded area.
(Source: http://www.fhwa.dot.gov/BRIDGE/signinspection03.cfm)

For the inspection of welded areas either by PT or MPI, the American Welding Society (AWS) *D1.1 - Structural Welding Code – Steel Inspection* should be followed. The code establishes the acceptance criteria for production welds criteria, the standard procedures for performing visual inspection and NDT, and the qualifications and responsibilities of inspectors.

Some of the drawbacks associated with MPI are the following:

1. the low sensitivity to detect cracks that run parallel to the magnetic field. In this circumstance there is little disturbance to the magnetic field and it is unlikely that the crack is detected. To avoid this limitation it is recommended that the inspection surface is magnetised in two directions at 90° to each other. Alternatively, techniques using swinging or rotating magnetic fields can be used to ensure that all orientations of crack are detectable.

2. the selection of the magnetization method must be pondered. It depends on the geometry of the component and whether or not the whole specimen is to be magnetised. Permanent magnets are attractive for on-site inspection, as they do not need a power supply. However, they tend only to be used to examine relatively small areas and have

to be pulled from the test surface. Despite needing their own power supply, electromagnets (yokes) find widespread application. Their main attraction is that they can be used to concentrate the field at the surface where it is needed, they are easy to remove (once the current has been switched off), and the magnetic field strength can be varied. Hand-held electrical prods are useful in confined spaces. However, arc strikes at the prod contact points can damage the specimen surface and, because the particles must be applied when the current is on, the inspection becomes a two-man operation.

3. residual magnetic fields left after the inspection is terminated may interfere with welding repairs. These can be removed by slowly wiping the surface with an energised AC yoke.

4. deeply embedded flaws cannot be detected

5. cannot be used for non-ferromagnetic materials, such as aluminium, copper or austenitic stainless steel.

6. length of the inspection time.

According to the survey MPI is used for welded areas.

It has been estimated that the cost of a typical highway sign support infrastructure may range from $40,000 to $200,000, including labour cost. Such range is associates with the level of sophistication of the equipment used. The cost of white contrasts or black particles is around $10 per each 16 oz. can. Similar to penetrant testing each can should be sufficient to cover an area of 25-30 sq.ft.

5.1.4 Ultrasonic Testing

Ultrasonic testing (UT) is one of the most widely used NDT methods today (Shull 2002). UT is based on the propagation of stress waves with frequencies higher than 20 kHz. A stress wave is characterized by its frequency, wavelength, and speed. In unbounded media two types (modes) of waves can propagate: the longitudinal bulk mode also, referred as P-wave (pressure wave), and the shear bulk mode (S-wave or T-wave). In the longitudinal mode the particle displacement is parallel to the direction of wave propagation; conversely, in the shear waves the particle displacement is orthogonal to the propagation direction.

Ultrasonic NDT is known for common applications like thickness gauging, flaw detection, material properties characterization, and acoustic imaging. Changes in one or more of four measurable parameters associated with the passage of a wave through a material— transit time, attenuation, scattering, and frequency content—can often be correlated with changes in the material's physical properties or geometry, and with the presence of damage.

Bulk waves are the most commonly used waves because only two modes can be measured without the complication of the multimode wave propagation typical of the guided waves (see discussion later in this chapter).

Sound pulses are normally generated and received by piezoelectric transducers that are acoustically coupled to the test material. In most cases a single transducer coupled to one side of the test piece serves as both transmitter and receiver (pulse/echo configuration).

A sound wave is launched by exciting the transducer with either a voltage spike or a continuous wave impulse. The sound wave travels through the test material, either reflecting

off the far side to return to its point of origin (pulse/echo), or being received by another transducer (pitch-catch) (Fig. 5.3). The received signal is then amplified and analyzed.

Disadvantages of bulk wave-based UT are the low sensitivity to the following: 1) detect discontinuities oriented parallel to the direction of propagation of the ultrasonic energy, 2) discontinuities that are similar or smaller than the material's grain structure, and 3) thin sections for which very high frequencies are necessary

A variety of commercial instrumentation is available for this purpose, utilizing both analog and digital signal processing. The pricing of corrosion gauges including one transducer, ranges from $1,360 to $3,800 depending on model and optional features. Precision (thickness) gauges, including one transducer, ranges from $2,500 to $5,000. Additional transducers for either type of gauge are typically $300-$500. Portable ultrasonic flaw detectors could be used for both thickness inspection and subsurface crack detection in welds and base metal. They range in price from $4,500 to $7,500 not including transducers which typically cost $300-$500 each.

Besides the responses obtained from the survey, it is known that some state DOTs use UT routinely to inspect anchor bolts at the bases of sign structures (FHWA 2005). Usually this inspection is conducted by certified personnel
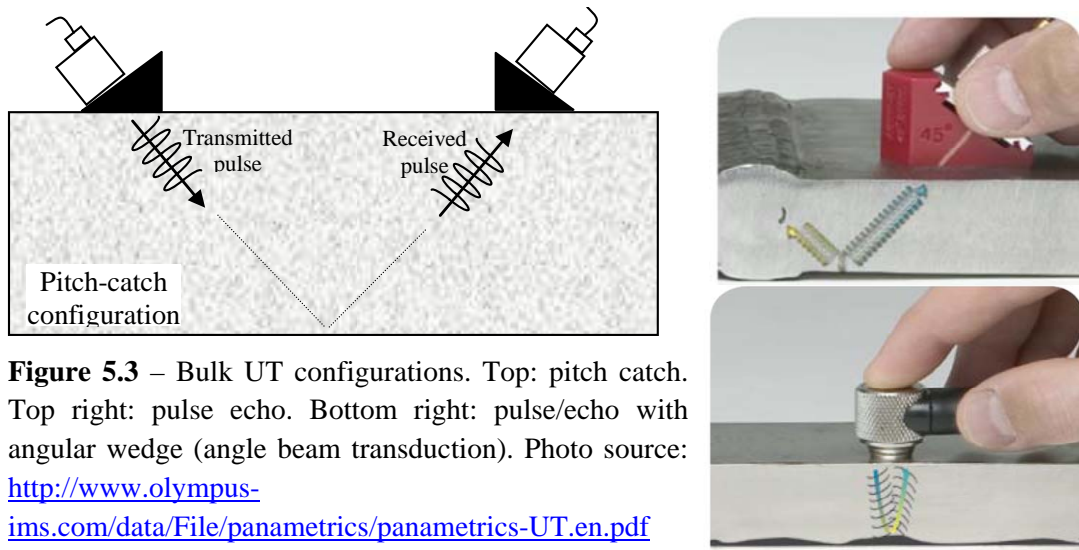
Figure 5.3 – Bulk UT configurations. Top: pitch catch. Top right: pulse echo. Bottom right: pulse/echo with angular wedge (angle beam transduction). Photo source: http://www.olympus-ims.com/data/File/panametrics/panametrics-UT.en.pdf

5.2 INSPECTION PROCEDURES

As previously outlined, there is no nationwide consensus or uniform strategy to inspect sign support structures. Unlike bridges, the inspection frequency for sign supports is not demanded by federal regulations. As the inspection of sign supports has similarities to highway bridges, the qualification for inspection personnel follows the National Bridge Inspection Standards (23 CFR 650)

Although these inspection types follow those typically performed for bridge inspections, in the current practice, the frequency for sign structure inspection is dependent on several factors such as material and structural redundancy.

All responding DOTs uses VIM. The New York State *Overhead Sign Structure Inventory and Inspection Manual* describes two inspection team members: the team leader and the assistant team leader. The guidelines of FHWA includes both of these positions and an additional position of program manager that should be registered as a Professional Engineer or have 10 years of experience in structures inspection (FHWA 2005). The job involves the scoping, scheduling, cost control, and quality assurance of an inspection project. Both documents agree that the team leader should be a professional engineer, but differ on the amount of inspection experience required to fill this position if the inspector is not a professional engineer. The NYSDOT says at least three years is sufficient, while the FHWA document recommends five years of experience.

The general indications to inspect sign structures were recently defined by the FHWA (FHWA 2005) and are summarized in what follows.

5.2.1 Initial Inspection

An initial inspection takes place shortly after the sign structure is constructed. This practice is particularly necessary for bolts which may become loose. Usually this inspection is conducted within 60 days after construction is complete.

5.2.2 Routine

This can simply consist of a ground level inspection with no attempt to close traffic lanes. This type of inspection is employed during the beginning of the sign structure inspection program to quickly look for deficiencies. However, as many structural deficiencies such as weld cracks in the overhead truss cannot be identified from a ground level inspection, this type of inspection is not recommended to occur normally in subsequent inspection cycles.

5.2.3 In-Depth

In–depth inspection is recommended as a typical inspection of a sign structure.

An **interim inspection** would be recommended by the inspector if a sign structure is found to have deficiencies or other problems that require more frequent inspections or after repairs or countermeasures are made. Such repairs can occur when cracks are found in the overhead sign truss. These measures may be simply the removal of sign panels to reduce wind load, the installation of dampeners, or the retrofit of cracked connection by using fiber composite material.

Damage inspection is conducted after a sign is damaged by, for instance, the impact of vehicles on posts or the hit over the truss or a sign panel by a passing truck.

5.2.4 Recommendations

As aluminum truss type span structures have shown increased problems due to fatigue deficiencies it is recommended that a two-year frequency of in-depth inspections be conducted while for steel structural components the inspection frequency may be longer.

High strength anchor rods have been more problematic than mild steel.

Cantilever sign structure supports only have one main support instead of two or more with span type structures. A four year frequency is recommended.

Sign structures associated with another structure such as a bridge-mounted sign may be inspected as the bridge is inspected during a normal two-year frequency. A typical two tower, two or four post sign bridge with a steel superstructure need only be inspected hands-on every six years. Routine or ground inspections can be conducted more frequently to check for corrosion of posts or connection problems.

Finally, it must be pointed out that other relevant factors influencing inspection frequency are traffic control and accessibility to the structure.

The following inspection program strategy may be outlined (FHWA 2005):

1. Perform field reconnaissance and collect inventory information

2. Perform a random sampling inspection project of perhaps 10% of total inventory

3. Based on findings of sample project, continue full inspection program, by prioritizing the following structures:

• Aluminum sign bridges

• Sign Bridges with long span

• Non Redundant cantilever sign structures

• Sign Structures greater than 20 years old

• Sign Structures where sign panel sizes exceed those originally designed for.

5.2.5 The example of Arkansas DOT

The Arkansas DOT integrated the survey response with the following document.

Inventory Inspection – This inspection is made after initial erection to assure proper construction. This will also serve as the first inspection made for initial documentation purposes. A copy of this inspection will be sent to Bridge Division.

Routine Inspection – Most inspections will be made every four (4) years after the inventory inspection. Bridge mounted sign structures whether overhead, overhead cantilever, or bracket mount will be inspected at a minimum of every two (2) years.

Special Inspection – Special inspections will be made after a major wind event or traffic incident that might have damaged the structure. Special inspections will be made to inspect specific areas of concern (that the inspector deems necessary).

FORM I
MAJOR SIGN STRUCTURE
INSPECTION

Identification Number: _____	Date: ___/___/____
Route Section Log Mile: ___/___/___	Inspector:
Descriptive Location:	

Condition (0-9): _____

Foundation.....__
  Concrete Footing
  Pedestal
  Cracks

Column.........__
  Anchor Bolts
  Bearing Plate
  Members
  Nuts and Bolts
  Pack Rust
  Cracks

Comments and Location

Super Structure.....__
  Members
  Nuts and Bolts
  Cracks
  Rust
  Connections

Type Structure:

Material:

Comments And Sketches:

Figure 5.4 – Major sign structure inspection form

Inspection Procedures:

1. *Inspect the foundation for cracks and concrete deterioration.*

2. *Inspect the anchor bolts for rust deterioration, missing nuts, cracks and broken bolts.*

3. *Inspect the base plates for rust deterioration and cracks especially around welds.*

4. *Inspect support columns and towers for cracks in welds, bulging from the effect of freezing water in closed sections that do not drain, and rust from the inside of closed galvanized sections that were not galvanized on the inside.*

5. *Inspect bolted connections for broken, missing and loose nuts and bolts. Also check for rust deterioration in connections due to incorrect bolt type – stainless steel or aluminum bolts should be used in aluminum.*

6. *Check space frame members for cracks and breaks. Aluminum welds are prone to fatigue cracking.*

7. *Check signs and fixtures for proper attachment.*

Watch for locations where sign structures are set close enough to the road that winter salt spray and snow plow wind rows can accumulate on the base support and cause deterioration of anchor bolts and concrete pedestals.

A template of major sign structure inspection form used by AR-DOT is shown in Fig. 5.4

5.3. POTENTIAL INSPECTION/MONITORING TECHNIQUES

In the last decade academia and industry have devoted an increasing attention toward advanced NDT methods and toward the implementation of inexpensive SHM solutions. The latter approach evolves the maintenance paradigm from "time-based" to "condition-based". In "time-based" maintenance the inspection is conducted at predefined times or intervals established by federal regulations, state policies, or owners' guidelines regardless of the condition of the components. Condition-based maintenance implies that a sensing system is integrated with the structure to provide real-time stream-like information of the structure's health. Safety and economic benefits are realized if the monitoring system provides sufficient warning such that corrective action can be taken before the damage or degradation evolves to some critical level.

The trade-off associated with implementing such a philosophy is that it requires a more sophisticated monitoring hardware to be deployed on the system and it requires a sophisticated data analysis procedure that can be used to evaluate the measured data (Farrar 2006).

This section reviews other NDT methods and novel SHM techniques that show promise for implementation for the inspection (NDT approach) or real-time monitoring (SHM approach) of sign support structures. In the context of time-based maintenance the methods of eddy current and X-ray are reviewed. Guided Ultrasonic Waves (GUWs) and Acoustic Emission (AE) testing can be used instead either as NDT method or SHM approaches. Finally the SHM approach of the Electromechanical Impedance (EMI) is described.

5.3.1 Eddy Current

Eddy Current Testing (ECT) measures a material's response to electromagnetic fields over a specific frequency range, typically a few kHz to MHz (Shull 2002).

An ECT is based on inducing electrical currents in the material under investigation and observing the interaction between the currents and the material. Eddy currents are generated by electromagnetic coils in the test probe, and monitored simultaneously by measuring the probe electrical impedance.

The basic principles are as follows. A current flowing in a wire generates a magnetic field that encircles the wire. A magnetic field in proximity with the metal surface under inspection (to be monitored) produces a voltage. The EC measurement consists of four steps, namely 'signal excitation', 'material interaction', 'signal pickup', and 'signal conditioning and display'. One coil (excitation coil) is excited with an AC signal and the other coil (pick-up coil) is connected to a voltmeter. The first coil produces a magnetic field, part of which passes through second coil. The pickup voltage reading will remain constant until the whole set up (first and second coils) is placed near the metal surface (ferromagnetic material). The disturbance to magnetic field is measured in the form of voltage at second coil. This is because the first coil when placed near any ferromagnetic material induces current in the material, which travels in closed circular paths, known as eddy currents (Shull 2002).

ECT is suitable to assess material conditions such as hardness and thickness or to detect the presence of corrosion or defects such as porosity and cracks. The method is adopted in automotive and aircraft manufacturing processes and it is an integral part of inspection and maintenance in the power generation and aircraft industries (Shull 2002).

ECT has the advantages of being versatile and sensitive. Contact between the probe and the surface is not required, the surface does not need to be specifically prepared (unlike for liquid penetrant, magnetic particle). However, such a method is limited to the inspection of conductors and it is sensitive to a wide range of parameters, which can represent a drawback. Other limitations include shallow-depth of penetration, lift-off effects, surface conditions, and sensitivity only to cracks perpendicular to the interrogating surface.

Portable eddy current flaw detectors may be of use for inspecting thin non-ferrous structures and surface breaking cracks on welds. They range in price from \$5,500 to \$8,200 not including probes which typically cost about \$200 each.

In the sign support industry, the technique of eddy currents can be applied leveraging the experience of research outcomes in the area of crack detection in aircraft skins (Pellettier et al. 2006), stainless steel piping (Diaz et al. 2007), structural steel (Lamtenzan 2000), and welds (Laubach et al. 2007).

5.3.2 X-ray

Radiographic techniques (specifically X-rays) are one of the few NDT methods that can examine the interior of an object and the only NDT method that works on all materials (Shull 2002). An X-ray (or Röntgen ray) is a form of electromagnetic radiation with a wavelength in the range of 0.01 to 1 nanometers, corresponding to frequencies in the range of $3x10^{17} – 3 x10^{19}$ Hertz.

X-rays have high electromagnetic energy. These rays tend to pass through object that block visible light. This allows "seeing" the interior of the material/structure under investigation. The amount of X-rays that pass through a material is dependent on the elemental composition, density, and thickness of the material, and the energy and amount of X-rays (Shull 2002). This method can detect cracks, flaws, and thickness reduction.

X-ray based NDT has the advantages of being accurate, inherently pictorial, adoptable to examine shapes and sizes, and sensitive to the discontinuity that causes a reasonable reduction of cross-section thickness. However, this method carries the burden of safety hazard concerns. It can be time-consuming and expensive. It also requires extensive experience and trained personnel to safely carry the inspection and to properly interpret the images.

As radiographic methods were proposed to inspect corrosion in pipes (Balasko et al. 2005) and more in general pipeline structures (U.S. Patent 1999), the use of X-ray technology can be extended to monitor tubular components and welded areas in sign support structures.

5.3.3 Guided ultrasonic waves

When an ultrasound propagates into a bounded media, a GUW is generated. The wave is termed "guided" because it travels along the medium guided by the medium geometric boundaries. Different types of guided waves exist: Rayleigh waves, Lamb waves, and cylindrical waves. Rayleigh waves are waves propagating along the surface of semi-infinite space. In plate-like structures Lamb waves propagate. They occur in two different basic modes, the symmetrical or dilatational mode, and the asymmetrical or bending mode. In a slender, isotropic, traction-free cylindrical waveguide, three types of vibrational modes can exist: longitudinal, flexural, and torsional waves. The first two waves are analogous to symmetric and anti-symmetric Lamb waves, respectively.

The application of guided waves is more complicated than bulk waves because guided waves are multimode (many vibrating modes can propagate simultaneously) and dispersive (the propagation velocity and the attenuation depend on the wave frequency).

Methods based on GUWs gained popularity owing to the capability of inspecting moderately large areas using a single probe attached or embedded in the structure while maintaining high sensitivity to small flaws. GUWs can travel at relatively large distances with little attenuation and offer the advantage of exploiting one or more of the phenomena associated with transmission, reflection, scattering, mode-conversion and absorption of acoustic energy that have shapes. As sign support structures contain several hollow cylindrical components (mast, vertical poles, truss members) and these components may be welded, the use of GUWs is feasible and offers the same advantages offered by any general GUWs application.

5.3.4 Acoustic Emission

AE is a passive method that monitors the transient stress waves generated by the rapid release of energy from localized sources within a material. The elastic energy propagates as a stress wave (AE event) in the structure and it is detected by one or more sensors attached to

or embedded in the structure (Fig. 5.5). Such an event can be linked to the onset of new damage or to the growth and propagation of existing anomalies. AE differs from most other NDT techniques in two key respects. First, the signal has its origin in the material itself, not in an external source. Second, AE detects movement, while most other methods detect existing geometrical discontinuities. Different AE sources may produce different AE waveforms. The AE source mechanism results in different received signals if the source is oriented differently with respect to the geometry of the medium or the propagation path to the detector.

AE is suitable for global monitoring, real-time evaluation, and remote sensing. By using an array of AE sensors, a global region or volume of material can be monitored and damage onset and propagation can be detected. Other advantages are associated with the ability to discriminate among different sources of events, i.e. sources of damage. Finally, in AE monitoring, time consuming and expensive point by point scanning is not required. As with any method related to the propagation of stress waves, AE may suffer from attenuation and be subjected to extraneous noise. It is a contact method, i.e. it requires contact between the sensing technology and the structure under investigation. Not always the previous loading history of the structure can be determined and the presence of existing damage cannot be appreciated. To determine the location of the AE event multiple sensors are required.
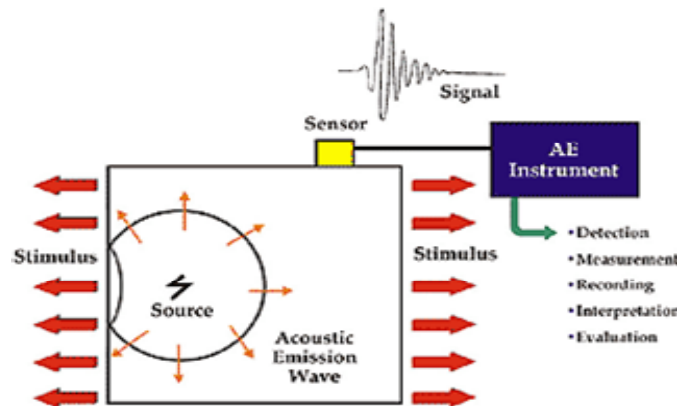
Figure 5.5 – AE principles. Source: http://www.pacndt.com/index.aspx?go=research

There are countless applications of AE in the civil infrastructure industry. The feasibility of using it to monitor pole connections in signal structures was carried out by Wang (Wang 1999) in a laboratory setting.

The cost to implement AE in a structure depends on the number of sensors deployed and therefore on the number of channels the data acquisition system has. The cost of commercially available monitoring systems can range from $18,000 to $24,000. Such systems include 8 sensors, 8-channels data acquisition system, and a laptop and software for signal processing and data storage. In the last few years a great effort has been made in academia and in the industry to reduce the cost of such equipment by achieving even higher levels of performance and robustness.

5.3.5 Electromechanical Impedance

The EMI method measures the resistance of a structure to the vibrations. A damaged/cracked structure offers less resistance to vibration when ones compared to undamaged structure. Liang and co-authors (1994) presented the first application of EMI on one dimensional skeletal structure for NDE applications.

In the last decade EMI applications spanned from small sized laboratory structures to real sized aerospace structures.

Piezoceramic or piezoelectric are employed as source of vibration. These patches are surface bonded on the host structure to be monitored (Fig. 5.6).

The governing principle is that harmonic electric field excites it to produce a structural response which is known as the 'admittance signature'. The signature is a function of the stiffness, mass, and damping of the host structure being monitored (Sun et al. 1995), and the length, width, thickness and orientation of the patch (Wetherhold 2003). The changes in the admittance signature, which is the inverse measure of the structure's mechanical impedance, are indicative of the presence of damage.

Figure 5.6 - PZT bonded on aluminum and steel beams.

The EMI technique was employed for various prototypes of line pipelines, aerospace and civil structures. However, because this method is relatively novel, its applications to real world structures are still rare.

In academia, methods based on EMI were proposed to monitor spot welded structural joints (Giurgiutiu et al. 1999), fatigue crack (Hoon et al. 2004, Xing et al. 2007), and bolted connections of pipeline systems (Park et al. 2003).

Several different types of patches can be used for the EMI method. The cost of each unit may vary between $10 to $200 depending on the material, roughness, manufacturer, etc. The unit to measure the parameters that are conventionally exploited in this methodology can cost between $16,000 (LCR meters) and $42,000 (impedance analyzers). However, in the last few years research groups, especially at Virginia Tech and Los Alamos Laboratories have developed circuitry units that cost few hundred dollars and that can be used in lieu of impedance analyzers.

5.4 LITERATURE REVIEW

5.4.1 Collins and Garlich (1997)

Collins and Garlich stated that the main mode of sign inspection is visual examination; hammers, scrapers, and mirrors on extended rods aid in this process. Other non destructive

techniques that may be used include: dye penetrant to locate and define the extent of cracks, magnetic particle or ultrasonic techniques to evaluate welds, ultrasonic thickness devices to measure the remaining thickness of members, and ultrasonic flaw detectors to examine anchor bolts. Although it is not truly NDE, drilling small holes in tubes to detect trapped water is also included in this list. Along with inspection methods, the authors also listed several common problems found during the inspection of sign structures. These include: cracked anchor bolts, loose nuts and missing connectors on anchor and structural bolts, cracked and broken welds, split tubes, plugged drain holes leading to debris accumulation and corrosion, internal corrosion of tubular members, poor fit up of flange connections with cracking and missing bolts, and structure overload.

5.4.2 NCHRP Report 469 (2002)

One of the outcomes of this study was the division of sign structures into Class A and Class B. Class A structures are those more susceptible to wind-induced fatigue damage and they should be inspected at least every four years. Class B should be inspected at least every eight years. The authors cite visual inspection as the main way to inspect cracks. This inspection should consist of close up or hands on view of the base, of the post, and the mast arm or truss to post connection. The rest of the structure may be inspected from the ground, however if evidence of cracks is noted they must be inspected more closely. Some NDE methods were also suggested for inspection. Like Collins and Garlich (1997), this report recommended magnetic particles or liquid penetrant as a means to detect cracks, but adds that these should only be used when a sound reason to suspect cracking exists.

Ultrasonic testing can also be used for crack detection. This report suggested that when an inspector notices a fatigue crack in the connection on one structure it is likely to late to repair that structure, but it may be practical to apply ultrasonic testing to similar connections in the same area in hopes of catching other cracks at a stage where they may be remediated.

5.4.3 Li (2005)

In this study, Li identified visual inspection as the primary mode of inspection, which can be carried out in combination with other NDE methods such as dye penetrant test, magnetic particle testing, or ultrasonic testing. Penetrant testing is inexpensive and can reliably find cracks on smooth surfaces. Magnetic testing can detect defects on and just below the surface, but its accuracy is not great when testing welded material. Ultrasonic testing an also detect surface and subsurface cracks, but unlike the previous three it requires a high level of inspector training thus making it more expensive.

5.4.4 Rizzo et al. (2008)

In Rizzo et al. (2008) the results of a survey sent to the DOT Departments nationwide determined that the methods of visual inspection, dye penetrant, magnetic particle, and ultrasonic testing are currently used for inspecting sign structures. The survey has been partially reproduced in Ch. 3 and, for convenience, is synthesized in this section.

Because no federal regulation mandates the inspection of sign support structures at a specified interval, the study determined a common trend among state DOTs in terms of frequency of inspection.

The survey determined the inspection policy currently in use. Such policies include: 1) inspection frequency based the type of sign being inspected (WA), 2) routine inspections on one cycle and more in depth inspections on another cycle (NY and PA12); 3) structures age and material (IL, MO, PA4, and PA8). These last two reasons are why we assume that New York checked both once/year and once every two years. Five out of seven PA districts reported a three year inspection cycle. PA district 9 inspects structures in accordance with SOL 431-04-03, now incorporated into PennDOT, Pub.238. After a cantilever with single pole carrying traffic signs failed, a number of such structures were re-inspected. The last regular inspection cycle occurred in 2005.

Seven DOTs inspect some structures on a four year cycle, five DOTs follow a five year cycle. The state of Washington inspect cantilevers with only four anchor bolts every four years, monotube cantilevers every eight years, and monotube bridges every ten years, and the remaining structures every five years. In the state of Illinois "*if no deficiencies are found the structure is placed in a five year detailed inspection cycle. If minor cracks are found in welds and internal members, the structure is placed on a three year detailed inspection cycle with a ground inspection cycle in eighteen months. If there are numerous cracked welds and broken members the structure is placed in annual inspection cycle until replaced or repaired*". Missouri noted that they are in a three year contract to inspect all of their sign structures and will use the results of these inspections to plan future inspection intervals. Finally the province of Alberta reported an inspection cycle of 21 months.

The survey confirmed that the four methods of visual inspection, liquid penetrant, magnetic particle, and ultrasonic testing are currently considered for sign support structures.

All DOTs use visual inspection. Arkansas, Missouri, and Tennessee do not use any inspection method other than visual inspection. In most cases liquid penetrant and magnetic particle testing are used as an extension of visual inspection. NJ-DOT reported that liquid penetrant is used if a crack is suspected, while NY and WA DOTs use it if a crack is visually located, i.e. if potential cracks have been located visually. Wisconsin DOT uses all three methods if a crack is suspected.

Liquid and magnetic particle are used: 1) "*to determine the limits of cracked welds or internal members that can not be visually determined when recommended by the Bureau of Bridges & Structures after a review of the structure's inspection report*" (IL_DOT), 2) if crack is suspected (CT_DOT and IA_DOTs), and 3) if a defect is found (WY_DOT). PA 9 reported that liquid penetrant are used if visual signs of cracks in paint or protective coating or cracks in welds and/or steel are visible. In the aftermath of the failure of a cantilever with single pole carrying traffic signs, magnetic particle was used to inspect all of the pole/base plate welds of all of the similar signs.

Ultrasonic Testing is most often used to test the anchor bolts at the base of the structure. Connecticut DOT has reported that UT is used to inspect all anchor bolts in tension on cantilever sign supports. Kansas, Iowa, New Jersey, and New York DOTs use UT to determine length and to detect the presence of defects in anchor bolts. It is estimated that the inspection time is five minutes per bolt. The state of New York has reported that UT testing

is used to routinely determine the thickness at the base of poles. This inspection can be conducted using ultrasonic thickness gauge and it can be extended to determine internal corrosion as well.

NY-DOT uses methods like hammer-based impact sounding as a part of regular inspection of loose foundation bolts and ultrasonic thickness gauging to routinely determine the thickness of the base of the pole. Once NY_DOT hired a company to do digital radiograph imaging on one particular structure.

The survey attempted to quantify the amount of personnel involved in the inspection process and therefore to estimate the cost of labor associated with each inspection. Most DOTs (67%) use two people for all types of inspections, however all the numbers given vary between needing one and five people to do the job. For instance, the Connecticut DOT has indicated that for visual inspection (conducted on every sign support), liquid penetrants, and magnetic particle (conducted only if crack is suspected) two inspectors are involved. For ultrasonic testing, used on all anchor bolts in tension on cantilever sign supports, one inspector and one technician are involved. The DOT that specified five people (PA District 4) included the people needed to aid in traffic control.

5.5 COST ESTIMATE

To provide a cost-estimate of the inspection methods several NDT companies were contacted. It was asked to estimate the cost to inspect a sign support structure like the one modelled in the fatigue analysis. Figure 5-7 was provided and it was requested to fill Table 5-1. A "note" column was provided in order to receive comments on the best method to detect critical damage such as corrosion, cracks at welds, surface cracks, cracks at foundations, loose bolts and fixtures.
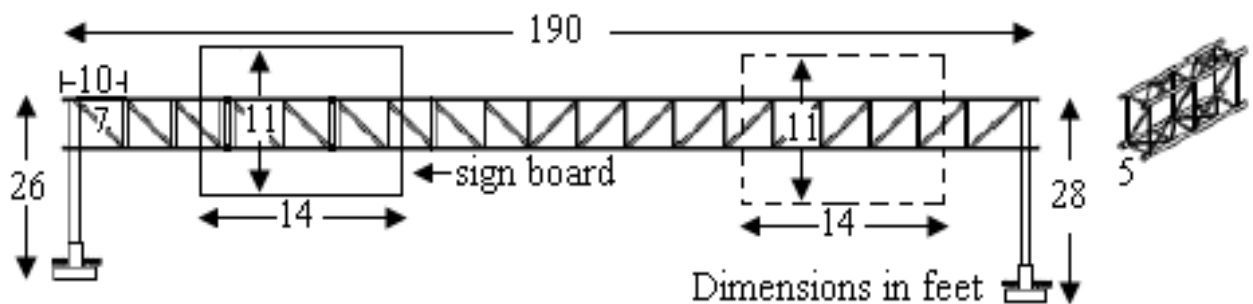
Figure 5-7. Envelope of the sign structure considered for the inspection cost-estimate.

Fourteen responses, i.e. about 20% of the contacted companies, were received. Each of the following tables reports on a specific NDT method and lists the response from each company, arbitrarily identified with a progressive number. It must be noted that the opinion expressed in Table 5-2 are solely those of the responders and not necessarily those of this report's authors.

Inspection method	Equipment cost [min –Max range]	Service cost (if provided)	Labor hours required for service	Note
Acoustic emission (transducers, software etc)				
Eddy Current (Analyzers, software, etc)				
Guided ultrasonic waves (Analyzers, oscilloscopes, transducers, etc)				
Liquid penetrant (dyes, liquids etc.)				
Magnetic particle (magnaflux products, magnetic materials, etc)				
Ultrasonic testing (Analyzers, oscilloscopes, transducers, software, etc)				
Visual inspection (Boroscope, Fibrescope, Videoscope, etc)				
X-rays				

Table 5-1. Sample table submitted to NDT companies to inquire about inspecting a sign support like the one shown in Fig. 5-7.

Table 5-2. Summary of responses obtained from NDT companies.

Company #	Acoustic Emission			Note
	Equipment cost	Service cost	Time, labor hours	
6	See note 1			
8	$27-$30k 8-channel Sensor Highway II	$11k for 1st month. For each month after $4k	Two days to install $1850/day.	One month should be done to allow for wind loading cycle.
10	$50-100k			Reliability is questionable
12				Acoustic Emission testing of structures are basically monitoring techniques for Dynamic structures. With regards to its application in the transportation industry, it is usually applied to large steel bridges, and may not be a cost effective inspection for support structures. Cost of AE set up with equipment is minimum $ 200K.
14		$400/hr		Two technicians

	Eddy Current			
Company #	Equipment cost	Service cost	Time, labor hours	Note
1	$8k – $15 k	$250/day	$5,600	2 men for 5 days @ $70.00/day
3	> $8,325			
4	$10k – $11.5 k			Only for surface crack detection on weld surface and around weld surface
6	See note 1			
10	$25-50k			N/A
12				EC is not usually applied to steel structures. Other NDT methods such as Magnetic Particle inspection or ACFM (Alternate Current Field Measurement) are applied.
14		$160/hr		One technicians

	Guided Ultrasonic Waves			
Company #	Equipment cost	Service cost	Time, labor hours	Note
6	See note 1			
8	$30k			
10	$250k			Reliability is questionable
12				See note 4
14		$520/hr		Two technicians

	Liquid Penetrant			
Company #	Equipment cost	Service cost	Time, labor hours	Note
1		$700 for materials	$6,720	2 men for 7 days @ 60.00/hour
3	~$900			
5	$200 - $400	$5,000	4-5 days plus travel & expenses	
6	$200 - $1,000	See note 3	See note 2	See note 3
10	$200	$600/day		Low cost for surface inspection
12	$ 750	$ 1000	50 man-hours	Either Liquid Penetrant or Magnetic Particle methods are employed for steel structures. Usually, the welds on these structures are inspected by these methods.
13	UV Lamp $559			Penetrant dyes are not supplied
14		$800/hr		One technician

	Magnetic Particles			
Company #	**Equipment cost**	**Service cost**	**Time, labor hours**	**Note**
1	$2k – $4 k	$70/day	5 days. $4,800	2 men for 5 days @ $70.00/ hour
3	~$1k			
5	$500 - $1,000	$5,000	4-5 days plus travel & expenses	
6	$200 - $1,000	See note 3	See note 2	See note 3
10	$ 500	$600/day		Very reliable and fast for surface flaw detection
12	$ 2500	$1000	50 man-hours	Note 5 and 7: Either Liquid Penetrant or Magnetic Particle method are employed for steel structures. Usually, the welds on these structures are inspected by these methods.
14		$80/hr		One technicians

	Ultrasonic Testing (Bulk Waves)			
Company #	**Equipment cost**	**Service cost**	**Time, labor hours**	**Note**
1	$4k – $15 k	$70/day	5 days. $4,800	2 men for 5 days @ $70.00/ hour
2	$695 - $ 2295			Wall/coating thickness measurement
3	$8k-$17.8k			
5	$8k - $12k	$5,000	4-5 days plus travel & expenses	
6	See note 1	See note 3	See note 2	See note 3
8	$8k - $15k			
10	$8k - $10k	$1500/day		Volumetric weld inspection. Dependent on operator skill
12	$ 15000	$ 2500	40 man-hours	See note 5
14		$140/hr		One technician

	Visual Inspection			
Company #	**Equipment cost**	**Service cost**	**Time, labor hours**	**Note**
1			5 days. $1,920	2 men for 2 days @ $70.00/ hour
3	$1,000 - $2,100			
5	$1,000 - $3,000	$3,000	2-3 days plus travel & expenses	Ballpark estimates of equipment and inspection costs and times
6	$3k - $15k	See note 3	See note 2	See note 3
10		$800/day		
12		$ 2000	30 man-hours	Performed by AWS Certified Welding Inspector on all welds and structures.
14		$80/hr		One technicians

	X-rays			
Company #	Equipment cost	Service cost	Time, labor hours	Note
1	$60k – $90 k	$2k / week	3 weeks. $63k	3 men for 3 weeks @ $175.00/hour
6	See note 1	See note 3	N/A	N/A
9	~ $30k			
10	$50k (with truck)			Volumetric inspection. Requires barricading area
11	$211k - $260k	Does not provide inspection services at this time	See note 6	2-3 people.
12	$ 50000	$ 5000	60 man-hours	See note 5
14		$150/hr		Two technicians

Note #1. Company#6 does not typically sell off the shelf, hand held equipment, however they sell custom NDT systems and chemicals for Dye Penetrant and Magnetic Particle Inspections.
Note #2. These inspections would / could be included in the sign support structure.
Note # 3. This inspection project would / could include the use of Eddy Current to check corrosion, (surface cracks) deterioration, Liquid Penetrant and/or Magnetic Particle for structure surfaces or weld crack inspection and Ultrasonic for sub surface (corrosions) structure and weld inspection. Ultrasonic is a good alternative to x-ray in the field because it requires no radiation or stopping of traffic, it is compact, operation is less expensive, and it yields instant results. We would / could also include AWS visual weld inspection and bolt inspection / replacement and torquing. This appears to be a 2 technician project and would require the use of a basket type man-lift. Rates of $75./hr for straight time, up to 40 hrs. / wk., Mon. – Fri. $95./hr. over 8 hrs /day, 40 hrs./wk.. Sundays - $120./hr.. Travel time, lodging, mileage, per diem, and any equipment rental would be additional.
These inspections are typically governed by ASNT. With regard to purchasing equipment and performing these inspections internally, one would need to have employees meet these minimum requirements per ASNT- Technician Requirements: Dye Penetrant: 32 hours classroom training plus 400 hours OTJ (on the Job) training under the supervision of a level II/III inspector. Each of the inspection methods would require a governing approved written procedure by an ASNT representative.
Note # 4. These techniques are not applied for steel structures.
Note # 5. Either Ultrasonic or X-ray (Usually Gamma Radiography) are applied for detection of subsurface defect detection of welds. This inspection is usually not 100% on all welds but may be limited to a percentage of the length of welds.
Note # 6. Typical setup time is one hour. Inspection time is contingent upon requirements, the size of area of interest, and the technique required for acceptable results.

5.6. SUMMARY AND CONCLUSIONS

This chapter reviewed the main NDT methods used by State DOTs and private companies to inspect sign support structures. Visual inspection is by far the most used method. Other techniques such as liquid penetrant, magnetic particle, and/or ultrasonic testing are adopted only if damage is located or suspected.

The difference between inspecting (time-based maintenance) and monitoring (condition-based maintenance) was introduced to discuss other approaches. Such approaches,

successfully used in academia and/or the industry, show potential for inspecting/monitoring sign structures.

Defects	Current methods	Potential NDE/SHM methods
Cracked welds in overhead truss	VIM, PT, MPI	EMI, GUW, X-ray, EC
Fatigue Cracks at the arm to column weld	PT, MPI	AE, EMI, EC, GUWs, Microwaves[2]
Painted tubular steel end supports deteriorating from the inside out	VIM, MPI	GUW
Delamination of concrete foundations	VIM	Impact-echo
Loose sign connectors	VIM	EMI
Loose or missing bolts at various locations	VIM	EMI
Cracks in cast base plate connectors	VIM, PT	AE, EC, EMI, X-ray
Cracks in truss diagonal chord welds	VIM, PT, MPI	AE, EC, EMI, X-ray
Fatigue on bolts at the base	UT	EMI
Corrosion on bolts at base	UT	EMI
Internal corrosion of galvanized structures	PT	GUWs, X-ray
Corrosion of anchor bolts within grout pad	UT	X-ray
Bolted connection between mast and pole	VIM	EMI
Surface cracks	VIM, UT	EC, EMI, X-rays

Table 5.3 – Principal defects observed in sign structure support, and current and potential NDT/SHM techniques to detect them.

Thus, the principles and the advantages/disadvantages of eddy current testing, the guided waves approach, and EMI were discussed. The first one is potentially feasible to inspect surface and near-surface defects. The method of guided ultrasonic waves can be used either for damage detection inspection or for damage detection monitoring of any tubular component. Finally the third method is suitable for monitoring the approach of parts like bolts and tubular components.

To summarize, Table 5.3 reports the more relevant defects in sign support structures, the NDT methods are currently used to detect them, and the potential technology that can be alternatively used. Finally, a cost-estimate of each NDT technique discussed in this chapter was provided based on the responses received from companies working in the area of NDT.

---

[2] Not discussed here. See for instance [Ju 2001]

CHAPTER 6: LABORATORY TESTS

6.1 THE STRUCTURE

One real-size sign support structure was tested at the University of Pittsburgh. The structure was part of a variable message sign support structure located over I-80 Eastbound, one mile West of the junction with I-81 in Pennsylvania, USA in Penn DOT District 4-0. A photo of the structure in service is shown in Fig. 6.1 while its location is illustrated in Figs. 6.1b and 6.1c.

In May of 2006, a routine field inspection found two large cracks in two of the upper chords of this four chord truss. Cracks' positions on a truss are presented in Fig. 6.2. The structure was removed from service as a preventative measure. An investigation of the cause of the observed cracking, a forensic investigation, was conducted (Connor 2008). As a result, selected joints were requested by Robert J. Connor and Associates LLC for examination. Both cracked and uncracked joints were sent to the Bowen Laboratory of Purdue University in West Lafayette, IN for destructive examination.

The laboratory examination identified an additional crack in one of the connections. The results of the study suggest that the cracking was present when the structure was erected and no evidence of fatigue crack growth was observed on the fracture surface. The cracking is believed to be the result of Liquid Metal Embitterment (LME), a phenomenon resulting in brittle fracture of a usually ductile steel in the presence of liquid metal. The fractures likely initiated in the Zinc bath, but remained undetected until the recent field inspection. Upon finding the additional crack and after suspecting LME was the cause of the cracks, Dr. Connor suggested that Penn DOT perform more in depth inspection on all similar structures in the inventory (i.e., those truss structures carrying VMS structures of the same vintage) using dye penetrant and ultrasonic inspection. Since the third crack was not found during the original inspection, there was concern that other cracks may be present in other structures.

The center to center bearing span of the original truss was 17.4 m (58.5 ft), with the bearings located on the vertical support columns. A bolted field splice was located mid-span of the truss. The chord is made from ASTM A-53 steel.

One of the two trusses connected with bolts in the original structure was delivered at the University of Pittsburgh. Photos of the delivery are presented in Fig. 6.3.

The three-dimensional rendering of the truss and the dimensions is presented in Fig. 6.4a. The structure was accommodated at the Watkins-Haggart Structural Engineering Laboratory (Figs. 6.4b and 6.4c). The dimensions of the truss are reported in Fig. 6.4c and 6.4d.

(a)

(b)

(c)
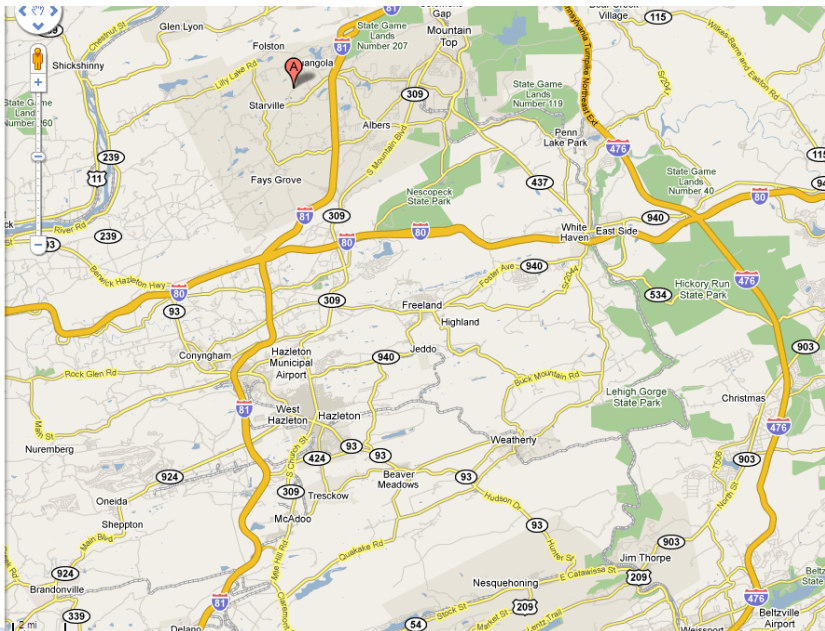
Figure 6.1 – (a) Photo of the sign support structure when in service. (b) Original location c) Original location (close up view).
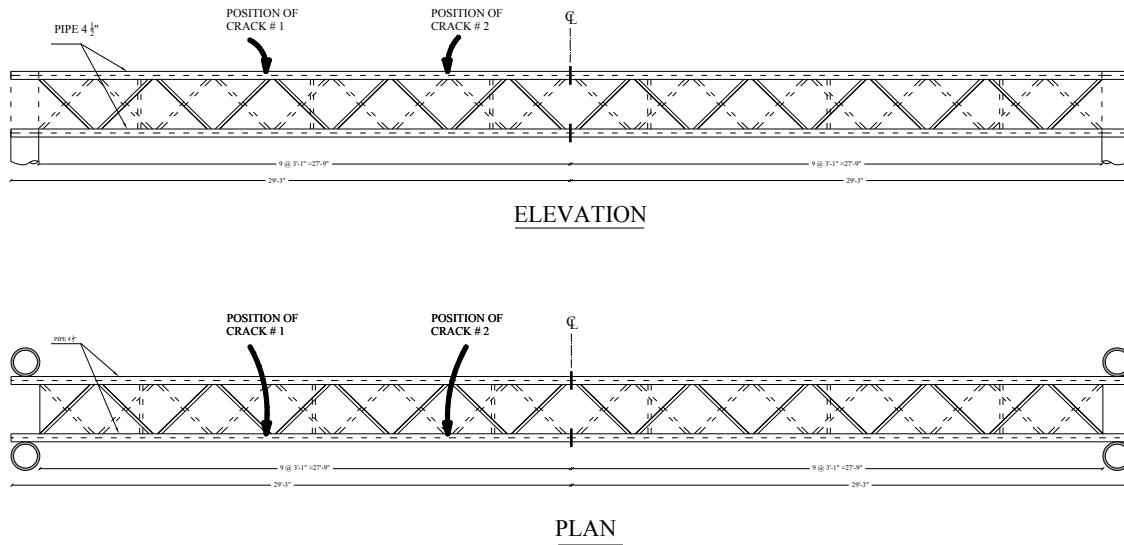
Figure 6.2 – Location of cracks found during the investigation conducted in Connor (2008).

Figure 6.3 – Delivering the truss at the University of Pittsburgh.

(a)

(b)

(c)

Outer diameter
114.3 mm

Thickness
8.6 mm

914.4mm

914.4 mm

(d)

939.8 mm

8458.2 mm

Figure 6.4 – (a) 3-D rendering of the truss. (b-c) Photo of truss set onto the supports. (d) Sketch and dimensions.

6.2 HARDWARE – SOFTWARE – SETUP

A static analysis was conducted by using finite element commercial code ANSYS to find the stresses of the truss subjected to a static load. The interested reader is referred to the publication

Zhu, P., Rizzo, P., and Tajari, M. (2010). Sensing Technology for Damage Assessment of Sign Supports and Cantilever Poles – Task 4, Year 2 Report, Pennsylvania Department of Transportation, Contract No. 519691-PIT 008, University of Pittsburgh.
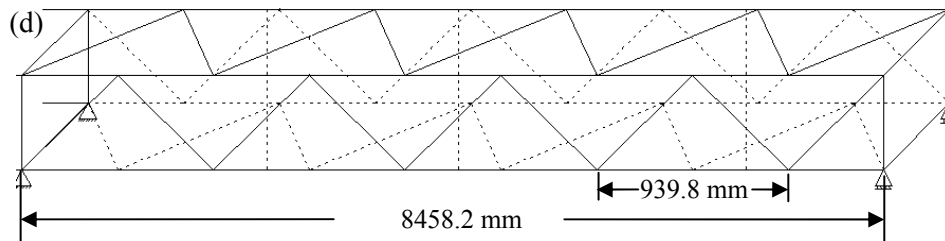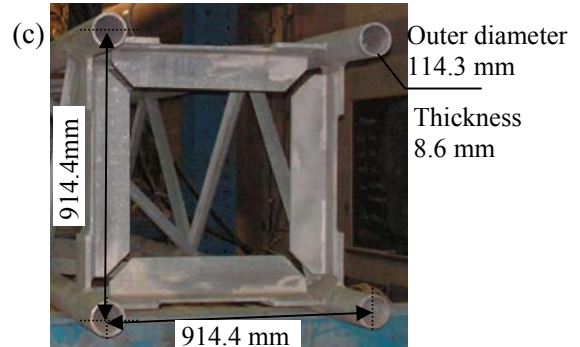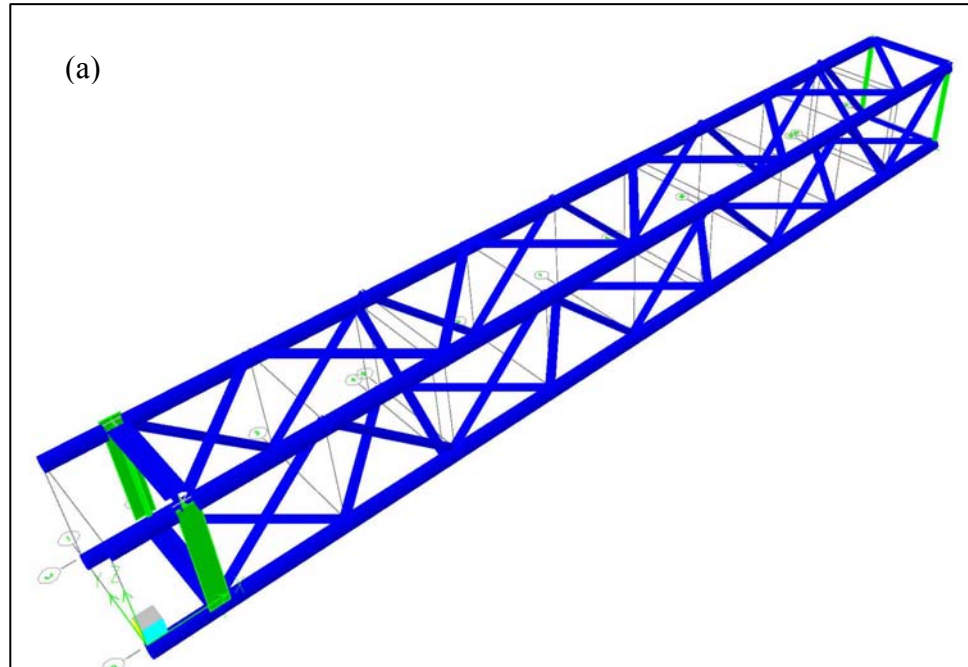
In this section the hardware and the software utilized in this study is described. The experimental setup is illustrated in the second part of the chapter.

6.2.1 The sensors

PKI-502-Navy type II PZT transducers (Model# PKI P/N SP0.330-0.330-0.120-502) from Piezo-Kinetics (http://www.piezo-kinetics.com) were employed in this study. The dimensions of the transducers were 0.33 in × 0.33in × 0.12in. The applied field voltage output of these transducers can be in through thickness or shear horizontal as shown in Fig. 6.5.
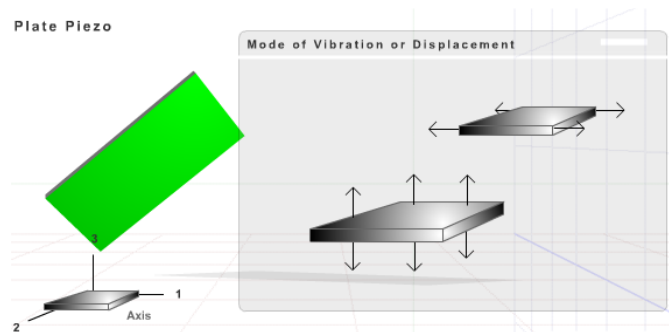
Figure 6.5 - Mode of vibration of the PZTs used in this study. Source: http://www.piezo-kinetics.com/21_plate_movie.htm

6.2.2 The Data Acquisition System

A National Instruments PXI unit running under LabView, integrated with a reed relay matrix switch module PXI 2530, and combined with TB 2643 and SCB 264X as terminal block, was employed for signal generation, detection, and acquisition.

For the guided waves excitation a 5-cycle, 10 V peak-to-peak sinusoidal toneburst, modulated with a Gaussian window was used. The detected signals were amplified 20 times by a linear amplifier, sampled at 10 MHz, averaged 10 times to increase the signal-to-noise ratio, and stored for post-processing analysis. A LabView program was designed to operate the switch so that every PZT could act as a transmitter or as a receiver. For instance, it will be seen that in Test 1 and Test 2, eleven transducers were used. For convenience these transducers were named S0, S1,…, S10. The switch module and the software was coded such that when PZT S0 was transmitting the toneburst, S1-S10 acted as sensors. Then PZT S1 was switched into an actuator and PZTs S0, S2-S10 acted as receivers. The operation was

repeated for every PZT. The program was designed such that the operator can select the number of cycles and voltage amplitude. In addition the program provides the flexibility to select the center frequency of the toneburst and to execute a frequency sweep between a lower and an upper limit selected by the operator.

To apply the EMI measurement, an electric circuit was designed and a second Labview program was created. The PXI acted as a function generator directing a 1 Volt, 50-cycles sinusoidal wave in the frequency range 50 - 500 KHz with frequency step equal to 0.5 KHz. More details of the circuitry and the mode of employment of the PXI to conduct the EMI measurements are provided in Chapter 8.

Photos of the hardware setup and of the software designed for both the GUW and the EMI studies are presented in Fig. 6.6. The front panel and the corresponding block diagram developed for the GUW measurements are presented in Fig. 6.6b and Fig. 6.6c, respectively. The Function Generator Parameter tab shown in this figure has the controls to select the following toneburst parameters: window functions; initial, final, and step of the desired frequency sweep; amplitude; repetition rate; and number of tonebursts per desired frequency.
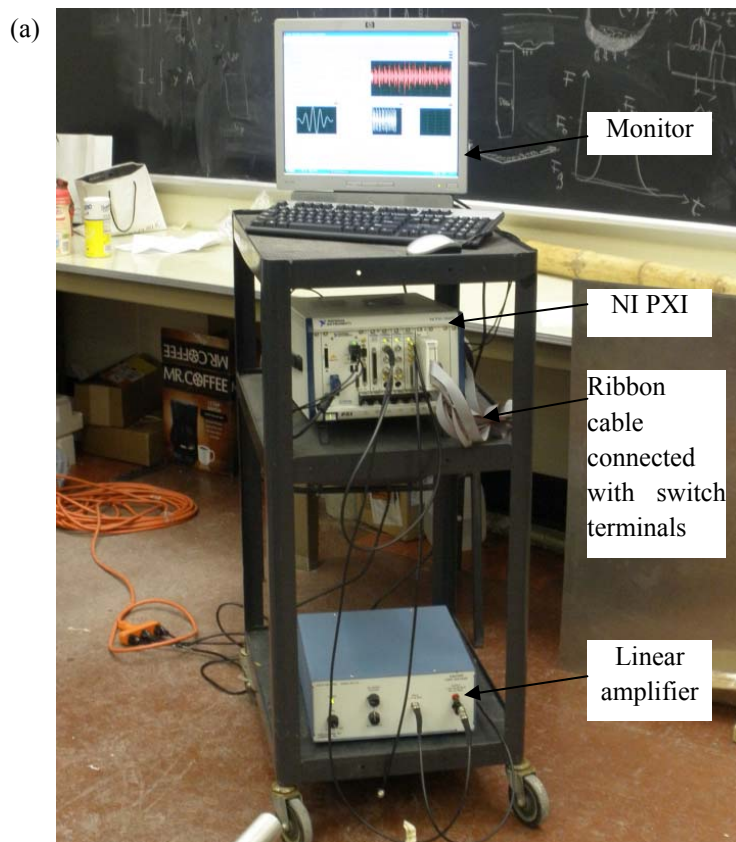
Figure 6.6 - (a) Hardware setup for the UWG. (b-c) LabView program front panel and block diagram created to control the GUW measurements. (d-e) LabView program front panel and block diagram created to conduct the EMI-based experiments.

(b)

(c)

(d)

(e)
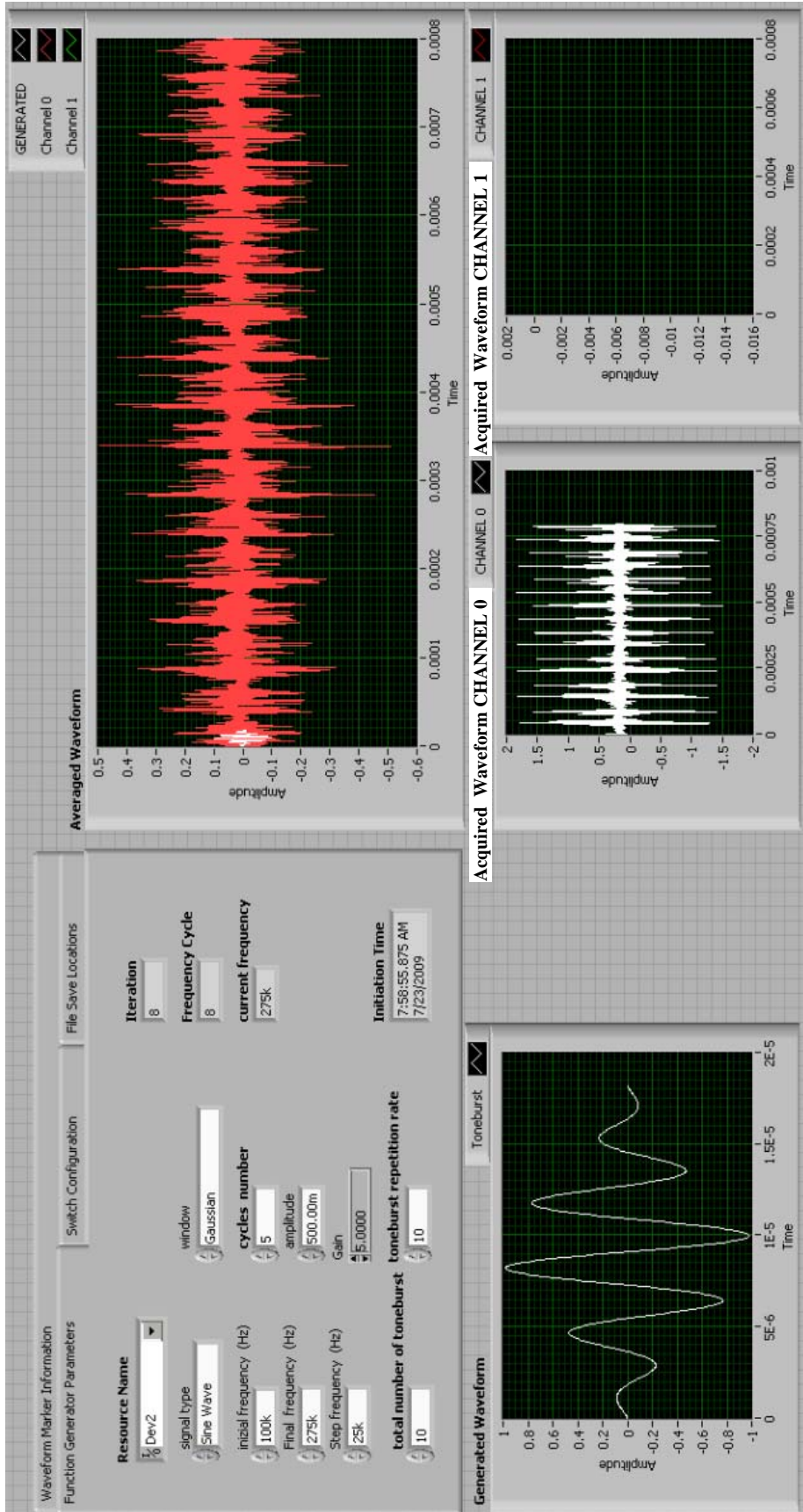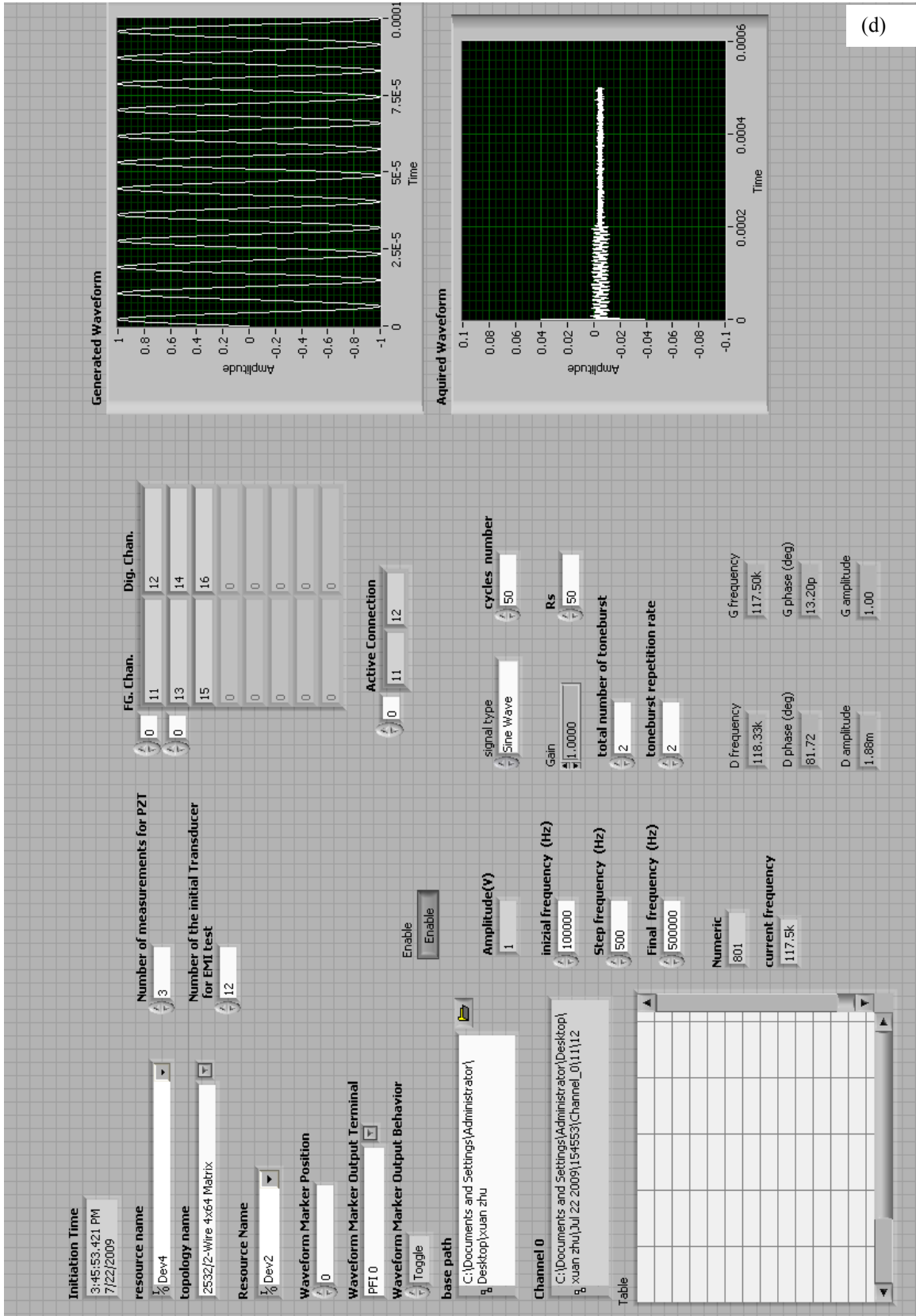
The front panel and the corresponding block diagram developed for the EMI measurement is presented in Fig. 6.6d and Fig. 6.6e, respectively. Some of the controls available in the panel are initial, final, and step of the desired frequency sweep; type of wave being generated; and number of cycles.

6.2.3 Test Protocol 1

For Tests 1 and 2, eleven of through-thickness PZTs were used for the generation and detection of GUW. The relative position of these eleven transducers on the truss is shown in Fig. 6.7a, and 6.7b, respectively. For convenience they are sequentially identified as S0, S1, …, S10. For illustrative purposes a close up view of PZT S5 and S1 is presented in Figs. 6.7c and 6.7d, respectively.

Three PZTs were used for the EMI method. The relative position of these three transducers, named EM1 EM2 and EM3, on the truss is shown in Fig. 6.8.
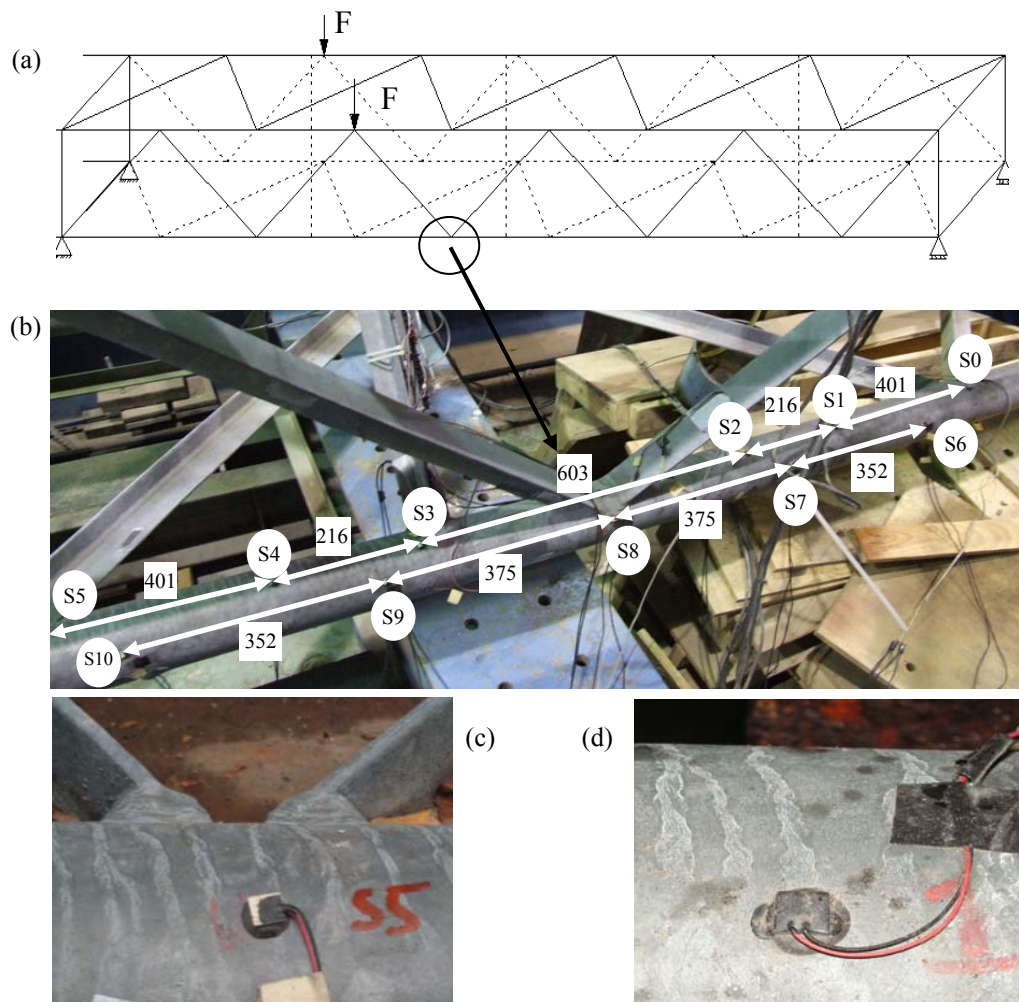
Figure 6.7 - (a) Sketch of the truss structure. (b) Location and relative distance of the PZTs. (c-d) Close up view of PZT S5 and S1. Dimensions in mm.
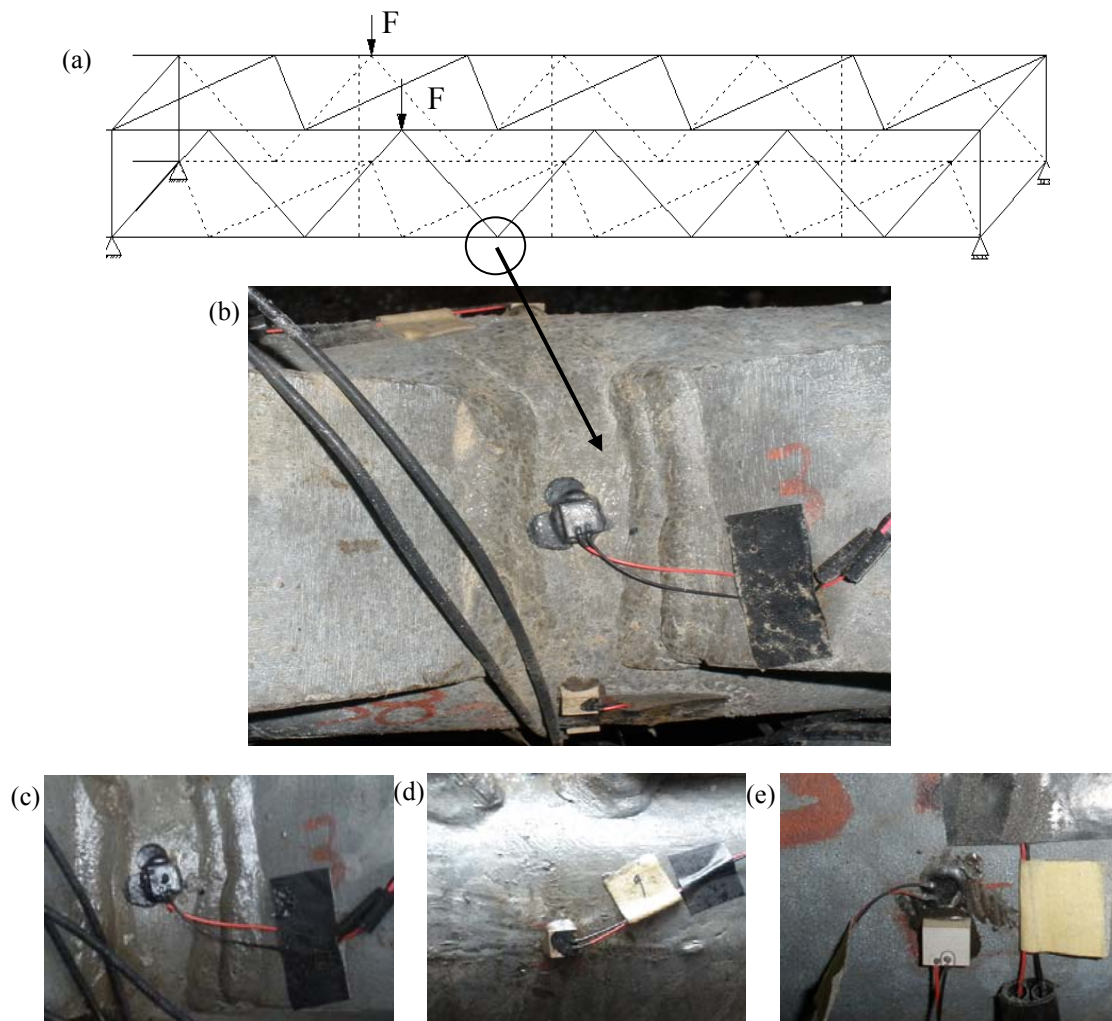
Figure 6.8 - (a) Sketch of the truss structure. (b) View from the top of the joint under investigation and PZT EM1. (c-e) Close up view pf for EM1 located between two joints (d) close up view for EM2 located inner side of the chord (e) close up view for EM3 located outer side of the chord.

To investigate the capability of GUWs and EMI to detect crack initiation and growth, two artificial notches were machined and progressively increased in size. The first one was devised near the weld toe at the joint illustrated in Fig 6.7a. The position and orientation of the notch are shown in Fig. 6.9a. The structure was subjected to 1 Hz sinusoidal cyclic load to simulate steady-state vibrations, induced by wind or traffic-induced gusts. The loading setup, shown in Fig. 6.9b, consisted of a 1290 mm-long steel beam that distributed over two joints the force generated by a hydraulic actuator. The load was cycled from 8.9 kN to 125 kN, resulting in a load range of 116 kN. During the first 25,000 load cycles, the notch size was artificially increased using a Dremel MultiPro Machine. The load history of the crack, i.e. the crack size as a function of the number of cycles, is presented in Fig. 6.9c. The area of the crack is approximately the length of the notch along the surface multiplied by the depth. Following every few thousand cycles the cyclic loading was paused and a static load of 66.7

kN was applied. Under this constant load, the size of the crack was measured and ultrasonic and EMI-related data from the PZTs were collected.

The square dots in Fig. 6.9c indicate the moment at which the crack size was measured. Measurements were also taken during the active cyclic loading. A total of 192 acquisitions were taken. The acquisition number (1-192) as a function of the number of load cycles is superimposed in Fig. 6.9c. It should be observed that the loading after 40,000 cycles had a limited effect on the crack growth. The modest scatter of the crack area value above 50,000 cycles is likely related to the variability of the manual measurement.
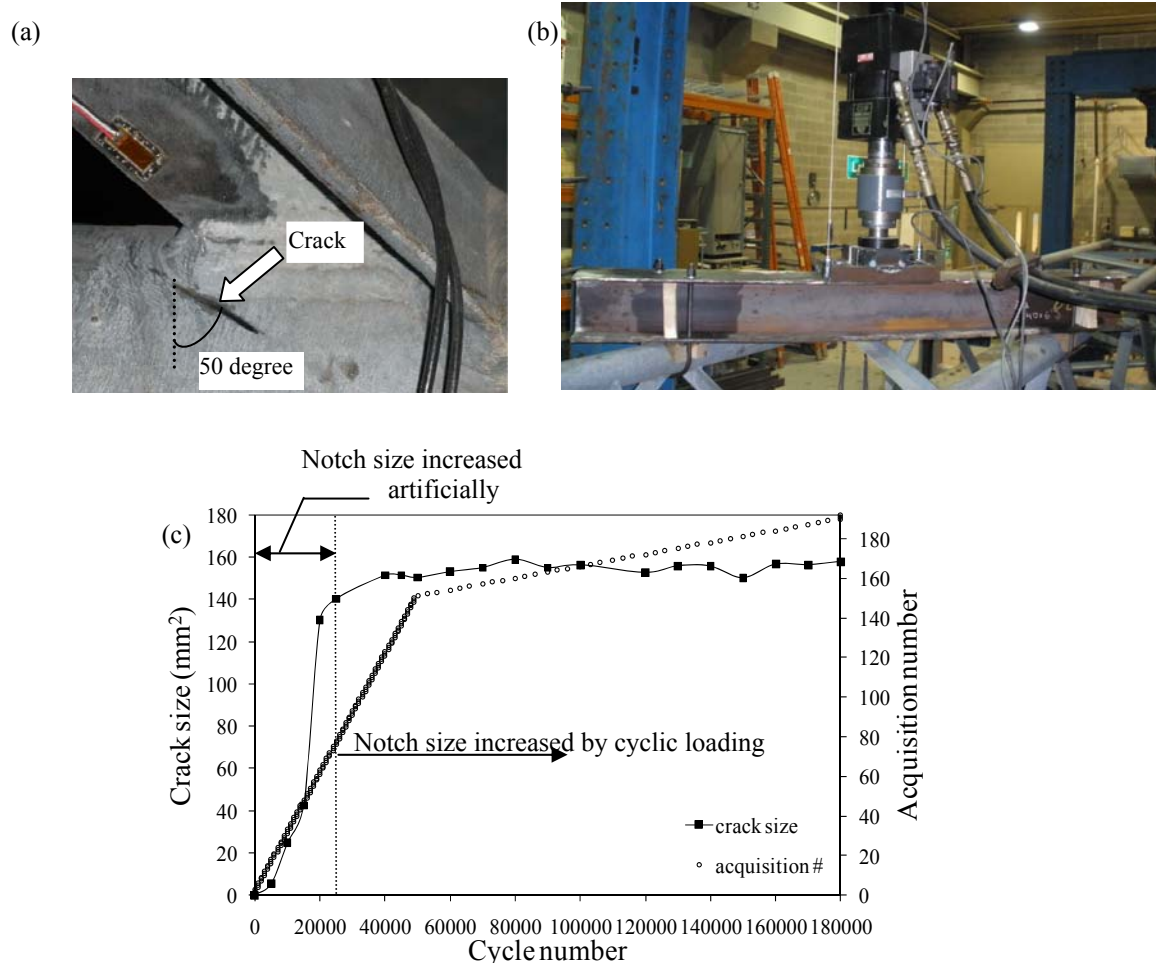
Figure 6.9 - (a) Close-up view of the artificial notch machined along the weld between the chord and one angular diagonal member. (b) Loading setup (c) Crack size and acquisition number as a function of cycle loading number.

6.2.4 Test Protocol 2

A second crack was devised near the weld toe of the second diagonal member concurring in the same joint as illustrated in Fig 6.10a. Similarly to Test 1, the crack was progressively machined and its position and orientation are shown in Fig. 4.6b. The same loading setup visible in Fig. 6.9b was adopted to apply a 1 Hz sinusoidal load ranging from 8.9 kN to 151.2 kN.

The load history of the crack, i.e. the crack size as a function of the number of cycles, is presented in Fig. 6.10c. As Test 2 followed Test 1, the cycle number count associated to Test 2 is considered starting at cycle 180,001. During the first 150,000 load cycles (cycles range 180,001-330,000) the notch size was artificially increased. Following every 5,000 cycles, the dynamic loading was paused and a static load of 80 kN was applied. Under this constant load, the size of the crack was measured and data from the PZTs were collected. The square dots in Fig. 6.10c indicate the moment at which the crack size was measured. Measurements were also taken during the active cyclic loading. A total of 124 acquisitions were taken. The acquisition number (193-316) as a function of the number of load cycles is superimposed in Fig. 6.10c. The modest scatter of the crack area value above 330,000 cycles is likely related to the variability of the manual measurement.

For both tests, the size of the notch was estimated by inserting a small piece of paper inside the notch and penciling the contour along the external surface of the chord. It was assumed that the internal part of the paper was adherent to the internal portion of the crack. Then the area under the penciled contour was measured. It is acknowledged that this approach might have some degree of inaccuracy.
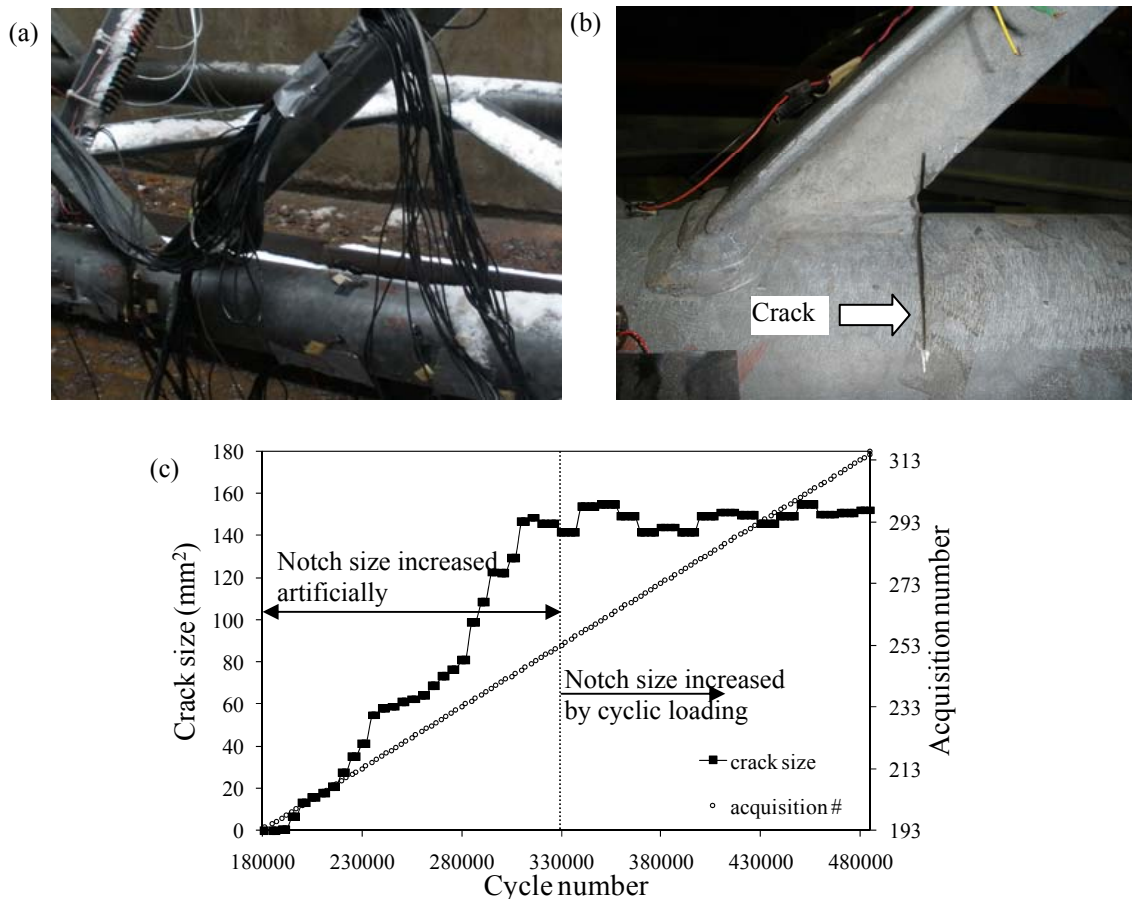
Figure 6.10 - (a) Close-up view of the joint where artificial notch was machined (b) the artificial notch along the weld between the chord and one angular diagonal member. (c) Crack size and acquisition number as a function of cycle loading number. 101

6.2.5 Test Protocol 3: Environmental Test

In practical SHM applications, environmental factors such as temperature, humidity, and electromagnetic inference may affect the performance of the damage detection algorithm. Any temperature variation, for instance, slightly changes the geometric and mechanical properties of the structure. If sensors are used, the properties of the sensors and of the adhesive utilized to bond them to the structure may also change due to temperature or moisture. If the sensors are made by piezoelectric crystals, the piezoelectric coefficients and the dielectric permittivity terms are both temperature-sensitive. Finally the presence of snow or rain changes the boundary conditions around the structure and this may change the physical characteristics of the nondestructive method being used.

If the propagation of guided waves is being used for SHM purposes, all the factors mentioned above may contribute to the variation of wave velocity and wave distortion. Thus, any variation of the wave energy characteristics due to environmental factors might shadow any effect associated with the presence of damage, or conversely may produce the presence of false positives.
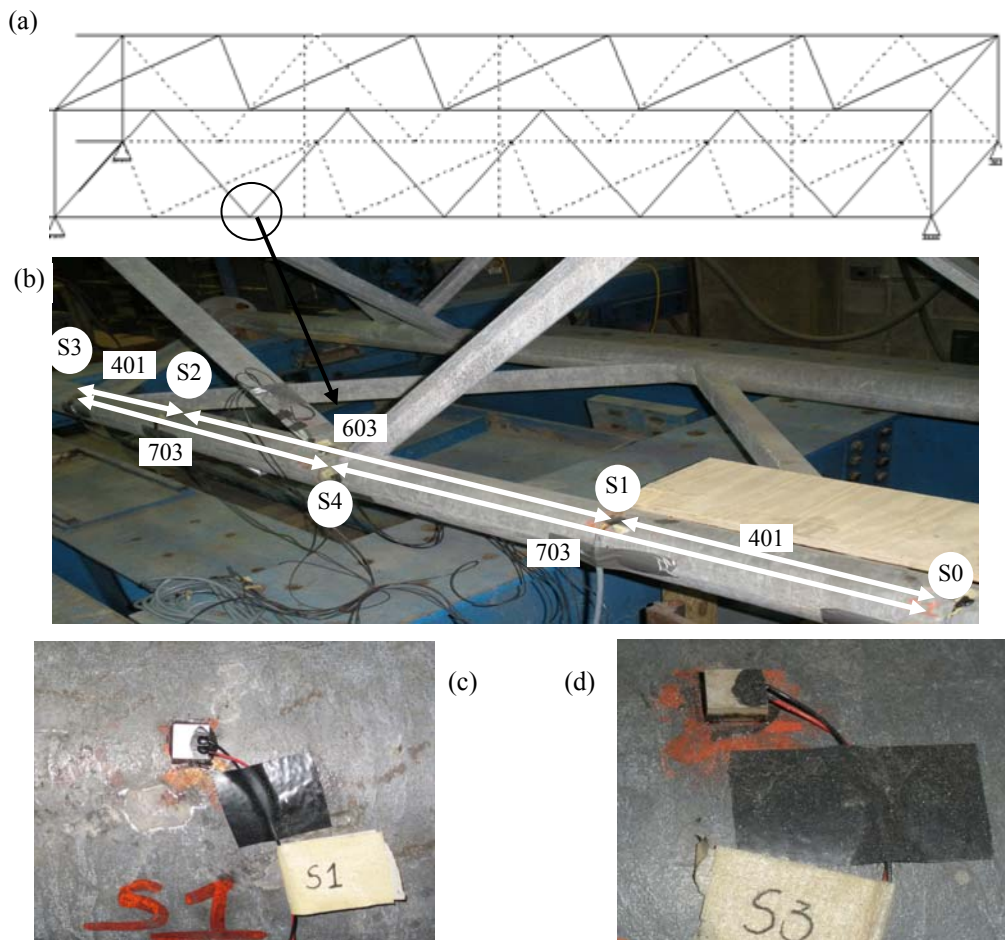
Figure 6.11 - (a) Sketch of the truss structure. (b) Location and relative distance of PZTs S0,…,S4. (c) Close up view of PZT S1. (d) Close up view of PZT S3. Dimensions are expressed in mm.

To assess the role that environmental conditions play on the SHM of the truss structure being investigated a third experiment was conducted at Pitt's WHSEL. With the same aim, a field test was executed and will be discussed in Chapter 9.

The welded joint under observation is circled in Fig. 6.11a. It can be remarked that in this third test, the horizontal chord under investigation was the one opposite to the chord monitored in Tests 1 and 2. Therefore the joint under investigation was close to the splice that served to connect this truss to the truss studied in Connor (2008).

Five PZTs in shear displacement were used for the generation and detection of GUW. The relative position of these five transducers on the truss is shown in Fig. 6.11b. The transducers were named as S0, S1…S4. For illustrative purposes a close up view of PZT S5 and S1 is presented in Figs. 6.11c and 6.11d, respectively.

A sixth PZT was attached in between the diagonal members converging into the joint and serve to evaluate the effect of temperature and boundary conditions on the EMI measurement. The relative position of the transducer, named EM1, on the truss is shown in Fig. 6.12. Unfortunately, this PZT malfunctioned after few measurements and its role will not be discussed in this report.

In this third experiment, three control variables were considered: temperature, boundary condition and damage. Eighty-five measurements were taken under different combinations of these parameters.
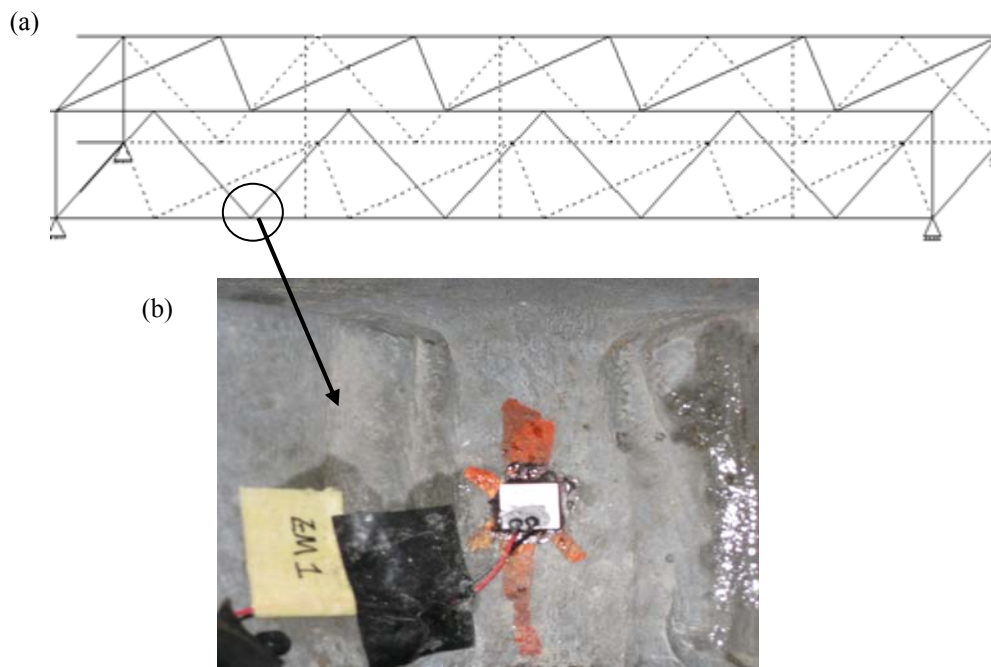
Figure 6.12 - (a) Sketch of the truss structure. (b) View from the top of the joint under investigation and PZT EM1.

As the experiment was conducted during winter the temperature was controlled by bringing the truss inside the laboratory or leaving it outside in the lab's pit. During internal measurements, the temperature was controlled by regulating the heating system. The temperature was measured attaching a portable thermocouple to the structure.

The boundary condition was varied by exposing the truss to snow or rain precipitation. When left inside, the structure was tested under dry conditions or under melting snow that was brought from the outside. To raise the temperature of the material a heat gun was used and the best efforts were made to make the chord's temperature along the wave paths as uniform as possible.


Figure 6.13 - (a) Close-up view of the artificial notch machined along the weld between the chord and one angular diagonal member. (b) Close-up view of enlarged crack. (c) Snowing condition.

Finally, the truss was monitored under three different structural conditions: pristine, crack, and enlarged crack. The enlarged crack was as twice as large. The defect was devised near the weld toe at the joint illustrated in Fig. 6.12a and 6.13a. As shown in Fig. 6.14a and 6.14b, the crack consisted of a notch oriented perpendicular to the orientation of the chord. The photo in Fig. 614c shows, instead, the measurement conducted while the structure was exposed to snow.

The experimental setup configuration is presented in Table 6.1 where the temperature of the chord, the boundary conditions (dry, snow, melting snow) and the damage level are reported.

Measurement #	Temp C	Boundary	Inside/outside	Damage
1	17.7	dry	i	pristine
2	17.7	dry	i	pristine
3	17.7	dry	i	pristine
4	17.7	dry	i	pristine
5	17.7	dry	i	pristine
6	17.7	dry	i	pristine
7	17.7	dry	i	pristine
8	17.7	dry	i	pristine
9	17.7	dry	i	pristine
10	17.7	dry	i	pristine
11	6.7	melting snow	i	pristine
12	6.7	melting snow	i	pristine
13	6.7	melting snow	i	pristine
14	6.7	melting snow	i	pristine
15	6.7	melting snow	i	pristine
16	6.7	melting snow	i	pristine
17	6.7	melting snow	i	pristine
18	6.7	melting snow	i	pristine
19	6.7	melting snow	i	pristine
20	6.7	melting snow	i	pristine
21	8.2	dry	i	pristine
22	8.2	dry	i	pristine
23	2	dry	o	pristine
24	2	dry	o	pristine
25	2	dry	o	pristine
26	2	dry	o	pristine
27	2	dry	o	pristine
28	2.7	dry	o	pristine
29	2.7	dry	o	pristine
30	2.7	dry	o	pristine
31	2.7	dry	o	pristine
32	2.7	dry	o	pristine
33	0.2	snow	o	pristine
34	0.2	snow	o	pristine
35	0.2	snow	o	pristine
36	0.2	snow	o	pristine
37	0.2	snow	o	pristine

38	0.2	snow	o	pristine
39	0.2	snow	o	pristine
40	0.2	snow	o	pristine
41	0.2	snow	o	pristine
42	0.2	snow	o	pristine
43	-2	snow	o	pristine
44	-2	snow	o	pristine
45	-2	snow	o	pristine
46	-2	snow	o	pristine
47	-2	snow	o	pristine
48	6.5	dry	i	pristine
49	6.5	dry	i	pristine
50	22	dry	i	pristine
51	22	dry	i	pristine
52	17.2	dry	i	damage 1
53	17.2	dry	i	damage 1
54	22	dry	i	damage 1
55	22	dry	i	damage 1
56	3	melting snow	i	damage 1
57	3	melting snow	i	damage 1
58	3	melting snow	i	damage 1
59	3	melting snow	i	damage 1
60	3	melting snow	i	damage 1
61	3	dry	i	damage 1
62	3	dry	i	damage 1
63	3	dry	i	damage 1
64	3	dry	i	damage 1
65	3	dry	i	damage 1
66	3	dry	i	damage 2
67	3	dry	i	damage 2
68	3	dry	i	damage 2
69	3	dry	i	damage 2
70	3	dry	i	damage 2
71	0.3	melting snow	i	damage 2
72	0.3	melting snow	i	damage 2
73	0.3	melting snow	i	damage 2
74	0.3	melting snow	i	damage 2
75	0.3	melting snow	i	damage 2
76	10	dry	i	damage 2
77	10	dry	i	damage 2
78	10	dry	i	damage 2

79	10	dry	i	damage 2
80	10	dry	i	damage 2
81	22	dry	i	damage 2
82	22	dry	i	damage 2
83	22	dry	i	damage 2
84	22	dry	i	damage 2
85	22	dry	i	damage 2

Table 6.1 - Experimental setup configuration for Test 3.

6.3 DIGITAL SIGNAL PROCESSING

6.3.1 GUW-related Signal Processing Algorithm

The overall SHM algorithm implemented in this study for the GUW study is illustrated in the flowchart in Fig. 6.14. Among all the actuator-sensor pairs activated by the NI-switch, only a selected number of waveform paths were examined and presented in this report. For each of the selected paths, all the time waveforms acquired during the tests were analyzed.
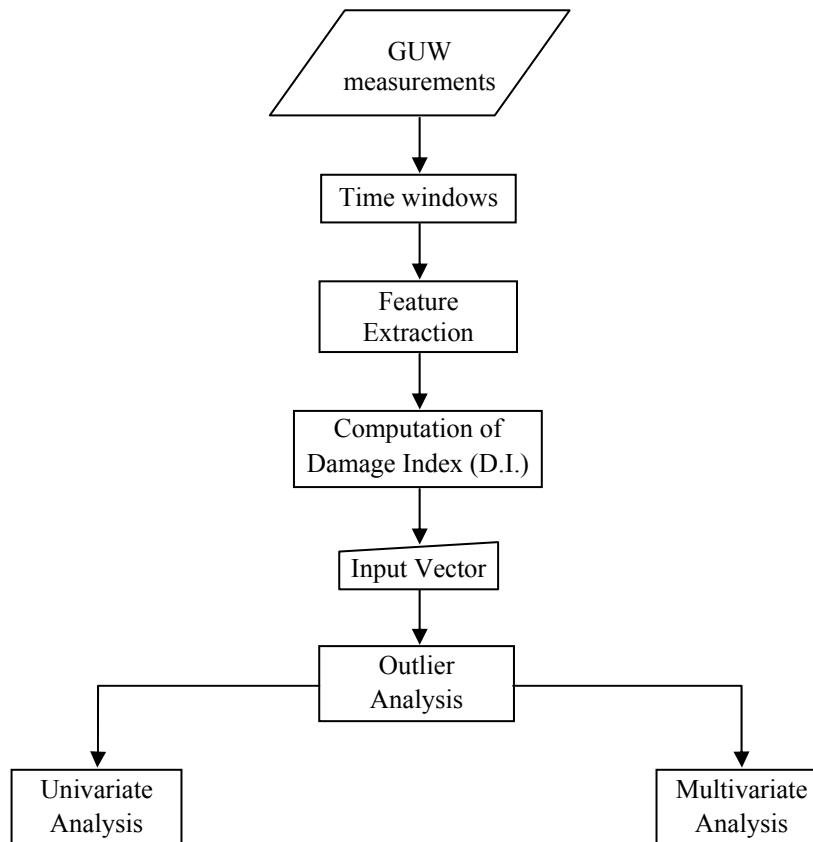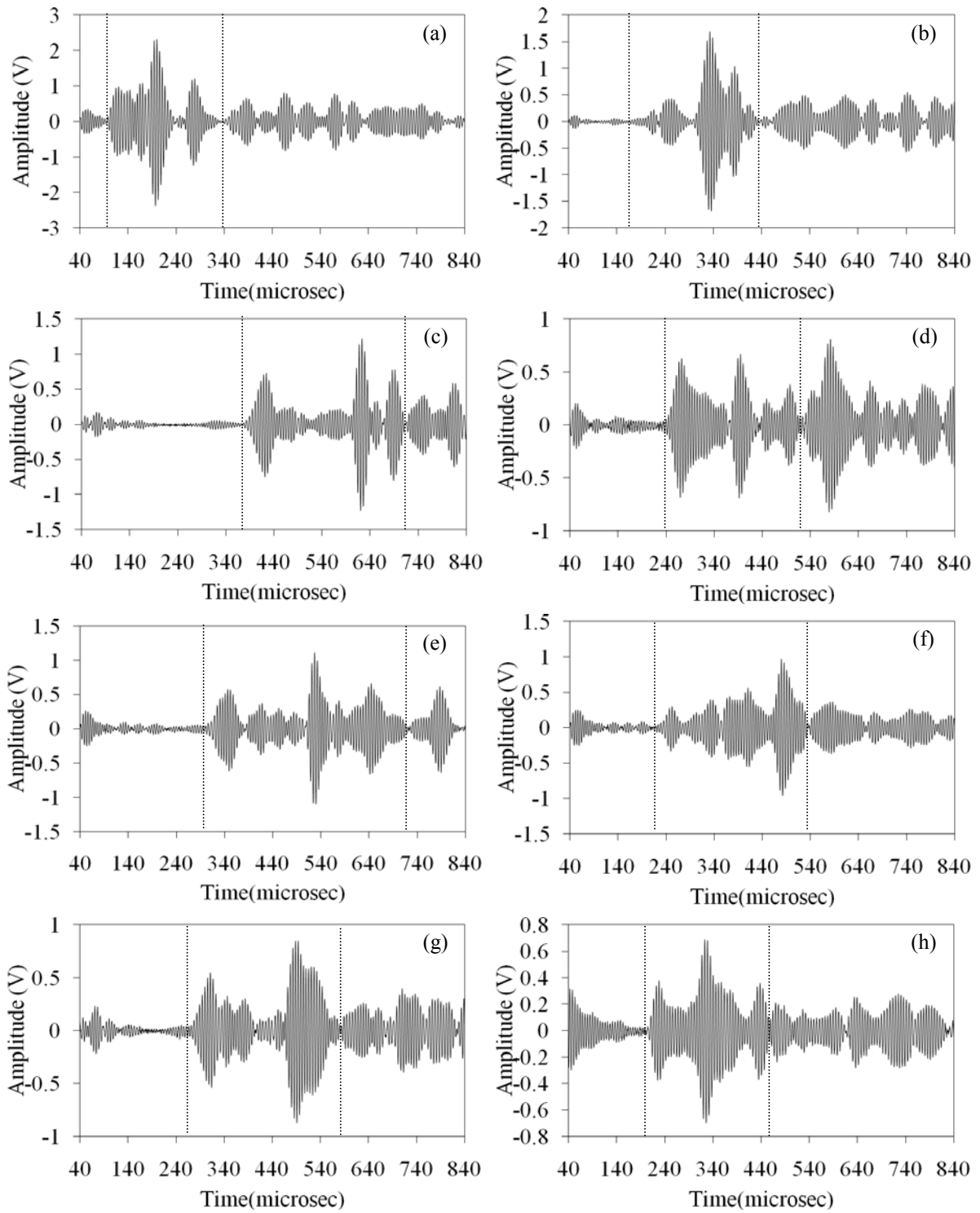

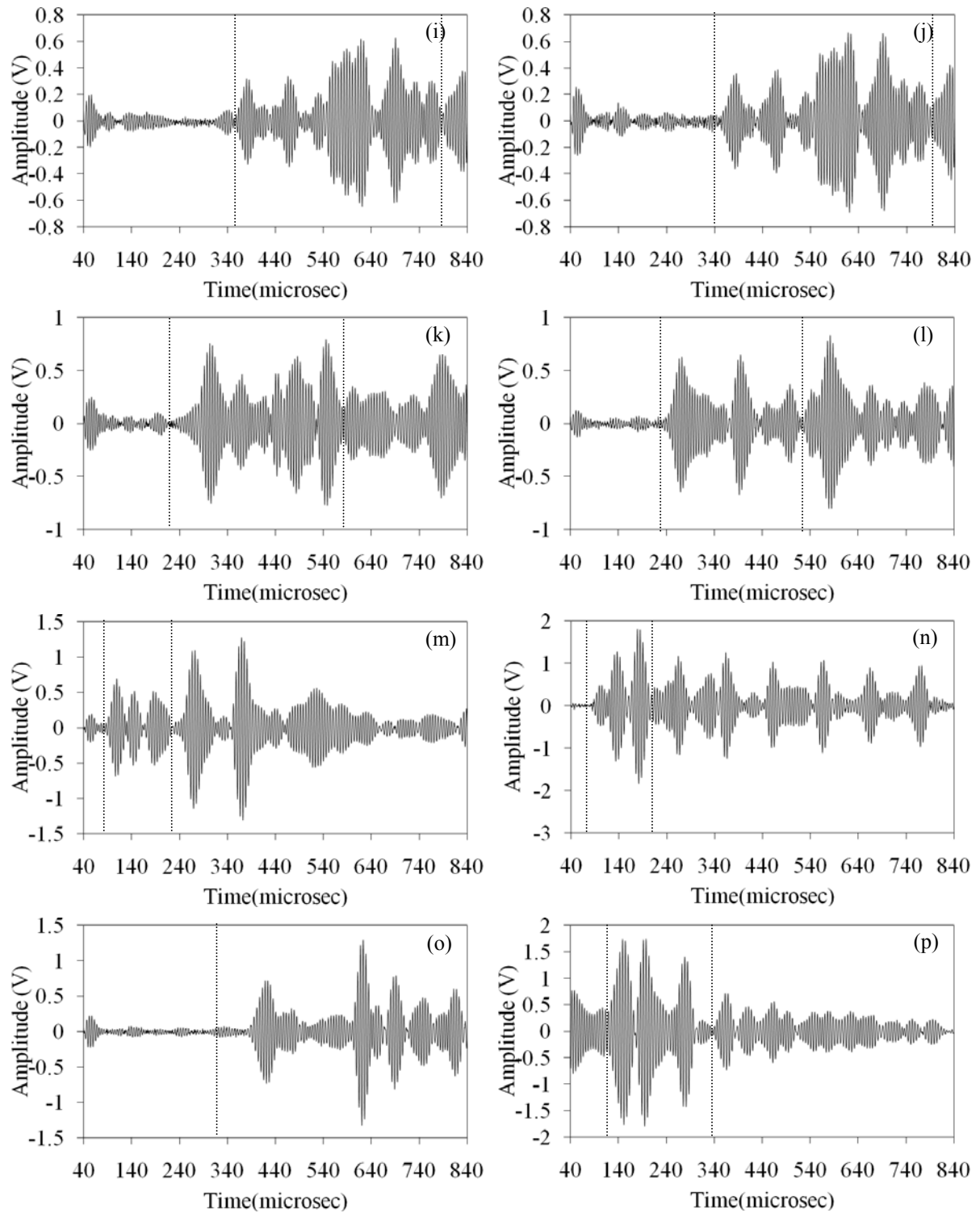**Figure 6.14** - Flowchart of the defect detection procedure.

Figure 6.15 - Time waveforms recorded at the beginning of the experimental program from actuator-sensor pairs: (a) S5=>S4 (b) S5=>S8 (c) S5=>S0 (d) S9=>S6 (e) S0=>S4 (f) S1=>S4 (g) S9=>S0 (h) S9=>S1 (i) S5=>S6 (j) S6=>S5 (k) S6=>S4 (l) S6=>S9 (m)S9=>S8 (n) S6=>S7 (o) S0=>S5 (p) S0=>S1.

Typical time waveforms recorded at the baseline, i.e. in pristine conditions, are shown in Fig. 6.15. The plots are relative to pairs S5=>S4, S5=>S8, S5=>S0, S9=>S6, S0=>S4, S1=>S4, S9=>S0, S9=>S1, S5=>S6, S6=>S5, S6=>S4, S6=>S9, S9=>S8, S6=>S7, S0=>S5, and S0=>S1, where the first number identifies the PZT acting as actuator and the second number indicates the PZT acting as sensor. As predicted by the numerical modeling (see Chapter 7.1), the presence of several guided waves' modes are visible. Many of these modes are flexural modes. Other wave packets are likely originated by mode conversion, generated from the interaction of the guided waves with the truss' angular members at the joints.

It is worth noting that although PZT 5 and PZT 0 were almost 2 m apart, the signal to noise ratio of the time waveform in Fig. 6.15c was still high. This demonstrates that the method is promising in gauging long distance along the chord of the truss by means of a pair of transducers only.

The first step of the damage detection algorithm was to retain the portion of the signal containing the three (or four) fastest modes, corresponding to the first three (or four) packets observed in each detected baseline waveform. The vertical dotted lines shown in Fig. 6.15 delimit the window applied to the time waveforms associated with the illustrated sensing paths.

Statistical features F_i were then extracted from the time-windowed waveforms. A feature is basically some set of values derived or calculated from measured data. Here maximum (max.) amplitude, peak-to-peak (ppk) amplitude, variance (var), root mean square (rms), kurtosis (krt), crest factor (cf), and k-factor (kf) were selected. Figure 6.16 shows the rms and the ppk as a function of the number of loading cycles extracted from the retained time series associated with the actuator-sensor pairs discussed in Fig. 6.7. At a given actuator-sensor pair the rms and the ppk appear to be slightly different. As expected, different paths provide different results. Guided waves along path S5 =>S4 should not have been affected by the presence of the notch. This is confirmed by observing that values of the rms and ppk (Fig. 6.16a and 6.16b, respectively) are dispersed within 1.5%.

The statistical features shown in Fig. 6.16c and 6.16d, associated with path S5 =>S8, denote a strong dependency on the number of cyclic loadings, and therefore on the size of the damage . This result is expected, given that sensor S8 is a few centimeters from the notch.

The values of the ppk (Fig. 6.16d) appear to be less dispersed. Overall, both statistical values at the most severe conditions are 25% less than the corresponding values at the pristine condition. The features associated with pair S5=>S0 (Figs. 6.16e and 6.16f) have about a 5% dispersion and they seem to slightly increase as the damage progressed. Because the sensing path is along two welded joints, wave scattering and leakage into the diagonal members is expected. The geometry along path S5=>S0 is complex, so any result associated with the features needs to be further investigated. Finally, the rms and the ppk associated with waveforms related to pair S9 =>S6 (Figs. 6.16g and 6.16f) provide two opposite trends, with statistical values dispersed between 11%-13%.

It should be noted, when observing Fig. 6.16, that overall no significant difference exists between data obtained from static loading and dynamic loading. The same can be said by observing the many wave paths considered in this study that, due to space constraints, cannot be shown here. This demonstrates that low-frequency vibration does not affect the propagation of guided waves and their ability to probe small cracks.
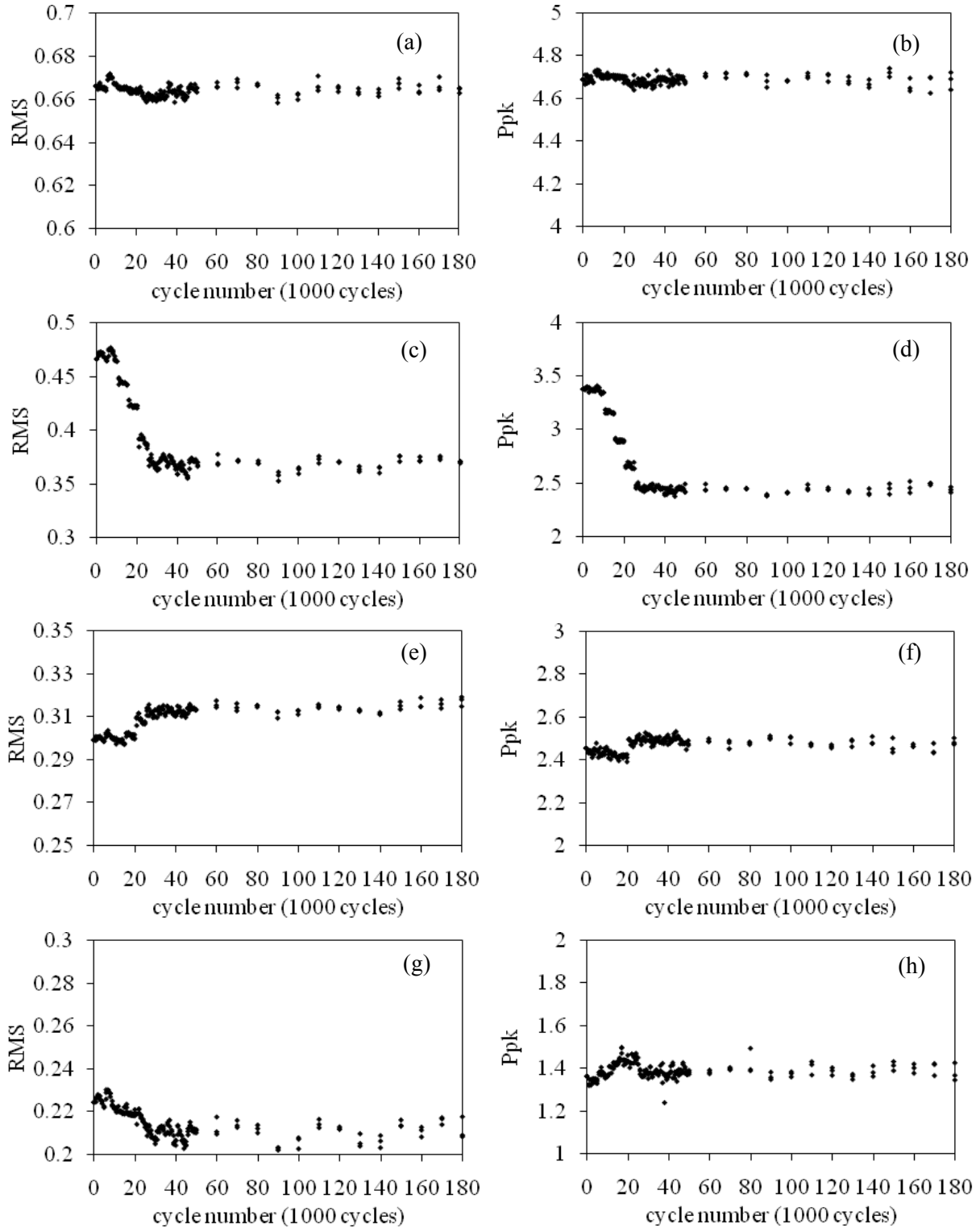
Figure 6.16 - Statistical features as a function of the loading number of cycles. (a) RMS S5=>S4 (b)Ppk S5=>S4 (c) RMS S5=>S8 (d) Ppk S5=>S8 (e) RMS S5=>S0 (f) Ppk S5=>S0 (g) RMS S9=>S6 (h) Ppk S9=>S6.

The next step of the algorithm was to compute a Damage Index (D.I.) as the ratio between a certain statistical feature $F_{a \Rightarrow b}$ and the same feature $F_{c \Rightarrow d}$:

$$D.I._{ab/cd} = \frac{F_{a \Rightarrow b}}{F_{c \Rightarrow d}}$$ (6.1).

where the generic subscript (a, b, c, and or d) indentifies one of the eleven PZTs.

In this study the 26 D.I.s listed in Table 6.2 were considered. The statistical features F_i were the same as discussed above, but normalized with respect to the value found at zero loading cycle.

Damage Index Number	Waveform path in the D.I. numerator/ Waveform path in the D.I. denominator
1	S5=>S2/S5=>S4
2	S5=>S1/S5=>S4
3	S5=>S0/S5=>S4
4	S0=>S4/S0=>S1
5	S0=>S5/S0=>S1
6	S0=>S4 / S0=>S2
7	S0=>S5 / S0=>S2
8	S6=>S8 / S6=>S7
9	S6=>S9 / S6=>S7
10	S9=>S7 / S9=>S8
11	S9=>S6 / S9=>S8
12	S5=>S8 / S5=>S4
13	S5=>S7 / S5=>S4
14	S5=>S6 / S5=>S4
15	S0=>S8 / S0=>S1
16	S0=>S9 / S0=>S1
17	S0=>S8 / S0=>S2
18	S0=>S9 / S0=>S2
19	S6=>S4 / S6=>S7
20	S6=>S5 / S6=>S7
21	S9=>S0 / S9=>S8
22	S9=>S1 / S9=>S8
23	S9=>S2 / S9=>S8
24	S1=>S4 / S1=>S2
25	S1=>S5 / S1=>S2
26	S9=>S0 / S9=>S8

Table 6.2 - Damage Index in the form of Waveform path in the D.I. numerator/ Waveform path in the D.I. denominator

The D.I.s were then used to feed an unsupervised learning algorithm, based on the outlier analysis. An outlier is a datum that appears inconsistent with the baseline, i.e. a set of data that describes the normal condition of the structure under investigation. Ideally, the baseline should include typical variations in environmental or operative conditions (e.g. temperature,

humidity, and loads) of the structure. In the analysis of one-dimensional elements, the detection of outliers is a straightforward process based on the determination of the discordancy between the one-dimensional datum and the baseline. Here the discordancy test based on the deviation statistics:

$$z_\zeta = \frac{|x_\zeta - \overline{x}|}{\sigma} \tag{6.2}$$

where x_ζ is the potential outlier, and $\overline{x}$ and σ are the mean and the standard deviation of the baseline, respectively. The mean and standard deviation can be calculated with or without the potential outlier depending on whether "inclusive" or "exclusive" measures are preferred.

For p-dimensional (multivariate) elements, the discordancy test equivalent to Eq. (2) is expressed by the Mahalanobis Squared Distance (MSD), D_ζ, which is a non-negative scalar defined as follows:

$$D_\zeta = (\{x_\zeta\} - \{\overline{x}\})^T \cdot [K]^{-1} \cdot (\{x_\zeta\} - \{\overline{x}\}) \tag{6.3}$$

where $\{x_\zeta\}$ is the potential outlier vector, $\{\overline{x}\}$ is the mean vector of the baseline, *[K]* is the covariance matrix of the baseline, and *T* symbolizes the transpose operation. Both vectors $\{x_\zeta\}$ and $\{\overline{x}\}$ are p-dimensional, whereas *[K]* is a square matrix of the order *p*.

As in the univariate case, the baseline mean vector and covariance matrix can be "inclusive" or "exclusive". In the present study, because the potential outliers are always known a priori, both z_ζ and D_ζ are calculated "exclusively" without contaminating the statistics of the baseline data.

A new datum is an outlier if the corresponding value of *z* or *D* falls above a set threshold. In the present study, the baseline was computed from the first 18 time histories that, according to Fig. 6.9c, were collected within the first 5,000 cycles. Once the values of the baseline distribution were determined, the threshold value was taken as the usual value of 3σ equal to 99.73% of the Gaussian confidence limit.

6.3.2 EMI-related Signal Processing Algorithm

The overall SHM algorithm applied to the EMI measurements is discussed in Chapter 8.

CHAPTER 7: EXPERIMENTAL RESULTS from GUWs

This chapter describes the experimental results obtained from the measurement of the propagation of the guided waves. The chapter is divided into three sections. The first section shows the numerical prediction of the wave modes that are expected to be observed. The second part describes the analysis of the GUW associated with the propagation of stress waves at 175 kHz. Finally, the remaining part of the chapter is devoted to the illustration of the data associated with the propagation of frequencies ranging from 125 kHz to 275 kHz.

7.1 NUMERICAL PREDICTION

Semi-analytical computations were performed to gain insight about the guided waves propagating along the main chord. The guided waves' dispersion curves associated with a straight steel tube made of the same material properties and geometry of the truss were sought. To date, different analytical and numerical tools are available to predict the dispersive behavior of waveguides. In particular, analytical models based on the Superposition of Bulk Waves (SPBW), pure Finite Element (FE) procedures, and Semi-Analytical Finite Element (SAFE) based formulations, have been proposed. SPBW approaches formulate the dispersive wave equation as superposition of the partial plane bulk waves that can propagate in the material with respect to the waveguide boundary conditions. Dispersive solutions are obtained as a minimum of the characteristic equation by using root-finding routines. In FE approaches the waveguide is meshed by using plate (when symmetry conditions apply) or brick elements. The dispersive properties of the structure are calculated by performing a series of modal analysis for a series of waveguides with different lengths under appropriate boundary conditions. Compared to SPBW approaches, limited to waveguides with standard cross-sections, FE-based methods can also deal with waveguides with arbitrary cross-sections. However, while SPBW approaches deal with exact wave solutions, FE models can only obtain an approximate solution that, for a given number of finite elements, is less accurate when the computation frequency is high. Nonetheless, the FE-based procedure, requiring a modal analysis for a large number of waveguides, results in time-consuming processes.

An alternatively efficient way to extract the dispersive spectrum of waveguides consists of using Semi-analytical Finite Element (SAFE) formulations. The SAFE Dispersive Wave Equation is obtained by equating zero to the variation of the waveguide Lagrangian that is based on a hybrid wave displacement field built by coupling a finite element mesh over the waveguide cross-section and by setting exact harmonic functions along the waveguide propagation direction.
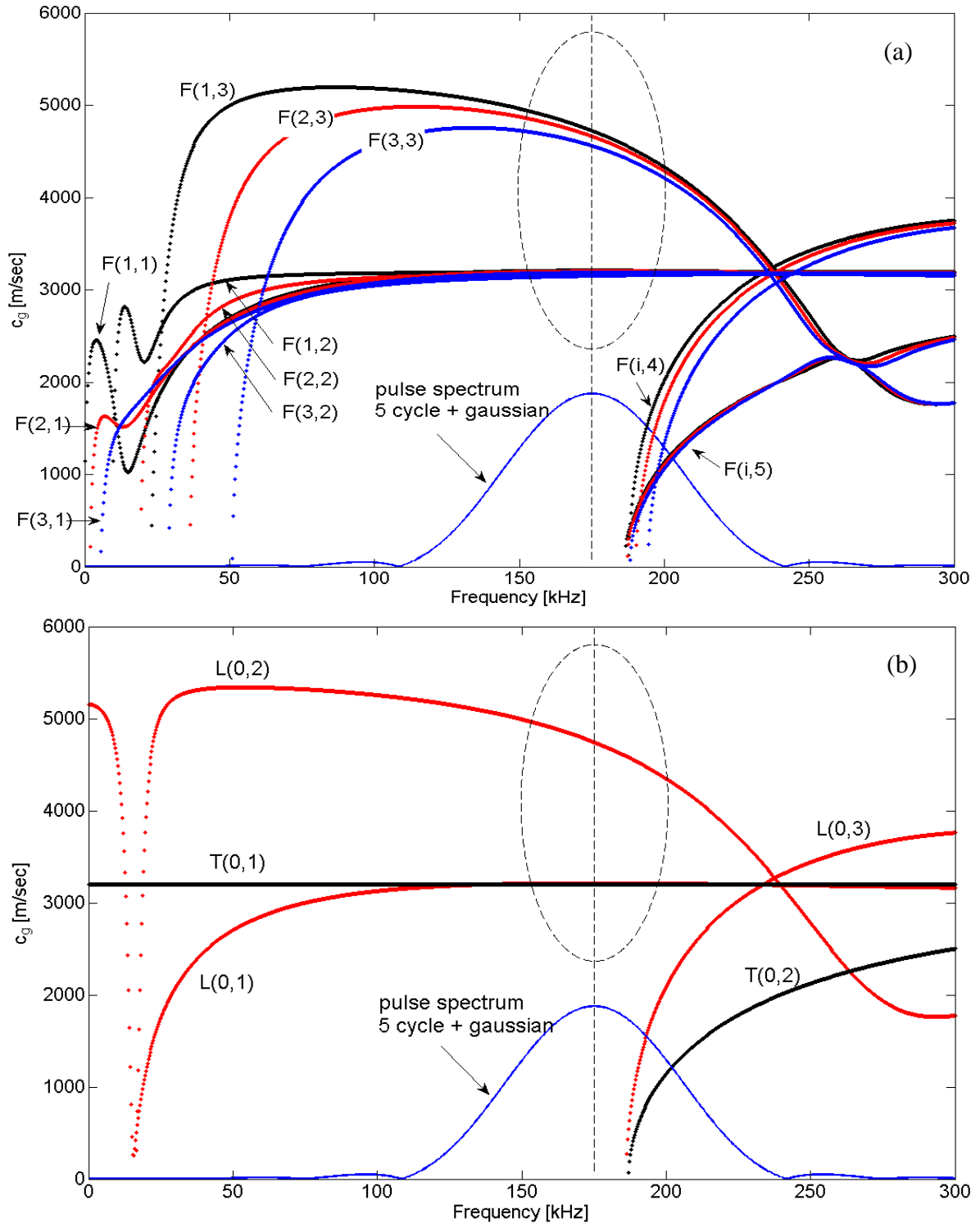
Figure 7.1 - (a) Group velocity dispersion curves for the first three orders of flexural waves and (b) first three longitudinal modes and first two torsional modes in a pipe. An ASTM A-53 pipe of outer diameter 114.3 mm and wall thickness of 8.6 mm was considered.

The wave equation results may be described by an algebraic eigensystem, from which dispersive roots can be obtained by using standard routines for eigenvalue problems.

Compared to SPBW methods, SAFE models have the advantage of handling waveguides with arbitrary cross-sections, such as square beams, rail, etc. Compared to pure FE procedures, where standard FE packages can be used, SAFE formulations are less time-consuming even if the construction of the Lagrangian requires an ad-hoc developed formulation.

In this study, the SAFE formulation was used considering the following geometrical and mechanical parameters: outer diameter 114.3 mm; wall thickness 8.6 mm; Young's Modulus 210 GPa; Poisson's Ratio 0.3; density 7900 Kg/m^3. Figure 7.1a shows the group velocity dispersion curves for the flexural modes in the 0-300 kHz range for the main truss' chord. The flexural waves of order one $F(1,i)$, two $F(2,i)$ and three $F(3,i)$ are represented. Owing to the PZT employed in this study, flexural waves are expected to be the most excitable modes in the chord, due to the local (point) action of the PZT's transducers. The frequency range 100-200 kHz appears suitable to consider because flexural modes of different orders have a similar group velocity. Operating within this range would lead to simpler time waveforms to be analyzed. For the sake of completeness the group velocity dispersion curves associated with the longitudinal and torsional modes in the frequency range 0 – 300 kHz are illustrated in Fig. 7.1b.

7.2 TEST 1

7.2.1 Univariate Analysis

This section presents the outlier analysis results when the statistical features F_i were considered separately and the propagation of the wave at 175 kHz was exploited. Figure 7.2 shows the discordancy as a function of the crack area for some of the features and wave paths considered in this study. In particular, the damage indexes $D.I._{58/54}$, $D.I._{96/98}$, $D.I._{50/54}$, $D.I._{56/54}$, $D.I._{51/54}$, $D.I._{04/02}$, $D.I._{05/01}$, $D.I._{04/01}$, and $D.I._{91/98}$ associated with the ppk and the rms are presented. The values of the respective thresholds are superimposed and illustrated by means of a horizontal line. It is evident that the rms and the ppk perform differently at a given wave path. For a small notch, a large number of inliers, i.e. false negative indications are visible. As discussed before, at a given damage size, measurements were taken under dynamic or static loads. Nonetheless, the dispersion of the damage index at a given crack extension is small.

The values of the discordancy show that only certain wave paths, both in terms of orientation and direction, are affected by the presence of damage. For instance, by comparing Fig. 7.2i to Fig. 7.2o, it is evident that when the actuator is on the same side of the notch (with respect to the truss joint), the wave is more affected. In fact, the wave path S5=>S1 is symmetric to the path S0=>S4. However, as the notch is closer to the actuator S5, the first path is more affected by the presence of damage than the second path. This evidence suggests that the algorithm not only is effective in detecting the presence of anomalies and in estimating its severity, but it may represent a valuable means to localize the position of the damage itself. In addition by observing the plots on the left side of Fig. 7.2, and comparing the corresponding values on the right side of Fig. 5.1 it is evident that the selection of the

appropriate feature can be pivotal in enhancing the sensitivity of the probing system. It should be noted that all figures are purposely plotted on a different y-axis scale.
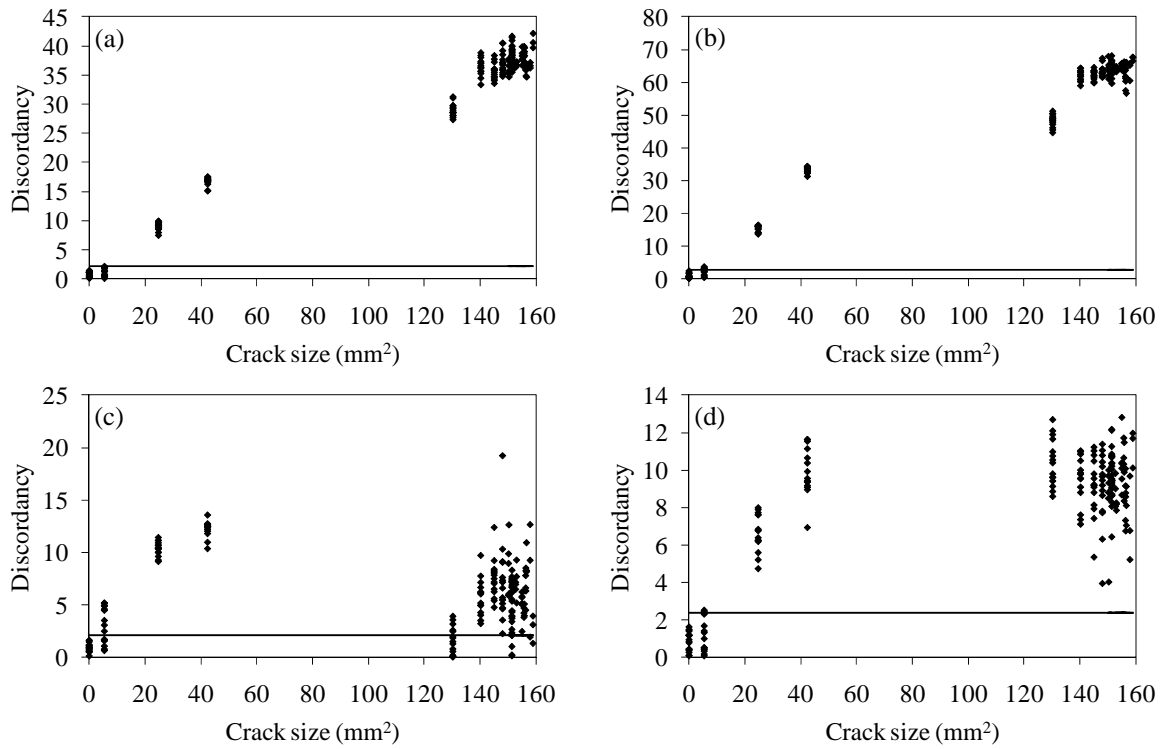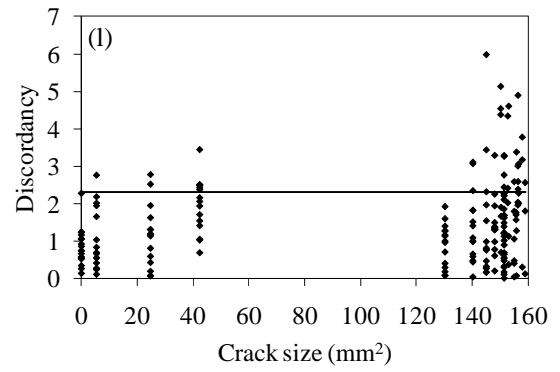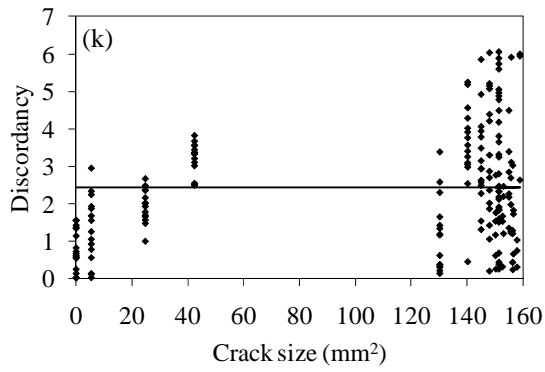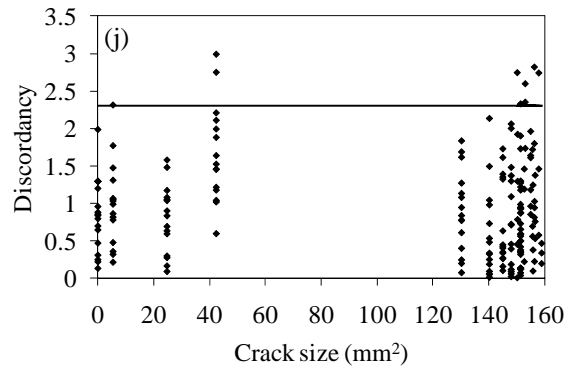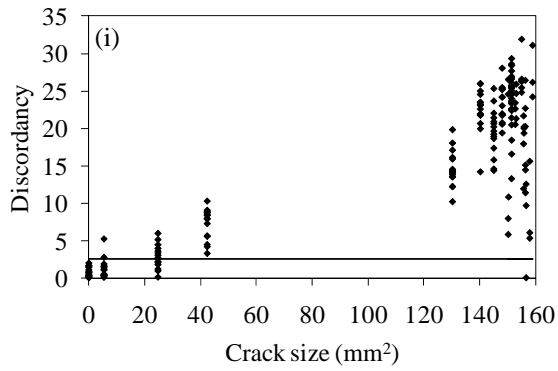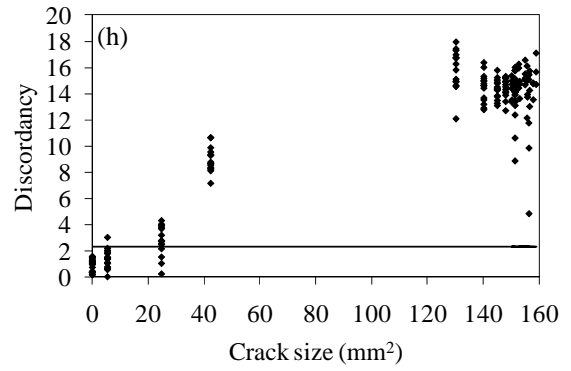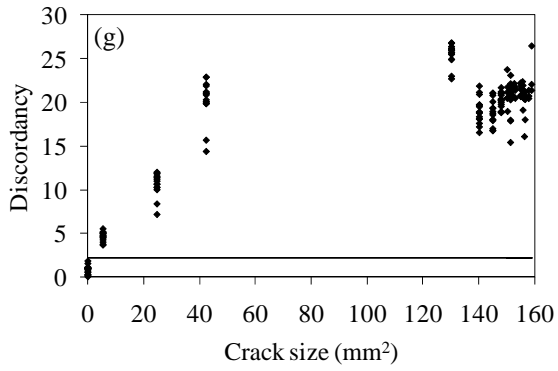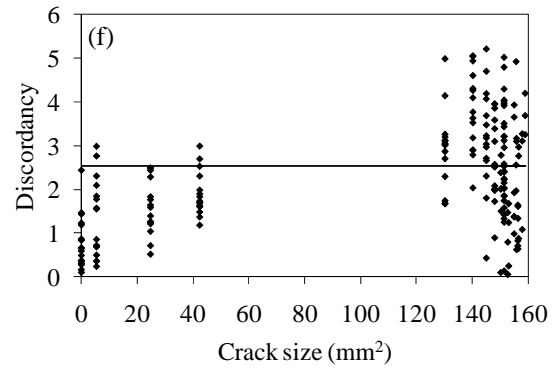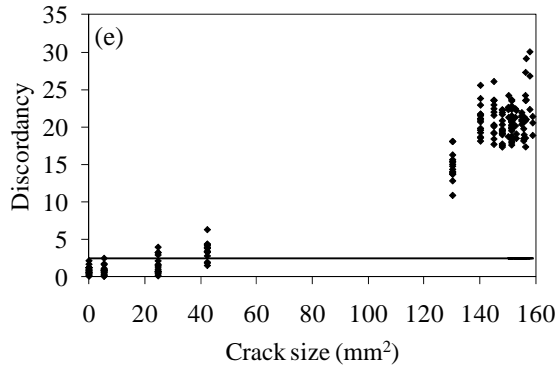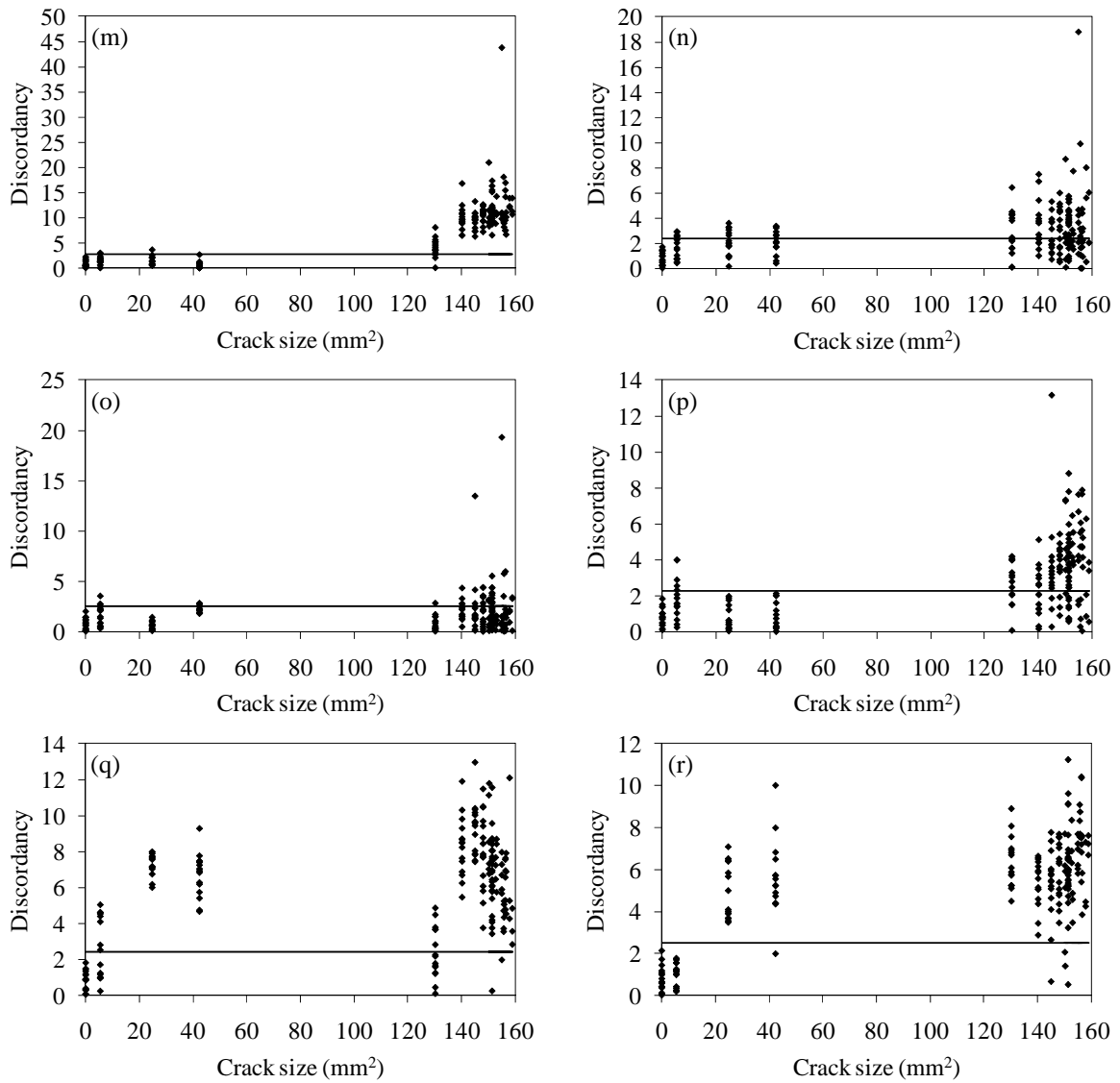
Figure 7.2: Univariate analysis. Discordancy as a function of the crack size for the following features and actuator-sensor pairs: (a) RMS_S5=>S8/S5=>S4 (b) Ppk_S5=>S8/S5=>S4; (c) RMS_S9=>S6/S9=>S8 (d) Ppk_S9=>S6/S9=>S8 (e) RMS_S5=>S0/S5=>S4 (f) Ppk_S5=>S0/S5=>S4; (g) RMS_S5=>S6/S5=>S4 (h) Ppk_S5=>S6/S5=>S4 (i) RMS_S5=>S1/S5=>S4 (j) Ppk_S5=>S1/S5=>S4; (k) RMS_S0=>S4/S0=>S2 (l) Ppk_S0=>S4/S0=>S2 (m) RMS_S0=>S5/S0=>S1 (n) Ppk_S0=>S5/S0=>S1; (o) RMS_S0=>S4/S0=>S1 (p) Ppk_S0=>S4/S0=>S1 (q) RMS_S9=>S1/S9=>S8 (r) Ppk_S9=>S1/S9=>S8.

The damage detection rate, i.e. the percentage of outliers of the features selected in this study associated with six actuator-sensor pair's ratios, is summarized in Table 7.1. The table demonstrates that the proper selection of wave path and statistical features are pivotal to enhancing the damage sensitivity of the hardware system. Because paths S5=>S4 and S0=>S1 should not be affected by the presence of damage at or around the joints, these paths can be used to normalize ultrasonic data in order to mitigate any effect due to changes in the environmental conditions, electronic noise/power, and PZT-structure interaction. Although

119

the sensing paths S5=>S1 and S5=>S0 are similar, it is interesting to note that the detection rate for some features is quite different. The same can be said about sensing paths S0=>S4 and S0=>S5. Observing the last two columns of Table 7.1, it can be noted that although actuators S0 and S5 are placed symmetrically with respect to sensor S8, sensing path S5=>S8 is strongly affected by the presence of the crack. This result suggests that the algorithm can be indirectly used to identify the position of the crack. Somehow it is surprising to observe the effect of the damage on certain features associated with guided waves propagating along path S0=>S1.

Feature	S5=>S1 /S5=>S4	S5=>S0 /S5=>S4	S0=>S4 /s0=>S1	S0=>S5 /S0=>S1	S5=>S8 /S5=>S4	S0=>S8 /S0=>S1
Krt	58.05%	94.25%	80.46%	31.61%	95.40%	61.49%
RMS	87.93%	83.33%	23.56%	74.14%	92.53%	90.23%
Variance	87.93%	83.33%	23.56%	74.14%	92.53%	93.68%
K-factor	4.022%	36.21%	43.68%	55.17%	94.25%	10.34%
Max	5.172%	43.68%	55.75%	51.72%	95.40%	8.046%
Ppk	10.92%	54.6%	62.64%	35.06%	83.91%	57.47%
Crest	50.0%	78.74%	25.29%	81.03%	94.25%	27.01%

Table 7.1 - Univariate Analysis: the percentage of outliers detected using statistical features applied to waveform data associated with some of the actuator-sensor pairs considered in this study.

7.2.2 Multivariate Analysis

The features considered separately in the previous section were used simultaneously to construct a multi-dimensional D.I. vector for the outlier analysis. The "exclusive" MSD for each of the 192 measurements was calculated using Eq. (6.3). The purpose of combining features was to increase the sensitivity to damage compared to the single-feature analysis. However, the use of all may not be necessary and the selection of all features may degrade the detection performance. To investigate this aspect, a parametric analysis was carried out. All of the features discussed in the previous section were considered, ranging from all combinations of two-dimensional D.I. vectors to the single combination of the 7-dimensional vector. A total of 3,120 cases were analyzed. The total is the result of the application of all 120 possible features' combinations to each of the 26 D.I.s considered in this study.

Figure 7.3 shows the results of the single combination of the 7-dimensional vector formed by the statistical features applied to the following features' ratios: S5=>S0/S5=>S4, S9=>S6/S9=>S8, S5=>S8/S5=>S4, S5=>S6/S5=>S4, S5=>S1/S5=>S4, S0=>S4/S0=>S2, S0=>S5/S0=>S1 and S0=>S4/S0=>S1, respectively. The improvement of the sensitivity is immediately visible by comparing the ordinate axis of Fig. 7.3 with the ordinate axis of Fig. 7.2. The improvement implies that variation in crack sizes determine large variations of the MSD value. By comparing the MSD presented in Fig. 7.3, it also evident that a certain waveform path, i.e. position of the PZTs, outperforms other paths. For instance, the values presented in Fig. 7.3c show a small scatter at a given damage size and better stepwise
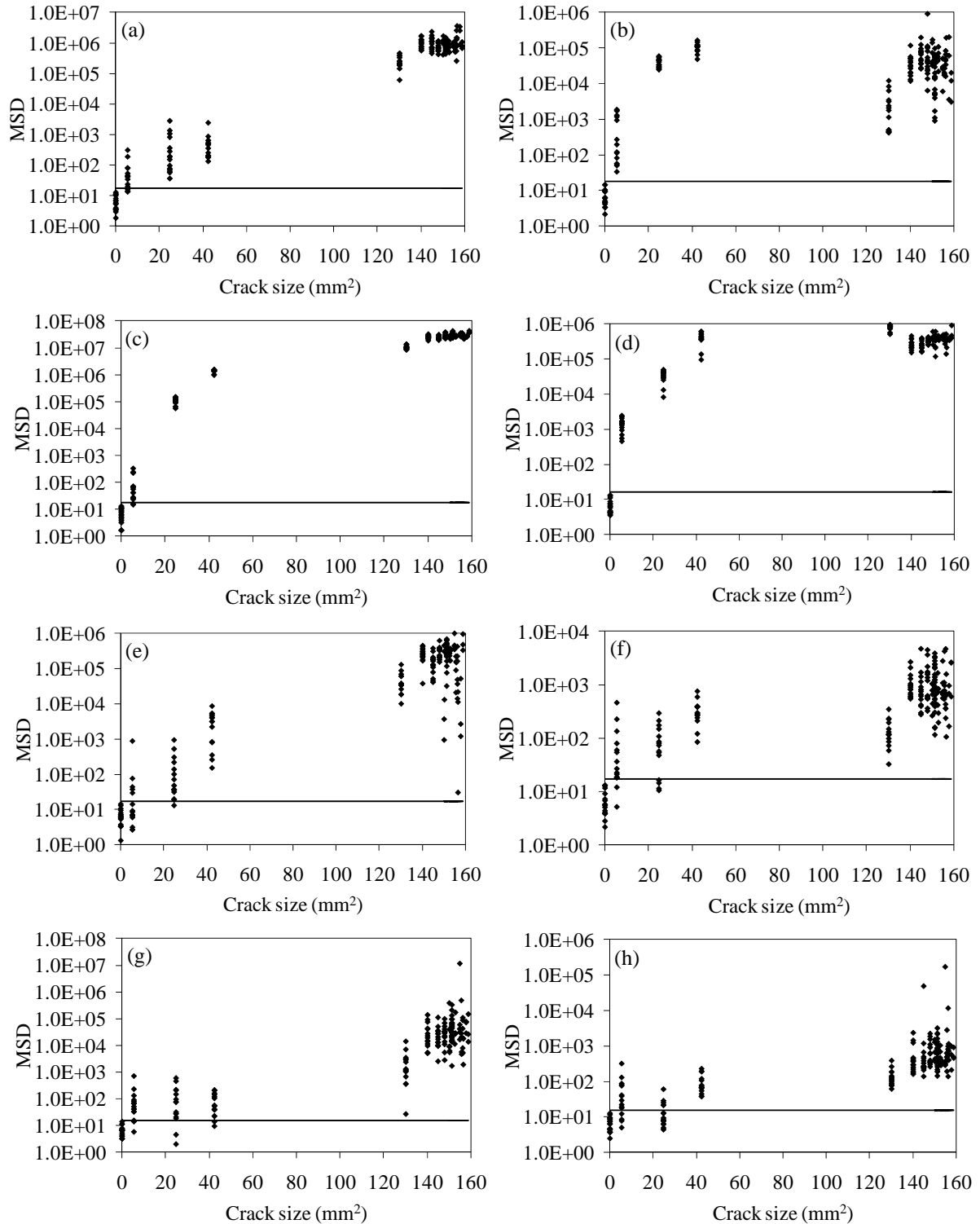
Figure 7.3 - Multivariate analysis. Mahalanobis squared distances as a function of the crack size for the actuator-sensor pairs considering all seven features: (a) S5=>S0/S5=>S4; (b) S9=>S6/S9=>S8; (c) S5=>S8/S5=>S4; (d) S5=>S6/S5=>S4; (e) S5=>S1/S5=>S4; (f) S0=>S4/S0=>S2; (g) S0=>S5/S0=>S1; (h) S0=>S4/S0=>S1.
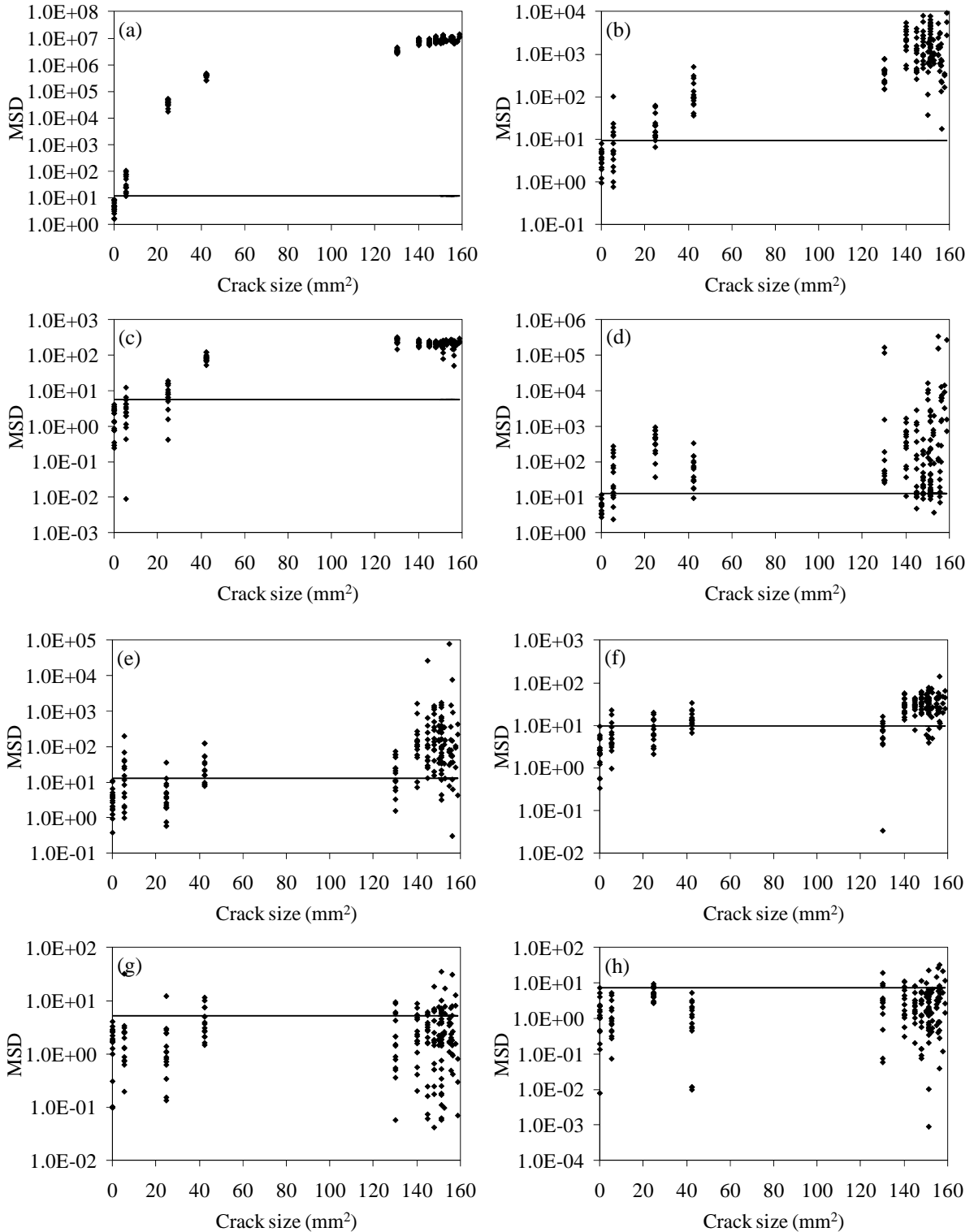
Figure 7.4 - Mahalanobis squared distances as a function of the crack size for the actuator-sensor pairs: (a) S5=>S8/S5=>S4 with krt, cf, kf ppk and max; (b) S5=>S2/S5=>S4 with krt, var, cf, kf, max and ppk; (c) S5=>S6/S5=>S4 with kf and max; (d) S5=>S7/S5=>S4 with krt, var, cf, kf, max and ppk; (e) S0=>S4/S0=>S1 with rms, var, kf and max; (f) S0=>S4/S0=>S2 with rms, cf and ppk; (g) S5=>S2/S5=>S4 with max and ppk; (h) S0=>S8/S0=>S1 with max and ppk; krt, rms, var, cf, kf, max and ppk.

behavior. To find, empirically, the best feature combination and the best wave propagation path, a quantitative study was performed using the values of the MSD associated with each of the 3,120 cases. The selection was done on the logarithmic magnitude values of the measurements and it was based on the ranking of their performance as novelty detectors. Figure 7.4 shows the results associated with from the best to the worst combination cases. The combination ranked '1st' provided the largest number (100%) of outliers and the largest ratio of the Mahalanobis distance over the threshold. Figure 7.4a shows the MSD as a function of the crack area from the time waveforms associated with paths S5=>S8/S5=>S4 and statistical features krt, cf, kf, ppk, and max. Fig. 7.4h presents the result of the multivariate analysis associated with D.I.$_{08/01}$ and features max and ppk. Only 12.07% of the outliers were properly identified.

7.2.3 Multiple frequencies analysis

In order to investigate the effect of the propagating frequency on the damage detection performance of the GUW approach, a portion of the study was devoted to the generation and detection of toneburst center at frequencies ranging from 100 kHz to 275 kHz at 25 kHz step. The results of this investigation to detect the presence of damage in Test 1 are presented in this section.

An example of time waveforms detected at various frequencies when the transducer pair S5=>S0 were activated are presented in Fig. 7.5. Because the generation and detection of 100 kHz toneburst led to a poor signal to noise ratio, its further analysis was excluded. By observing Figs. 7.5a – 7.5h, it is possible to observe that the frequency range 150 – 200 kHz provides the highest signal to noise ratio.

The vertical dotted lines identify the time window analysis considered for the subsequent structural health monitoring algorithm. For consistency with the analysis described in the previous section the same features and the same outlier analysis was applied to each and every frequency examined in this study.

The quantitative results of the detection rate of the discordancy tests (multivariate analysis) applied to the damage index associated with all seven features and the selected windowed time waveforms are shown in Fig. 7.6. In Fig. 7.6, the histograms are shown as a function of frequency for all seven features and selected wave paths considered in this study. In particular, the damage indexes D.I.$_{50/54}$, D.I.$_{96/98}$, D.I.$_{58/54}$, D.I.$_{04/01}$, D.I.$_{65/67}$, and D.I.$_{05/01}$ associated with the krt, var, RMS, max, ppk, crest and kf are presented. By comparing all six wave paths and seven features the krt-based, var-based and RMS-based damage indexes extracted from the selected windowed time waveforms provided the highest detection rate and 150 kHz, 175 kHz and 200 kHz are the optimal frequencies.

Moreover, by comparing the performance of the detection rates for a specified frequency and certain feature, the histograms demonstrate that the proper selection of wave paths are pivotal to enhancing the damage sensitivity of the hardware system. As mentioned earlier, paths S5=>S4, S0=>S1 and S6=>S7 should not be affected by the presence of damage at or around the joints. Thus, these paths were used to normalize ultrasonic data in order to mitigate any effect due to changes in the environmental conditions, electronic noise/power, and PZT-structure interaction.
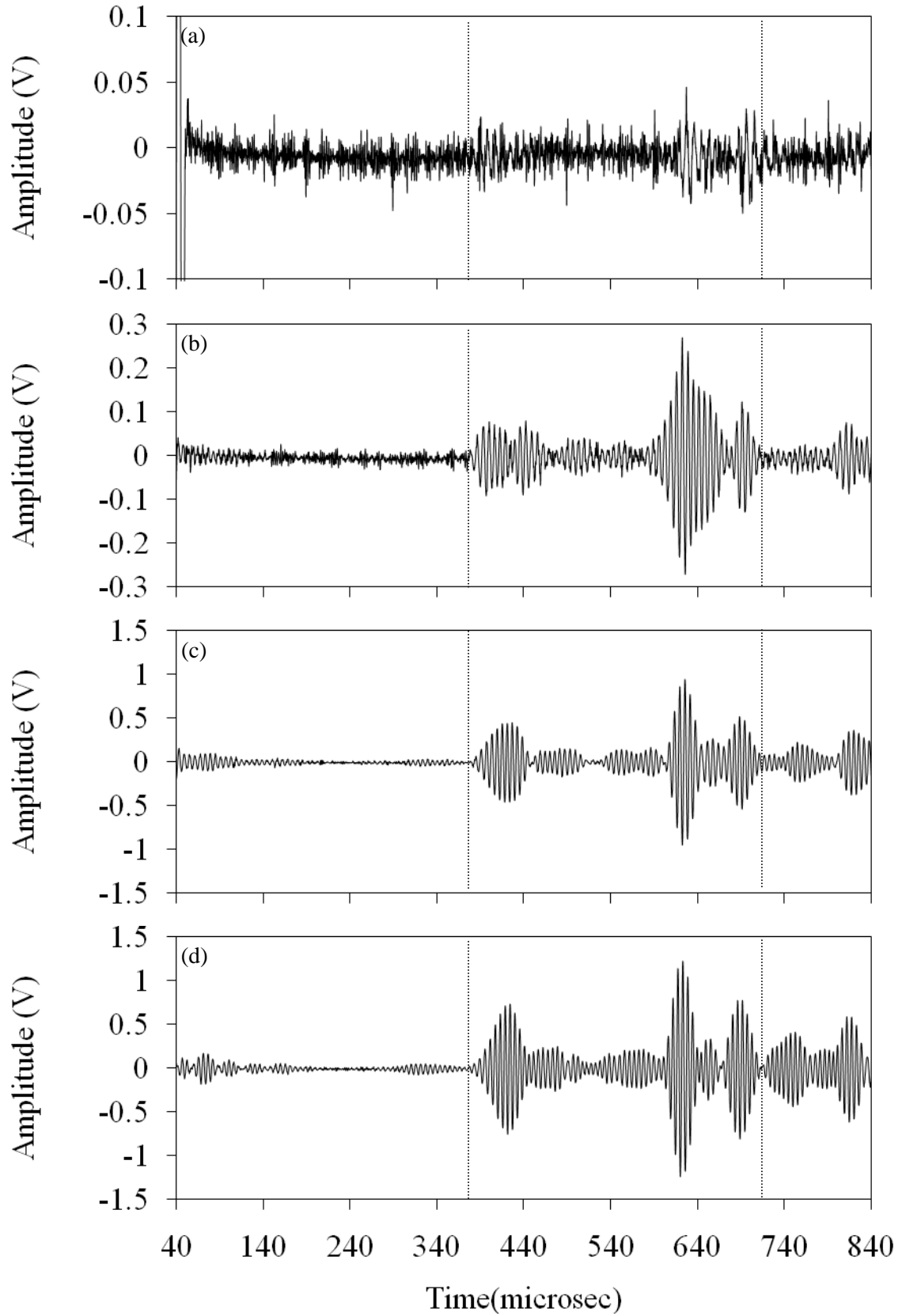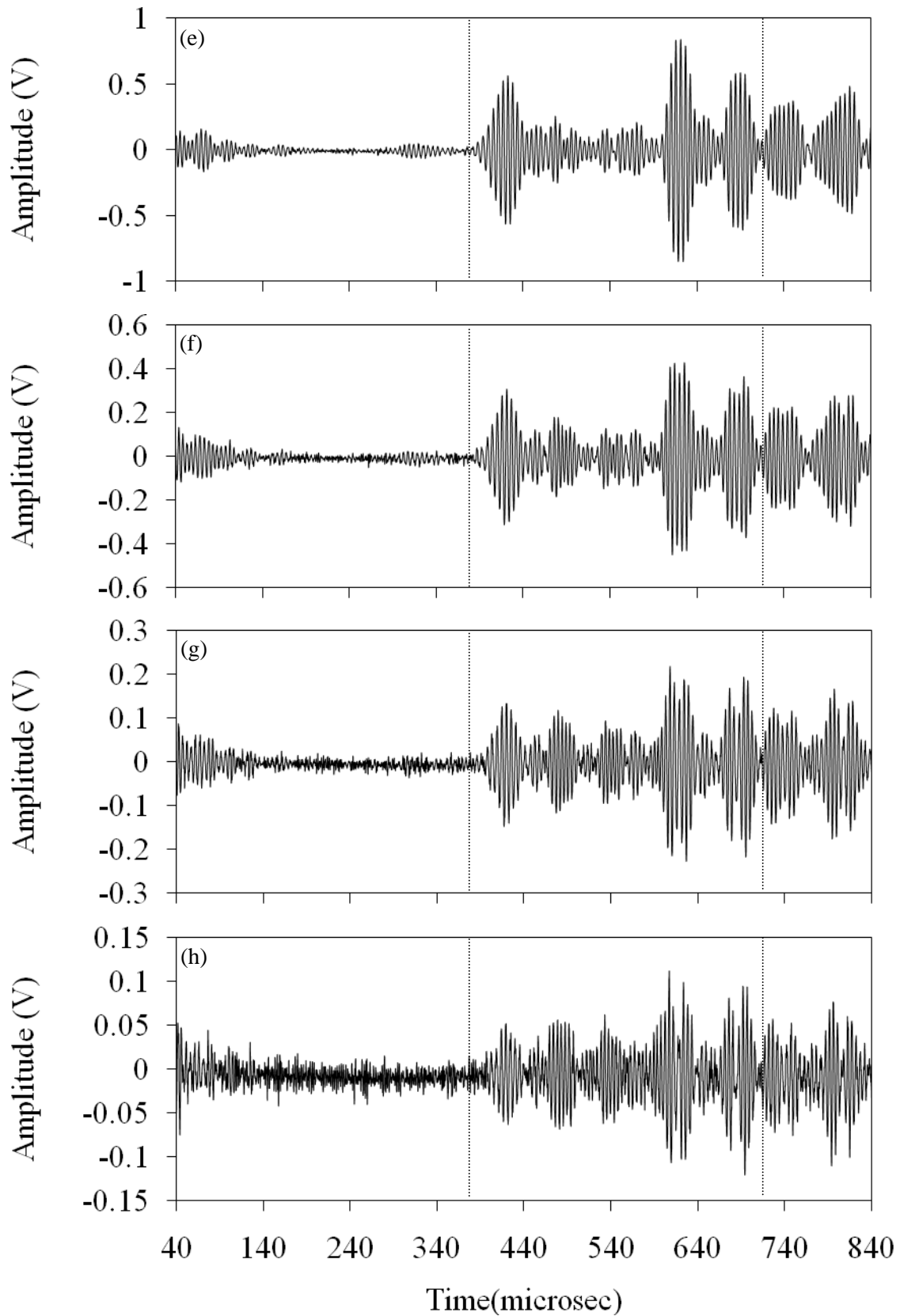
Figure 7.5 - Time waveforms of S5=>S0 in different frequencies: (a) 100 KHz; (b) 125 KHz; (c) 150 KHz; (d) 175 KHz; (e) 200 KHz; (f) 225 KHz; (g) 250 KHz; (h) 275 KHz.
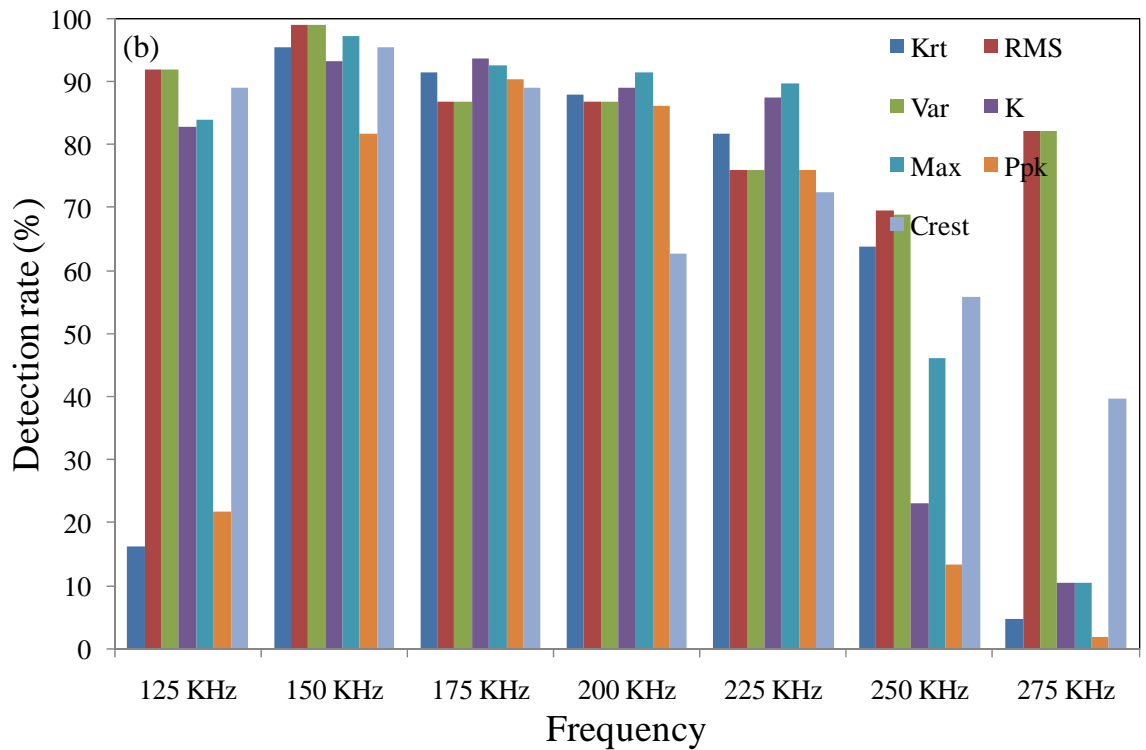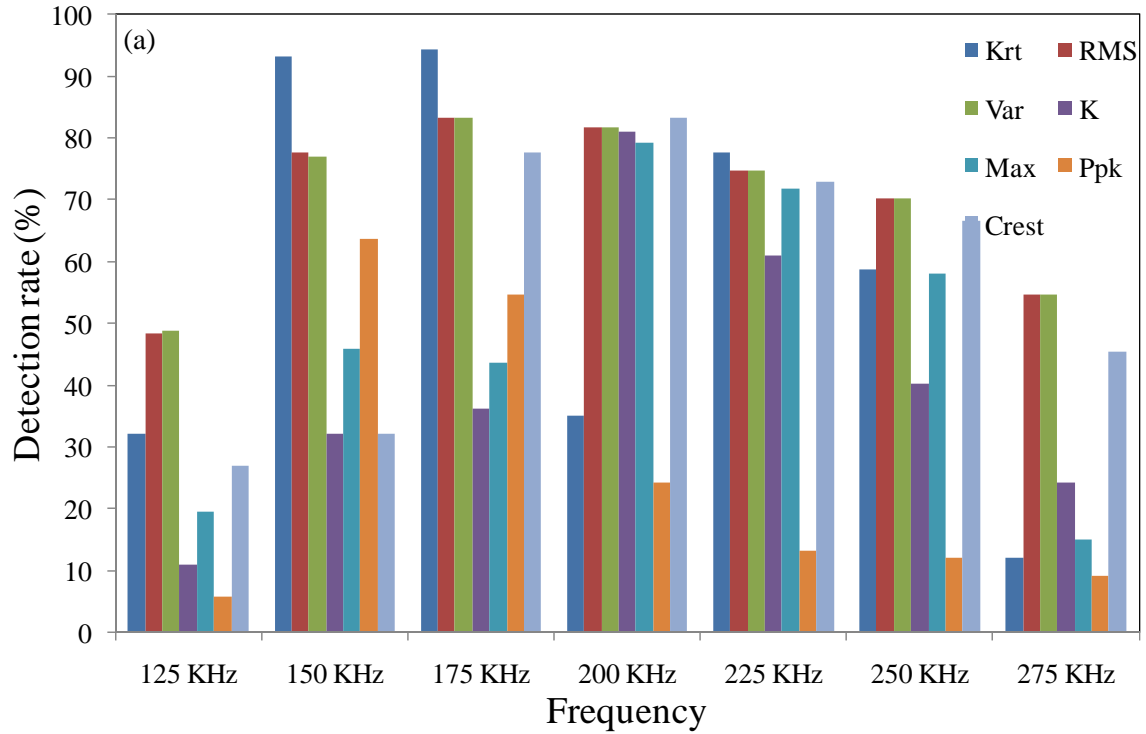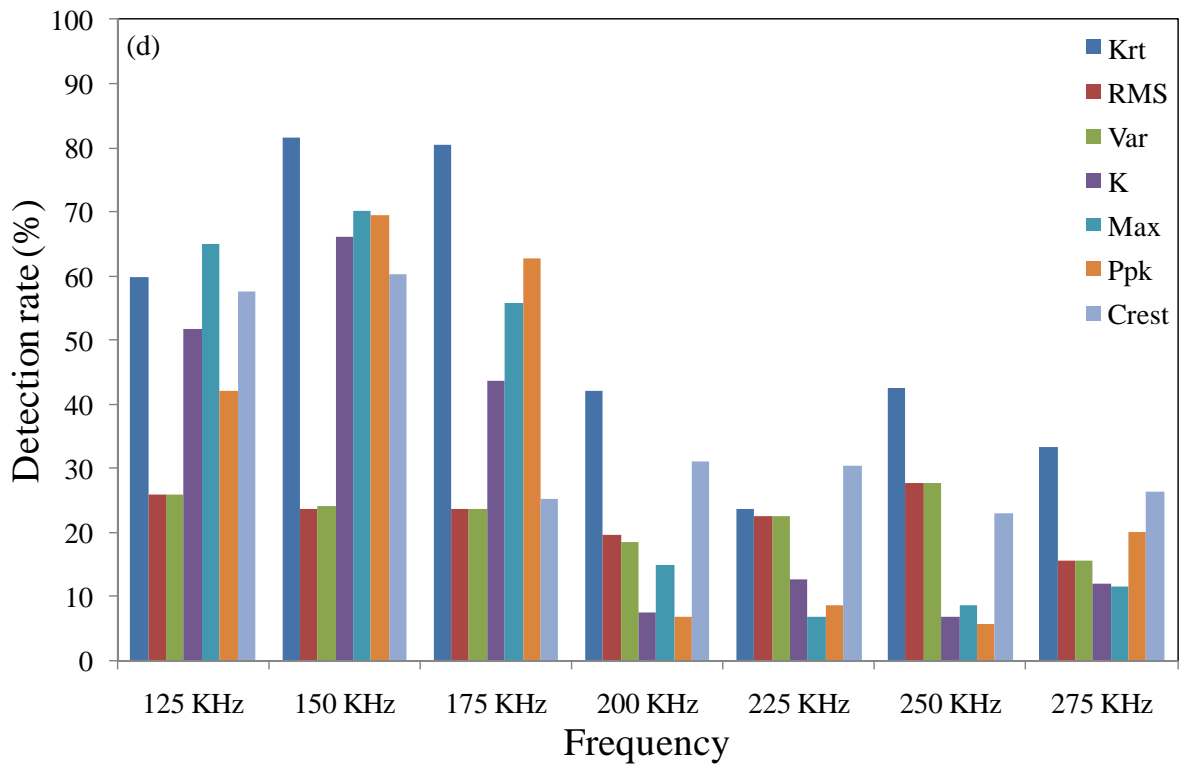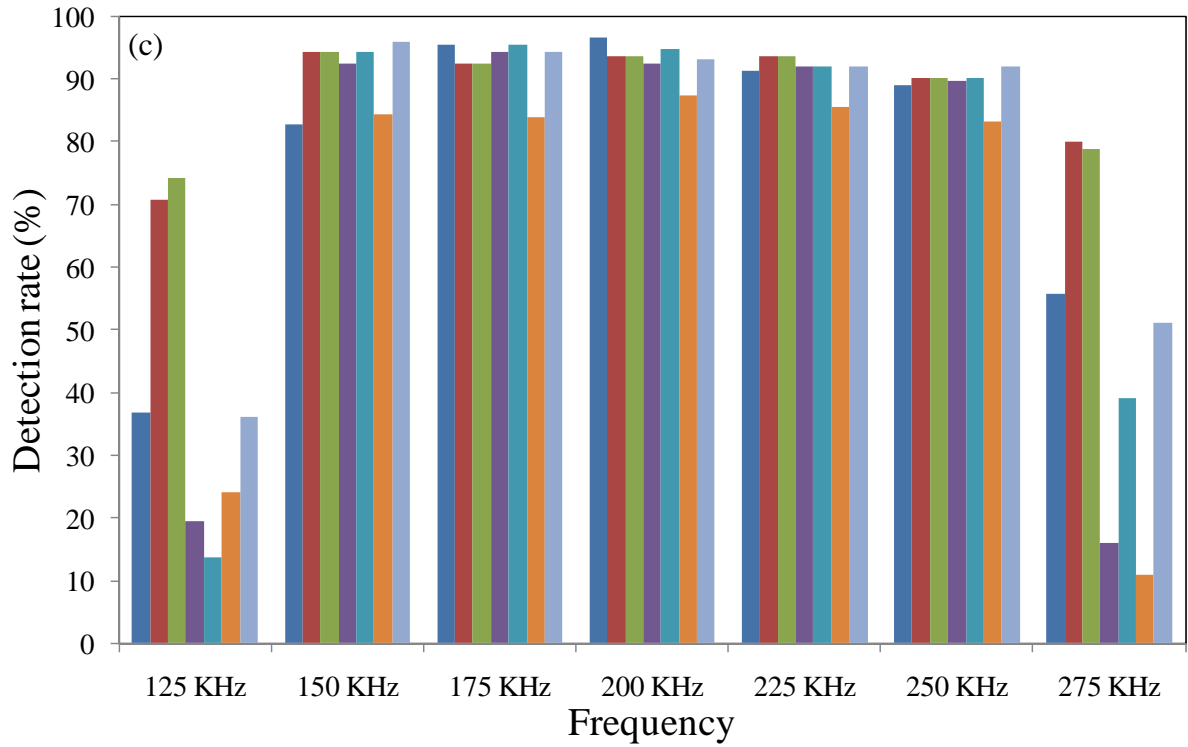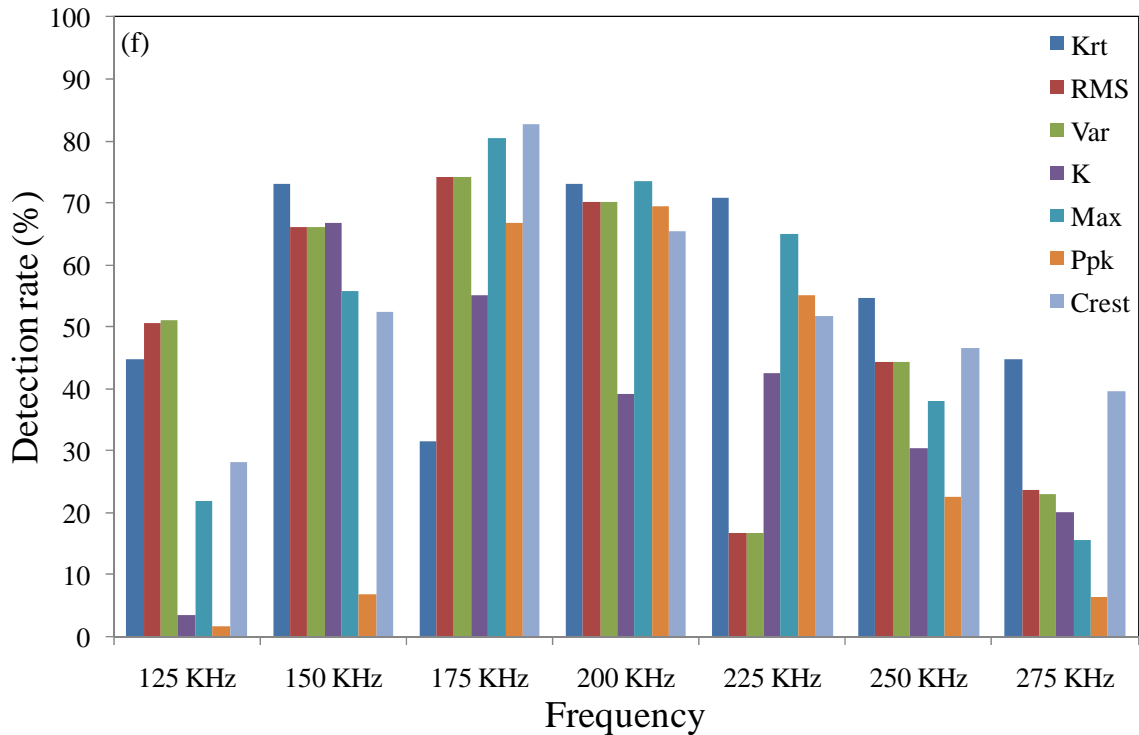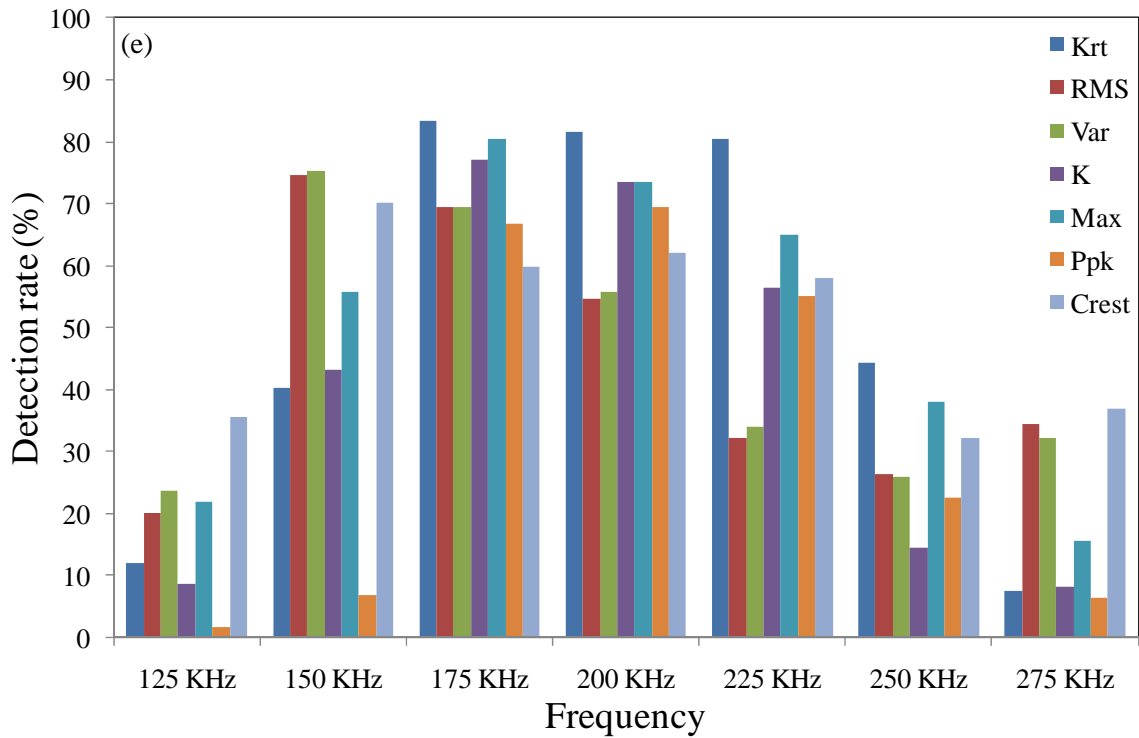
Figure 7.6 - Univariate analysis. Detection rate as a function of frequency for the following features: (a) S5=>S0/S5=>S4 (b) S5=>S6/S5=>S4; (c) S5=>S8/S5=>S4 (d) S0=>S4/S0=>S1 (e) S6=>S5/S6=>S7 (f) S0=>S5/S0=>S1.

The sensing path S5=>S8 is strongly affected by the presence of the first crack is as observed in Fig. 7.6 (c). Considering the symmetrical case of S5=>S0/ S5=>S4 (Fig. 7.6 (a)) and S0=>S5/ S0=>S1 (Fig. 7.6(f)), the different performances suggests that the algorithm could be indirectly used to identify the position of the crack.

Figure 7.7 shows instead the results of the multivariate analysis when all seven features were considered for eight different paths.
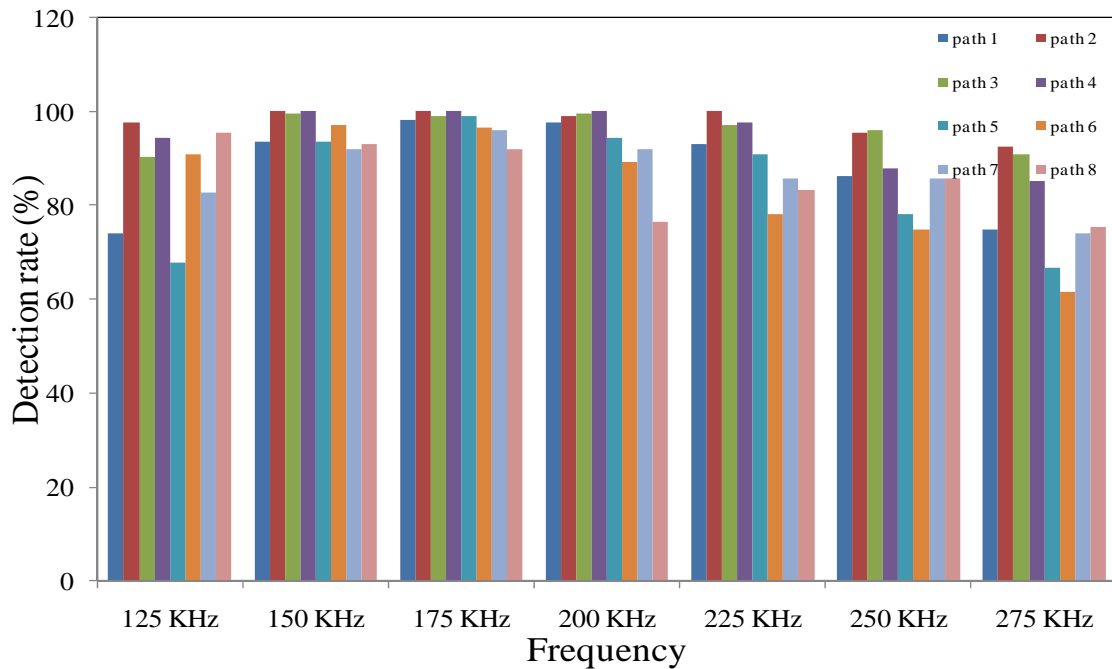
**Figure 7.7** - MSD considering all seven features: path (1) S5=>S0/S5=>S4; (2) S9=>S6/S9=>S8; (3) S5=>S8/S5=>S4; (4) S5=>S6/S5=>S4; (5) S5=>S1/S5=>S4; (6) S0=>S4/S0=>S2; (7) S0=>S5/S0=>S1; (8) S0=>S4/S0=>S1.

7.3 TEST 2

In Test 1, the multivariate analysis was proven to be more effective in terms of crack growth detection in comparison with univariate analysis. Thus, only the multivariate analysis was performed to analyze the data from Test 2. The features considered in the previous section were used simultaneously to construct a multi-dimensional D.I. vector for the outlier analysis. The "exclusive" MSD for each of the 124 measurements was calculated using Eq. (6.2). As was done for the data associated with Test 1, all of the seven feature types discussed in the previous section were considered, ranging from all combinations of two-dimensional D.I. vectors to the single combination of the seven-dimensional vector. A total of 3,120 cases were analyzed. The total is the result of the application of all 120 possible features' combinations to each of the 26 D.I.s considered in this study.

Figure 7.8 shows the results of the single combination of the 7-dimensional vector formed by the statistical features applied to the following features' ratios: S9=>S6/S9=>S8, S9=>S1/S9=>S8, S5=>S6/S5=>S4, S5=>S1/S5=>S4, S0=>S4/S0=>S2, S0=>S5/S0=>S1, S0=>S4/S0=>S1, and S5=>S0/S5=>S4 against cycle number respectively. Because the

abscissas range from 0 to 480,000, the plots present the results associated with both Test 1 (0 – 180,000) and Test 2 (180,001 - 380,000). By comparing the MSD presented in Fig. 7.8, it is once more evident that certain waveform paths outperform other paths in terms of crack growth detection. In figures (a), (b), (c) and (d), the MSD values increased during the first 180,000 cycles and stayed relatively constant from 180,000 to 485,000. For instance, the wave path S5=>S6/S5=>S4 increased dramatically at the first 25,000 cycles in which crack 1 was artificially increased, and stayed constant in Test 2 for the reason that crack 2 was 'shadowed' by the welding joints. In figures (e), (f) and (g), increasing tendency could be observed from 180,000 to 330,000 cycles, which suggests crack growth along this period. Thus, different behaviors of one PZT wave path in different tests and of different PZT wave path in same test suggest the possibility of crack growth detection and crack localization.

It can be remarked that the cluster of data observed in Figs. 7.8a, 7.8b, and 7.8c and located between 295,000 and 340,000 cycles are related to lost connections occurring at sensors 6, 7, and 8. After the connection was re-established, a small shift of MSD values was observed.

To find, empirically, the best feature combination and the best wave propagation path able to detect the second crack, a quantitative study was performed using the values of the MSD associated with each of the 3,120 cases. The ranking was first executed in terms of percentage of outliers detected. Among the wave paths and feature combinations that were able to detect all damaged states, the combination ranked '1st', provided the largest ratio of MSD values between values after 330,000 cycles and values between 40,000 and 180,000 cycles.

For comparative purposes, Figure 7.9 shows the best and worst cases. Figure 7.9 a shows the MSD as a function of the cycle number from the time waveforms associated with path of S1=>S4/S1=>S2 and statistical features rms and var. Different patterns comparing MSD values of Test 1 which is the first 180,000 cycles and Test 2 suggests that the path of S1=>S4/S1=>S2 with features of rms and var was sensitive to the 2nd crack (stepwise behavior at Test 2) and 'deaf' to the first crack (constant behavior with variance at Test 1). Fig. 5.6h presents the result of the multivariate analysis associated with D.I. of S5=>S6/S5=>S4 with features of krt, rms, var, cf, kf, and max, which suggests that this path with this set of features was sensitive for the first crack (stepwise behavior at first 25,000 cycles) and not affected by the second crack (stay constant till the connection lost). The difference between Fig. 7.9a and Fig. 7.9c was caused by the different feature setting which has been discussed in section 5.1.2.
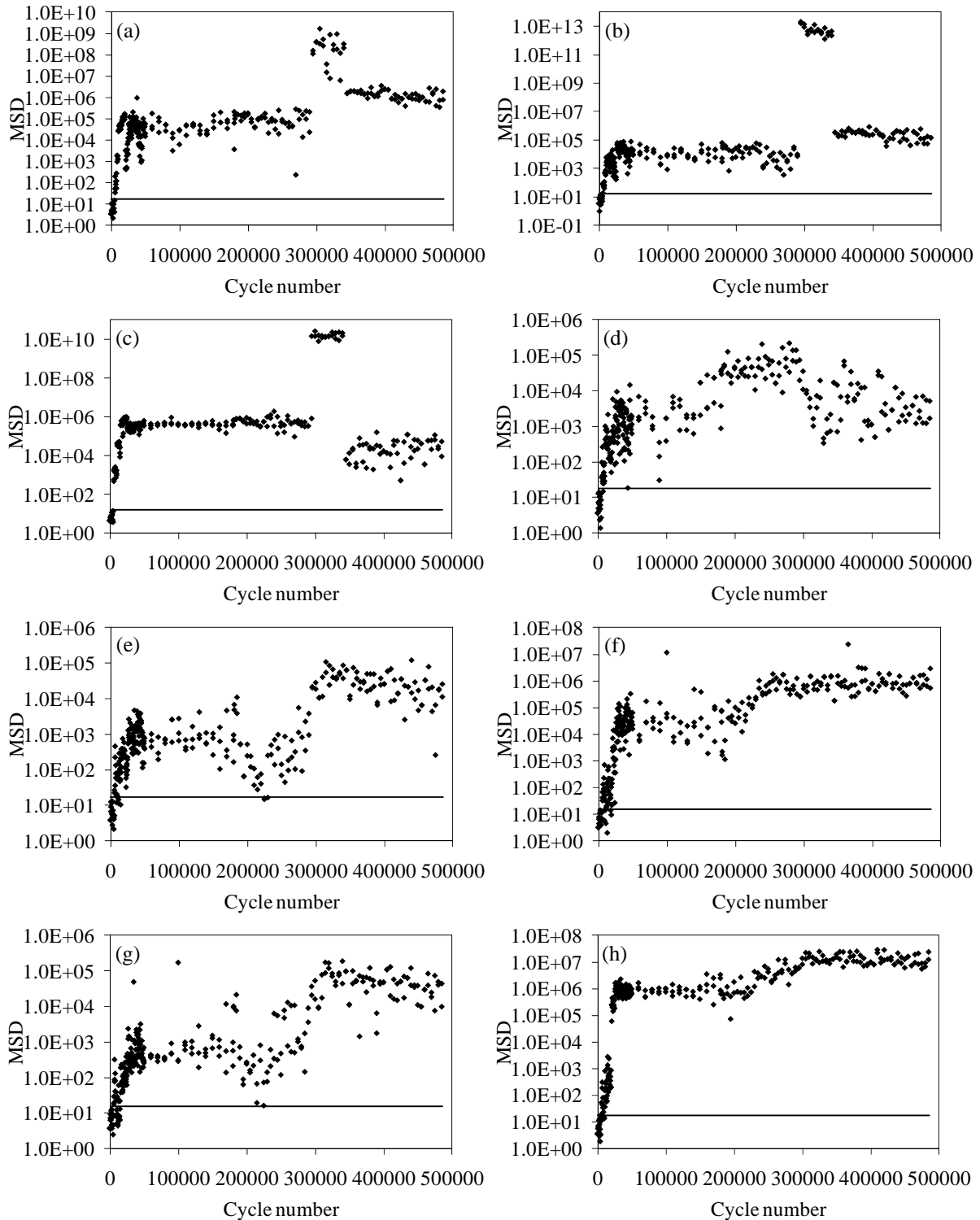
Figure 7.8 - Multivariate analysis. Mahalanobis squared distances as a function of the crack size for the actuator-sensor pairs considering all seven features: (a) S9=>S6/S9=>S8; (b) S9=>S1/S9=>S8; (c) S5=>S6/S5=>S4; (d) S5=>S1/S5=>S4; (e) S0=>S4/S0=>S2; (f) S0=>S5/S0=>S1; (g) S0=>S4/S0=>S1; (h) S5=>S0/S5=>S4.
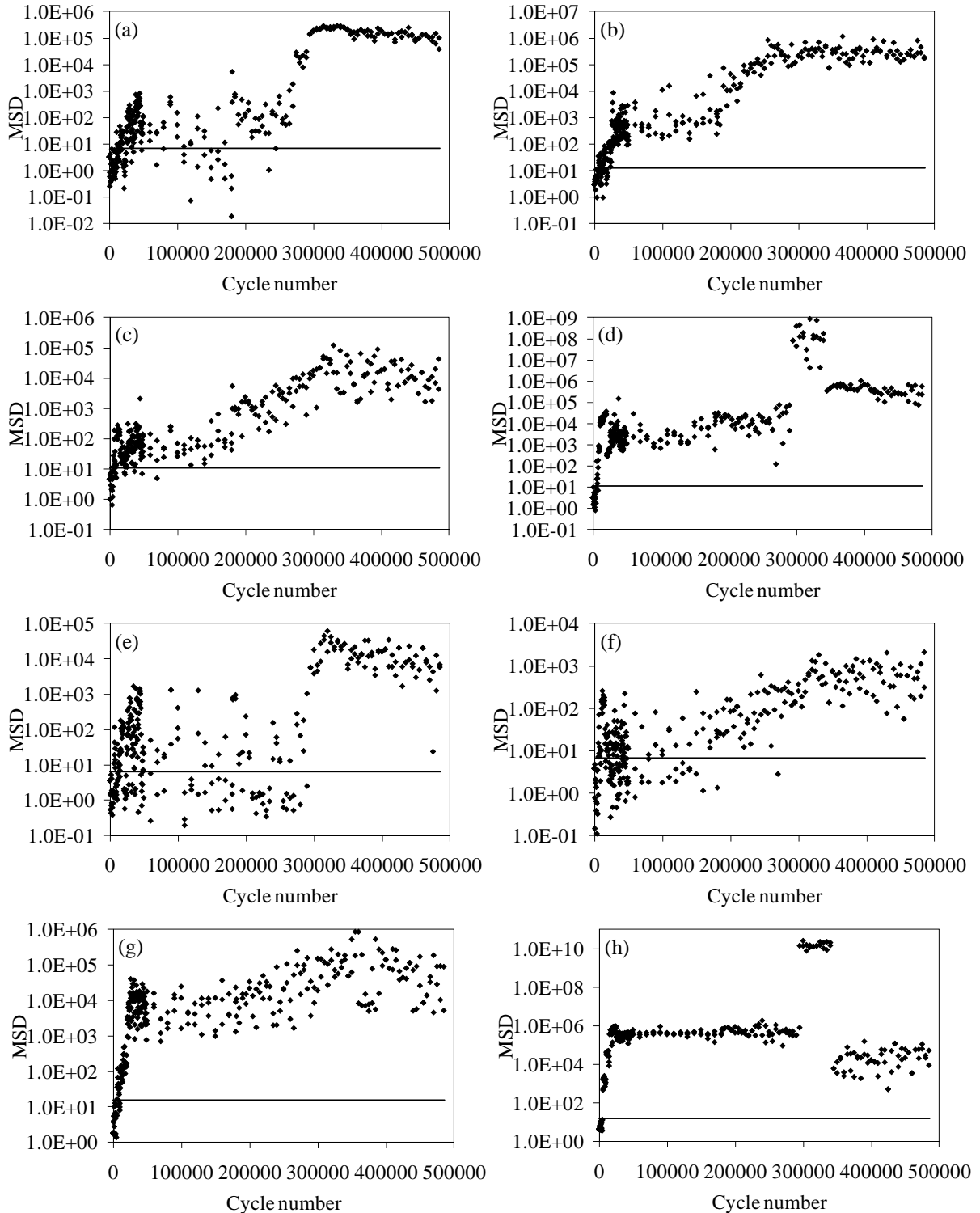
Figure 7.9 - Mahalanobis squared distances as a function of the crack size for the actuator-sensor pairs: (a) S1=>S4/S1=>S2 with rms and var (b) S0=>S5/S0=>S1 with krt, var, cf, kf, and ppk (c) S1=>S5/S1=>S2 with krt, var, cf, and kf (d) S9=>S6/S9=>S8 with rms, var, cf, and ppk; (e) S0=>S4/S0=>S2 with rms and var; (f) S1=>S4/S1=>S2 with krt and max;(g) S5=>S0/S5=>S4 with krt, rms, kf, max and ppk; (h) S5=>S6/S5=>S4 with krt, rms, var, cf, kf, and max.

7.4. TEST 3

Following the outcomes from tests 1 and 2, a few wave paths were considered for the analysis of the data associated with Test 3. The procedure used for the analysis of the time waveforms was the same adopted for Test 1 and 2, i.e. the first three or four wave energy packets were considered for the extraction of the seven statistical features discussed in Chapter 6.3.1.

For convenience, Table 6.1 is summarized in Table 7.2, which clusters several measurements under a certain combination of temperature, boundary condition, and damage level.

Measurement #	Temp C	Boundary	Inside/outside	Damage
1 - 10	17.7	dry	i	pristine
11 - 20	6.7	melting snow	i	pristine
21 - 22	8.2	dry	i	pristine
23 - 27	2	dry	o	pristine
28 - 32	2.7	dry	o	pristine
33 - 42	0.2	snow	o	pristine
43 -47	-2	snow	o	pristine
48 -49	6.5	dry	i	pristine
50 - 51	22	dry	i	pristine
52 - 53	17.2	dry	i	damage 1
54 - 55	22	dry	i	damage 1
56 - 60	3	melting snow	i	damage 1
61 - 65	3	dry	i	damage 1
66 - 70	3	dry	i	damage 2
71 - 75	0.3	melting snow	i	damage 2
76 - 80	10	dry	i	damage 2
81 - 85	22	dry	i	damage 2

Table 7.2 – Test 3. Summary of boundary condition, steel temperature, and joint condition.

Figure 7.10 shows the values of the RMS as a function of the measurement points for the following wave paths: S3=>S4/S3=>S2; (b) S3=>S0/S3=>S2; (c) S0=>S3/S0=>S1; (d) S0=>S4/S0=>S1. Paths S3=>S2 and S0=>S1 were chosen since the relative position of the sensors were such that the direct propagation of the wave from S0 to S1 or from S3 to S2 should not be affected by the presence of damage. Therefore evaluating the ratio of features using S3=>S2 or S0=>S1 is expected to normalize any effect associated with temperature or boundary conditions.

Given the positions of the transducers with respect to the location of the flaw, the damage index ratio S3=>S4/S3=>S2 plotted in Fig. 7.10a is expected to be affected by the presence of the damage, while the S0=>S4/S0=>S1 damage index plotted in Fig. 10d is likely to be immune by the notch.
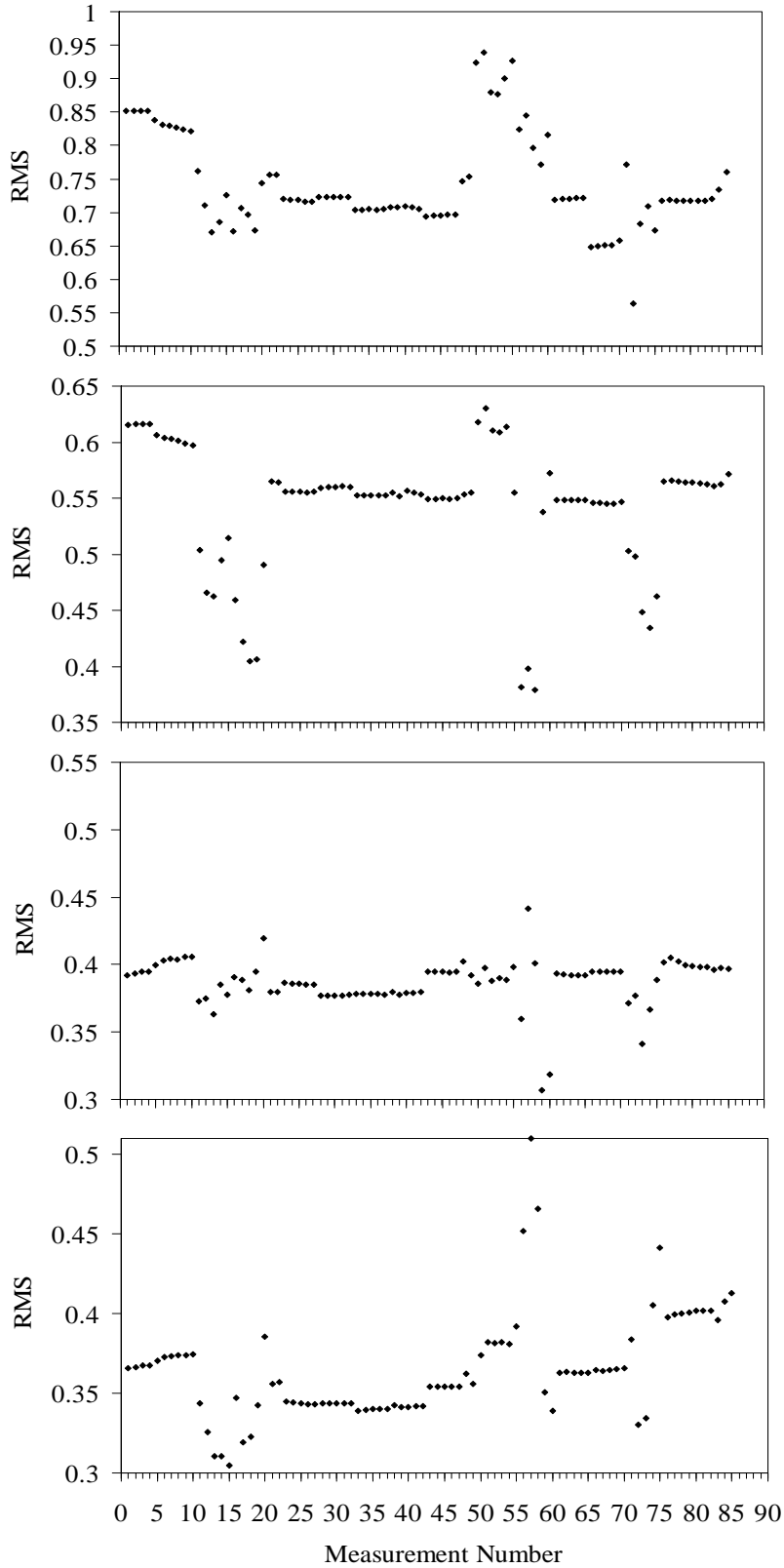
Figure 7.10 – Root Mean Square values as a function of the measurement number for: (a) S3=>S4/S3=>S2; (b) S3=>S0/S3=>S2; (c) S0=>S3/S0=>S1; (d) S0=>S4/S0=>S1.

Although damage index ratios are considered, it is evident from Fig. 7.10 that the values of the RMS are affected by the environmental conditions. By looking at Fig. 7.10a, a drop is visible in the RMS values in the measurement number range 11-49 when the structure was in pristine condition but the temperatures were several degrees Celsius below the baseline (17.7 C = 63.9 F). When the temperature of the steel was raised up to 22 C (71.6 F) by means of a heat gun and the structure was still pristine, the value of the RMS ratio was about 12% higher than the baseline, i.e. data taken during the first ten measurements. It should be noted that the heat gun was used with the objective of heating the chord along the span between sensors S0 and S3 uniformly. However, owing to the nature of the approach, it should not be excluded that a temperature differential between sensors was possible.

When the small notch was present and the structure was cooled a decrease in the value of the RMS is visible.

A step wise behavior is visible in Fig. 7.10a between a range of 61-65 and 66-70. Both ranges were under the same temperature and boundary conditions. The latter range was measured with larger crack. This means that the step clearly visible in Fig. 7.10a is associated with the increase of the size of damage. This hypothesis is corroborated by comparing the values of the RMS along the same range for Fig. 7.10b, 7.10c, and 7.10d. These three figures also confirm that the wave paths used in the analysis were not affected by the presence of damage, due to the relative position of the PZTs with respect to the notch.

The presence of melting snow on portions of the chord along the wave paths (measurements 11 – 20) caused a large scattering of the RMS values. The scattering is probably due to non-uniform melting that created various boundary conditions across different measurements. When compared to the baseline RMS values at 21 and 22 were taken under lower temperatures. An 11.76% decrease in Damage Index values suggests a positive correlation between the selected D.I. and temperature. For the measurement from 23 to 47, snow and temperature drop affected the wave propagation and the characteristics of the piezoelectric transducers.

The decrease in the ratio values across measurements 52 to 60 confirms the hypothesis that a decrease in temperature induces a decrease in RMS ratio observes looking across the measurement range 1-20.

The size of the artificial defect was augmented after measurement 65. Within measurements 61 to 70, the temperature and boundary conditions were purposely left the same. Therefore, the step visible in Fig. 7.10a should be associated with the increase of damage size. During the last twenty measurements (66 - 85) stepwise increases were observed as a consequence, most likely, of temperature increase.

Overall, by comparing the values plotted in Fig.7.10a, the range of the RMS values with respect to the baseline spans from +11.7% (measurement 51) to -35.2% (measurement 72).

Similar considerations can be made by observing Figures 7.10b-7.10d. For these three figures it should be noted that the scattering from the baseline data is lower when compared to Fig. 7.10. The effect of the temperature over the values of the RMS ratio seems higher than the effects associated with the boundary conditions and the boundary condition.
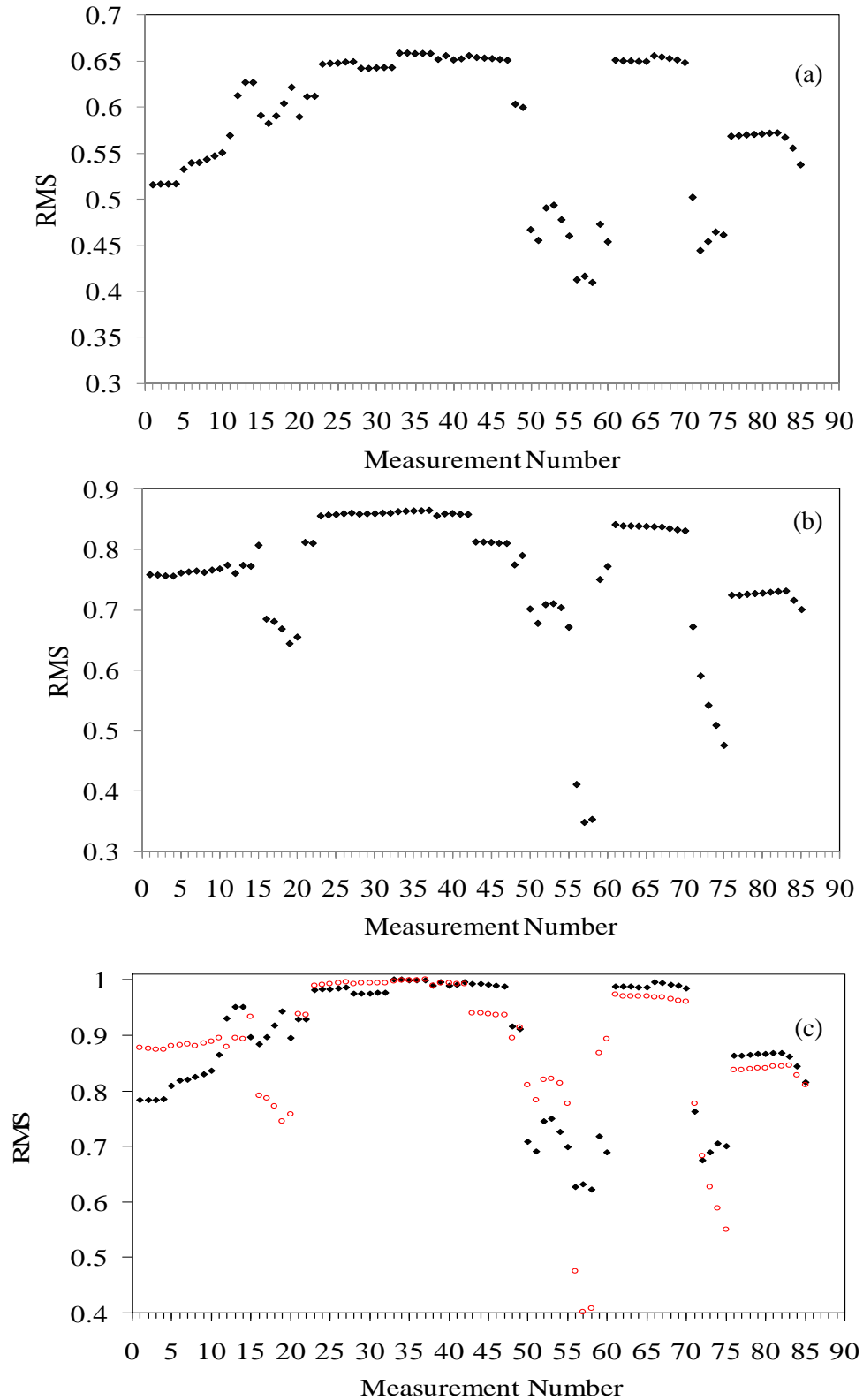
Figure 7.11 – Test 3. RMS for path: (a) S3=>S2; (b) S0=>S1; (c) Normalized RMS for S0=>S1 (red circles) and S3=>S2 (black dots).

To isolate the effect of the temperature and boundary conditions from the effect of damage, the statistical features associated with the time waveforms along paths S3=>S2 and S0=>S1 were investigated. Owing to the position of PZTs S0, …, S3, these two path must have been immune from defect, as long as the portion of the time series considered did not interfer with any reflections from the notch. The values of the RMS, as a function of the measurement number associated with these two paths, are presented in Fig. 7.11a and 7.11b. The normalized values of the RMS are overlapped in Fig. 11c. Figure 11 shows that although there are some quantitative differences in the values of the RMS, the overall changes associated with varying conditions are quite similar.

Interestingly the effect of the temperature seems to be opposite of that observed in Fig. 7.10. In fact, the temperature decrease determined an increase in the value of the RMS. Within the range 61 – 70 there was not a visible variation of the RMS. Within this range the damage state of the notch changed but all other conditions were the same. Across the range 23 – 42 a constant response of the time waveform statistical feature is observed. This range covers absolute temperatures of about 2 C (3.6 F) and with pristine structure. Surprisingly it seems that the presence of snow does not affect the measurements.

To quantify the effect of the temperature and boundary conditions on the other features considered in this study, Fig. 7.12 is presented. It contains the values normalized with respect to the first measurement of the baseline, which therefore assume a value of 100%. The percentage scale was used to provide a quantitative estimate of the data scattering from the baseline. Figure 7.12 illustrates the results associated with paths S3=>S2 and S0=>S1, because the effect of damage was purposefully ignored.
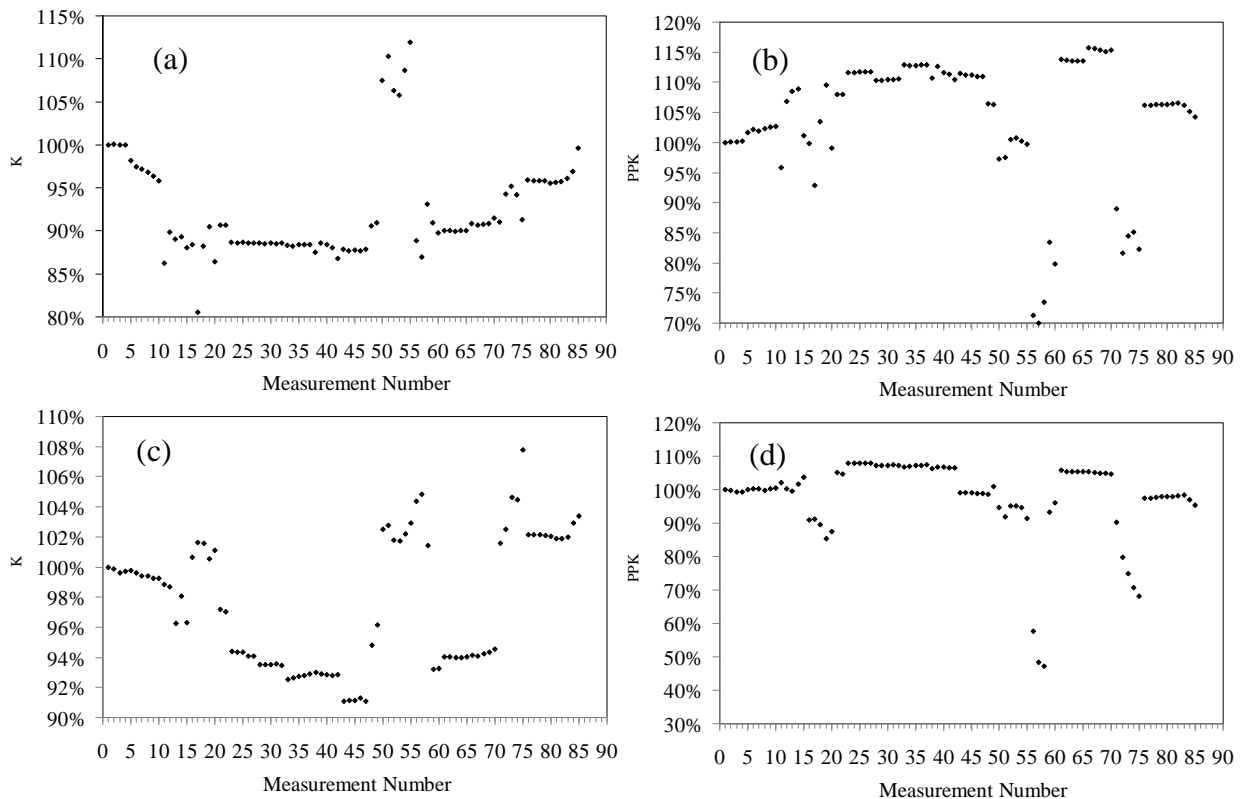
Figure 7.12 – Test 3. Path S3=>S2 (a) K–factor, (b) peak-to-peak. Path S0=>S1 (c) K–factor, (d) peak-to-peak.

137
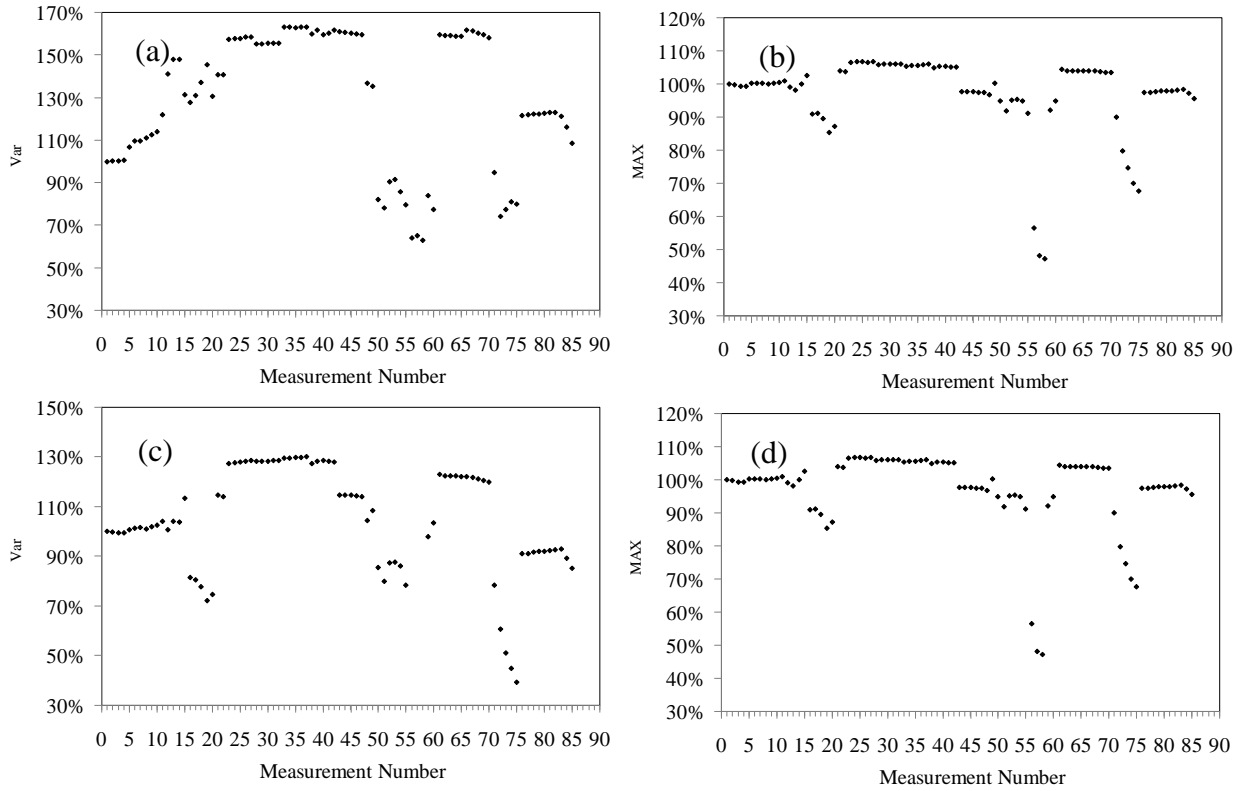
Figure 7.13 – Test 3. Path S3=>S2 (a) variance, (b) maximum. Path S0=>S1 (c) variance, (d) maximum.
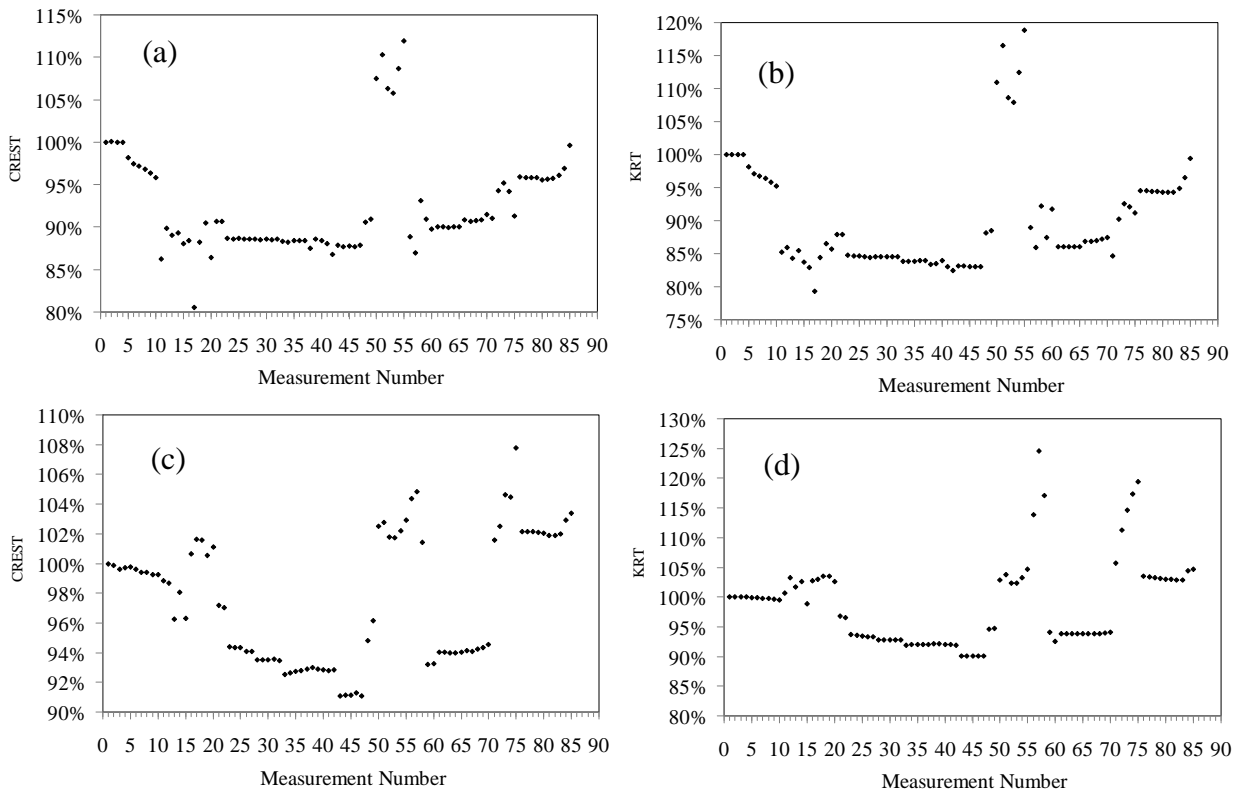
Figure 7.14 – Test 3. Path S3=>S2 (a) crest factor, (b) kurtosis. Path S0=>S1 (c) crest factor, (d) kurtosis.

Overall, the trend is similar although by comparing the values on the y-axis, some features are less sensitive to the temperature variation.

The damage index ratios S3=>S4 /S3=>S2 and S0=>S4 / S0=>S1 associated with six statistical features are presented in Fig. 7.15a and 7.15b, respectively. The graph of the chord's temperature is overlapped and its values are plotted against the right ordinate axis. The two vertical lines indentify the measurement at which the small crack was devised and
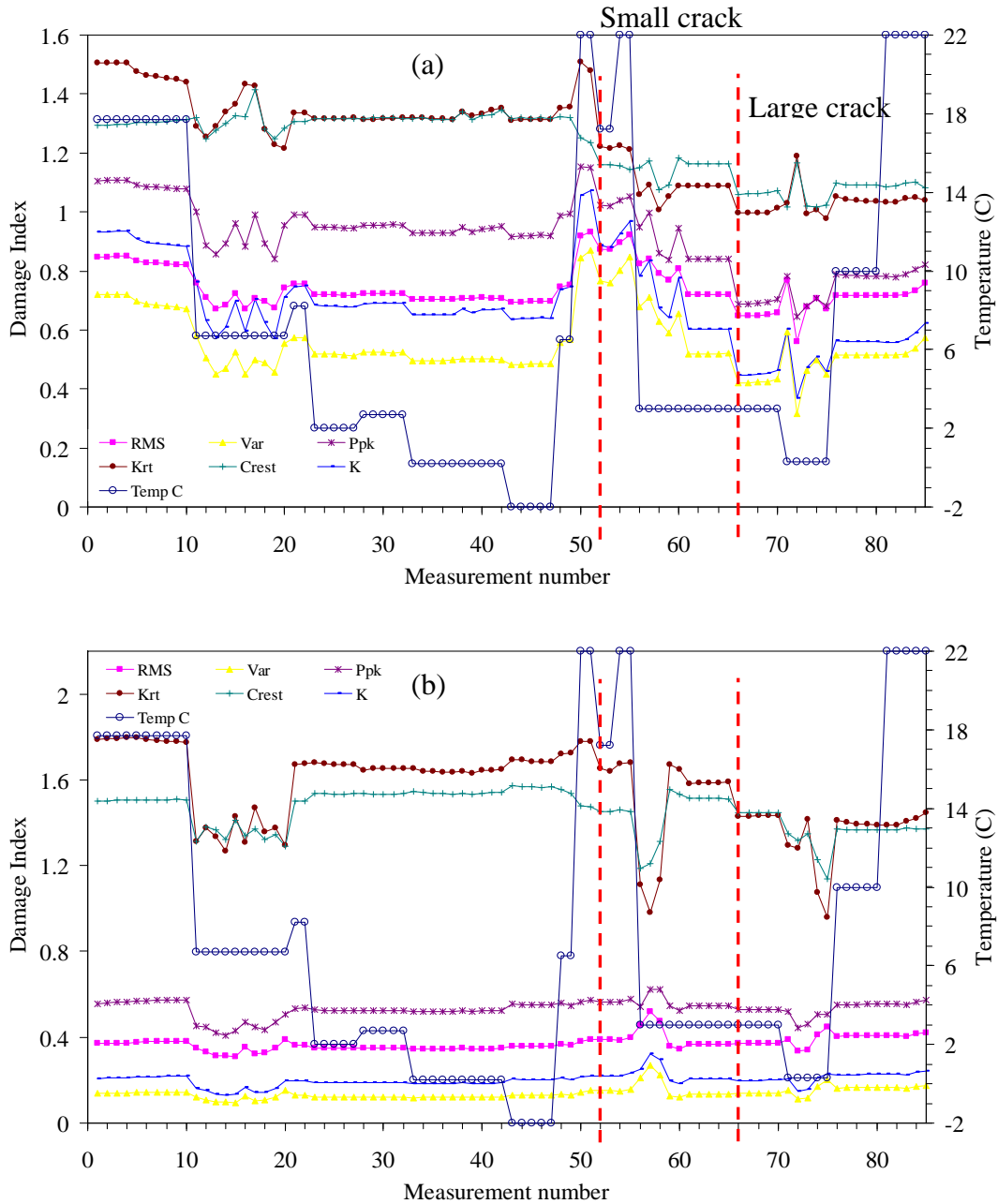
Figure 7.15 – Damage Index as a function of the measurement number associated with six features. (a) Ratio S3=>S4 /S3=>S2. (b) Ratio S0=>S4 / S0=>S1. The value of the temperature at each measurement number is scaled on the y-axis on the right.

when the small crack was enlarged.

In both Fig. 7.15a and Fig. 7.15b there is no clear stepwise behavior associated with the formation of the small crack after measurement 51. However after measurement 65, when the small crack was expanded, a step is visible in all six features associated with the damage index ratio S3=>S4 /S3=>S2, which was expected to be affected by the presence of damage. A step between measurement 65 and 66 is also visible in the plot of the crest and kurtosis associated with the ratio S0=>S4 / S0=>S1. Such behavior was not expected and could be used to ignore such statistical features.
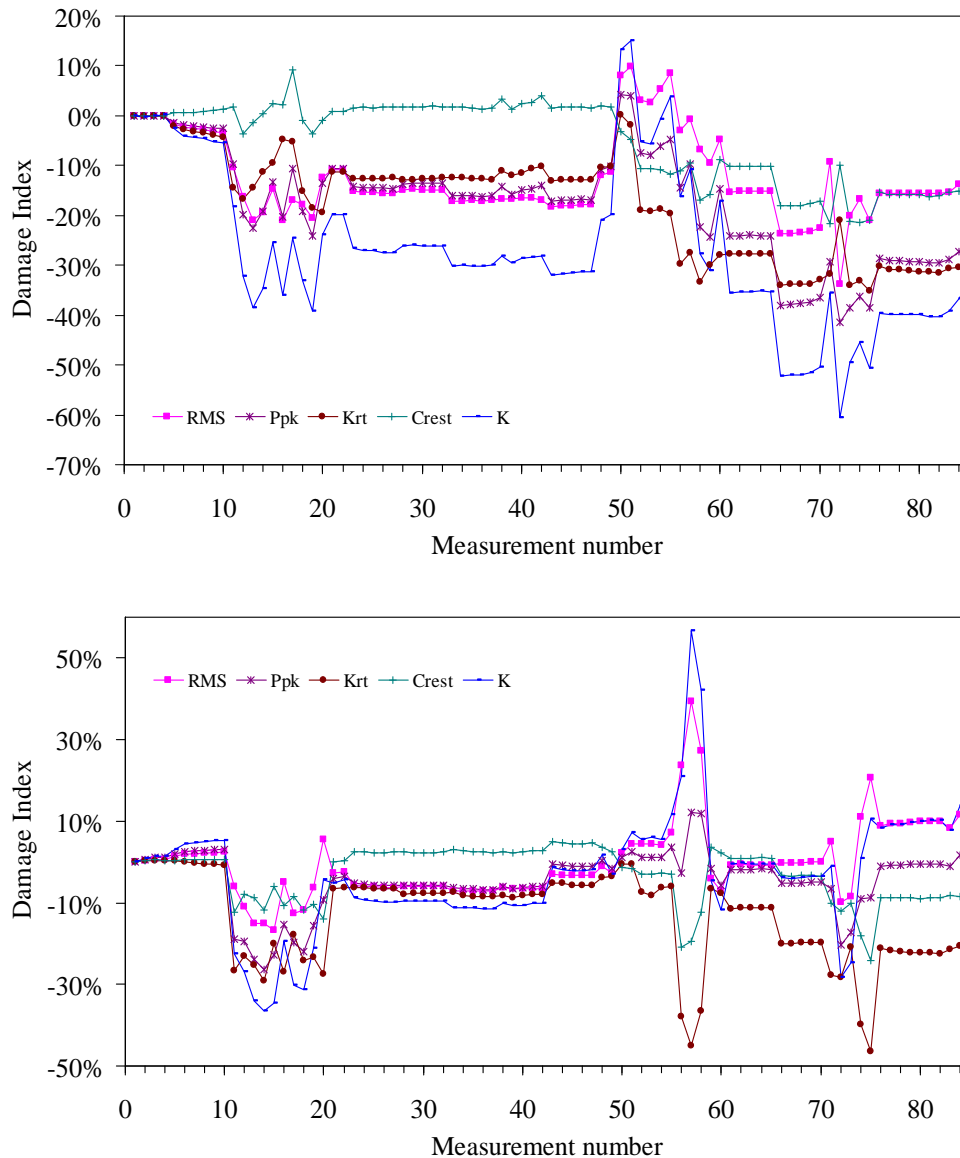
Figure 7.16 – Percentage variation of the damage index as a function of the measurement number associated with six features with respect to the value calculated during the first measurement. (a) Ratio S3=>S4 /S3=>S2. (b) Ratio S0=>S4 / S0=>S1. The value of the temperature at each measurement number is scaled on the y-axis on the right.

To quantify the variation in percentage of the damage index with respect to the first measurement, Fig. 7.16 is presented. The figures show that the K-factor and the RMS had the largest variation.

The temperature dependency of the results observed in the previous Figures is mainly due to the characteristics of the PZT. A recent work by Lanza di Scalea and Salamone (2008) has investigated the effect of temperature on the guided Lamb wave propagation. The temperature-dependent properties of the PZTs are the following: Young's moduli, Poisson's ratios, piezoelectric coefficients; dielectric permittivity; and length and thickness.

Other factors that affected the results are the following: 1) not uniform distribution of the temperature when the heat gun was used; 2) variation in size and thickness of the adhesive; 3) variation of the adhesive mechanical properties.

To shed some light on the cause of such a discrepancy associated with the various measurements the time waveforms associated with propagation paths S3=>S2 and S3=>S4 are presented in Fig. 7.17 and 7.18, respectively. The plots refer to measurement number 1, 25, 61, and 68. All these measurements had dry conditions in common.

From Fig. 7.17 it is possible to observe that except for the first arrival at about 110 microseconds, the shape of all the ultrasonic packets is overall similar. As is said earlier, wave path S3=>S2 was not influenced by the presence of damage. Although wave path S3=>S4 should be affected by the presence of damage, Fig. 7.18 does not show any evident shape/amplitude difference among the four cases presented.
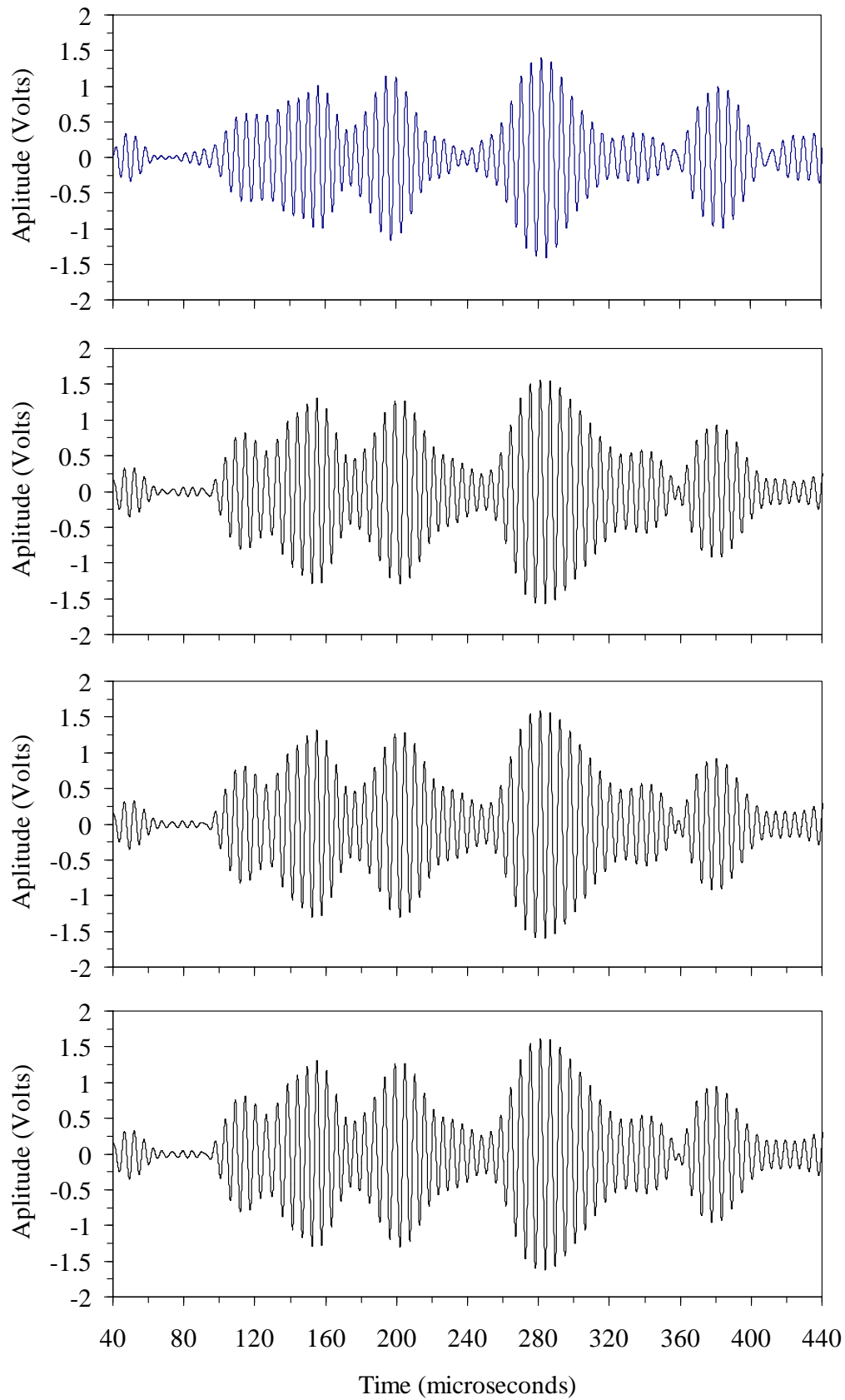
Figure 7.17 – Time waveforms generated by actuator S3 and sensor S2. From top to bottom: measurement number 1. 25. 61, 68.
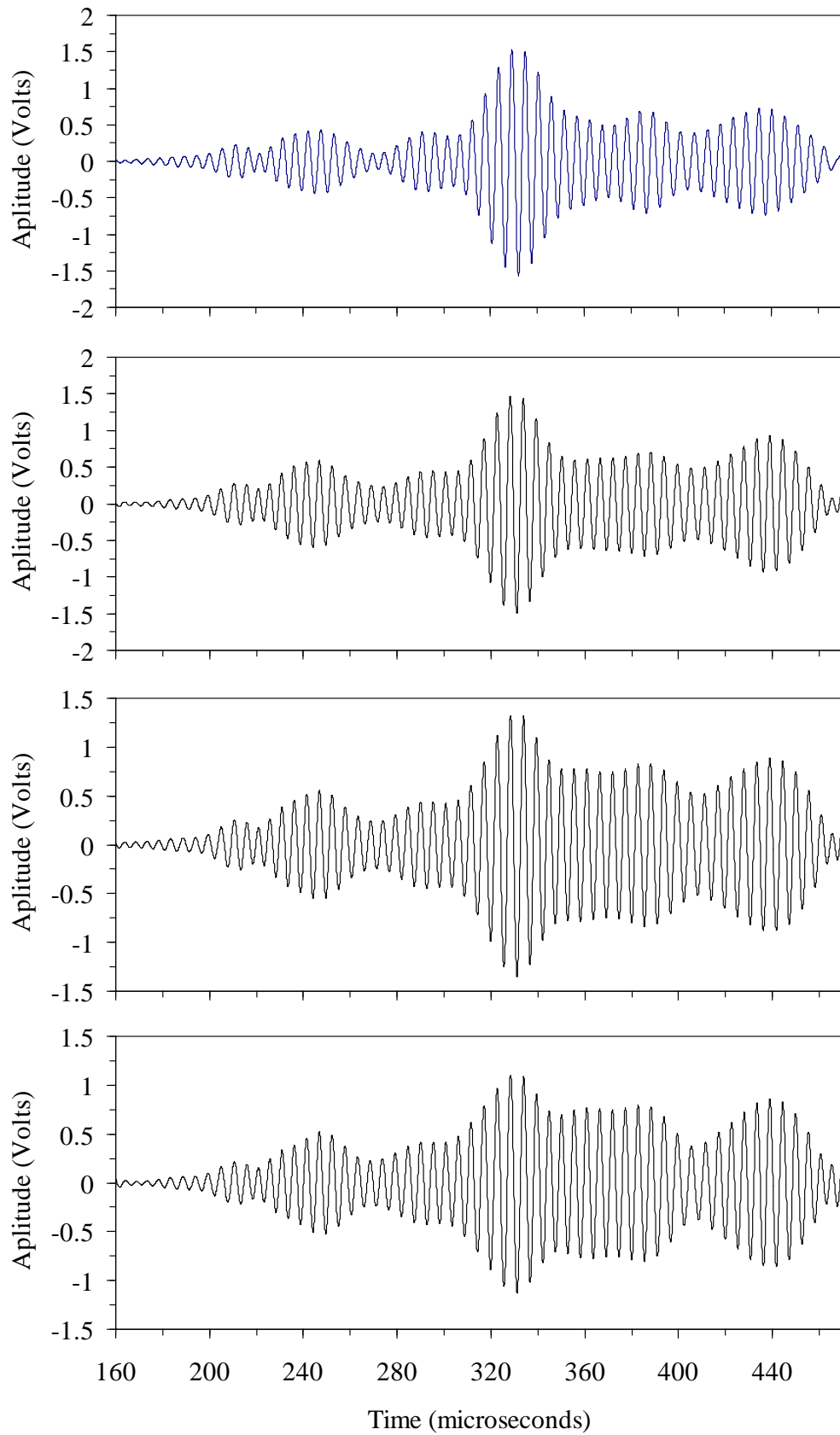
Figure 7.18 – Time waveforms generated by actuator S3 and sensor S4. From top to bottom: measurement number 1. 25. 61, 68.

To complete the analysis of Test 3, the outlier analysis was conducted. The MSD associated with the seven features calculated for four damage index ratios is presented in Fig. 7.19. In this analysis the first ten measurements only were considered for the baseline, and therefore for the computation of the threshold level. Clearly, all data were classified as outliers and there is no evidence that data from a damaged state could be discriminated.
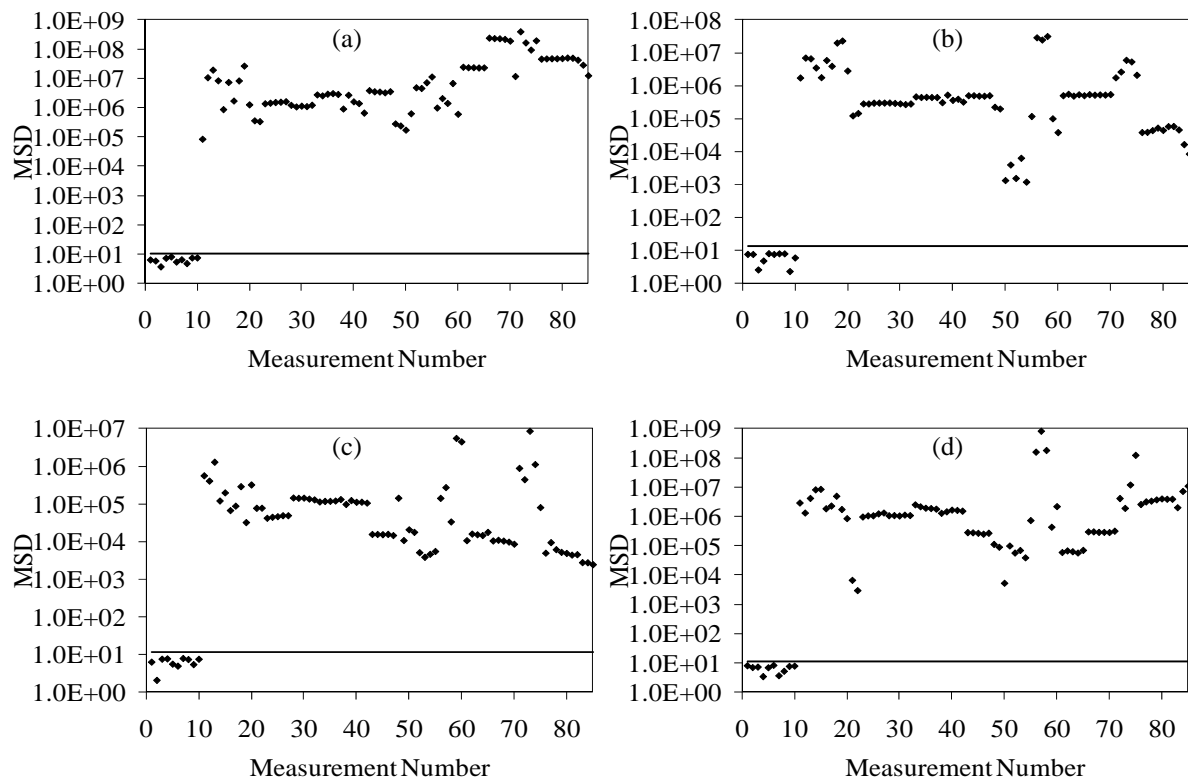
Figure 7.19 - Multivariate analysis. Mahalanobis squared distances as a function of the measurement number considering all seven features for the following: (a) S3=>S4/S3=>S2; (b) S3=>S0/S3=>S2; (c) S0=>S3/S0=>S1; (d) S0=>S4/S0=>S1.

Because the scope of any outlier analysis applied to ultrasonic-based damage detection strategy is to find structural anomalies, the number baseline data were increased to include the first 51 measurements. The results of this multivariate analysis are presented in Fig. 7.20. Clearly an improvement in the success rate is visible. In fact Fig. 7.20a shows the largest number of outliers. This is expected as the data refers to C3=>C4/C3=>C2, which is affected by the presence of damage. On the contrary, the plot in Fig. 7.20d, which is related to the damage index ratio C0=>C4/C0=>C1, shows few outliers.

Finally, the same computation was made by considering the first 41 measurements a baseline. The results are reported in Fig. 7.21.
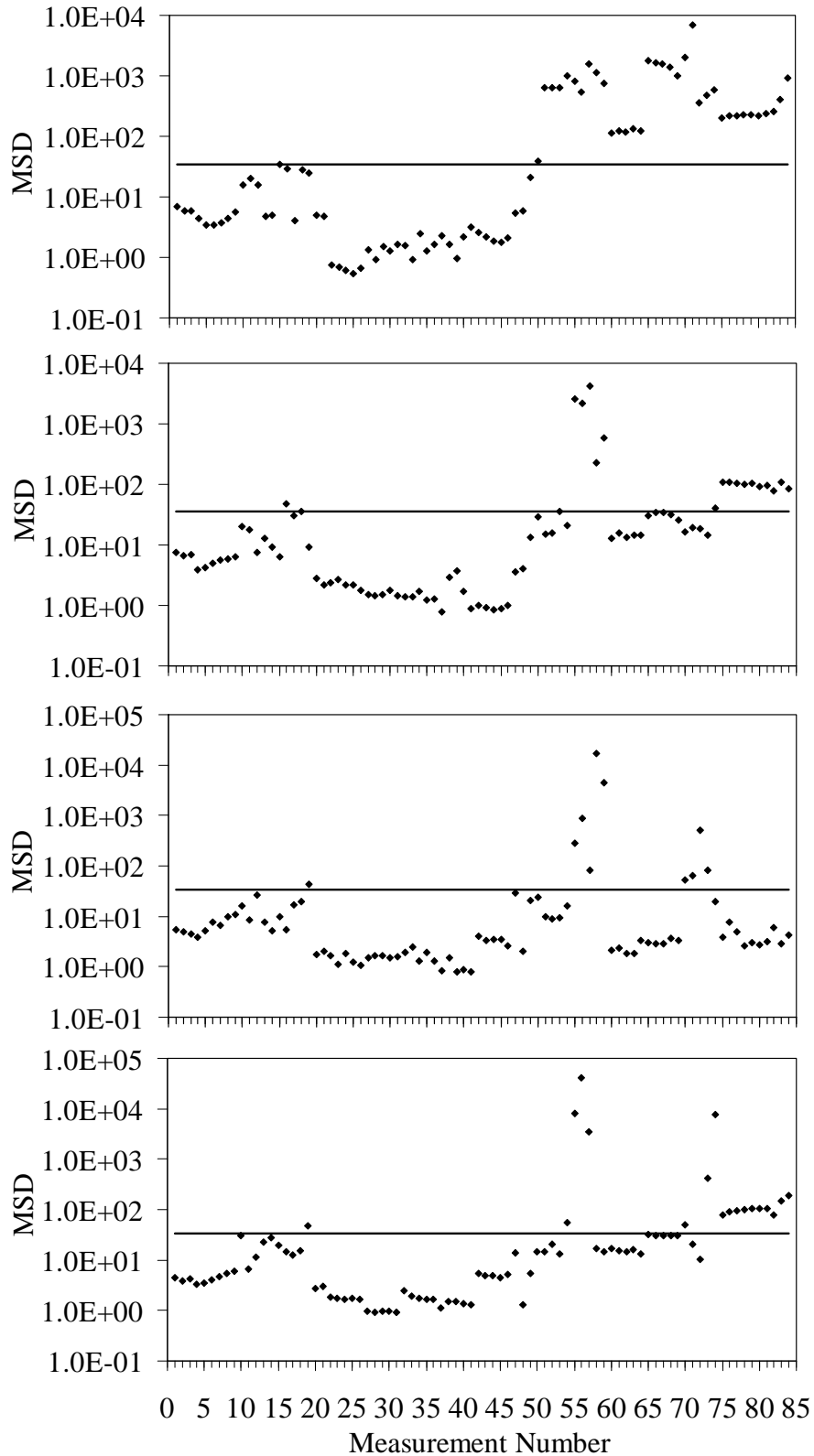
Figure 7.20 – MSD as a function of measurement number for paths (a) C3=>C4/C3=>C2, (b) C3=>C0/C3=>C2, (c) C0=>C3/C0=>C1, and (d) C0=>C4/C0=>C1. The first 51 measurements were considered a baseline.
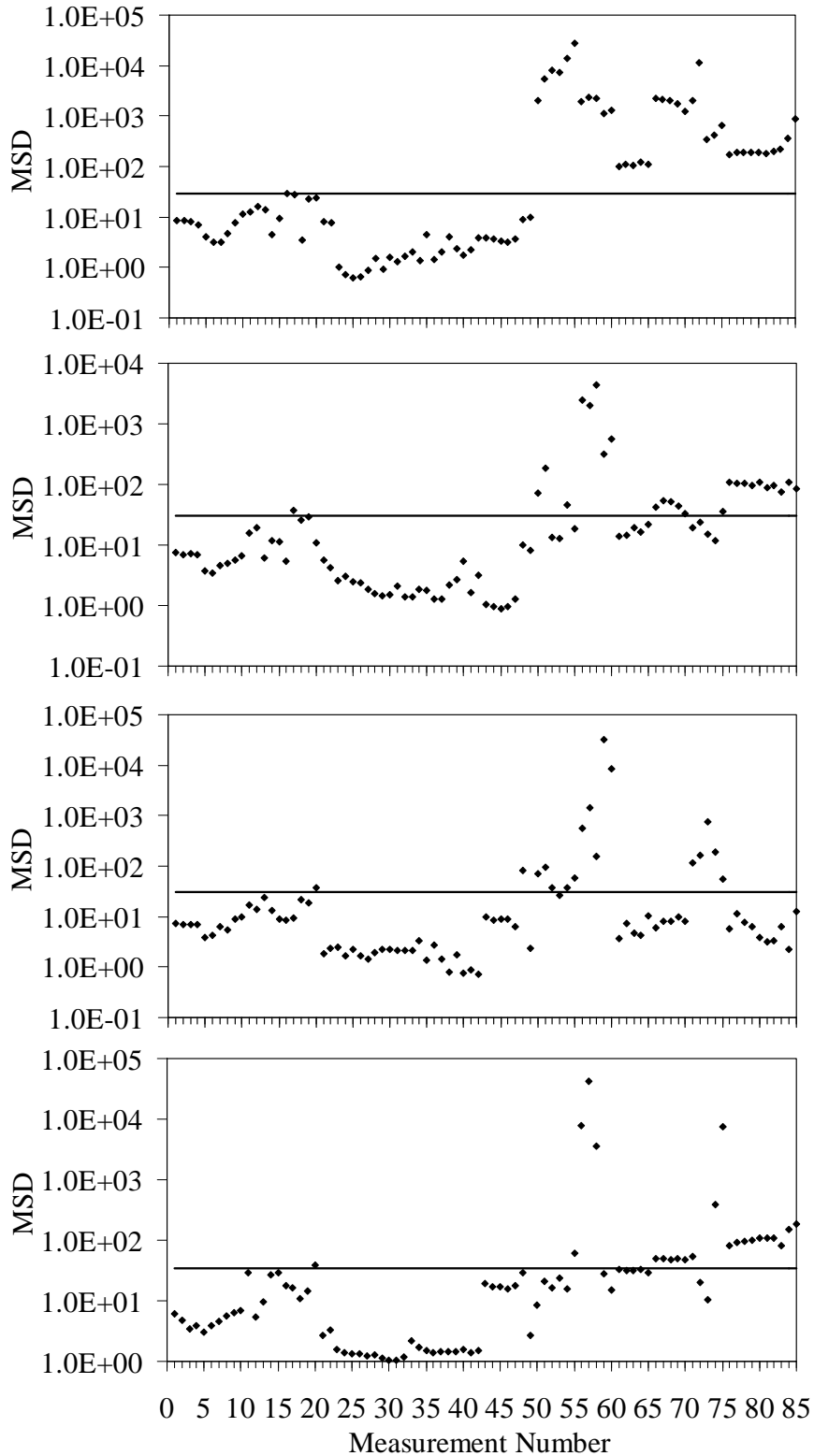
Figure 7.21 – MSD as a function of measurement number for paths (a) C3=>C4/C3=>C2, (b) C3=>C0/C3=>C2, (c) C0=>C3/C0=>C1, and (d) C0=>C4/C0=>C1. The first 51 measurements were considered as baseline.

CHAPTER 8: EXPERIMENTAL RESULTS from EMI

8.1 LOW-COST CIRCUITRY

To conduct the EMI measurements by means of the portable NI-PXI, a low cost electric circuit was designed. The aim was to develop a low-cost system that would not require the use of a conventional impedance analyzer or LCR meter.

According to the scheme illustrated in Fig. 8.1, the output of the function generator was connected to the circuit consisting of a PZT and a resistor. The nodes of the circuit were also connected to the PXI digitizer. The LabView program illustrated in Figs. 6.6d and 6.6e controlled the generation of a 1-Volt amplitude, 50-cycles sinusoidal wave. The sine wave frequency was driven from 100 KHz to 500 KHz with 0.5 KHz step.
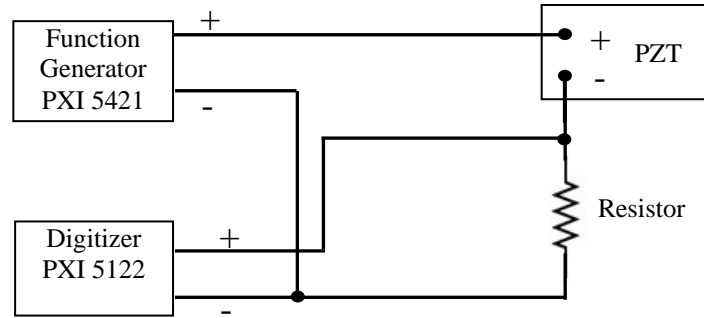
Figure 8.1 – Design of the circuit and its connection to the PXI for EMI measurement.

Once the digitizer collected the output waveform V_o from the resistor, the calculation of the PZT admittance $Y(j\omega)$ was executed by applying the following equations:

$$Y(j\omega) = \frac{1}{R_s} \cdot \frac{u_o(j\omega)}{u_i(j\omega) - u_o(j\omega)} = \frac{1}{R_s} \cdot \frac{V_o e^{j(\omega t + \beta)}}{V_i e^{j\omega t} - V_o e^{j(\omega t + \beta)}}$$

$$= \frac{1}{R_s} \cdot \frac{V_o \angle \beta}{V_i \angle 0 - V_o \angle \beta} = \frac{V_o}{R_s} \cdot \frac{\cos \beta + j \sin \beta}{V_i - V_o \cos \beta - jV_o \sin \beta}$$

$$= \frac{V_o}{R_s \cdot \sqrt{(V_i - V_o \cos \beta)^2 + (V_o \sin \beta)^2}} \cdot \frac{\angle \beta}{\angle arc \tan(-\frac{V_o \sin \beta}{V_i - V_o \cos \beta})}$$

$$= \frac{V_o}{R_s \cdot \sqrt{(V_i - V_o \cos \beta)^2 + (V_o \sin \beta)^2}} \cdot \angle(\beta - arc \tan(-\frac{V_o \sin \beta}{V_i - V_o \cos \beta}))$$

$$= M \cdot \cos \alpha - jM \cdot \sin \alpha \tag{8.1}$$

where is the admittance, u_i and u_o are the input and output signals, respectively, V_i and V_o are the amplitude of the input and output signals, R_s is the value of resistance and β is the phase shift between the input signal and output signal, $j^2=-1$, ω is the angular frequency.

In Eq. 8.1, M and α are defined as follows:

$$\alpha = \beta - arc\tan(-\frac{V_o\sin\beta}{V_i - V_o\cos\beta}), M = \frac{V_o}{R_s \cdot \sqrt{(V_i - V_o\cos\beta)^2 + (V_o\sin\beta)^2}}$$

(8.2)

To assess the performance of this circuit, a comparative study between the Labview program combined with the designed circuit and a commercial LCR meter was conducted. The EMI signatures of two PZTs were measured by both methods and the results are shown in Figure 8.2. Figures 8.2a and 8.2b present the conductance and the susceptance, respectively, as a function of frequency associated with the first PZT. The results from the test on the second PZT are presented in Fig. 8.2c and 8.2d. By observing these figures it is evident that the PXI system is capable of identifying the main peaks for both conductance and susceptance and it agrees very well with the results obtained from the LCR meter. The differences could be a result of the impedance introduced by NI PXI and the switch module. Meanwhile, the conductance became coarse and 'noisy' at higher frequency.
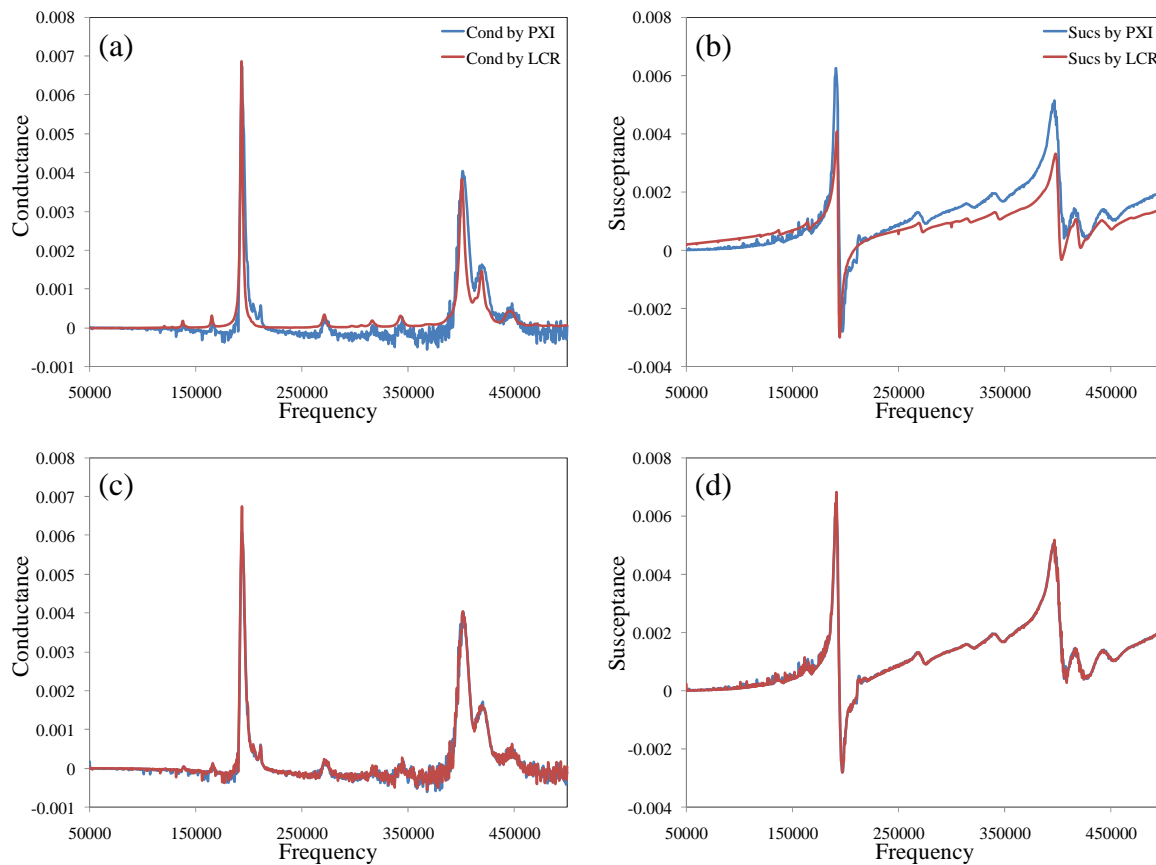
Figure 8.2 – Comparative study between LCR and low-cost circuit conducted on two PZTs. Conductance as a function of frequency for (a) PZT 1 and (c) PZT 2; susceptance as a function of frequency for (a) PZT 1 and (c) PZT 2.
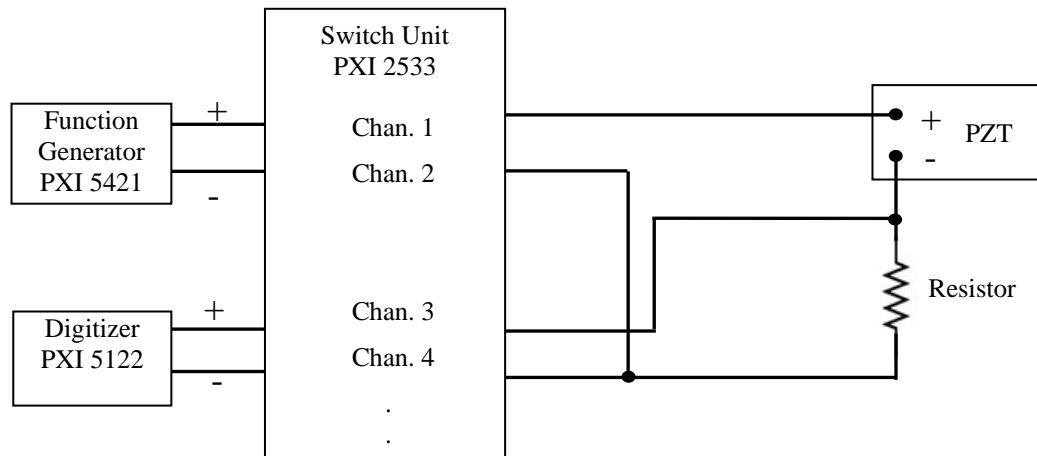
Figure 8.3 - Design of the circuit and its connection to the PXI and the switch for multiple EMI measurement

As for the structure, many PZTs were potentially used, and the low cost circuit had to be integrated with the PXI switch unit. The function generator output was connected to the switch unit according to the scheme illustrated in Fig. 8.3.

A photo of the hardware system is presented in Fig. 8.4

Figure 8.5 illustrates the connection setup for the EMI measurement coupled with PXI: in Fig. 8.4 (a), high-density matrix switch module PXI-2532 is directly connected with the front-mounting terminal block TB-2643, and the SCB-264X terminal block provides screw terminal access to the row and column connections of the PXI-2532 switch via an NI TB-264x terminal; the physical connection scheme in the screw terminal for the situation in Fig. 8.2 is shown in Fig. 8.4 (b). The PZTs and the circuits interact with the screw terminal and the channel switching is controlled by the LabView program and the topology for the specified switch module.

The program was designed to control as many as 16 PZTs by using the connection topology illustrated in Fig. 8.5. In this topology r0 and r1 are the positive and negative outputs of the PXI digitizer, respectively, and r2 and r3 are the positive and negative outputs of the PXI function generator, respectively. In the topology c0, …, c63 denominates the terminals of the PXI switch unit. In this particular experiment, for instance, c0…, c3 serve to connect EM1 to the PXI following the scheme illustrated in Fig. 8.2. The LabView program designed for the EMI measurement, and illustrated in Fig. 4.4d and 4.4e, relayed the driving signal from the function generator to the proper EMI sensor.

To further validate the proposed measurement system, the admittance signatures from one of the PZTs bonded to the truss structure, namely EM1, was measured by both methods. The results are shown in Fig. 8.6. Overall the agreement is satisfactory.
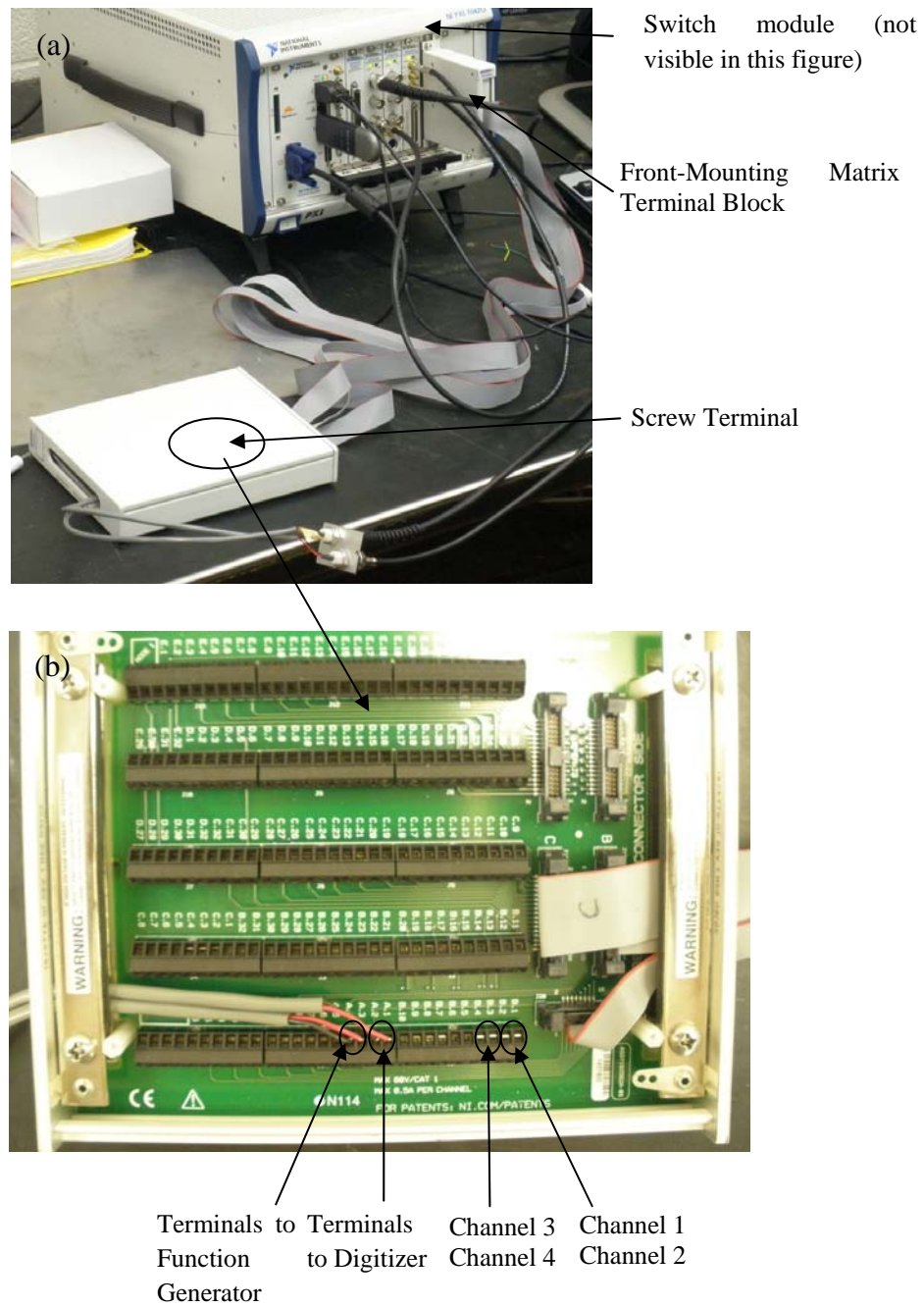
Figure 8.4 – Hardware for the EMI measurement. (a) PXI, switch module, terminal block and screw terminal. (b) Inside view of the screw terminal.

.
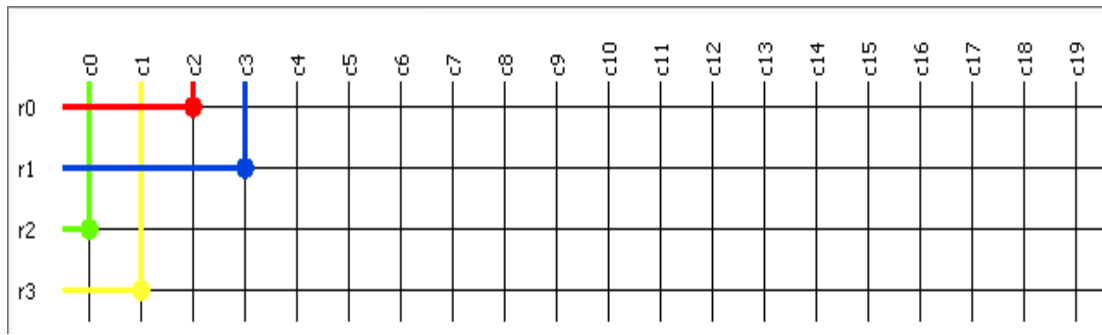
Figure 8.5 - Connection topology adopted for the NI Switch front panel and first PZT.
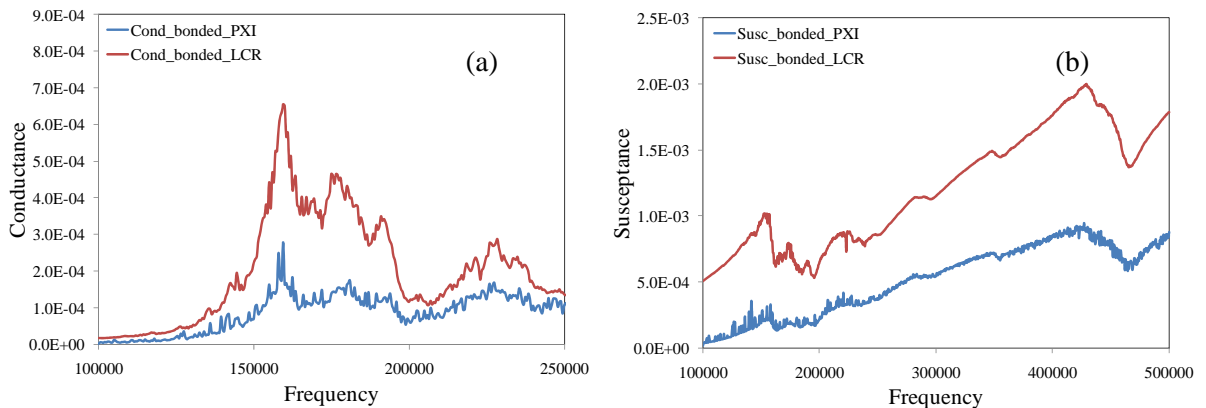
Figure 8.6 - (a) Conductance resulted from PXI and LCR meter for EM1 bonded with the truss structure; (b) Susceptance resulted from PXI and LCR meter for EM1 bonded with the truss structure.

8.2 EMI-RELATED SIGNAL PROCESSING ALGORITHM

The overall SHM algorithm implemented in this study for the EMI study is illustrated in the flowchart in Fig. 8.7.

The first step consisted of the measurement of the conductance signatures. Example of signatures acquired from EM1 and EM2 at different cycle number and focused in the frequency range 100 – 250 kHz are shown in Fig. 8.8. The figures show that as the crack increased, there was a shift of the conductance peak.

From each conductance signature (conductance as a function of frequency) the features of the variance, RMS, max amplitude, kurtosis, and skewness were calculated. Moreover, the area under the signature and the RMS Deviation (RMSD) were computed as well. The RMSD is defined as follows:

$$RMSD\ (\%) = \sqrt{\frac{\sum_{i=1}^{N}\left(y_i^k - y_i^1\right)^2}{\sum_{i=1}^{N}\left(y_i^1\right)^2}} \times 100 \qquad (8.3)$$

151
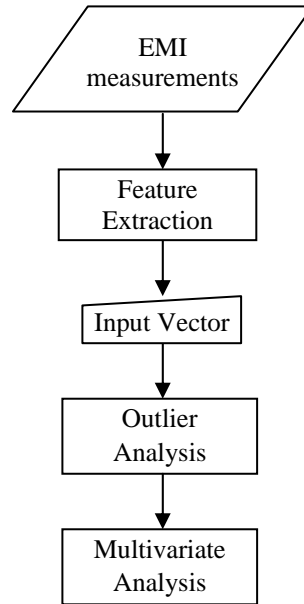
Figure 8.7 - Flowchart of the defect detection procedure

where y_i^k , y_i^1 are respectively k-th and baseline state admittance at a frequency i, N represents the upper limit (i.e. in a range comprising of N frequencies) and $\overline{y^k}$ is the mean of the admittances obtained at k-th state for N frequencies. This feature compares the quantitative deviation of the *k-th* measurement with the baseline signature.

The RMSD as a function of the cycle number associated with the measurements conducted with EM1 and EM2 in the frequency range 100 - 500 KHz are shown in Fig. 8.9.

Figure 8.10 shows the values of the remaining features as a function of the cycle number. The plots in the left column are associated with EM1 while the plots on the right column are associated with transducer EM2. When compared with the performance of the ultrasonic measurement, both Figs. 8.9 and 8.10 do not reveal significant patterns that relate the features to the presence of damage.
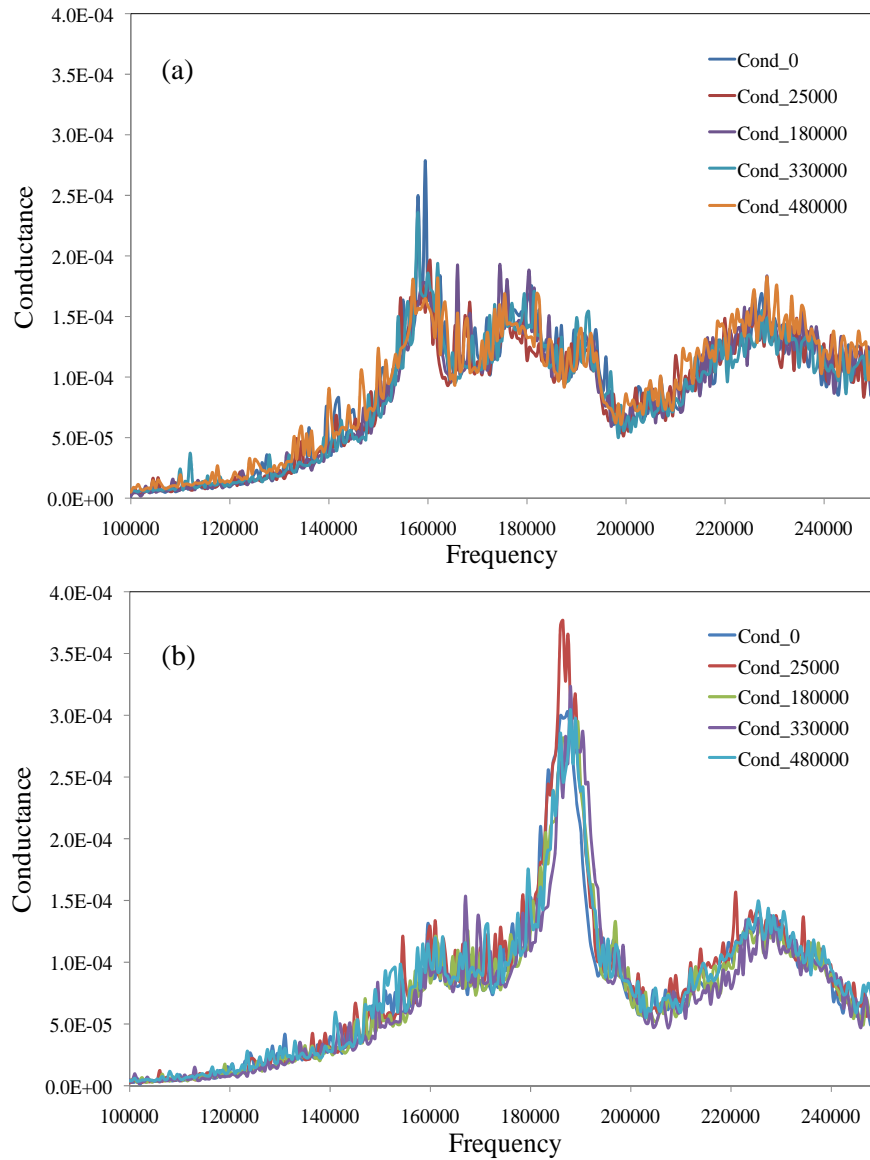
Figure 8.8 - (a) Conductance signature for EM1 resulted from PXI at 5 different periods; (b) Conductance signature for EM2 resulted from PXI at 5 different periods.
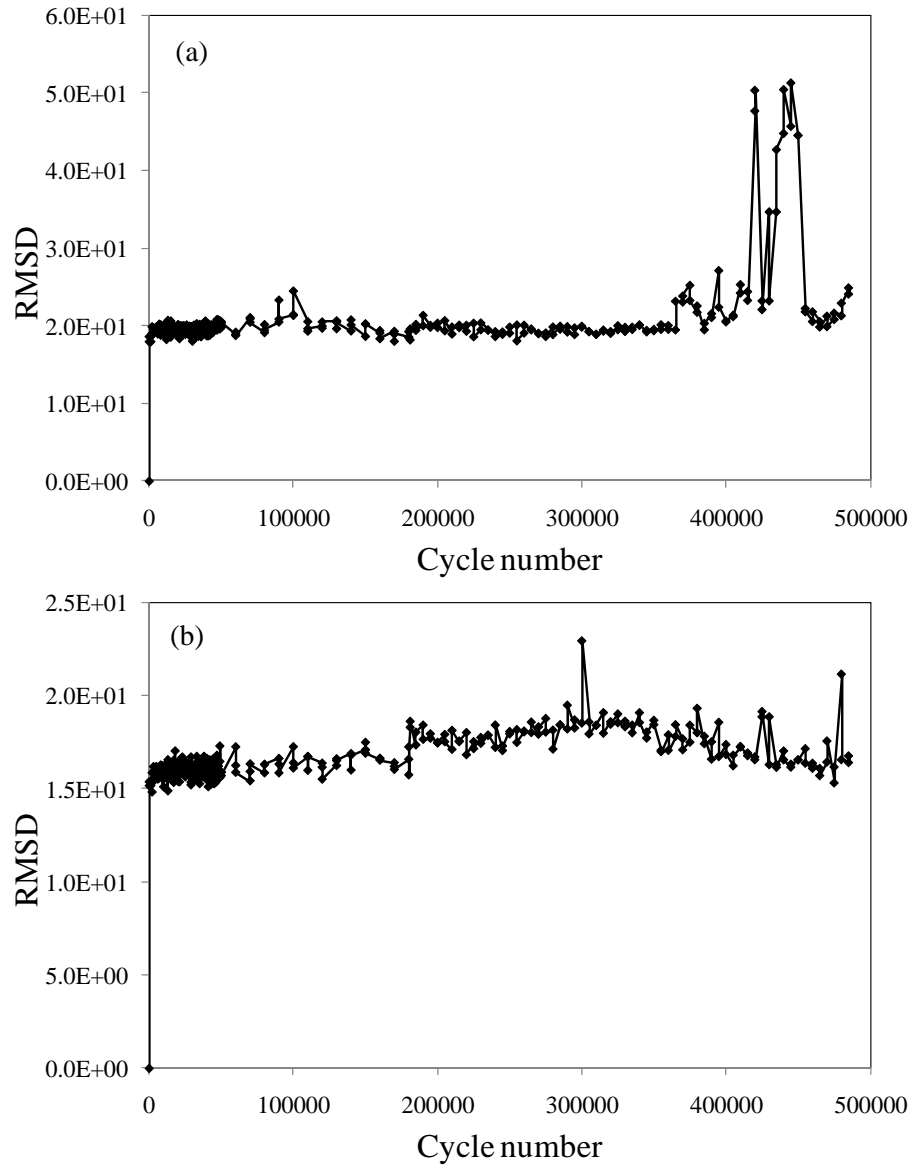
Figure 8.9 - RMSD values from 100 KHz to 500 KHz of (a) EM1; (b) EM2
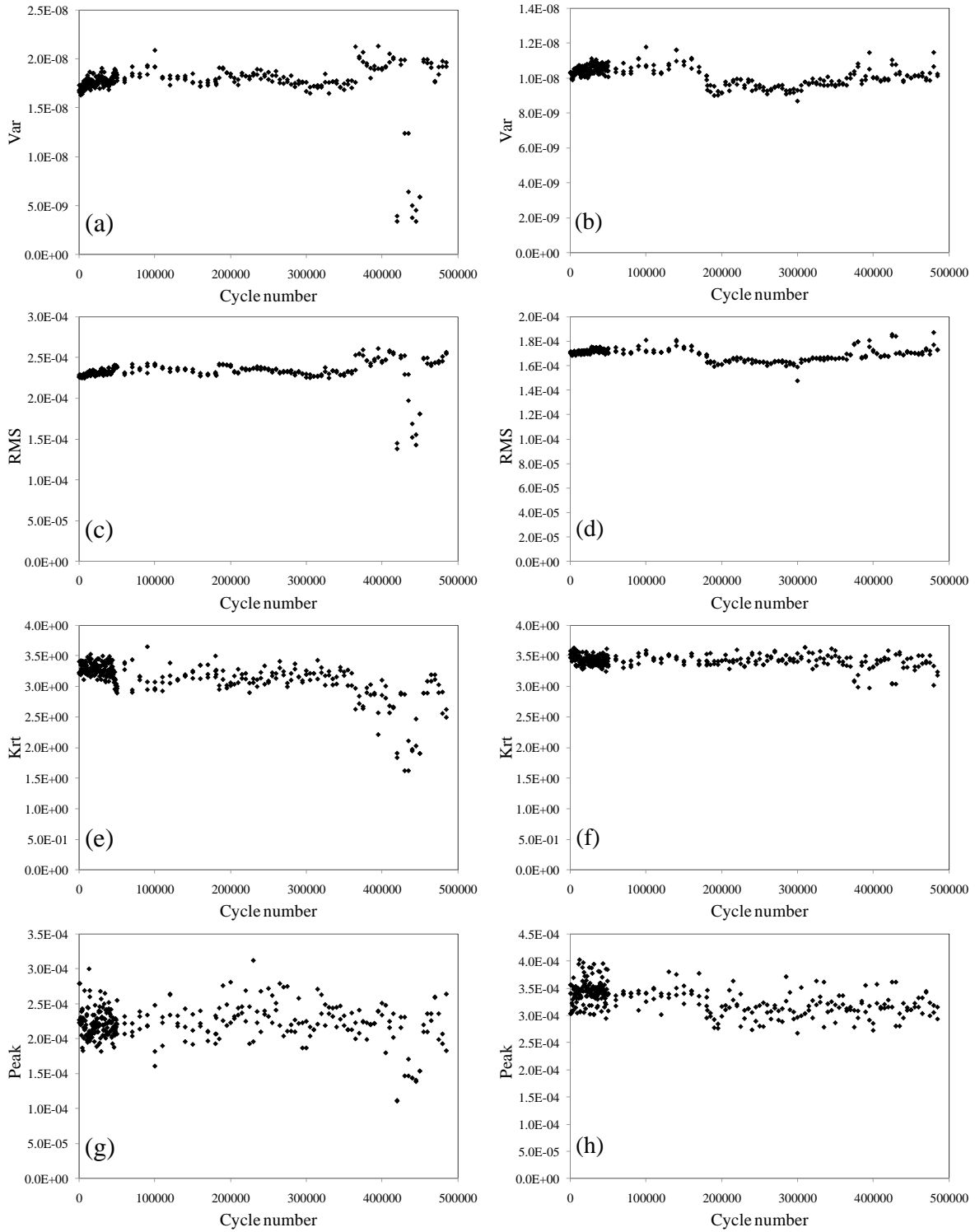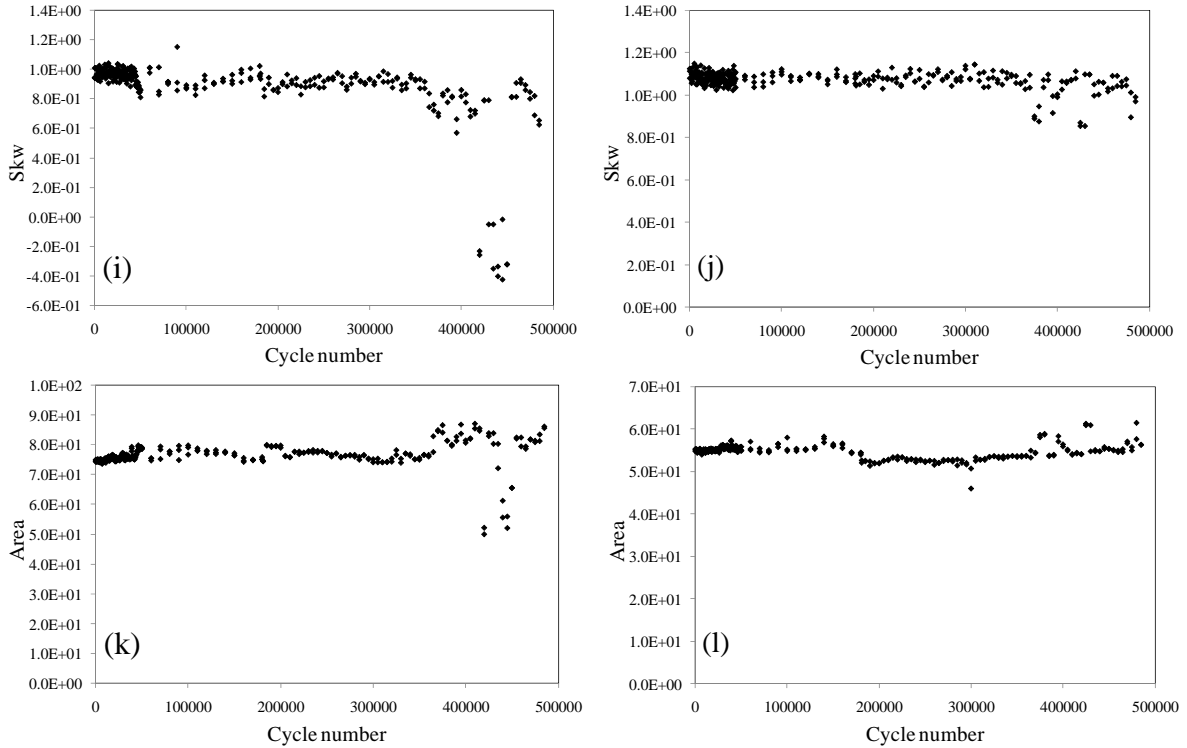
Figure 8.10 - Statistical features as a function of the loading number of cycles. (a) Var EM1; (b) Var EM2; (c) RMS EM1; (d) RMS EM2; (e) Krt EM1; (f) Krt EM2; (g) Peak EM1; (h) Peak EM2; (i) Skw EM2; (j) Skw EM1; (k) Area EM2; (l) Area EM1.

In Fig. 8.10 there are some scattered values of the features associated with PZT EM1 around 420,000 cycles. This is due to a sudden decrease in value of the conductance at its peak frequency at about 190 kHz (see Fig. 8.8). The origin of this decrease is under investigation.

It should be noted, when observing Figs. 8.9 and 8.10 that overall no significant difference exists between data obtained from static loading and dynamic loading. This demonstrates that the dynamic loading applied to the truss structure does not affect the EMI measurement

The last step of the signal processing algorithm consisted of applying the multivariate outlier analysis , by combining the seven features discussed above. The "exclusive" MSD for each of the 316 measurements was calculated using Eq. (6.3).

8.3 EXPERIMENTAL RESULTS: LABORATORY TEST

In the multivariate analysis all of the features discussed in the previous section were considered: all combinations of two-dimensional vectors (i.e. vectors containing two out of seven features) up to the single combination of the seven-dimensional vector. Thus, 120 features' combinations were examined. Data from EM1 and EM2 were considered.

To determine the threshold, the data from the first 18 measurements (0 – 5,000 cycles) were considered.

Figure 8.11a and 8.11b show the MSD associated with the seven-dimensional vector as a function of the cycle numbers PZTs EM1 and EM2, respectively. The improvement of the sensitivity is visible because a very large number of outliers were detected. However, it should be noted that the MSD does not show a step-wise trend because the size of the crack increased with the increase of the number of cycles.
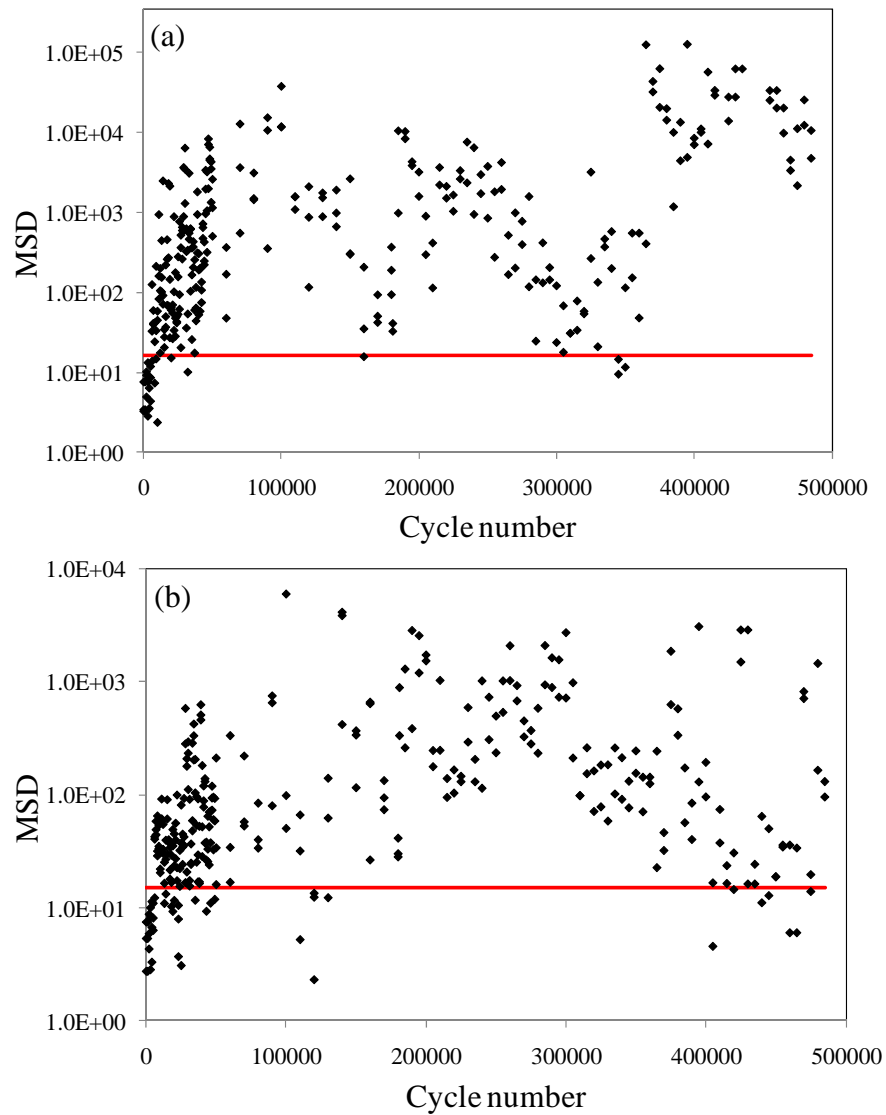
Figure 8.11 - Multivariate analysis. Mahalanobis squared distances as a function of the cycle number considering all seven features for: (a) EM1; (b) EM2.

157
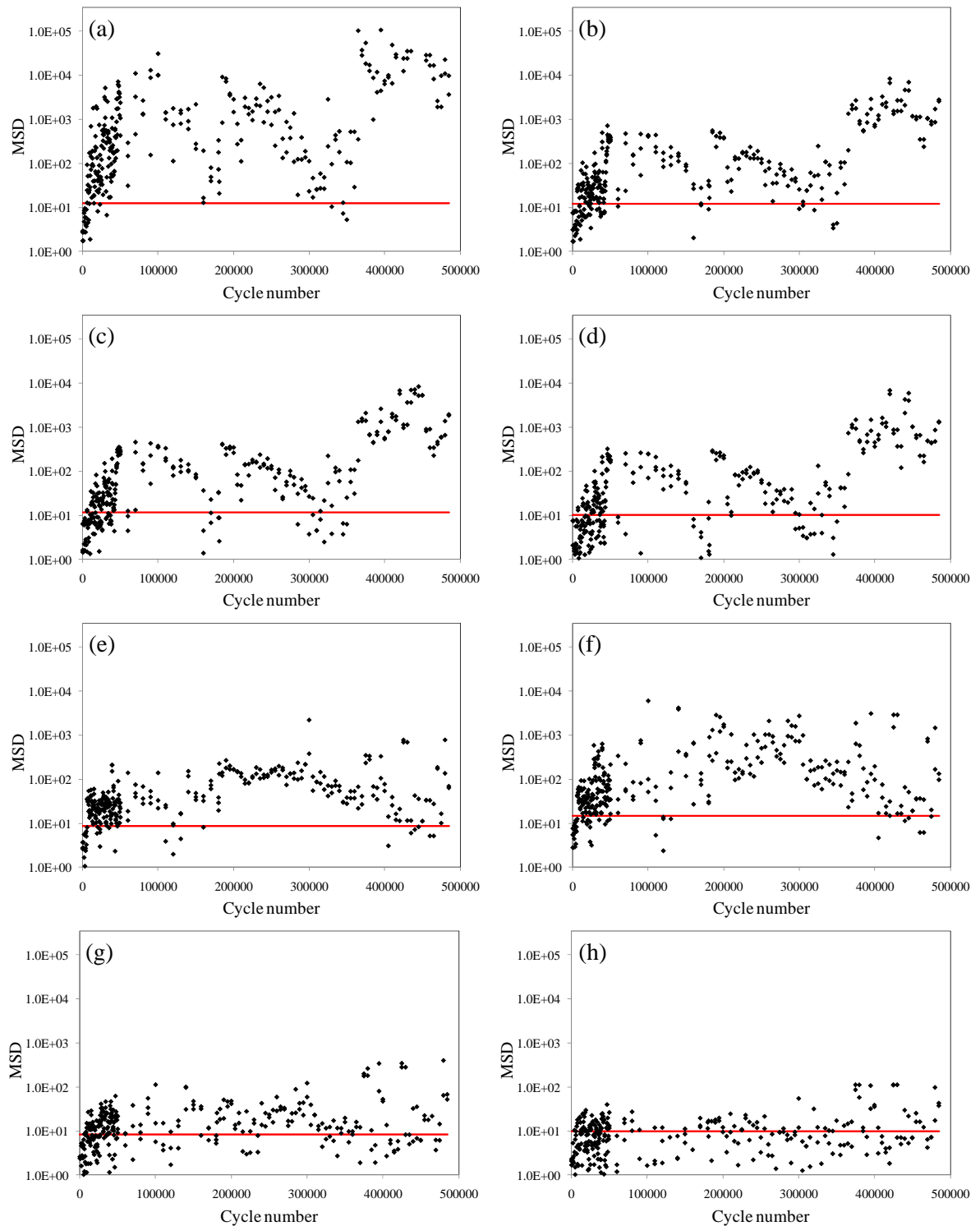
Figure 8.12 - Multivariate analysis. Mahalanobis squared distances as a function of the cycle number for: (a) EM1 with krt, rms, peak, area, skw, var and rmsd (b) EM1 with krt, peak, area, var and rmsd (c) EM1 with krt, rms, peak and skw (d) EM1 with peak, area and rmsd; (e) EM2 with rms, peak, area and skw; (f) EM2 with krt, rms, peak, area, skw, var and rmsd;(g) EM2 with peak, skw and var ; (h) EM2 with peak, area and rmsd.

As was conducted for the ultrasonic measurement, a parametric analysis was carried out to investigate the feature combination that better performed in terms of damage detection sensitivity. To find, empirically, the best feature combination in terms of crack detection, a quantitative study was performed using the values of the MSD associated with the 240 cases. The combinations were ranked according to the percentage of outliers properly detected. Figure 8.12 shows the results associated with the Mahalanobis squared distances as a function of the cycle number for the following: (a) EM1 with krt, RMS, peak, area, skw, var and RMSD (96.6%) (b) EM1 with krt, peak, area, var and RMSD (86.5%) (c) EM1 with krt, RMS, peak and skw (78.1%) (d) EM1 with peak, area and RMSd; (68.4%) (e) EM2 with RMS, peak, area and skw (93.2%) (f) EM2 with krt, RMS, peak, area, skw, var, and RMSD (85.9%) (g) EM2 with peak, skw and var (66.4%) (h) EM2 with peak, area, and RMSD (41.6%) from the best to the worst combination cases. Therefore, the combination ranked '1st' provided the largest number (96.6%) of outliers and it is shown in Fig 8.12a. It is the result of combining all seven features obtained from EM1. Its opposite, the worst combination, provided only 33.21% of the outliers properly identified.

8.4. EXPERIMENTAL RESULTS: ENVIRONMENTAL TESTS

Due to the malfunctioning of the single PZT transducer used in this portion of the experiment, useful results could not be reported about the effect of temperature on the performance of the EMI measurement.

Park et al. (1999) studied the temperature's effects on the electrical impedance of piezoelectric materials and the structures. Considering the effect on piezoelectric materials, the dielectric constant exhibits the most significant effect on electrical impedance. It modifies the capacitive admittance, causing a baseline shift of the electrical impedance. The piezoelectric coupling constant and complex young's modulus also result in a baseline shift, but the effect on the overall impedance can be negligible compared with the dielectric constant. Previous experimental work conducted by Park et al. (1999) examined the effects of temperature on a free PZT. It was shown that an increase in temperature leads to a decrease in the impedance magnitude. Furthermore, Park and co-authors analyzed the real part of the electrical impedance for the reason that the real part is more reactive to damage rather than the imaginary part. The change of the resistive part of EMI of free PZT versus change in temperature shows a relatively insignificant change, keeping the magnitude unchanged or a slight downward shifting of the impedance curve.

Considering the temperature effect on structure, the Young's modulus varies slightly with temperature and the thermal expansion of the material will induce stresses in constrained structures. To investigate the temperature effect on structure, a conventional modal analysis was conducted at high frequency ranges on a free carbon-steel beam. The increase in temperature led to shifting of resonance frequencies and fluctuations in peak response magnitudes, which indicated that the change in temperature would leads to a horizontal shift and magnitude change of the impedance peak.

A temperature controller set the temperature in the oven from 25 C to 75 C in steps of 12.5 C. The beam was excited with a PSI-5A piezoceramic bonded in the middle and each measurement was taken under a steady-state temperature. The fluctuations of magnitude and the horizontal shift of resonant frequencies would be observed with the change in temperature as shown in Figure 3. This is due to the fact that the PZT materials as well as the structural properties exhibit strong temperature dependence.

To eliminate the temperature effect, 'baseline bank' of the collection of preliminary impedance measurements of free PZT was proposed by Krishnamurthy et al. (1996).

A damage detection strategy based on the correlation coefficient was proposed by Koo (Koo et al 2007). The correlation coefficient between the reference impedance data and measurement impedance data was computed considering the maximum correlation which corresponds to the maximum likelihood estimator of frequency shift. This technique combined with outlier analysis was applied to a lab-sized steel truss bridge member and an artificial notch was detected under the temperature varying environment. Park proposed a damage metric of the sum of the real impedance change squared as temperature compensation, taking advantage that the variation in impedance is dominated by horizontal shift of peak values (Park et al. 1999). This technique was applied in real-time monitoring application in pipes connected by bolted joints to minimize the effects of temperature and normal variations (Park et al. 2000 and Park et al. 2000).

CHAPTER 9: FIELD TEST

Two structures were monitored during the field testing program conducted in spring and summer 2010. The results from the first structure are presented in section 9.1. Section 9.2 instead illustrates the setup and the results associated with the second structure.

9.1 STRUCTURE 1: SETUP and RESULTS

The first field test was performed on the sign support structure shown in Fig. 9.1a. The structure is located on the Mc Knight Road ramp along Interstate 279 (40.49153,-80.009442) few miles north of downtown Pittsburgh, Pennsylvania. The structure is denoted as L.R.1021 3-C.

(b)

(a)

Figure 9.1 – (a) Photo of the first structure monitored in the field. (b) Particular of the welded connections instrumented with PZTs.

The main chords consist of tubular elements have 6.625 inches (168.275 mm) outer diameter and 0.432 inches (10.97 mm) thickness. Diagonal angular members (type 2.0 x 3.85) are welded to the structure. A zoom in view of one of these welded connections is shown in Fig. 9.1b.

The sensing system was deployed along the bottom chord on the rear side with respect to the traffic direction (Fig.9.2a). Eight PZTs were bonded to the structure along the part of the chord lying above the shoulder (Fig. 9.2b). The choice of the sensors' location was such that during the installation the closure of traffic lanes was not necessary.
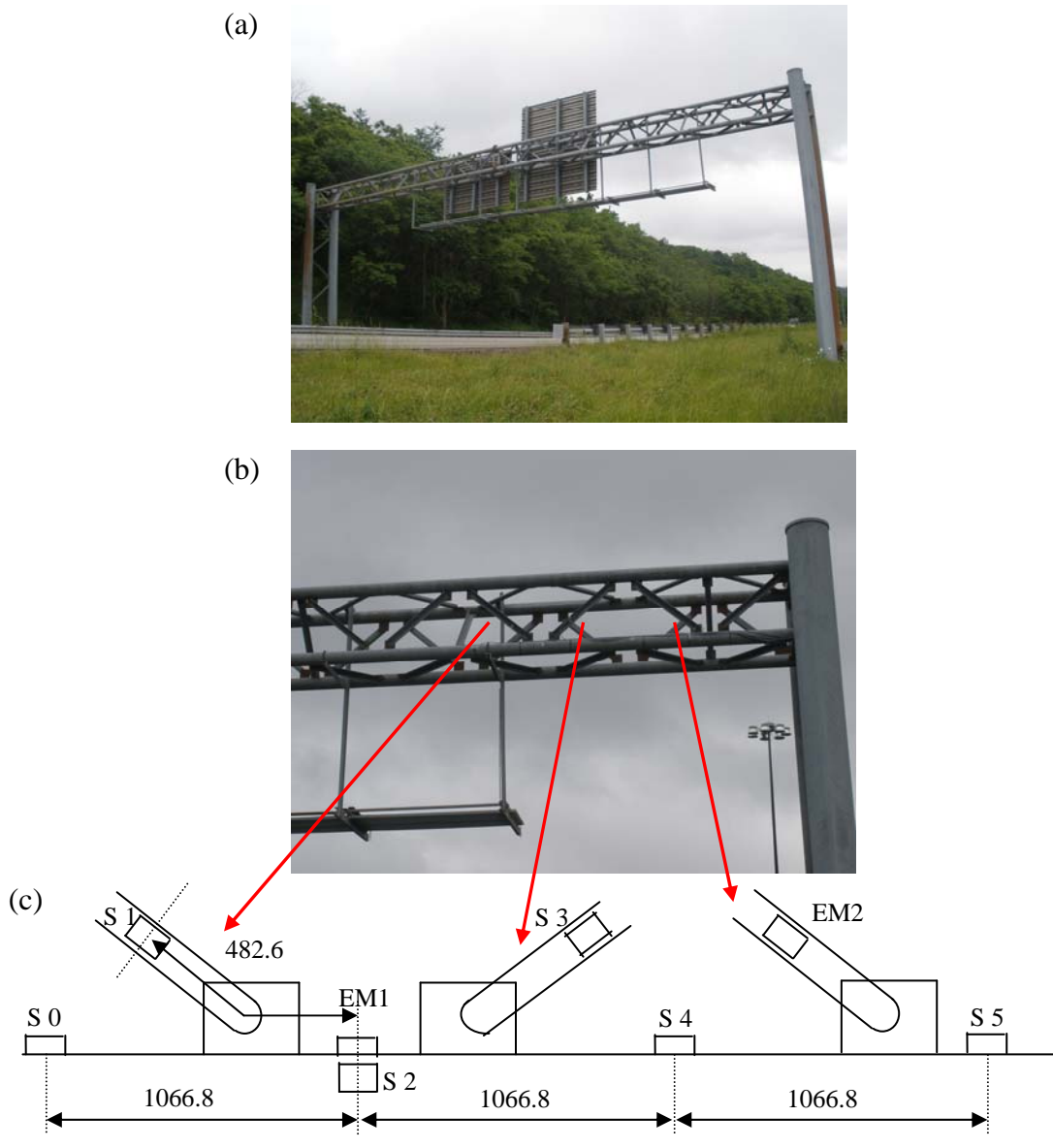
Figure 9.2 (a) Photo of structure 1. (b) Close-up view of the part that was monitored. (c) Location of the sensing system. The red arrows indicate the diagonal members involved in the field test. Distances are expressed in mm.

Six PZTs in shear modes were used for the generation and detection of UGW. The relative position of these transducers on the truss is shown in Fig. 9.2c. The transducers were named as S0, S1…S5. Two PZTs were used for the EMI method and are indicated as EM1 and EM2 in Fig. 9.2c.

The sensors were connected to the data acquisition system by means of a flexible multi-conductor cable shielded 20/3 AWG cables. The same program software used for the indoor tests was used in the field.

The LabView program described in section 6 was updated to allow for acquisitions being taken at regular intervals without the intervention of an operator. Measurements were taken every fifteen minutes. Phases of the installation and of assembling the wires to the data acquisition system are shown in Fig. 9.3.

The data associated with the ultrasonic measurement were taken over the May – June 2010 period. The measurements were taken on a weekly basis. In order to monitor the structure under different environmental conditions, the measurement days were chosen based upon the weather forecast. Table 9.1 lists the temperature of the air and of the steel pole as well as the weather conditions. It should be noted that the air temperature was retrieved through the following link http://weather.org/weatherorg_records_and_averages.htm while
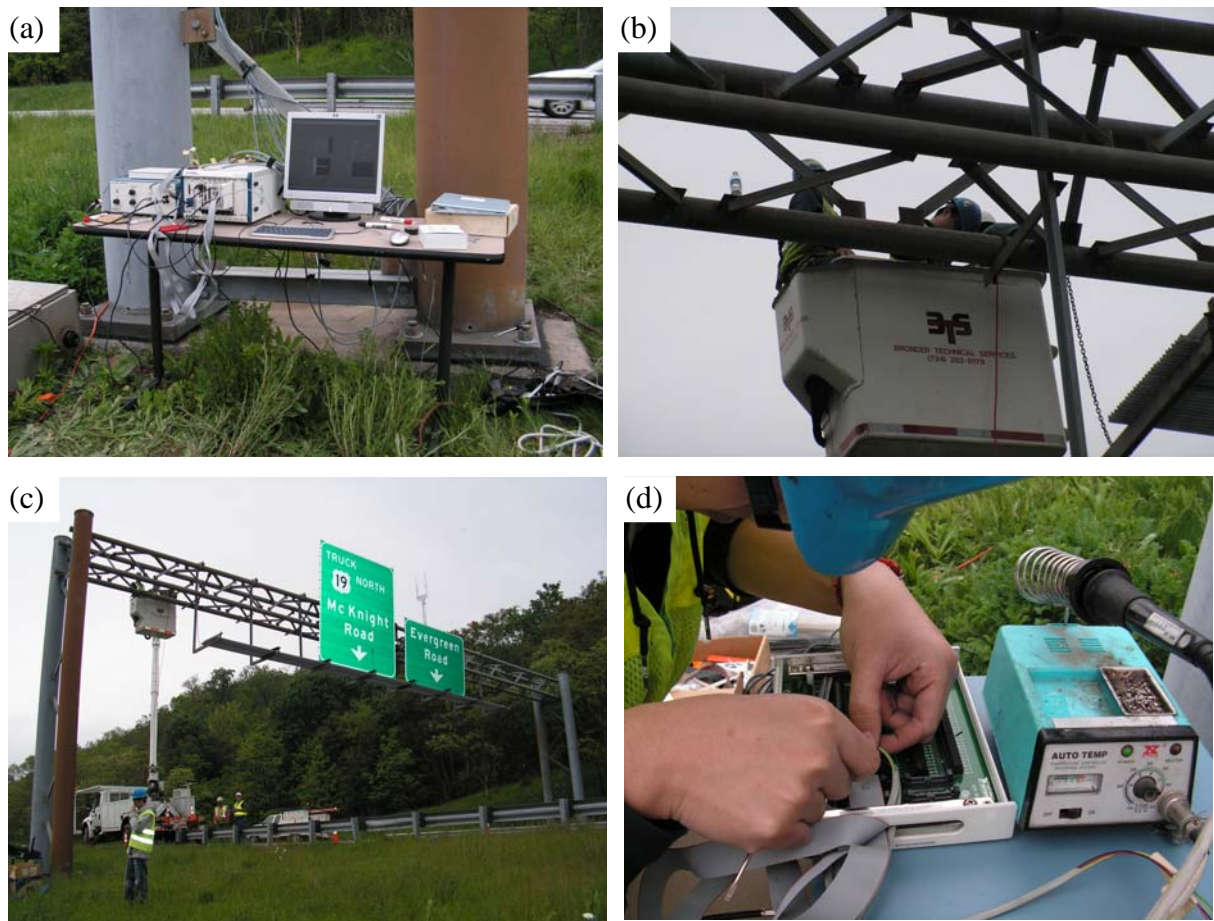
Figure 9.3 – Structure 1. (a) Data acquisition system. (b-c) Bonding the PZTs to the structure. (d) Connecting the coaxial cables to the screw terminal.

Meas. #	Date	Time	Air Temperature (C)	Time	Steel Temperature (C)	Dry / rain
1	12-May	8:53 AM	14.4		no measurement	dry
2		9:53 AM	14.4		no measurement	dry
3		10:02 AM	14.0		no measurement	dry
4		10:53 AM	13.9		no measurement	dry
5		11:45 AM	14.0		no measurement	dry
6		11:53 AM	14.4		no measurement	dry
7		12:53 PM	13.9		no measurement	dry
8		1:05 PM	13.0		no measurement	rain
9		1:28 PM	14.0		no measurement	rain
10		1:53 PM	14.4		no measurement	rain
11		2:53 PM	13.9		no measurement	rain
12	12-May	3:53 PM	13.9		no measurement	rain
13	17-May	8:49 AM	12.0		no measurement	rain
14		9:14 AM	12.0		no measurement	rain
15		9:53 AM	11.7		no measurement	rain
16		11:15 AM	12.0		no measurement	rain
17		11:53 AM	12.8		no measurement	rain
18		1:06 PM	13.0		no measurement	rain
19		1:53 PM	12.2		no measurement	rain
20	17-May	2:53 PM	12.2		no measurement	rain
21	20-May	9:04 AM	11.0	8:50 AM	16.4	dry
22				9:12 AM	19.1	dry
23		9:27 AM	11.0	9:26 AM	19.8	dry
24				9:45 AM	23.4	dry
25		9:53 AM	12.2	10:01 AM	26.3	dry
26				10:15 AM	29.3	dry
27				10:27 AM	31.5	dry
28				10:42 AM	32	dry
29		10:53 AM	16.1	10:59 AM	35	dry
30				11:12 AM	34.5	dry
31				11:28 AM	35.6	dry
32				11:42 AM	37.8	dry
33		11:53 AM	18.9	12:00 PM	38.9	dry
34				12:30 PM	40.3	dry
35				12:45 PM	41.1	dry
36	20-May	12:53 PM	21.1	13:00 PM	40.7	dry
37	26-May	8:53 AM	22.8	8:55 AM	23	dry
38				9:15 AM	27.8	dry
39				9:33 AM	28.6	dry
40				9:45 AM	30	dry
41		9:53 AM	24.4	9:59 AM	35.2	dry
42				10:17 AM	43.7	dry
43		10:53 AM	25.6	10:44 AM	41.1	dry
44				11:02 AM	44.6	dry
45				11:14 AM	46.5	dry
46				11:29 AM	46.7	dry
47		11:53 AM	27.8	11:45 AM	46.8	dry
48				12:00 PM	40.8	dry
49				12:14 PM	48.5	dry
50				12:29 PM	49	dry
51		12:53 PM	26.7	12:45 PM	42.3	dry
52				1:03 PM	39	dry
53				1:14 PM	36.9	dry
54				1:30 PM	36.6	dry
55	26-May	1:53 PM	27.8	1:45 PM	36.6	dry

Table 9.1 – Environmental conditions experienced during the first 55 measurements.

the temperature of the material was recorded by attaching a thermocouple to one of the uprights. The thermocouple was not used during the first two days.

On May 12 the measurements 8 – 12 were taken under light rain, while the test on May 17th (measurements 13 - 20) was performed under heavy rain. Tests on May 20 and 26 were performed in clear sky conditions that implied direct exposure to the sun which, in turn, caused a significant difference between air and steel temperature.

Time waveforms recorded during the second day (under heavy rain conditions) when the actuation frequency was equal to 175 kHz are presented on the left side of Figure 9.4. The time waveforms refer to the following wave paths: S0=>S2; S0=>S5; S0=>S3; S1=>S3; S5=>S0.

When compared to the laboratory data, the time waveforms collected in the field were overall noisier. For the specific case of May 17 records, it is plausible that the rain caused the noise and very low frequency signal fluctuations .

To reduce the presence of noise all time waveforms were filtered using a Butterworth band pass filter which allowed to remove unwanted background noise and low-frequency components. For the field test data passing bandwidth was equal to 100 ÷ 270 kHz. The filtered signals are presented on the right side of Fig. 9.4.

The structural health monitoring algorithm described in the previous chapters was then applied to the filtered time waveforms. Figures 9.5, 9.6, and 9.7 present the RMS, K factor, and variance respectively associated with the measurement executed during the month of May. The plots refer to four different paths, namely, C0=>C2/C0=>C5,   C0=>C3/C0=>C5, C1=>C3/C0=>C5, and C5=>C0/C0=>C5. The guided waves propagating at 175 kHz were considered for the analysis. It can be seen that the measurements obtained under heavy rain conditions produced a large scatter in the data.

Constant behavior was observed for S0=>S2/S0=>S5 (Fig. 9.5 (a), Fig. 9.6 (a) and Fig. 9.7 (a)) within the first day measurement and these measurements were used as training data in latter multivariate analysis.

The data collected under heavy rain show a large discordance when compared to all other data. Clearly the presence of rain altered the boundary conditions along the tubular member but most likely affected the actuation and sensing characteristics of each transducer which was directly exposed to the water drops.

For measurements 23-37 and 38-55, slight variation resulted from the variation of temperature, and there was an increased tendency from 16.4°C to 25.3°C corresponding to measurement 23-27 and an increased tendency from 35°C to 41.1°C corresponding to measurement 30-37. Similar behavior was observed within measurement 38-55.
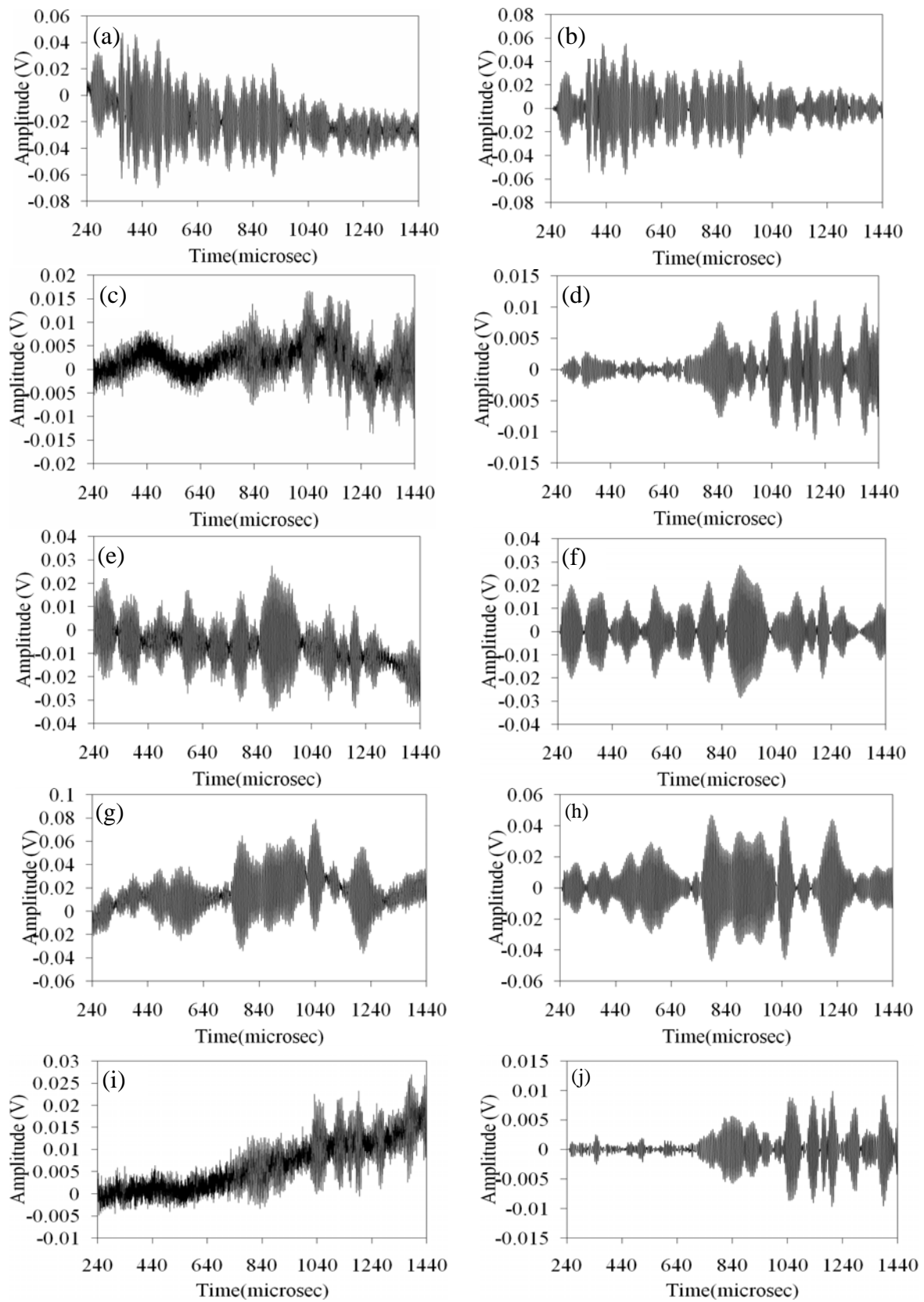
Figure 9.4 - Time waveforms recorded during May 17 and actuation frequency equal to 175 kHz. The left column shows original data. The right column shows the corresponding waveforms filtered using a Butterworth filter. (a,b) S0=>S2; (c,d) S0=>S5; (e,f) S0=>S3; (g,h) S1=>S3; (i,j) S5=>S0.
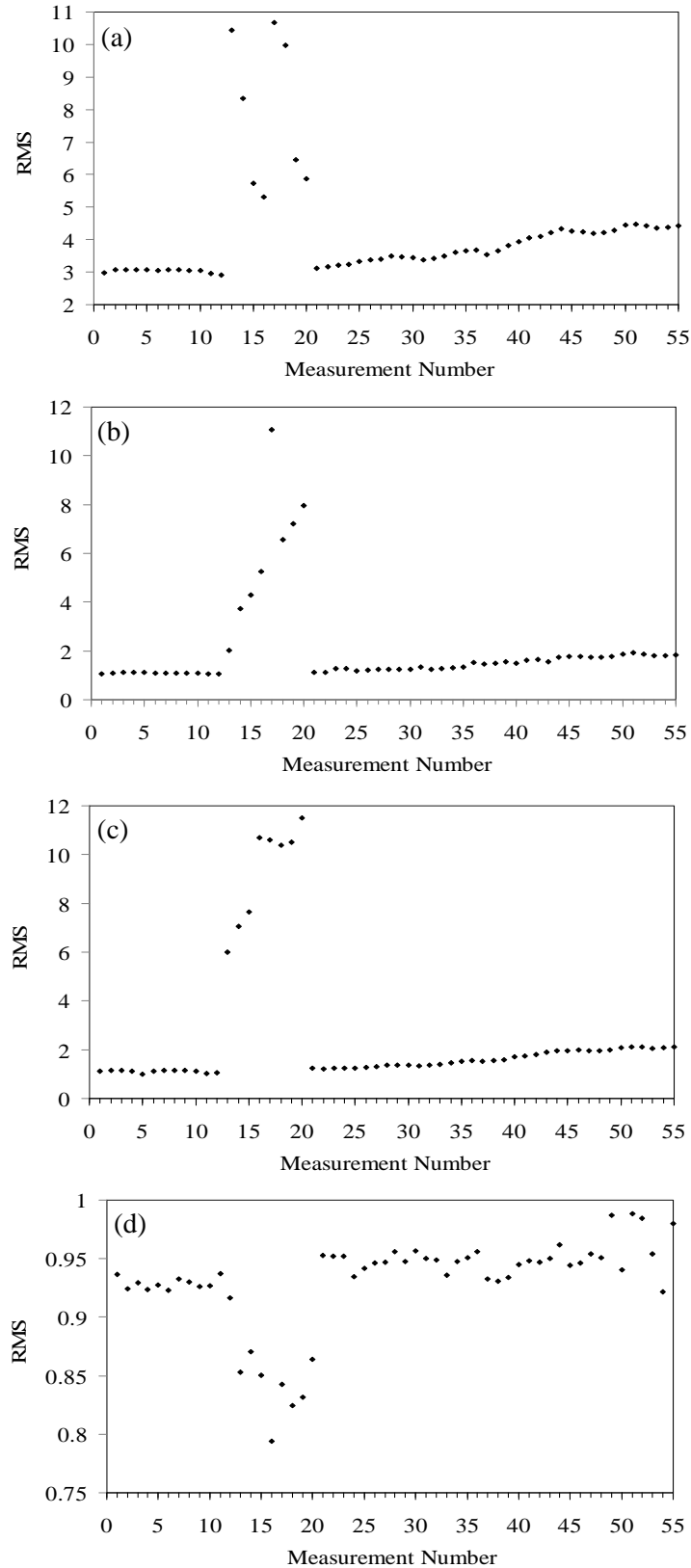
Figure 9.5 - Test 1, May. RMS – based damage associated to waveform paths: (a) C0=>C2/C0=>C5; (b) C0=>C3/C0=>C5; (c) C1=>C3/C0=>C5 and (d) C5=>C0/C0=>C5.
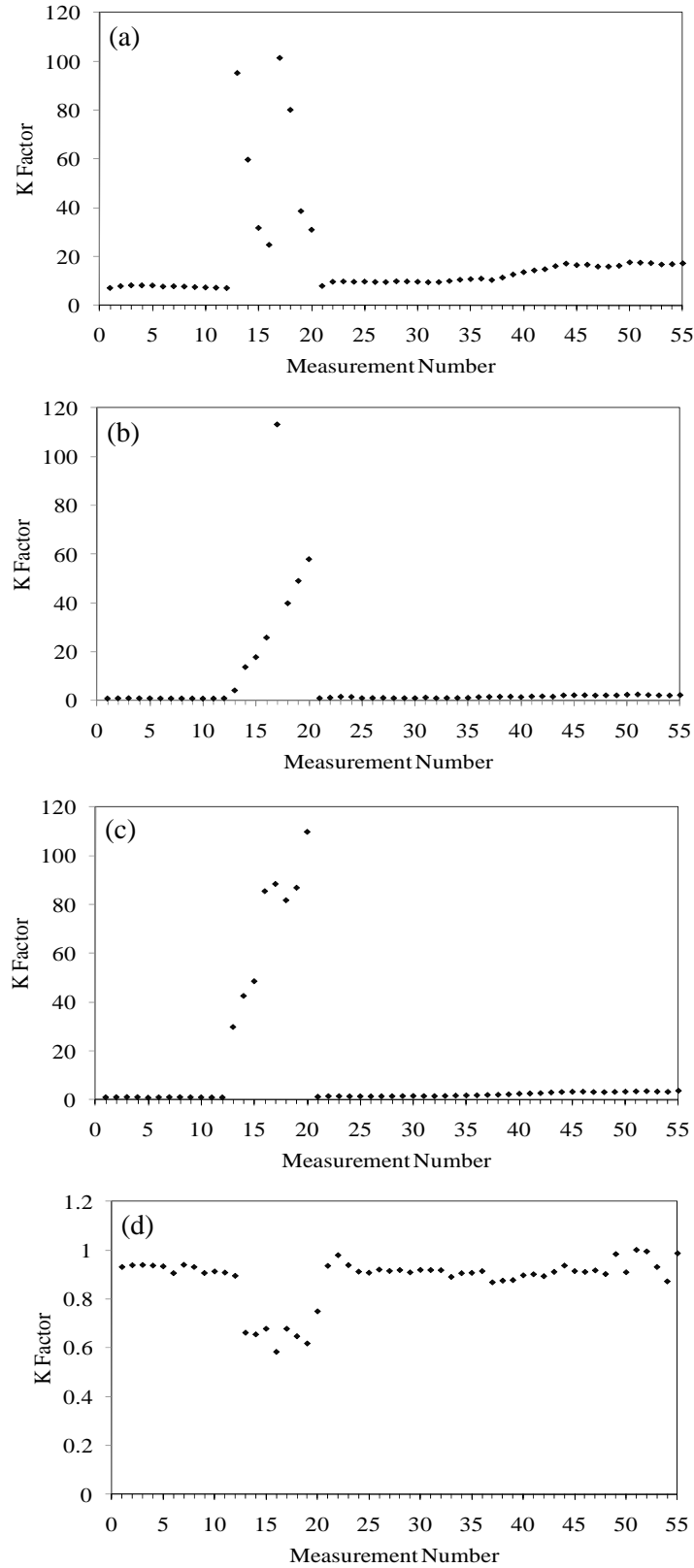
Figure 9.6 - Test 1, May. K factor – based damage associated to waveform paths: (a) C0=>C2/C0=>C5; (b) C0=>C3/C0=>C5; (c) C1=>C3/C0=>C5 and (d) C5=>C0/C0=>C5.
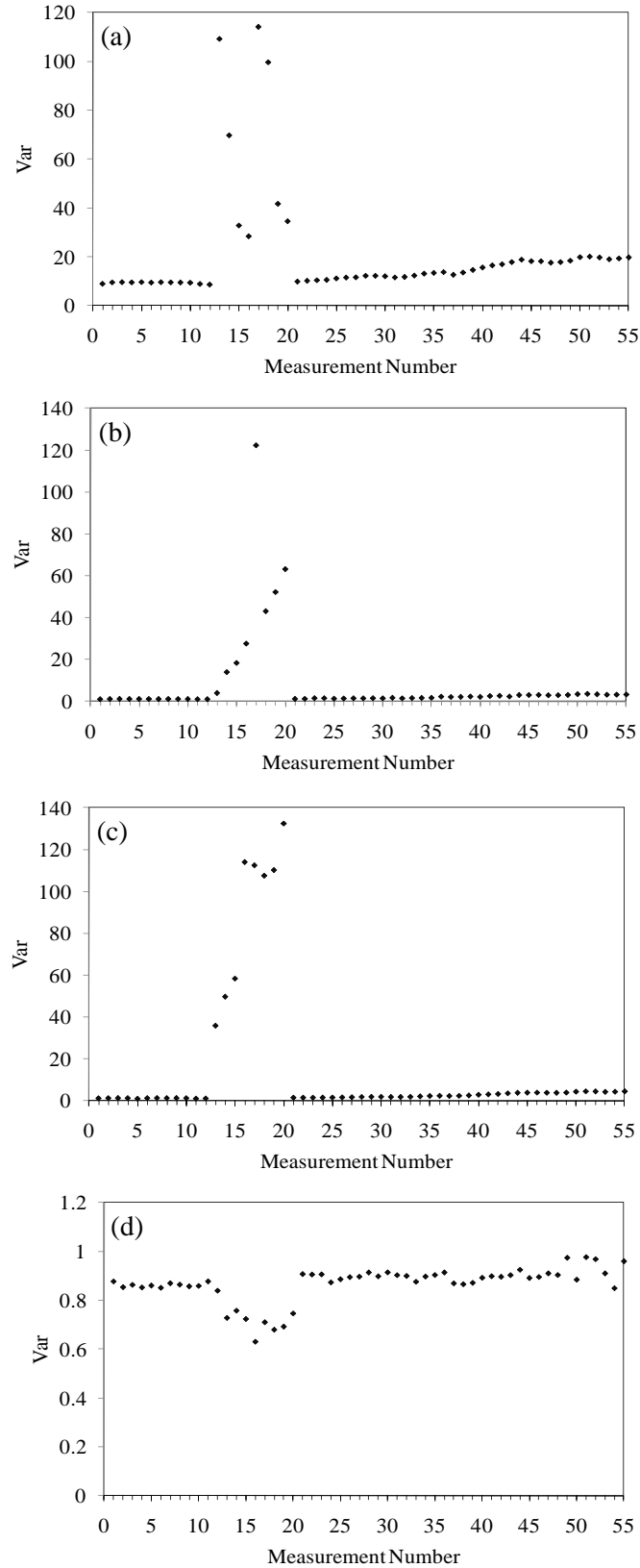
Figure 9.7 - Test 1, May. Variance – based damage associated to waveform paths: (a) C0=>C2/C0=>C5; (b) C0=>C3/C0=>C5; (c) C1=>C3/C0=>C5 and (d) C5=>C0/C0=>C5.

During the month of June a total of 40 measurements were taken within three days. As done for table 9.1, Table 9.2 summarizes the weather conditions occurred during the test. Tests on June 1 and 3 there were performed under clear sky while the test on June 9 occurred under shower condition.

Meas. #	Date	Time	Air Temperature (C)	Time	Steel Temperature (C)	Dry / rain
56	1-Jun	8:53 AM	20	8:44 AM	21.4	dry
57				9:05 AM	21.6	dry
58		9:26 AM	21	9:21 AM	21.6	dry
59				9:40 AM	22	dry
60		9:53 AM	21.1	9:55 AM	23.6	dry
61				10:10 AM	26.5	dry
62				10:25 AM	26.7	dry
63		10:39 AM	22.0	10:40 AM	26.6	dry
64		10:53 AM	22.8	10:55 AM	25.8	dry
65		11:07 AM	22.0	11:10 AM	27	dry
66				11:24 AM	29.6	dry
67	1-Jun	11:44 AM	23.0	11:40 AM	25.3	dry
68	3-Jun	8:53 AM	18.9	9:13 AM	23.2	dry
69				9:25 AM	23.1	dry
70				9:40 AM	22.7	dry
71		9:53 AM	19.4	9:54 AM	23.2	dry
72				10:17 AM	24.7	dry
73				10:31 AM	25.3	dry
74		10:53 AM	19.4	10:45 AM	26.7	dry
75				11:06 AM	26.1	dry
76				11:21 AM	26.9	dry
77				11:37 AM	27.8	dry
78		11:53 AM	20.6	11:52 AM	27.8	dry
79				12:06 PM	28.2	dry
80				12:21 PM	27.6	dry
81				12:35 PM	26.9	dry
82		12:53 PM	22.2	12:50 PM	26.5	dry
83	3-Jun			1:11 PM	26.5	dry
84	9-Jun	9:14 AM	16.0	9:17 AM	17.9	rain
85		9:44 AM	16.0	9:37 AM	17.3	rain
86		9:53 AM	16.1	9:52 AM	17.7	rain
87		10:07 AM	17.0	10:08 AM	16.9	rain
88		10:23 AM	17.0	10:19 AM	16.9	rain
89				10:36 AM	16.2	rain
90		10:53 AM	17.2	10:59 AM	17.7	rain
91				11:08 AM	18.5	rain
92				11:22 AM	18.5	rain
93				11:37 AM	18.9	rain
94		11:53 AM	17.8	11:54 AM	18.7	rain
95	9-Jun			12:07 PM	18.7	rain

Table 9.2 – Environmental conditions experienced during measurements 56 ÷ 95.

Figure 9.8, 9.9 and 9.10 present the RMS-, K factor- and variance-based damage index associated with measurements 56 ÷ 95. The plots refer to the following path ratios: C0=>C2/C0=>C5, C0=>C3/C0=>C5, C1=>C3/C0=>C5, and C5=>C0/C0=>C5. The guided waves propagating at 175 kHz were considered. As observed along measurements 56 ÷ 67 and 68 ÷ 83 the damage index increased with the increase of temperature. This is the same trend observed during May.

For measurements 84 ÷ 95 some data scatter is visible but it is not as dramatic as the ones observed in May during the heavy rain measurements. It can be postulated that the presence of rain alter the performance and the sensitivity of the transducers and that the intensity of rain may cause significant variation on the transducers characteristics.

Figure 9.11 shows the Mahalanobis squared distance as a function of the measurement number for the four damage index ratios discussed in the previous six figures. The measurements taken during May 12 were considered as a baseline. As can be seen from Fig. 9.11, the algorithm was unable to classify all the data as inliers. This result demonstrates the importance of the proper selection of the baseline and the challenges associated with field application of algorithms that were successfully demonstrated in the laboratory. In addition, the selection of the first day of test only was not representative of the various environmental conditions that can be experienced in the field.

In Fig. 9.12 and Fig. 9.13 the baseline was considered by including the data from May 12 and May 17, and by including May 12 and May 26, respectively. As expected the amount of inliers strongly depend on the baseline data.
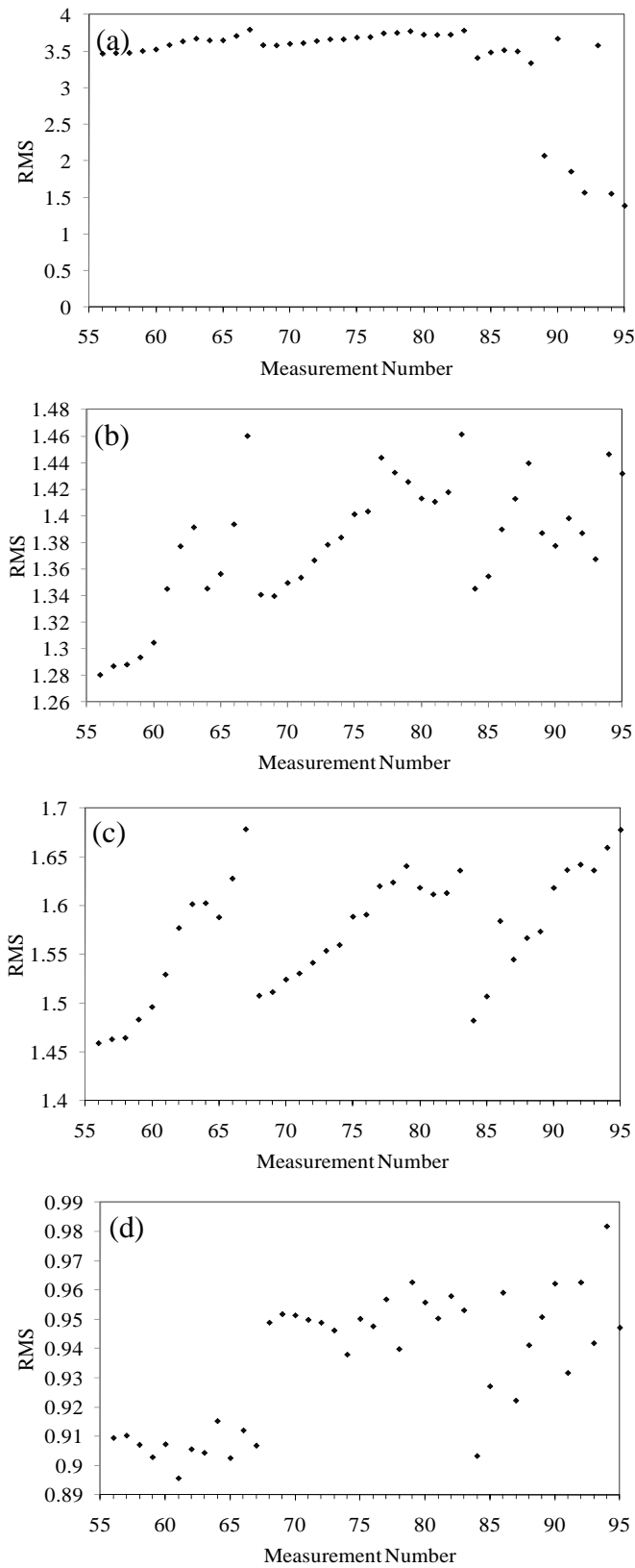
Figure 9.8 – RMS-based damage index from June data relative to paths: (a) C0=>C2/C0=>C5; (b) C0=>C3/C0=>C5; (c) C1=>C3/C0=>C5 and (d) C5=>C0/C0=>C5.
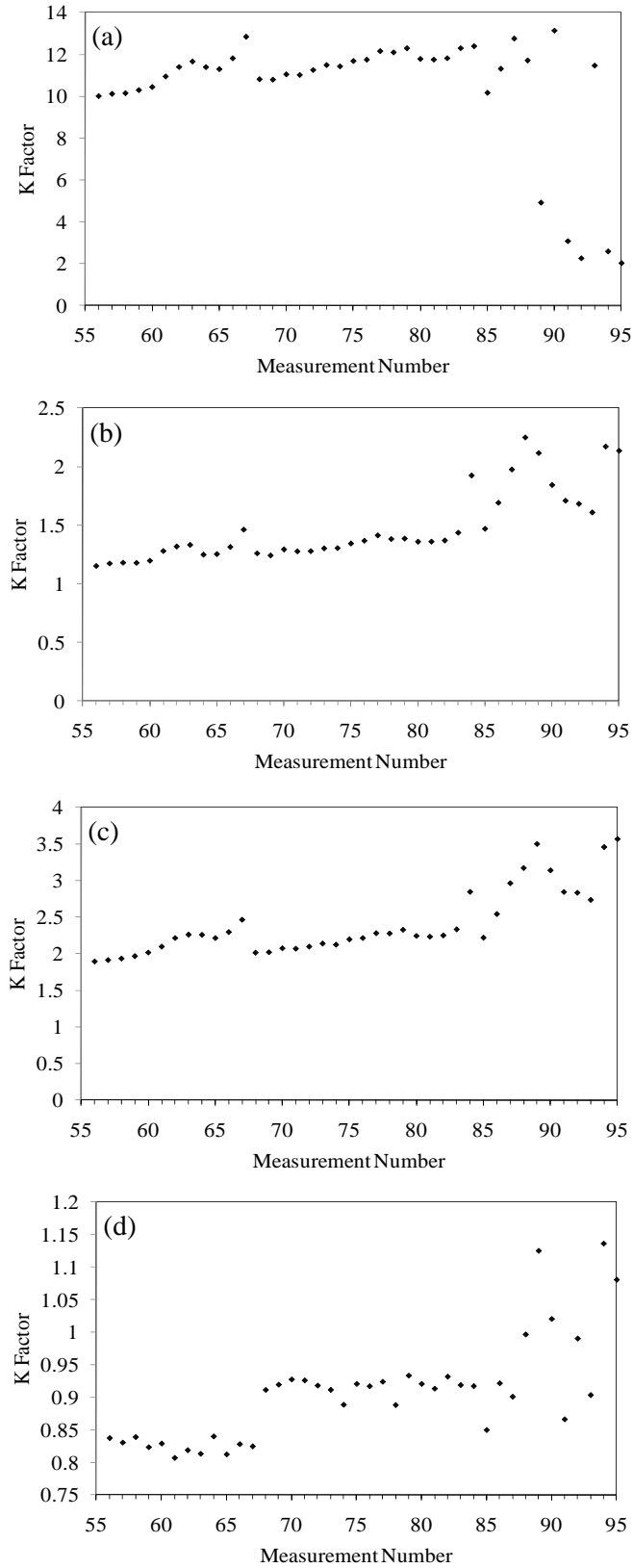
Figure 9.9 - K factor-based damage index from June data relative to paths: (a) C0=>C2/C0=>C5;
(b) C0=>C3/C0=>C5; (c) C1=>C3/C0=>C5 and (d) C5=>C0/C0=>C5.
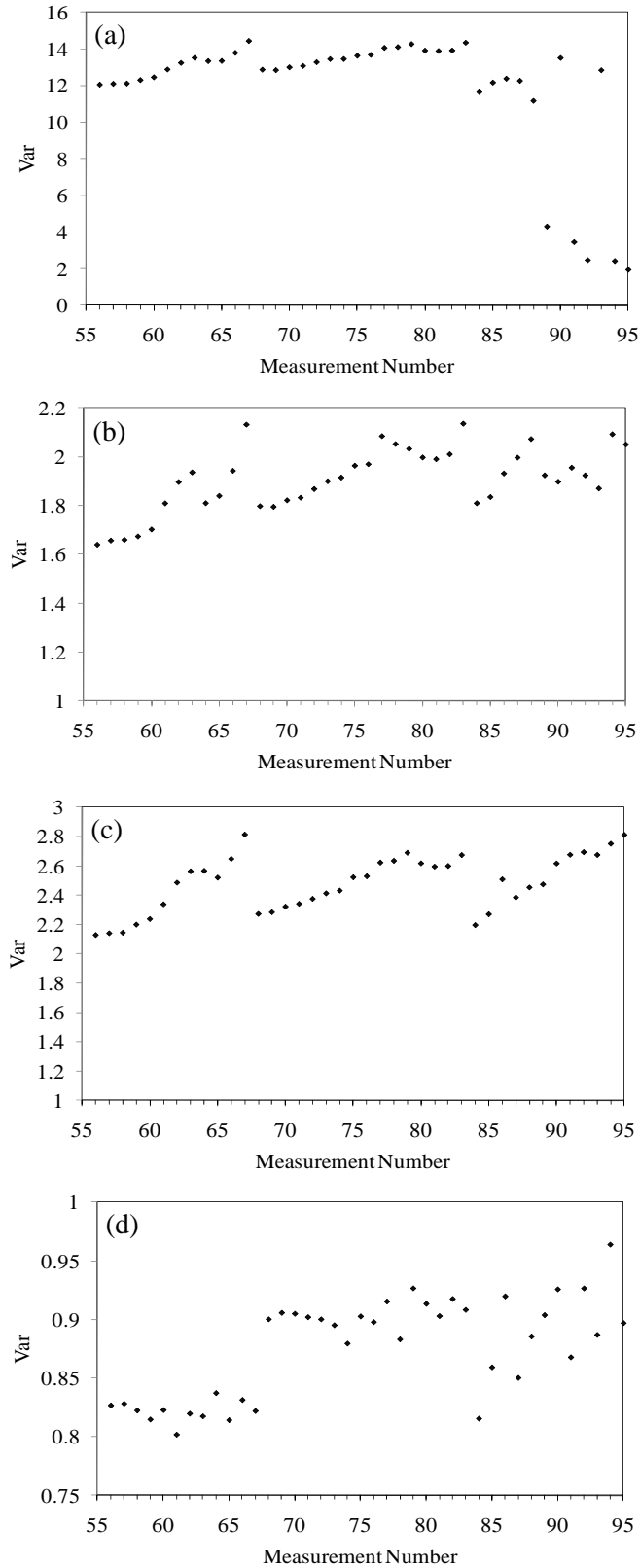
Figure 9.10 - Variance-based damage index from June data relative to paths: (a) C0=>C2/C0=>C5; (b) C0=>C3/C0=>C5; (c) C1=>C3/C0=>C5 and (d) C5=>C0/C0=>C5.
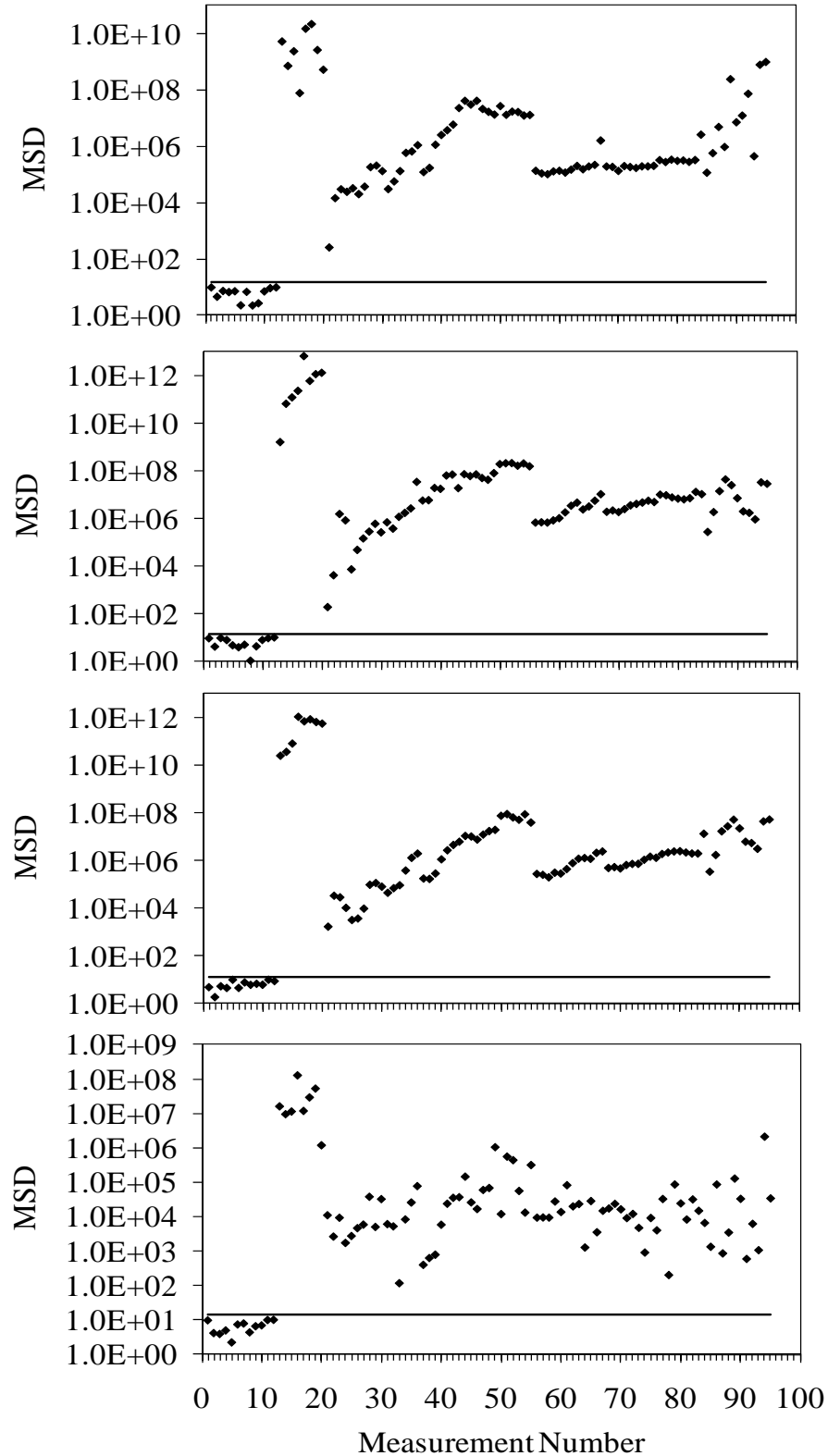
Figure 9.11 - MSD as a function of the measurement number. All seven statistical features and baseline from May 12 data considered. Paths: (a) C0=>C2/C0=>C5; (b) C0=>C3/C0=>C5; (c) C1=>C3/C0=>C5 and (d) C5=>C0/C0=>C5.
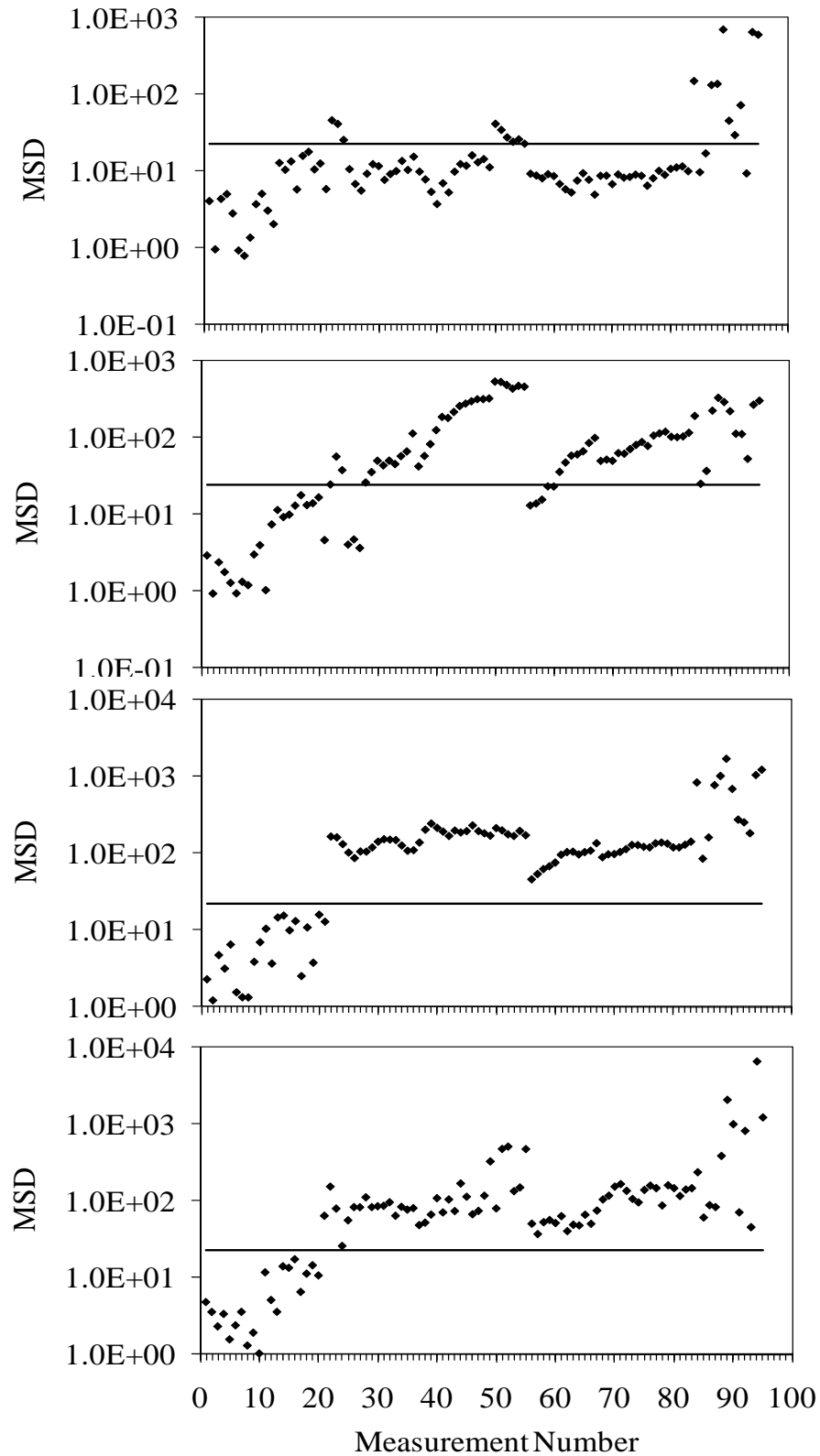
Figure 9.12 - MSD as a function of the measurement number. All seven statistical features and baseline from May 12 and May 17 data considered. Paths: (a) C0=>C2/C0=>C5; (b) C0=>C3/C0=>C5; (c) C1=>C3/C0=>C5 and (d) C5=>C0/C0=>C5
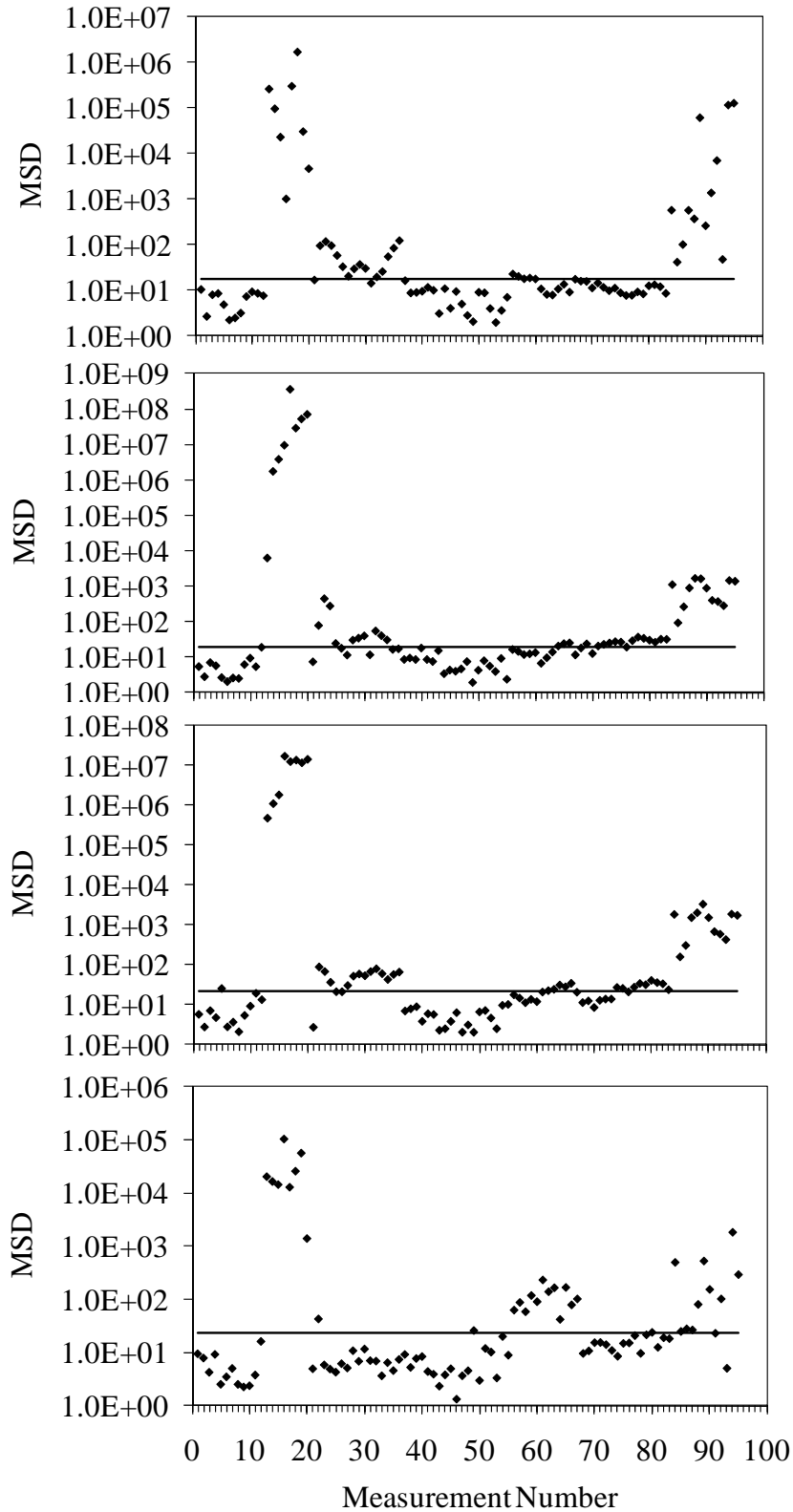
Figure 9.13 - MSD as a function of the measurement number. All seven statistical features and baseline from May 12 data considered. Paths: (a) C0=>C2/C0=>C5; (b) C0=>C3/C0=>C5; (c) C1=>C3/C0=>C5 and (d) C5=>C0/C0=>C5

9.2 STRUCTURE 2: SETUP and RESULTS

The second structure considered in this study is shown in Fig. 9.14a. The structure is located along Interstate 279 adjacent to the Mc Knight Road ramp.

The overhead truss consists of angular members. The diagonal and the vertical members are connected to the main chords by means of bolted connections and welds. A close-up view of one joint is presented in Fig. 9.14b.
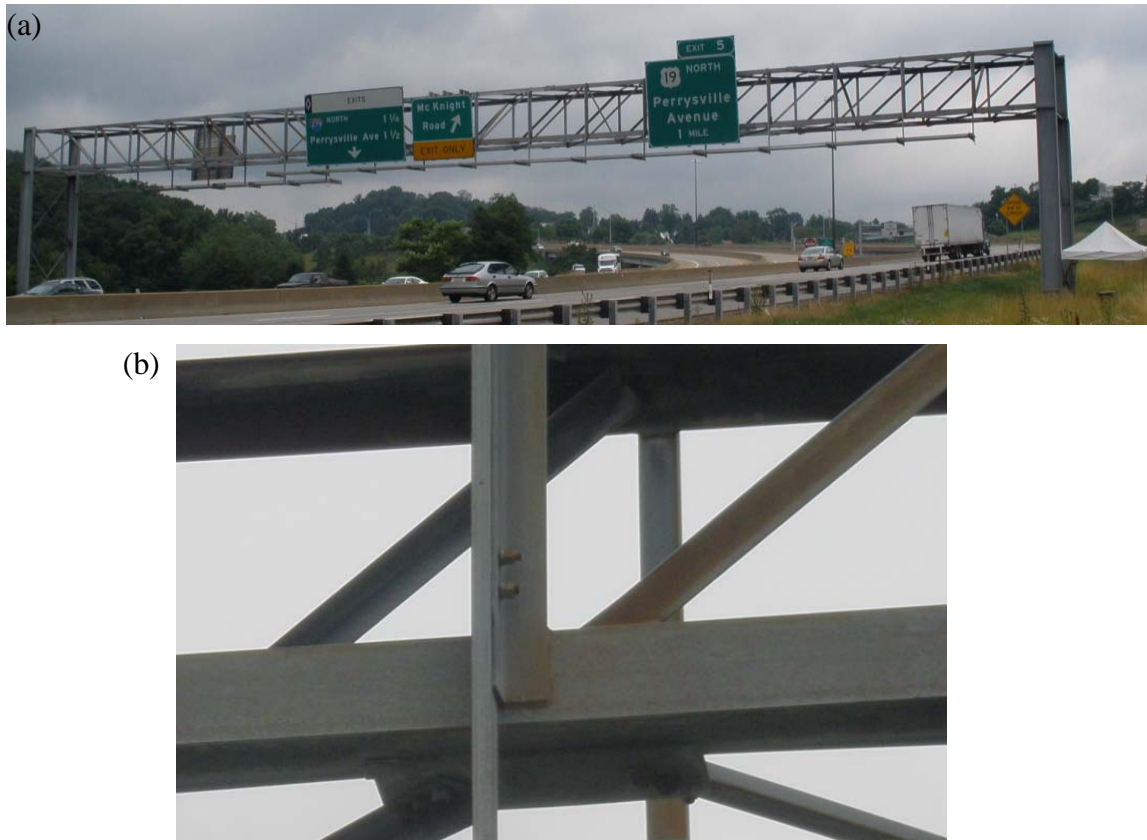
Figure 9.14 – (a) Photo of the second structure monitored in the field. (b) particular of the welded connections.

The sensing system was deployed along the bottom chord facing the northbound traffic and consisted of seven PZTs bonded at the locations shown in Fig. 9.15a and 9.15b.

During the installation one traffic lane was closed for safety consideration. All seven PZTs were used for the generation and detection of guided waves. The relative position of these transducers on the truss is presented in Fig. 9.16b. The transducers were named as S0, S1…S6. Photos of three transducers are shown in Fig. 9.15c, d and e. The sensors were connected to the data acquisition system by means of flexible multi-conductor cable shielded 20/3 AWG cables.

Phases of the installation are illustrated in Fig. 9.16.
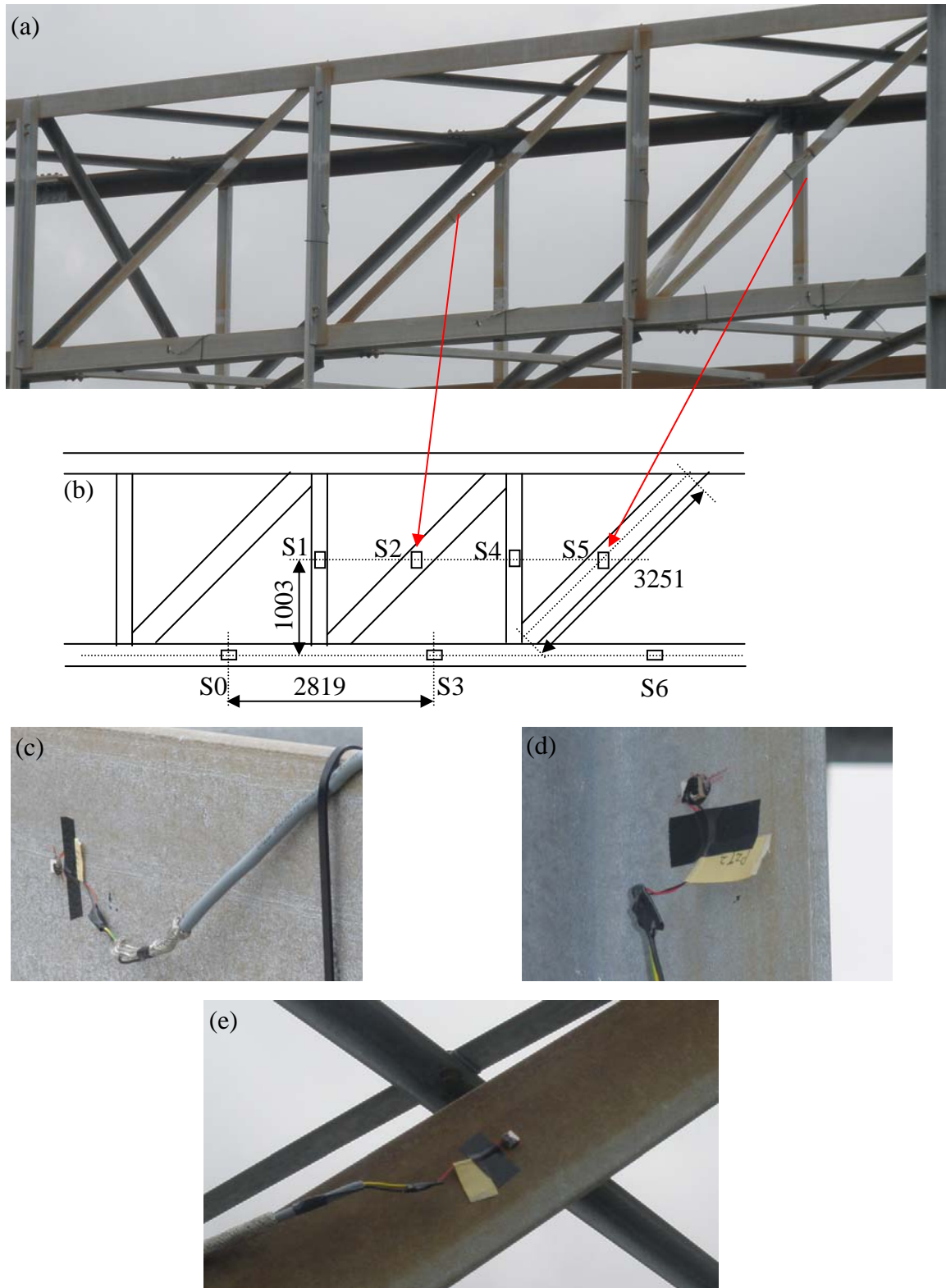
Figure 9.15 - (a) Close-up view of the part that was monitored. (b) Location of the sensing system. The red arrows shows the diagonal members involved in the field test. (c) Close-up view of S0. (d) Close-up view of S1. (e) Close-up view of S2.   Distances are expressed in mm.

(a)
(b)

Figure 9.16 – Field testing: (a) Set up the safety robe. (b) Measuring the geometry of the trusses.

For this second structure it was decided to record data every fifteen minutes. Data were collected during the six days listed on Table 9.3. A total of 74 measurements were taken. It is noteworthy that on June 22 there was a mild rain during the first six measurements and on July 20 there was rain during the first measurement.

Meas. #	Date	Time	Air Temperature	Time	Steel Temperature (C)	Dry / rain
1	17-Jun	1:53 PM	19.4	1:47 AM	28.9	dry
2				2:02 AM	28.3	dry
3				2:26 AM	29.8	dry
4				2:41 AM	29.3	dry
5		2:53 PM	19.4	2:56 AM	29.5	dry
6				3:10 AM	29.8	dry
7	17-Jun	3:53 PM	20.6	3:26 AM	34	dry
8	22-Jun	8:53 AM	20.6	8:52 AM	no measurements	rain
9		9:00 AM	21.0	9:07 AM	no measurements	rain
10		9:24 AM	21.0	9:22 AM	no measurements	rain
11		9:49 AM	21.0	9:41 AM	25.3	rain
12		9:53 AM	21.1	9:56 AM	27.2	rain
13				10:09 AM	28.6	rain
14				10:26 AM	31.4	dry
15		10:53 AM	22.8	10:45 AM	31.4	dry
16				11:02 AM	32	dry
17				11:17 AM	35.3	dry
18				11:31 AM	34.5	dry
19				11:42 AM	33.3	dry
20		11:53 AM	23.3	11:56 AM	33.5	dry
21		12:03 PM	24.0	12:02 PM	33.4	dry
22		12:18 PM	24.0	12:17 PM	33.3	dry
23	22-Jun			12:32 PM	33.3	dry
24	29-Jun	8:53 AM	20.6	8:45 AM	no measurements	dry
25				9:00 AM	no measurements	dry
26				9:15 AM	no measurements	dry
27				9:30 AM	24.7	dry
28		9:53 AM	20.0	9:45 AM	24.4	dry
29				10:00 AM	26.3	dry
30				10:15 AM	28.1	dry
31				10:30 AM	28.2	dry
32		10:53 AM	19.4	10:45 AM	29.5	dry
33				11:00 AM	31.2	dry
34				11:15 AM	31.2	dry
35				11:30 AM	29.5	dry
36		11:53 AM	19.4	11:45 AM	29.5	dry
37				12:00 PM	29.4	dry
38		12:12 PM	21.0	12:15 PM	29.9	dry
39	29-Jun	12:35 PM	20.0	12:30 PM	29.7	dry

40	8-Jul	8:53 AM	26.7	9:16 AM	27.8	dry
41				9:30 AM	28.5	dry
42		9:53 AM	28.3	9:45 AM	32.6	dry
43				10:00 AM	33.3	dry
44				10:15 AM	33	dry
45				10:30 AM	35.3	dry
46		10:53 AM	30.0	10:45 AM	38.7	dry
47				11:00 AM	42.4	dry
48				11:15 AM	44	dry
49				11:30 AM	46.2	dry
50		11:53 AM	30.0	11:45 AM	46.6	dry
51				12:00 PM	47.7	dry
52				12:15 PM	45.4	dry
53	8-Jul	12:53 PM	30.0	12:30 PM	45	dry
54	13-Jul	8:53 AM	23.3	9:45 AM	30.1	dry
55		9:53 AM	23.9	10:00 AM	30	dry
56				10:15 AM	31.1	dry
57				10:30 AM	33.3	dry
58		10:53 AM	25.0	10:45 AM	33.2	dry
59				11:00 AM	31.5	dry
60				11:15 AM	33.2	dry
61				11:30 AM	33.2	dry
62		11:53 AM	25.6	11:45 AM	36.9	dry
63				12:00 PM	37.4	dry
64				12:15 PM	36.2	dry
65	13-Jul	12:53 PM	26.1	12:30 PM	36	dry
66	20-Jul	9:21 AM	22.0	9:15 AM	22.8	rain
67				9:30 AM	23	wet
68		9:53 AM	22.2	9:45 AM	23.3	wet
69				10:00 AM	23.4	wet
70				10:15 AM	24	dry
71		10:33 AM	22.0	10:30 AM	24.8	dry
72		10:53 AM	22.8	10:45 AM	25.1	dry
73				11:00 AM	24.4	dry
74	20-Jul	11:25 AM	23.0	11:15 AM	26	dry

Table 9.3 – Environmental conditions experienced during the observation of the second structure.
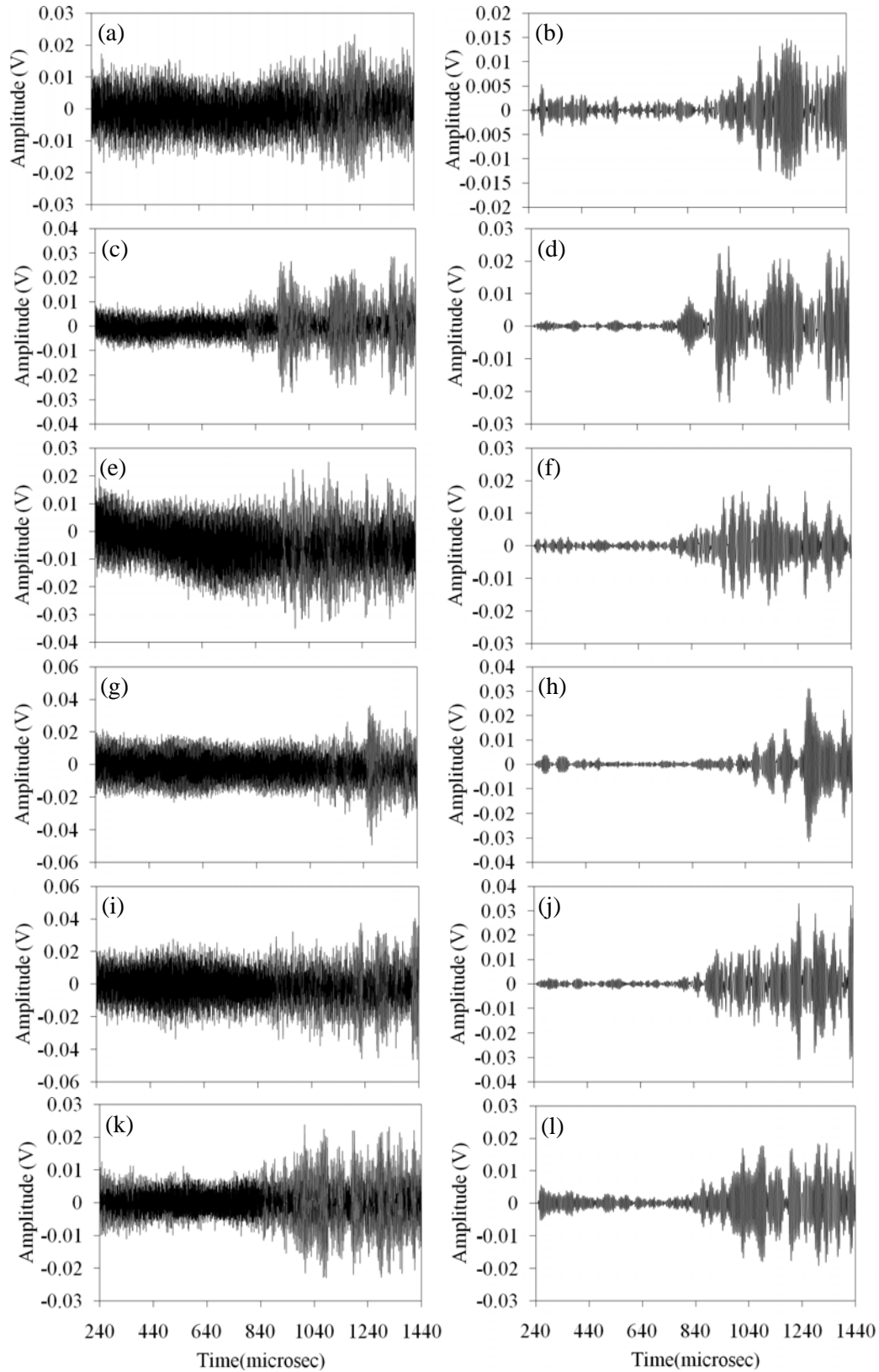
Figure 9.17 - Original time waveforms of 175 kHz for paths: (a) S0=>S2; (c) S0=>S3; (e) S3=>S4; (g) S3=>S5; (i) S3=>S6; (k) S1=>S0 and corresponding filtered waveforms of (b) S0=>S2; (d) S0=>S3; (f) S3=>S4; (h) S3=>S5; (j) S3=>S6; (l) S1=>S0 at the fourth measurement on June 17th.

183

As done for structure 1, the data were filtered using a Butterworth band pass filter.

Typical time waveforms recorded on June 17th are shown in Fig 9.17. The left column refers to the original signals. The right column shows the corresponding filtered signals. The following paths are presented: (a-b) S0=>S2; (c-d) S0=>S3; (e-f) S3=>S4; (g-h) S3=>S5; (i-j) S3=>S6; (k-l) S1=>S0. After signal filtering, time window were applied and statistical features were extracted from selected windowed information. With respect to structure 1, this second structure has different waveguide geometry and the relative distance among the transducers is also different. As such, the time of fight of the guided ultrasonic waves and the modes observed differ.
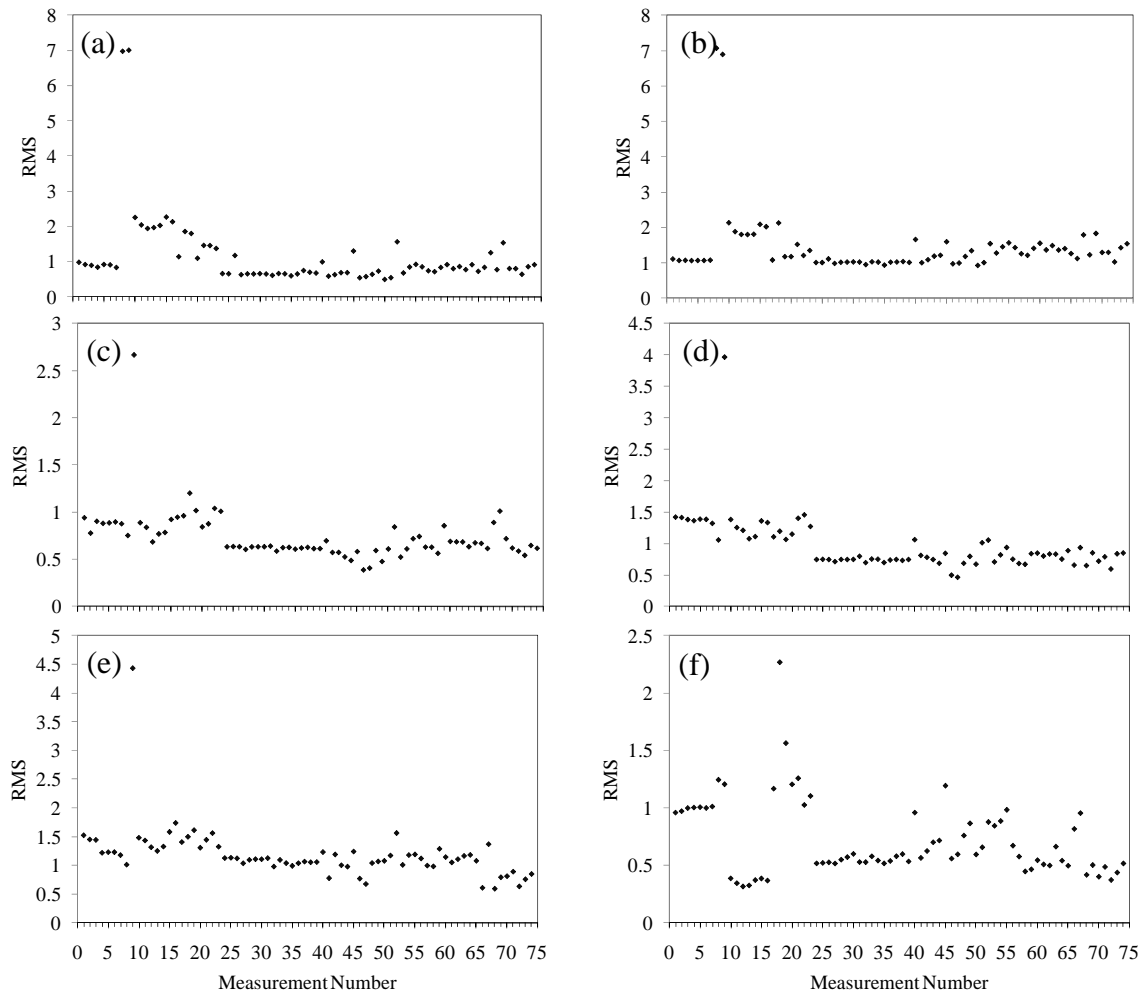
Figure 9.18 - Test 2. RMS-based damage index associated with paths: (a) S0=>S2/S3=>S0; (b) S0=>S3/S3=>S0; (c)S3=>S4/S3=>S0; (d)S3=>S5/S3=>S0;(e)S3=>S6/S3=>S0;(f) S1=>S0/S3=>S0.

184

Figures 9.18, 9.19, and 9.20 present the RMS-, K factor- and variance-based damage index. The plots refer to the following six damage indexes: S0=>S2/S3=>S0, S0=>S3/S3=>S0, S3=>S4/S3=>S0, S3=>S5/S3=>S0, S3=>S6/S3=>S0 and S1=>S0/S3=>S0, in which features extracted from S3=>S0 were used as normalization. The guided waves propagating at 175 kHz were considered for the analysis. It can be seen that the measurements obtained under mild rain conditions produced a decrease in the RMS values at measurement numbers 7, 8 and 9.

Overall an increase of the damage index with temperature increase was observed. This is the same response observed from the first structure. The scattering from measurement number 17 to 23 in Fig. 9.18 (f) is unexpected for the environmental conditions were stable along that period.
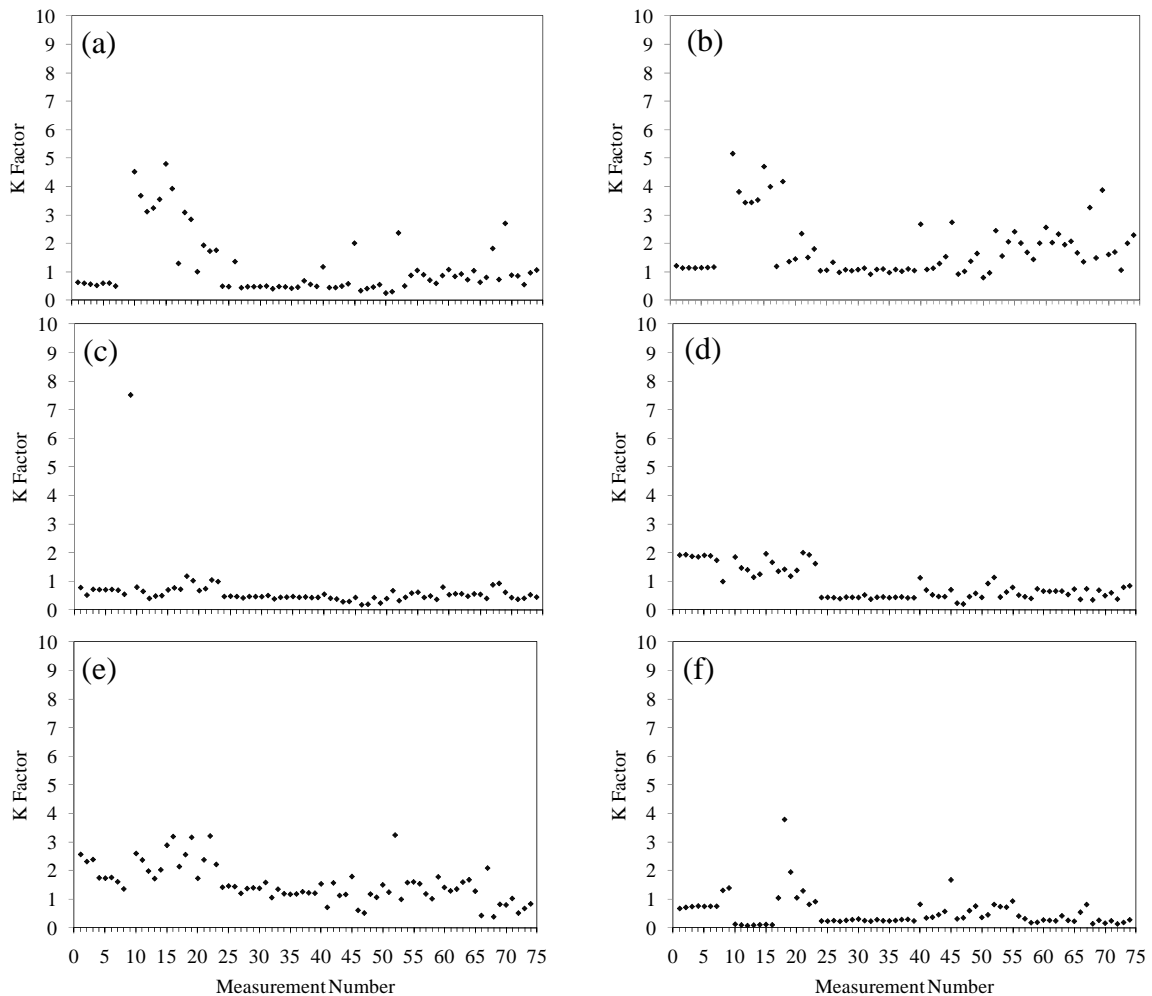
Figure 9.19 – Test 2. K-factor-based damage index associated with paths: (a) S0=>S2/S3=>S0; (b) S0=>S3/S3=>S0; (c)S3=>S4/S3=>S0; (d)S3=>S5/S3=>S0; (e)S3=>S6/S3=>S0; (f) S1=>S0/S3=>S0.
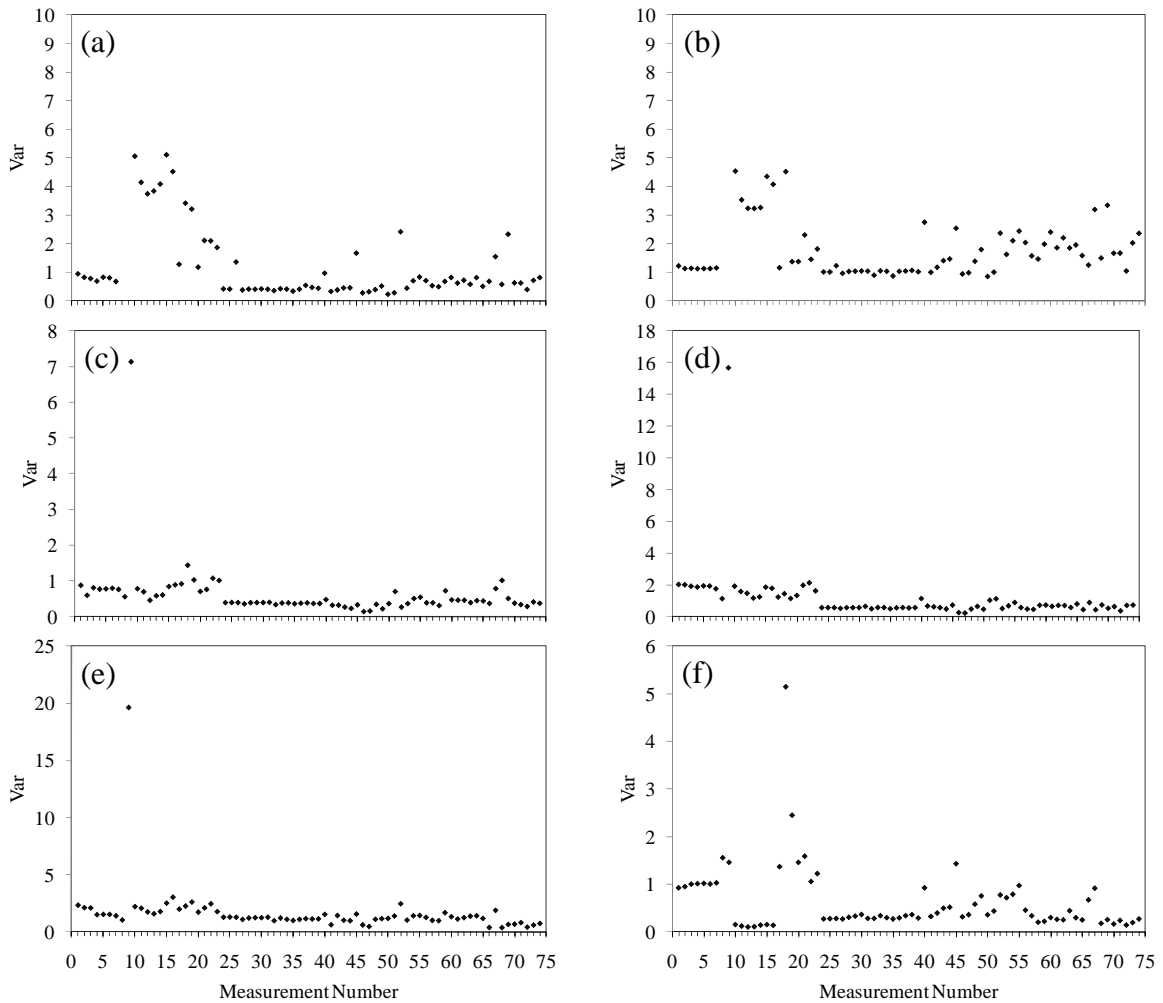
Figure 9.20 - Test 2. Variance-based damage index associated with paths: (a) S0=>S2/S3=>S0; (b) S0=>S3/S3=>S0; (c)S3=>S4/S3=>S0; (d)S3=>S5/S3=>S0; (e)S3=>S6/S3=>S0; (f) S1=>S0/S3=>S0.

Finally, Fig. 9.21 shows the multivariate analysis for the selected D.I.s. The measurements taken during the first two days of test were used as training data. As found for structure 1 the selection of the baseline data is pivotal to guarantee the robustness of the algorithm and more extensive data that include various environmental conditions should be included in the analysis.
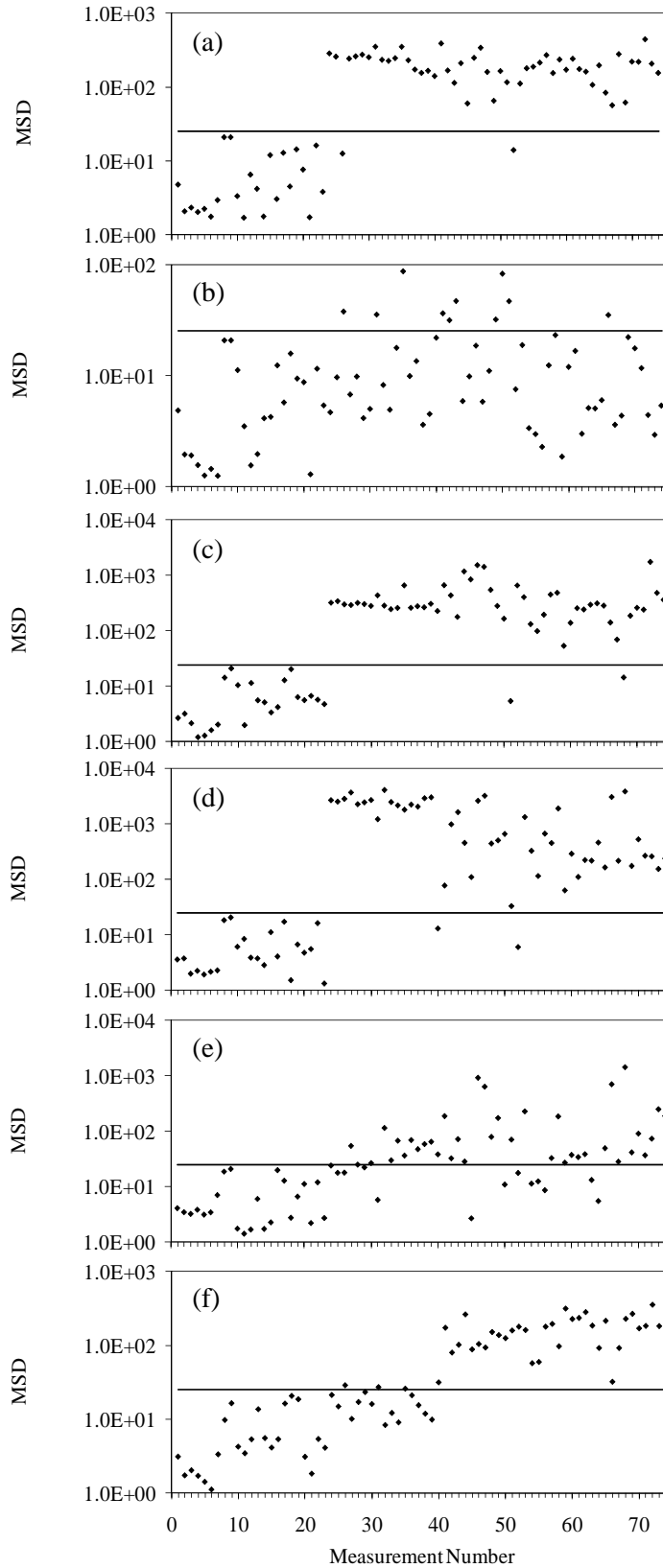
Figure 9.21 – MSD as a function of the measurement number associated with paths: (a) C0=>C2/C3=>C0; (b) C0=>C3/C3=>C0; (c) C3=>C4/C3=>C0; (d) C3=>C5/C3=>C0; (e) C3=>C6/C3=>C0 and (f) C1=>C0/C3=>C0.

187

CHAPTER 10: CONCLUSIONS

10.1 DISCUSSION

This report presents the results of a study about sensing technology for highway sign support structures. The objective of this study is two-fold: develop a numerical methodology aimed at determining the fatigue life of critical structural members and develop an inspection/monitoring technology to assess the structural soundness of such structures.

The report is articulated in three main parts.

The first part surveys the current technologies and procedures adopted by state DOTs all over the U.S. The review discusses strength, limitations, and cost-analysis of each approach and it includes potential techniques successfully adopted in other structures but not yet validated or proven on sign support elements. For instance, given that sign supports are mainly formed by welded hollow cylinders, a review of NDE methods in the pipeline industry is presented.

The second part of the report presents the findings associated with the use of commercial finite element method software to model an overhead four chord real sign support. The study aimed at predicting fatigue performance and residual lifetime of in-service sign support structures. In the framework of this part a review of the current algorithms to model the action of wind on structures and of the most recent fatigue theories applied to dynamic analysis to determine residual fatigue life of structures was conducted. Then, an accurate loading scenario for the structure under investigation was formulated. The scenario included wind loads. Finally, the action of wind loading was used to predict the residual lifetime of the structure under pristine condition and under few simulated damaged conditions.

Finally, the third part of this report presents the research and development outcomes of two NDE/SHM methodologies aimed at detecting damage in sign support structures. The first method consists of the excitation and detection of guided ultrasonic waves at frequencies ranging between 100 kHz and 300 kHz by means of an array of small PZTs. The detected waves were processed by extracting statistical features from the time waveforms and feeding an unsupervised learning algorithm based on the outlier analysis. The second NDE/SHM method investigated in this study was the electromagnetic impedance method, which exploits the mechanical impedance of a structure to monitor, in real-time, changes in structural stiffness and damping. Because direct measurements of the mechanical impedance of a structure are difficult to obtain, the electromechanical coupling effect of the host structure (the sign support in this work) and a PZT are measured. In fact, whenever a PZT is driven by an electrical current, the structure is deformed and produces a local dynamic response. This response is detected by the same PZT as an electrical response, which is analyzed by an impedance analyzer. Any damage in the host structure results in changes to its mechanical impedance, which will be observed by changes in the electrical impedance of the PZT material.

The following activities were performed to validate the sensing technology and the SHM proposed in this study: 1) large scale testing at the Watkins-Haggart laboratory at the University of Pittsburgh (Pitt); and 2) field testing along interstate 279 few miles north of Pittsburgh.

The experiments at Pitt aimed at developing a robust ultrasonic signal processing and an impedance method analysis for field deployment. Robustness against noise, low-frequency (very few Hertz) vibration, and environmental variations were considered. The density of the array (number of PZTs per unit length) was determined with the goal of minimizing the cost per sensing unit.

On one of the main chords of each structure tested in the field, PZT were bonded and data were collected on a weekly basis.

10.2 SUMMARY OF FINDINGS

Chapter 1 motivated the study and described the outline of the report.

Chapter 2 described the nomenclature in use for sign support structures. The materials that are utilized for the various structural elements were listed. Damage and factors inducing damage determined were discussed including corrosion, fatigue, and loads.

Chapter 3 presented the results of a survey conducted by the University of Pittsburgh. The answers given by the DOTs that responded to the survey show that, while sign structures across the US are pretty similar and are damaged in similar ways, the inspection processes are not very similar. For instance, there is no uniformity in the interval between two consecutive inspections.

Chapter 4 presented the results of the ANSYS model to evaluate the effect of natural wind on the fatigue life of five critical elements of the truss. A 5-second natural wind load was considered by using the Kaimal wind spectrum and base speeds in the range of 5-25 mph. The wind data were gathered from the NCDC website. The data from the Pittsburgh International Airport were considered. The analysis was carried out by considering: a) the structure in pristine conditions; b) the structure having one or two members partially damaged; c) the structure having one critical member fully damaged. It was found that the selected critical members have an infinite fatigue life. Even though the results predicted an infinite life, the exact conditions in the field cannot be predicted without monitoring the real structure and measuring the real wind loading. It was assumed that natural wind is the loading that most significantly contributes to fatigue damage. The computer procedure developed in this study is general and can be adapted to any type of overhead sign structure. The geometry and material properties of the new structure need to be accurately modeled in ANSYS or a similar program and the wind load algorithm described in Chapter 4.4 can be applied.

In general it was found that, although the fatigue life was found to be reduced by the presence of damage, it can still be considered as infinite. The fatigue life of the critical

members was also calculated by including the self-weight of the truss. In this case, the fatigue life of one element is found to be on the order of 13-15 years.

Chapter 5 demonstrated that currently only four NDE techniques are considered for the inspection of sign support structures: visual inspection, liquid penetrants, magnetic particles, and ultrasonic testing. Visual inspection is the most widely used and the most economic solution. However, it is ineffective to detect internal flaws. The cost to deploy other techniques for a structure such as the one modeled for fatigue, range from $1,000 to about $12,000. Potential techniques were identified. Some of them, however, are very expensive like the X-ray technique which also carried out safety issues related to radiation. Other technique like acoustic emission, ultrasonic guided waves, or EMI can be used although no practical employment in the field has been reported for overhead sign structures.

Chapter 6 described: 1) the structure tested at the University of Pittsburgh; 2) the hardware and software used for the experiments and the test protocol; 3) the structural health monitoring algorithm applied to the propagation of guided waves.

The sensing system adopted in this study cost about $10-15 a piece, excluding the wiring needed to connect them to the NI-PXI. The data acquisition system including the software is at about $12,000-$15,000 and can control up to thirty-two PZTs. As such, the hardware/software scheme presented in this chapter would be able to control up to $n \cdot (n-1)$ wave propagation paths, where $n = 32$.

The Labview program used to control both monitoring systems was built in house and is flexible to be modified at the user convenience and necessity. However, for a larger number of transducers the software tasks should be optimized to secure fast execution and lower time consumption.

Chapter 7 described the results of the SHM algorithm applied to GUW data. It was found that:

- PZT as far as 2 meters (~7 feet) are able to detect guided waves with large signal to noise ratio;

- several PZT pairs are able to detect the presence of a small size crack around the weld toe;

- certain waveform paths are more sensitive than other paths which therefore should be ignored;

- multivariate analysis outperforms univariate analysis;

- the appropriate combination of certain features may outperform the use of all of the features selected for the study;

- certain frequencies, namely 150 kHz, 175 kHz, and 200 kHz are more sensitive to the presence of damage than the other frequencies considered;

- few wave propagation paths can be used, which therefore implies that a lower number of PZT may be used to monitor a joint;

- the dynamic load would not affect the guided wave measurements and therefore the approach appears to be robust against field loading conditions;

- extreme care must be paid to the handling of the wiring connection and PZT conditions to mitigate false positives.

- environmental factors such as low-warm temperatures or dry-rain-snow conditions over the chord and the sensors may alter significantly the values of the damage index ratios considered in this study.

Chapter 8 described the results of the SHM algorithm applied to EMI data. It was found that:

- the hardware/software system proposed here may replace the use of high cost impedance analyzers or LCR meters which are conventionally used in the measurements of the electromechanical impedance;

- the method is less sensitive to the presence of damage growth when compared to the performance of the UGW measurement;

- the application of the outlier analysis greatly improves the sensitivity of the method;

- the position of the crack with respect to the EM transducers was very likely unfavorable, which means that for a bulk structure like the truss, the location of the PZT to exploit the EMI method must be carefully evaluated;

- extreme care must be paid to the handling of the wiring connection and PZT conditions to mitigate false positives.

Chapter 9 described the results of the field tests. It was found that:

- the methodology is robust for field deployment;

- temperature plays an important role in the quantitative measurement of the damage index ratios;

- raindrops may cause false positives.

10.3   RECOMMENDATIONS FOR FUTURE WORK

The following recommendations can be drawn based upon the work conducted during year 1 study.

1) Fatigue Analysis

   • Simulate the chain of events that would lead to the failure of more members allowing for the determination of complete structure failure.

   • Instrument the structure with wind sensors (anemometers for instance) to determine the wind loading scenario more accurately.

   • Extend the analysis to the uprights and the base in order to determine the condition of the pole and the nearby members when the structure is subjected to fatigue loading.

   • Extend the analysis carried out in this study to other types of structures in order to make an inclusive comparison among the fatigue lives of such structures.

2) Inspection/monitoring technology

   • Extend the field test over one year to include the widest possible temperature and weather conditions

   • Develop robust signal processing able to discriminate the effect of ambient conditions from damage conditions.

   • Carry out more tests to include structure's elements of various waveguide geometries.

   • Increase the typology of damage against which GUW and EMI methodology is proved.

   • Develop long term data collection, storage, and retrieval management.

REFERENCES

Abe, M., Park, G. and Inman, D. J. (2000). "Impedance-based monitoring of stress in thin structural members." Proc., 11th Int. Conference on Adaptive Structures and Technologies, Nagoya, 285–92.

Ahlborn, T., Lewis, M. Lindt, JV. (2003). "Optimization of Cost and Performance of Overhead Sign Structures." Michigan Tech Center for Strucututal Durability, Michigan Technological University, Michigan.

Ahlborn, T.M., van de Lindt, J.W., Uzcategui, A.J. and Lewis, M.E. (2004), Cost and performance comparison of U.S. overhead sign support structures, Transportation Research Record: Journal of the Transportation Research Board, No. 1892, 14–23.

Alleyne, D., Lowe, M. J. S., and Cawley, P. (1998). ''The Reflection of Guided Waves From Circumferential Notches in Pipes.'' *J. Applied Mechanics,* 65, 635–641.

American Association of State Highway and Transportation Officials (AASHTO). (1994). *Standard Specifications for Structural Supports for Highway Signs, Luminaires, and Traffic Signals.* With Interims, Washington, D.C.

American Association of State Highway and Transportation Officials (AASHTO). (2001). *Standard Specifications for Structural Supports for Highway Signs, Luminaires, and Traffic Signals, 4th Edition.* With Interims, Washington, D.C.

American Association of State Highway and Transportation Officials (AASHTO). (2004). *LRFD Bridge Design Specifications, 3rd Edition.* With Interims, Washington, D.C.

Annamdas, V.G.M. (2004). "Improved method of structural health monitoring using smart materials." First year report, Nanyang Technological University. Singapore.

Annamdas, V. G. M. (2007). "Characterization of Smart PZT transducer and admittance signatures using PZT-structure interaction models for structural health monitoring." PhD Thesis, Nanyang Technological University, Singapore.

Annamdas, V. G. M., Yang, Y. and Soh, C. K. (2007). "Influence of loading on the electromechanical admittance of piezoceramic transducers." *Smart Materials and Structures*, 16(5), 1888-1897.

Annamdas, V. G. M. and Soh, C. K. (2007a). "Three-Dimensional Electromechanical Impedance Model. I: Formulation of Directional Sum Impedance." *Journal of Aerospace Engineering*, 20(1), 53-62.

Annamdas, V. G. M. and Soh, C. K. (2007b). "Three-Dimensional Electromechanical Impedance Model. I: Damage Analysis and PZT Characterization." *Journal of Aerospace Engineering*, 20(1), 63-71.

Annamdas, V. G. M. and Soh, C. K. (2008). "Three Dimensional Electromechanical Impedance Model for Multiple Piezoceramic Transducers-Structure Interaction Model." *Journal of Aerospace Engineering*, ASCE, 21(1), 35-44.

ANSYS version 11.0, (2007), ANSYS Inc.

ASTM E 1049-85, *Standard practices for cycle counting in fatigue analysis*, ASTM International.

Ariduru, S. (2004) "Fatigue Life Calculation by Rainflow Cycle Counting Method." MSME thesis, Middle East Technical University, Ankara, Turkey.

Azzam, D.M. and Menzemer, C.C. (2008), Numerical study of stiffened socket connections for highway signs, traffic signals, and luminaire structures, ASCE Journal of Structural Engineering, 134(2), 173–180.

Balaskó, M., Sváb, E., Kuba, A., Kiss, Z., Rodek, L., and Nagy, A. (2005). "Pipe corrosion and deposit study using neutron-and gamma-radiation sources," *Nuclear Institute and Methods in Physics Research*, A.

Bannantine, J.A., Comer, J.J. and Handrock, J.L. (1990). *Fundamentals of Metal Fatigue Analysis.* Prentice Hall, New Jersey.

Bhalla, S. (2004). "A Mechanical Impedance Approach for Structural Identification, Health Monitoring and Non-Destructive Evaluation Using Piezo-Impedance Transducers" Ph.D Thesis, Nanyang Technological University, Singapore.

Bhalla, S. and Soh, C. K. (2004a). "Electromechanical Impedance Modeling for Adhesively Bonded Piezo-transducers," *Journal of Intelligent Material systems and structures*, 15, 955-972.

Bhalla, S. and Soh, C. K. (2004b). "Structural Health Monitoring by Piezo-impedance Transducers: I Modeling." *Journal of Aerospace Engineering*, ASCE, 17(4), 154-165.

Boller C. (2002). "Structural Health Management of Ageing Aircraft and Other   Infrastructure", Monograph on Structural Health Monitoring, Institute of Smart   Structures and Systems, 1-59.

Cheng, C. C. and Lin, C. C. (2005). "An impedance approach for determining optimal locations and shapes of multiple induced strain actuators." *Smart Materials and Structures*, 14, 1120-1126.

Collins, T. and Garlich, M. (1997) "Sign Structures Under Watch." *Road and Bridges.*

Cook, R.A., Bloomquist, D. and Agost, A.M. (1997). "Truck Induced Dynamic Wind Loads on Variable Message Signs." Transportation Research Board, 1954, Paper No. 970244, 187-193.

Connor, R.J., (2008). Draft Final Report – Results of the Investigation into the Cause of the Observed Cracking on VMS Support Structures in Penn DOT District 4-0, *Draft Final Report - Results of the Investigation into the Cause of the Observed Cracking on VMS Support Structures in Penn DOT District 4-0.*

Creamer, B.M., Frank, K.H. and Klinger, R.E. (1979). "Fatigue Loading of Cantilever Sign Structures from Truck Wind Gusts." Research Report 209-1F, Project 3-5-77-209, Center for Highway Research, The University of Texas, Austin, TX.

Davenport, A.G. (1961a) "The Spectrum of Horizontal Gustiness Near the Ground in High Winds." *Journal of the Royal Meteorological Society,* 87, 194-211.

Davenport, A.G. (1961b) "The Application of Statistical Concepts to the Wind Loading of Structures." *Proceedings of the Institute of Civil Engineers,* 19, 449-472.

Desantis, P.V. and Haig, P.E. (1996). "Unanticipated Loading Causes Highway Sign Failure." *ANSYS Conference Proceedings,* The Future of Simulation Tools – Computer Aided Design, ANSYS Convention, 3.99-3.108.

Dexter, R. J., K. Johns, and R. Di Bartolo, (2000). "Smart Sign Support," Civil Engineering, Nol. 70, No. 9, pp. 62-65.

Dexter, R.J. and Ricker, M.J. (2002). "Fatigue Resistant Design of Cantilevered Signal, Sign and Light Supports." NCHRP Report 469, Transportation Research Board, Washington, D.C.

Dexter, R.J. and Johns, K.W. (2005). "The Development of Fatigue Design Load Ranges for Cantilevered Sign and Signal Support Structures." *Journal of Wind Engineering*, 77, 315-325.

Diaz A.A., Mathews R.A., Hixon J. Doctor S.R. (2007). "Assessment of Eddy Current Testing for the Detection of Cracks in Cast Stainless Steel Reactor Piping Components" U.S. Nuclear Regulatory Commission Washington, DC 20555-0001, NRC Job Code Y6604.

Ditri, J. J. (1994). "Utilization of Guided Elastic Waves for the Characterization of Circumferential Cracks in Hollow Cylinders," *J. Acoust. Soc. Am.,* 96, 3769-3775.

EDSU. (1970). "Fluid Forces and Moments on Flat Plates." *Engineering Sciences Data Unit,* EDSU International, London.

Elspass, W.J. Kunzmann, J. Flemming, M. Baumann, and D. Design, (1995). "Manufacturing and Verification of Piezoceramics Embedded in Fiber-Reinforced Thermoplastics." Proc., Smart Structures and Materials 1995. Smart Structures and Integrated Systems, SPIE 2443, 327-333.

Farrar, C. (2006). *Structural Health Monitoring*, class notes, Univ. of California, San Diego.

Federal Highway Administration (FHWA). (2005). "Guidelines for the Installation, Inspection, Maintenance, and Repair of Structural Supports for Highway Signs, Luminaires, and Traffic Signals."

Finley, J. (2008). "TDOT to Inspect Signs After Collapse." 7 July, 2008. WSMV Nashville. http://www.wsmv.com/news/16813368/detail.html?rss=nash&psp=news#- [accessed 12 Nov, 2008.]

Fisher, J.W., Kulak, G.L and Smith, I.F.C. (1998), *A Fatigue Primer for Structural Engineers.* American Institute of Steel Construction, National Steel Bridge Alliance, Chicago, IL.

Fouad, F.H., Davidson, J.S., Delatte, N., Calvert, E.A., Chen, S.E., Nunez, E., and Abdalla, R. (2003). "Structural Supports for Highway Signs, Luminaires, and Traffic Signals." NCHRP Report 494, Transportation Research Board, Washington, D.C.

Fouad, F.H. and Calvert, E.A. (2005), Design of cantilevered overhead sign supports, Transportation Research Record: Journal of the Transportation Research Board, No. 1928, 39–47.

Ginal, S. (2003). "Fatigue Performance of Full-Span Sign Support Structures Considering Truck Induced Gust and Natural Wind Pressures." MSCE thesis, Marquette University, Milwaukee, WI.

Giurgiutiu, V. and Rogers, C. A. (1997). "Electromechanical (E/M) Impedance Method for Structural Health Monitoring and Non-Destructive Evaluation." Proc., International Workshop on Structural Health Monitoring: Current Status and Perspectives, 433-444.

Giurgiutiu, V. and Rogers, C. A. (1998). "Recent Advancements in the Electro-Mechanical (E/M) Impedance Method for Structural Health Monitoring and NDE," Proc., Smart Structures and Materials Conference, San Diego, California, SPIE, 536-547.

Giurgiutiu, V., Reynolds, A. and Rogers, C. A. (1999). " Details of the Electro-Mechanical (E/M) Impedance Health Monitoring of Spot-Welded Structural Joints." SPIE 6th Annual International Symposium on Smart Structures and Materials, Newport Beach, CA, Paper 3668-34.

Giurgiutiu, V. and Zagrai, A. N. (2000). "Characterization of Piezoelectric Wafer Active Sensors." *Journal of Intelligent Material Systems and Structures*, 11(12), 959-976.

Giurgiutiu, V. and Zagrai, A. N. (2002). "Embedded Self-Sensing Piezoelectric Active Sensors for On-Line Structural Identification." *Journal of Vibration and Acoustics*, ASME, 124(1), 116-125.

Hagood, N. W., Crawley, E. F., de Luis, J., and Anderson, E. H. (1988). "Development of Integrated Components for Control of Intelligent Structures." *Smart Materials, Structures and Mathematical Issues,* U.S. Army Research Office Workshop. 80-104. Blacksburg. VA. USA.

Holmes, J. D. (2007). *Wind Loading of Structures.* Taylor & Francis, New York, NY.

Hoon T, Toshihiko M, Tang C.K and Chiu W.K. "Fatigue Crack Detection Using Piezoelectric Elements," *SIF 2004 Structural Integrity and Fracture*, http://eprint.uq.edu.au/archive/00000836

Iannuzzi, A. and Spinelli, P. (1987). "Artificial Wind Generation and Structural Response." *Journal of Structural Engineering*, 113 (12), 2382-2396.

Kacin, J. (2009), Fatigue life estimation of a highway sign structure, M.S. Thesis, University of Pittsburgh, USA.

Kacin, J., Rizzo, P. and Annamdas, V.G.M. (2009), Sensing technology for damage assessment of sign supports and cantilever poles (Year 1), report submitted to the Pennsylvania Department of Transportation.

Kaczynski, M.R., Dexter, R.J. and Van Dien, J.P. (1998), Fatigue design of cantilevered signal, sign, and light supports, NCHRP Report 412, Transportation Research Board, Washington, D.C.

Kaimal, J.C., Wyngaard, J.C., Izumi, Y. and Cote, O.R. (1972). "Spectral Characteristics of Surface Layer Turbulence." *Journal of the Royal Meteorological Society,* 98, 563-589.

Kessler, S. S., Spearing, S. M., Attala, M. J., Cesnik, C. E. S. and Soutis, C. (2002). "Damage Detection in Composite Materials Using Frequency Response Methods," *Composites, Part B: Engr.*, 33, 87-95.

196

Koo, K.Y., Park, S., Lee, J.-J, Yun, C.-B., Inman, D.J. (2007), Impedance-Based Structural Health Monitoring Considering Temperature Effects, Proceedings of SPIE, 6532, 65320C.

Kozy, B. and Earls, C.J. (2007), Bearing capacity in long-span tubular truss chord, ASCE Journal of Structural Engineering, 133(3), 356-367.

Krishnamurthy, K., Lalande, F. and Rogers, C.A. (1996), Temperature effects on Piezoelectric Elements used as collocated Actuator/Sensors, Proceedings of SPIE North American Conference on Smart Structures and Materials, Vol. 2717, p. 302-310

Lamtenzan D, Washer G, and Lozev M, (2000). "Detection and Sizing of Cracks in Structural Steel Using the Eddy Current Method" US Department of Transportation, Federal Highway Administration, McLean, VA, FHWA-RD-00-018.

Lanza di Scalea, F. and Salamone, S. (2008). "Artificial Wind Generation and Structural Response." *J. Acoust. Soc. Am.,* Vol. 124, No. 1, 161-174.

Laubach M, Montgomery M, Cope D (2007). "Summary and Comparison Report on Teardown Evaluation of Cessna 402A and Cessna 402C Airplanes", U.S. Department of Transportation, Federal Aviation Administration DOT/FAA/AR-07/35.

Li, X. (2005). "Fatigue Strength and Evaluation of Highway Sign Structures." PhD thesis, Purdue University, West Lafayette, IN.

Li, X., Whalen, T.M. and Bowman, M.D. (2005), Fatigue strength and evaluation of double–mast arm cantilevered sign structures, Transportation Research Record: Journal of the Transportation Research Board, No. 1928, 64–72.

Liang, C., Sun, F. P. and Rogers, C. A. (1994). "Coupled electromechanical analysis of adaptive material systems- determination of the actuator power consumption and system energy transfer." *Journal of Intelligent Material Systems and Structures*, 5(1), 12-20.

Liu, H. (1991). *Wind Engineering: A Handbook for Structural Engineers.* Prentice Hall, New Jersey.

Logan, D.L. (2002). *A First Course in the Finite Element Method (3rd Edition).* Brooks/Cole, California.

Lowe, M. J. S., Alleyne, D. N., and Cawley, P. (1998). ''Defect Detection in Pipes Using Guided Waves,'' *Ultrasonics*, 36, 147–154.

Madhav, A. V. G. and Soh, C. K. (2007). "An electromechanical Impedance Model of Piezoceramic Transducer -Structure in Presence of Thick Adhesive Bonding." *Smart Materials and Structures*, 16(3), 673-686.

Madhav, A. V. G. and Soh, C. K. (2008). "Multiplexing and uniplexing of PZT transducers for structural health monitoring." *Journal of Intelligent Material systems and structures*, 19(4), 457-467.

Mall, S., and Hsu, T. L. (2000). "Electromechanical Fatigue Behaviour of Graphite/ Epoxy Laminate Embedded with Piezoelectric Actuator." *Materials and Structures,* 9, 78-84.

Mall, S. (2002). "Integrity of Graphite/Epoxy Laminate Embedded with Piezoelectric Sensor/Actuator under Monotonic and Fatigue Loads" *Smart Mater. Struct,* 11, 527-533.

Matsuishi, M. and Endo, T. (1968). "Fatigue of Metals Subjected to Varying Stresses." *Japanese Society of Mechanical Engineers,* Fukuoka, Japan.

McLean, T.W. (2004), Fatigue evaluation of a variable message sign bridge type support structure by analytical and experimental methods, M.S. Thesis, Auburn University, USA.

Mix, P.E. (2005). *Introduction to nondestructive testing : a training guide*, 2nd ed., Hoboken,   N.J. Wiley Interscience.

Naidu, A. S. K. and Soh, C. K. (2004). "Identifying damage location with admittance signatures of smart piezo-transducers." *Journal of Intelligent Material Systems and Structure*, 15, 627–642.

National Climate Data Center (NCDC). (2009). "NCDC: Unedited Local Climate Data." http://cdo.ncdc.noaa.gov/ulcd/ULCD?prior=Y [accessed 10/17/08].

Newsobserver (2008)"Driver Charged with DWI Following Early Morning Crash." 5 Oct, 2008. The News and Observer. http://www.newsobserver.com/news/story/1243763.html [accessed 12 Nov, 2008.]

New York State Department of Transportation. (1999). *Overhead Sign Structure: Inventory and Inspection Manual.* NYSDOT Region 10.

Ong, C. W., Yang, Y. W., Naidu, A. S. K., Lu, Y. and Soh, C. K. (2002). "Application of the electro-mechanical impedance method for the identification of in-situ stress in structures." Proc., Smart Structures, Devices, and Systems, SPIE, Melbourne, Australia 4935, 503-514.

Paget, C. A., Levin, K. (1999) "Structural Integrity of Composites with Embedded Piezoelectric Ceramic Transducer." Proc , Smart Struct and Mater. Smart Structures and Integrated Systems. SPIE. 3668, 306-313.

Paget, C. (2001). "Active Health Monitoring of Aerospace Composite Structures by Embedded Piezoceramic Transducers." PhD Thesis 0117, Royal Institute of Technology, Valenciennes University.

Paget, C. A. Levin, K. Delebarre, C. (2002) "Actuation Performance of Embedded Piezoceramic Transducer in Mechanically Loaded Composites." *Smart Mater. Struct.,* 11, 886–891.

Park, G., Kabeya, K., Cudney, H. and Inman, D.J. (1999), Impedance-based structural health monitoring for temperature varying applications, JSME International Journal, 42, 249-258.

Park, G., Cudney, H. H. and Inman, D. J. (2000). "Impedance-based health monitoring of civil structural components." *ASCE Journal of Infrastructure System*, 6, 153–60.

Park. G., Cudney. H. and Inman. DJ (2001), Feasibility of using impedance-based damage assessment for pipeline systems, Earthquake Engineering & Structural Dynamics Journal. 30. 1463 1474.

Park, G., Sohn, H., Farrar, C. R. and Inman, D. J. (2003). "Overview of Piezoelectric Impedance-Based Health Monitoring and Path Forward." *The Shock and Vibration Digest*, SAGE Publications, 35(6), 451-463.

Park, S., Ahmad, S., Yun, C. B. and Roh, Y. (2006). "Multiple Crack Detection of Concrete Structures Using Impedance-based Structural Health Monitoring Techniques." *Experimental Mechanics*, 46(5). 609-618.

Park, J.S. and Stallings, J.M. (2006). "Fatigue Evaluation of Variable Message Sign Structures Based on AASHTO Specifications." *KSCE Journal of Civil Engineering,* 10 (3), 207-217.

Pelletier E, Grenier M, Chahbaz A and Bourgelas T. (2006). "Array Eddy current for Fatigue Crack Detection of Aircraft Skin Structures" Proc., 5th Intl. Workshop, Advances in Signal Processing for Non Destructive Evaluation of Materials, Québec City, Canada, 85-92.

Piezo systems, Inc. (2008). Woburn, MA, USA. http://www.piezo.com/prodsheet1sq5A.html

Pun, Adarsh. (2001). "How to Predict Fatigue Life." *Design News.*

Ritdumrongkul, S., Abe, M., Fujino, Y. and Miyashita, T. (2004). "Quantitative health monitoring of Bolted joints using a piezoceramic actuator sensor." *Smart Materials and Structures*, 13, 20–9.

Rizzo, P., Annamdas, V.G.M., and Kacin, J. (2008). "Sensing Technology for Damage Assessment of Sign Supports and Cantilever Poles – Task 1." Draft Interim Report Contract No. 519691-PIT 008, University of Pittsburgh, Pittsburgh, Pa.

Rizzo, P., Bartoli, I., Marzani A., and Lanza di Scalea, F. (2005). "Defect Classification in Pipes by Neural Networks using Multiple Guided Ultrasonic Wave Features", *ASME Journal of Pressure Vessel Technology,* 127 (3), 294-303.

Rose, J. L., Ditri, J. J., Pilarski, A., Rajana, K., and Carr, F. T. (1994). ''A Guided Wave Inspection Technique for Nuclear Steam Generator Tubing,'' *NDT&E Int.*, 27, 307–330.

Rose, J. L., Jiao, D., and Spanner Jr., J. (1996) ''Ultrasonic Guided Wave NDE for Piping,'' *Mat. Eval.*, 54, 1310–1313.

Samman, M. M. and Biswas, M. (1994). "Vibration Testing for Non-Destructive Evaluation of Bridges II: Experiment." *Journal of Structural Engineering*, ASCE, 120(1), 290-306.

Shull P. J. (2002). *Nondestructive Evaluation – Theory, Techniques, and Applications*, Marcel Dekker.

Stephens, R.I. (2000) *Metal Fatigue in Engineering (2nd Edition).* John Wiley & Sons, New York.

Stevens, M.J. and Smulders, P.T. (1979). "The Estimation of the Parameters of the Weibull Wind Speed Distribution for Wind Energy Utilization Purposes." *Wind Engineering,* 3 (2), 132-145.

Sun, F. P., Chaudry, Z., Rogers, C. A., Majmundar, M. and Liang, C. (1995). "Automated real-time structure health monitoring via signature pattern recognition." Proc., Smart Structures Materials Conference, San Diego, California, SPIE, 2443, 236-247.

Tedesco J., Mcdougal W. and Ross, C. (1999). *Structural Dynamics: Theory and Applications.* Addison Wesley, California.

TWI 2008 http://www.twi.co.uk/content/ksijm001.html, last access July 10th 2008.

United States Patent (1999) *Method and apparatus for inspecting pipes using a digitized radiograph*, U.S. Patent 5864601.

Van de Lindt, J.M. and Ahlborn, T.M. (2005), Practical fatigue/cost assessment of steel overhead sign support structures subjected to wind load, Wind and Structures, 8(5), 343-356.

Wang, P. (1999). "Acoustic Emission Testing and FEA of Cantilevered Traffic Signal Structures." Mater thesis, University of Wyoming,

Wen, Y., Chen, Y., Li, P., Jiang, D., and Guo, H. (2007). "Smart Concrete with Embedded Piezoelectric Devices: Implementation and Characterization." *Journal of intell mater and sys.,* 18(3), 265-274.

Wetherhold, R.; Messer, M.; Patra, A. "Optimization of directionally attached piezoelectric actuators," *J. Engr. Mat. Techn.*, Vol 125, pp.148-152, 2003

Xing K. J and. Fritzen C.P "Monitoring of Growing Fatigue Damage Using the E/M Impedance Method", *Key Engineering Materials,* Vol. 347, pp 153-158, 2007.

Yang, Y., Hu, Y. and Lu, Y. (2008). "Sensitivity of PZT Impedance Sensors for Damage Detection of Concrete Structures." *Sensors*, 8, 327-346.

Zagrai, A. N. and Giurgiutiu, V. (2001). "Electro-Mechanical Impedance Method for Crack Detection in Thin Plates." *Journal of Intelligent Material Systems and Structures*, 12, 709-718.

Zalewski, B.F., Huckelbridge, A.A. (2005), Dynamic load environment of bridge-mounted sign support structures: a special student study, Report No. ST/SS/05-002. http://www.dot.state.oh.us/research/2005/Structures/134153-FR.PDF

Zhao, X., Gao, H., Zhang, G., Ayhan, B., Yan, F., Kwan, C. and Rose, J. L. (2007). "Active health monitoring of an aircraft wing with embedded piezoelectric sensor/actuator network: I. Defect detection, localization and growth monitoring." *Smart Materials and Structures*, 16(4), 1218-1225.

SUGGESTED READINGS

Alabama Department of Transportation (1994). *Procedures for Sampling and Inspection of Roadway Signs and Overhead Sign Structures.* Bureau of Materials and Tests, 2pp.

Albert, M.N. (2006). "Field Testing of Cantilevered Traffic Signal Structures Under Truck Induced Gusts." MSCE thesis, The University of Texas, Austin, Texas.

American Society for Testing and Materials (ASTM). (1986). *Annual Book of ASTM Standards,* Section 3: Metals Test Methods and Analytical Procedures, Vol. 3.01-Metals Mechanical Testing, ASTM, Philadelphia, PA 836-848.

Bhatti, A. and Constantinescu, G. (2008). "Improved Method for Determining Wind Load on Highway Sign and Traffic Signal Structures." Iowa Highway Research Board.

Bishop, N.W.M., Steinbeck, J. and Sherrat, F. (2000). *Finite Element Based Fatigue Calculations.* NAFEMS Ltd, Glasgow, Scotland.

Bowman, M. (2001). *Minutes of the Study Advisory Committee Meeting.* Purdue University Project SPR-2494: "Fatigue Strength and Evaluation of Sign Structures." Purdue University, West Lafayette, IN.

Consolazio, G.R., Dexter, R.J. and Johns, K.W. (1998). *Fatigue Performance of Variable Message Sign and Luminaire Support Structures: Volume 1.* FHWA 1998-009, New Jersey Department of Transportation.

Florida Department of Transportation. (2007). "Single and Multi-Post Inspection." Topic 850-055-025-g.

Fouad, F.H. and Calvert, E. (2004). "AASHTO 2001 Design of Overhead Cantilevered Supports" University Transportation Center for Alabama, The University of Alabama at Birmingham, Birmingham, AL.

Fouad, F.H. and Calvert, E. (2005). "Design of Overhead Cantilevered Sign Supports." *Transportation Research Record: Journal of the Transportation Research Board*, 1928, Transportation Research Board of the National Academies, 39-47.

Gilana, A and Whittaker, A. (2000a) "Fatigue Life Evaluation of Steel Post Structures I: Background and Analysis." *Journal of Structural Engineering,* 126 (3), 322-330.

Gilana, A and Whittaker, A. (2000b) "Fatigue Life Evaluation of Steel Post Structures II: Experimentation." *Journal of Structural Engineering,* 126 (3), 331-340.

Hancq, D.A. (2000). "Fatigue Analysis Using ANSYS." ANSYS inc.

Harnett, D.L. (1982). *Statistical Methods (3rd Edition).* Addison Wesley, Reading, Pa.

Illinois Department of Transportation (2007). *Sign Structures Manual.* Bureau of Bridges and Structures.

Provan, J.W. (1988). "An Introduction to Fatigue." *The Journal of Materials Education,* 11 (1) 1-104.

Scanlan, R.H. and Simiu, E. (1986). *Wind Effects on Structures (2nd Edition).* Wiley-Interscience, New York.

South, J.M. (1994). "Fatigue Analysis of Overhead Sign Structures." Report No. FHWA/IL/PR-115, Illinois Department of Transportation, Springfield, IL.